

# PRACTICAL MANUAL FOR FLUORESCENCE MICROSCOPY TECHNIQUES

Sohail Ahmed  
Sudhaharan Thankiah  
Radek Machán  
Martin Hof  
Andrew H. A. Clayton  
Graham Wright  
Jean-Baptiste Sibarita  
Thomas Korte  
Andreas Herrmann



# Foreword

Fluorescence describes the emission of photons upon excitation of a molecule by light or other electromagnetic radiation with certain well defined characteristics. These include: (i) the wavelength of excitation and emission being coupled, (ii) the process being time dependent in the region of ns, and (iii) photon emission being localized to within nm of the fluorescent molecule and influenced by its environment. Fluorescence has a long history dating back to the 1850s when George Stokes first analyzed the process using quinine and a prism in his treatise "On the Change of Refrangibility of Light". It was Albert Coons (1941) that linked fluorescein isothiocyanate (FITC) to antibodies and Gregorio Weber (1952) who developed dansyl chloride labeling of proteins that brought fluorescence into biology. Then in 1962, Osamu Shimoura and colleagues discovered the green fluorescent protein (GFP) of the jellyfish *Aequorea victoria*. GFP was cloned in 1992 by Douglas Prasher and expressed as an active fluorescent protein in *E. coli* and *C. elegans* by Martin Chalfie in 1994. Subsequent work by many people has developed GFP through side directed mutagenesis to optimize and diversify its uses. The use of GFP and its variants as genetically encoded fluorescent molecules has been key to using fluorescence to unravel the role of proteins in cell and molecular biology. Over the last few decades, these fundamental characteristics of fluorescence and the biology of "GFP" have been ingeniously used to probe protein dynamics, protein localisation and protein structure. In parallel to the development of fluorescent labeling techniques there has been significant developments in instruments to measure fluorescence inside biological specimens. These developments have included wide-field and confocal microscopy, two photon microscopy and most recently light sheet microscopy. In addition there has been significant improvements in lasers, detectors and software.

This practical manual has arisen through many courses and workshops that were run in Singapore between 2001 and 2016. The focus for this manual are the so-called F-techniques: FRET (fluorescence resonance energy transfer), FLIM (fluorescence lifetime imaging microscopy), FCS (fluorescence correlation spectroscopy) and FRAP (fluorescence recovery after photobleaching), and their use to probe protein structure and function. It is not our purpose here to describe the theory of the F-techniques in depth or all the discoveries that have been made with them. There are many excellent

reviews and scientific papers that cover these topics. In this practical manual we seek to help scientists to implement and utilize the F-techniques. We also hope the manual will serve as a resource for anyone interested in the F-techniques. Here, we focus on the core F-techniques, but recognize the development of many interesting variants that are in current use, such as fluorescence cross correlation spectroscopy (FCCS).

FRET is the method of choice to measure protein-protein interaction in a cellular context. FRET is the process of energy transfer between two fluorescent molecules in close proximity (1-10 nm) to each other. If certain conditions are met FRET can be used as a molecular ruler. In Chapter 1 the relatively simple indirect technique, Acceptor Photobleaching-FRET (AP-FRET), to measure FRET is described. AP-FRET utilizes laser induced bleaching of an acceptor in a region of interest (ROI) and monitoring changes in fluorescence intensity of the donor molecule in the same ROI. These measurements are made in fixed cells. The major advantage of AP-FRET is its simplicity allowing wide application. Chapter 2 describes Sensitised Emission-FRET (SE-FRET), a ratiometric method for measuring FRET. In SE-FRET changes in fluorophore spectra are used to monitor FRET. SE-FRET has utility for rapid events occurring in live cells. Chapters 3 and 4 describe methods to measure the lifetimes of fluorophores, in the frequency domain (FD-FLIM) and the time domain (TD-FLIM). FD-FLIM is an indirect method for measuring fluorescent lifetimes and has utility for rapid measurements in live cells. In contrast, TD-FLIM is a direct method that relies on measuring the time between excitation and photon release. Although more time consuming than FD-FLIM, TD-FLIM gives higher resolution of fluorescent lifetimes. TD-FLIM can be used to measure fluorescent lifetimes at sub-cellular resolution. Both FD-FLIM and TD-FLIM can be used to measure FRET. With TD-FLIM being the "gold standard" for estimating quantitatively whether there is FRET occurring between two fluorophores. In addition, TD-FLIM allows the proportion of interacting molecules to be measured. Chapter 5 introduces FCS, a powerful technique for measuring the movement of molecules within a defined (confocal) volume. Using mathematical analysis of FCS data two parameters can be estimated: protein diffusion rates and protein concentration. FCS has applications to follow protein association and dissociation (affinity constants) and protein complex formation.

Thus, FCS and the FRET methods described above can be used in parallel to measure protein-protein interaction. Lastly, Chapter 6 describes FRAP, a technique which measures protein diffusion by bleaching fluorophores in a ROI and then looking for recovery of fluorescence in the same ROI. FRAP is a semi-quantitative method that can be used in parallel with FCS to examine protein diffusion. Both FRAP and FCS are carried out on live cells. In conclusion, it is important to realize that the F-techniques are a powerful set of techniques that can be used to interrogate protein behavior in cells and can be used together by complimenting and/or validating each other. The F-techniques are not restricted to following protein behaviour and can also be used to follow DNA/RNA, as well as protein-DNA and protein-RNA interactions (protein-ligand interactions). This practical manual serves to promote and facilitate the use of F-techniques together by describing the implementation of the core techniques in a single resource.

Many people have contributed to bringing this manual into being. First and foremost I would like to thank the “PicoQuant team” (including Sandra Orthaus-Mueller, Jana Rudolph, Stefan Ruettinger, Nicole Saritas, Ben Kramer, Volker Buschmann) for their help in reviewing chapters, formatting text and figures, and their support in general. Particular thanks go to Sandra Orthaus-Mueller for co-ordinating activities and keeping the candle burning. Thanks are also due to Malte Wachsmuth and Lambert Instruments for help in reviewing the chapter on FCS and FD-FLIM, respectively. Other important contributions were made by Malte Wachsmuth, Thorsten Wohland and Ernst Stelzer through running EMBO courses in Singapore. Lastly, the Singapore government funding agency, A-STAR, Birgit Lane (Head of the Institute of Medical Biology, IMB) and the IMB Microscopy Unit (IMU) deserve special mention for funding the implementation of F-techniques in Singapore.

*Sohail Ahmed*  
September 2016

# Content

Chapter 1

## **Acceptor Photobleaching FRET (AP-FRET)**

*Thankiah Sudhaharan*

*Sohail Ahmed*

Chapter 2

## **Fluorescence Sensitized Emission FRET (SE-FRET)**

*Thankiah Sudhaharan*

*Sohail Ahmed*

Chapter 3

## **Frequency-domain Fluorescence Lifetime Imaging Microscopy (FD-FLIM)**

*Andrew H. A. Clayton*

Chapter 4

## **Fluorescence Lifetime Imaging Microscopy by TCSPC (TD-FLIM)**

*Thomas Korte*

*Andreas Herrmann*

Chapter 5

## **Fluorescence Correlation Spectroscopy (FCS)**

*Radek Machán*

*Martin Hof*

Chapter 6

## **Fluorescence Recovery After Photobleaching (FRAP)**

*Graham Wright*

*Jean-Baptiste Sibarita*



# Chapter 1

# Acceptor Photobleaching FRET (AP-FRET)

**Thankiah Sudhaharan and Sohail Ahmed**

Institute of Medical Biology, Singapore

Contact details of corresponding author: Thankiah Sudhaharan,  
sudhaharan.thankiah@imb.a-star.edu.sg

## Index

Abstract .....	3
1. Principle and Theory.....	3
2. Instrumentation .....	4
3. Methods.....	4
A. Materials Required.....	4
B. Sample Preparation .....	4
4. Data Acquisition.....	4
5. Data Analysis.....	6
A. FRET Efficiency .....	6
B. Pearson Product Moment Correlation Coefficient – “r” .....	7
6. Data Verification .....	7
7. Applications and Limitations .....	7
8. Conclusions .....	8
References .....	9
Appendix.....	11

## Abstract

Although the concept of FRET has been known since the 1960s, its first implementation in the context of cell experiments was not until the 1990s. Bastiaens, Jovin, and colleagues pioneered the use of FRET to study membrane trafficking and cell signaling pathways<sup>[1]</sup>. Acceptor photobleaching (AP)-FRET was first implemented to track cholera toxin complex formation using the cyanine dye pairs Cy3 and Cy5<sup>[2]</sup>. Subsequently, when GFP and its variants became available, AP-FRET was used to follow 5HT receptor dimerization<sup>[3]</sup>. Initially, CFP and YFP were the fusion proteins of choice for FRET experiments as their spectral characteristics were well suited to FRET. However, GFP/mRFP or mCherry are preferred nowadays. AP-FRET is the least complicated method to perform FRET. It can utilize GFP/mRFP or GFP/mCherry pairs, like other FRET methods, as donor and acceptor, respectively. Moreover, AP-FRET can be performed on standard confocal microscopes, which are usually available in most institutions. In this chapter we describe in detail how to perform AP-FRET, define positive FRET, and design controls.

## 1. Principle and Theory

In simple terms, Förster Resonance Energy Transfer (FRET) is a non-radiative energy transfer process

occurring due to interaction between the excited state of a donor and the ground state of an acceptor fluorophore. FRET occurs over distances of 10 nm or less (Figure 1). Hence FRET can be used as a molecular ruler working on the nanoscale. In biology FRET is widely used to measure biomolecular interactions such as protein-protein, protein-RNA, protein-ligand or protein-DNA. In this chapter, we focus on genetically encoded GFP and mRFP fluorescent proteins as tags to measure FRET between Cdc42 and CRIB fusion proteins by a method known as Acceptor Photobleaching (AP)-FRET. The fundamental aspect of the method lies in the comparison of donor fluorescence intensity (GFP) when in the presence or absence of an acceptor (mRFP or mCherry). If FRET is occurring between two fluorophores then it follows that eliminating the acceptor by means of photobleaching will increase donor fluorescence intensity. In contrast, in the absence of FRET, eliminating the acceptor should not affect the donor fluorescence intensity. Thus by measuring donor fluorescence intensity under these two different conditions should allow determining whether FRET is occurring or not. Another important advantage of AP-FRET is that it can be used to examine spatial aspects of protein-protein interactions in single cells under very precise conditions by choosing particular Regions Of Interest (ROIs). It should be noted that AP-FRET can only be performed on fixed samples, i.e. when fluorophore diffusion is prevented.

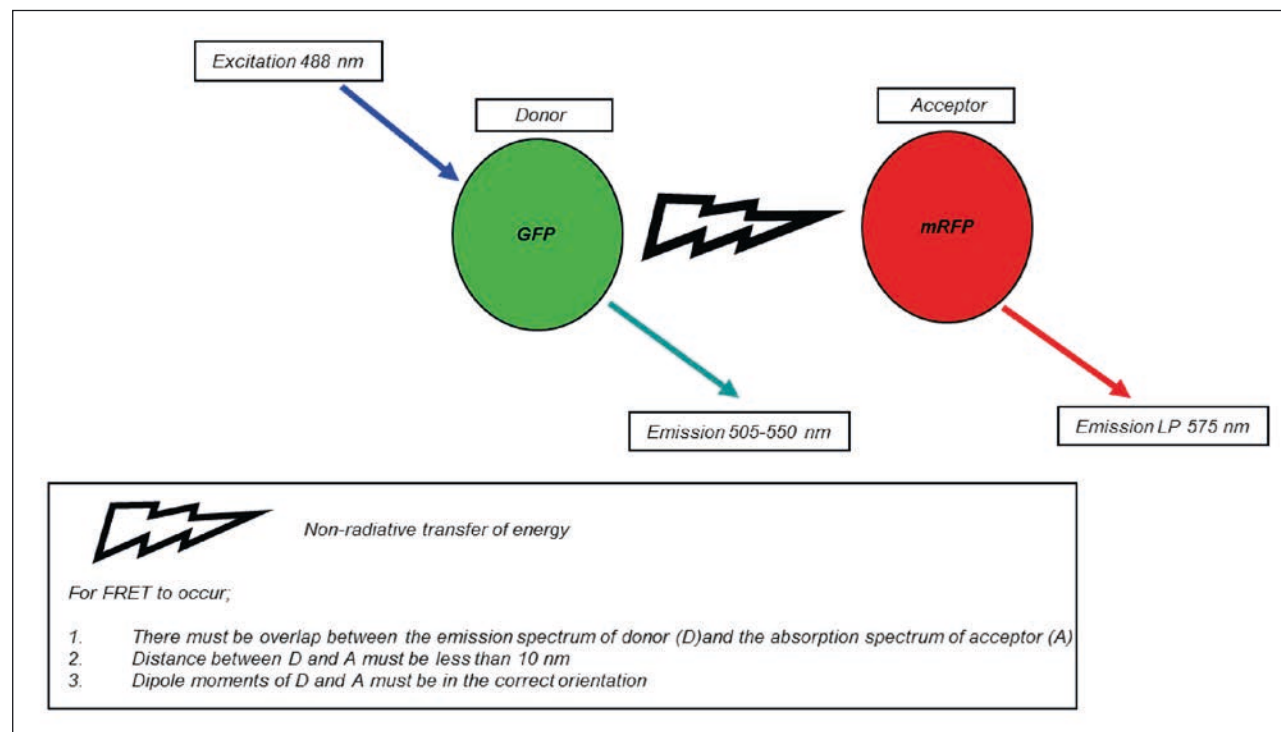


Figure 1 Shown here is the pictorial representation describing FRET occurrence.

## 2. Instrumentation

Either a confocal laser scanning microscope with lasers emitting at 488 and 561 nm for excitation with respective emission filter sets or a widefield microscope with appropriate filter sets and corresponding dichroic mirrors are necessary for the GFP and RFP pair. A 60 X water objective with high NA and either PMT detector (Confocal) or CCD camera (widefield) are also required.

## 3. Methods

### A. Materials Required

We use CHO cells as a starting point for AP-FRET because this cell line expresses a wide range of GFP and mRFP fusion proteins well. In principle, any cell line of interest can be used for AP-FRET. Other required material include: CO<sub>2</sub> incubators (37 °C), Fetal Bovine Serum (FBS), antibiotics (penicillin and streptomycin), trypsin, plasmids with fluorescent tags (expressing the acceptor and donor fusion proteins), cell culture medium (F-12K nutrient mixture [Kaighn's modification] for CHO cells), transfection reagent (Turbofect), coverslips (diameter 18 mm) and hemacytometer, six well plate dishes, T75 flasks and 10 ml pipettes, para-formaldehyde, mounting media (without antifade) and microscopy cover slides.

### B. Sample Preparation

CHO cells were grown in a 75 cm<sup>2</sup> tissue culture flask up to 90% confluence in the complete growth medium (1 x F-12K nutrient mixture [Kaighn's modification]) containing 10% fetal bovine serum qualified [FBS] and 1% antibiotics [penicillin and streptomycin]. Cells were detached from the flask, using 2 ml trypsin by incubating at 37 °C for 5 min and counted using a hemacytometer. For transfection, cells were seeded with a cell density of 1.5 × 10<sup>5</sup> cells in a 6-well tissue culture plate containing a 18 mm pre-washed and sterilized cover glass for 24 h. CHO cells were then transfected using Turbofect transient transfection reagent (other transfection reagents suited for the cell type can also be used) as per the following protocol. [Mix 3 µl of Turbofect with 1.5 µg of plasmid (1:2 (w/v), DNA/Turbofect) and 150 µl of serum free medium in a tube and let it stand for 25 min at RT]. Transfection mixes of respective plasmids were then transferred into different wells of a six well plate containing cells. The transfected cells in the six well plates were incubated at 37 °C in a CO<sub>2</sub> incubator for 24 h for protein expression to occur. Typically three transfections are used; (i) GFP-mRFP (tandem fusion) positive control. (ii) Co-expression of free GFP and mRFP (negative control). (iii) Co-expression

of mRFP-Cdc42 and GFP-CRIB as experimental model. These positive and negative controls are essential to correlate to potential positive FRET scenarios. Other controls including point mutants or deletion constructs, fusion protein/GFP, or mRFP combinations should also be considered for rigorous analysis. 24 h after transfection, cells are washed 3 times with 1 x PBS and are fixed using 4% para-formaldehyde for 15 min and quickly washed with 50 mM Tris pH 8.0, 100 mM NaCl to rinse excess fixative and then washed again for 5 min. It is advisable to use the right fixative to keep the cell structures intact. The cover slip containing fixed cells are mounted on a microscopy slide using Hydromount, an aqueous non-fluorescing mounting media, and allowed to dry overnight.

## 4. Data Acquisition

Any type of fluorescence microscope offering the necessary settings and controls can be used to perform the experiment. Although the Zeiss LSM

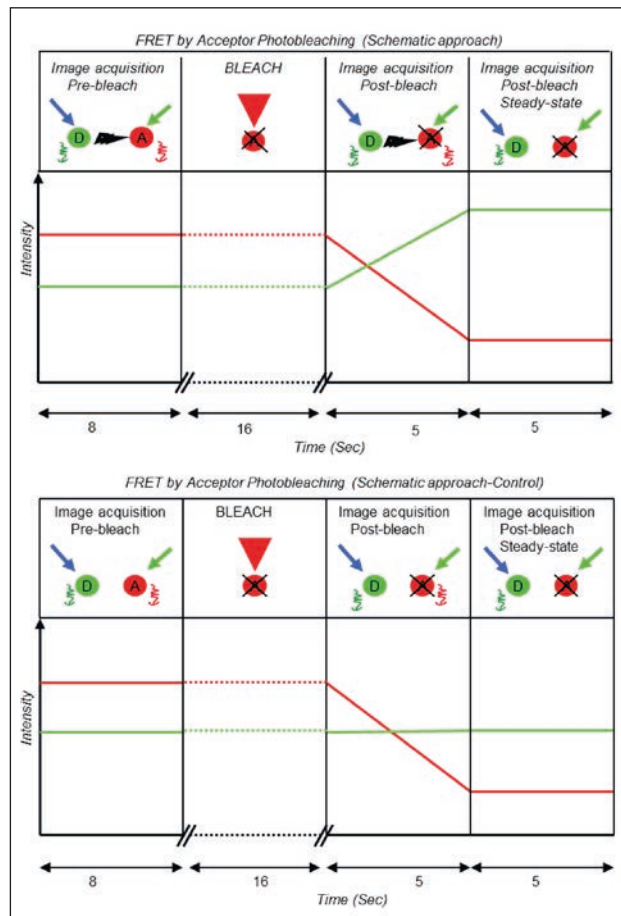


**Figure 2** Schematic representation is describing actual FRET and non-FRET situation expected from a typical FRET experiment.

510 confocal microscope is described in detail here, confocal microscopes from other manufacturers are suited as well. The software control sequences are given in the Appendix. If another type of confocal microscope is used, the equivalent software control windows have to be identified while the actual steps remain the same.

The AP-FRET experiment is running as a time sequence over a period of 35 s. Cells with similar modest levels of GFP/mRFP expression are chosen. Cells with high over expression should be avoided.

Dual channel recording (GFP and mRFP) is initiated pre-bleach and fluorescence intensity is measured for 8 s. Acceptor bleaching is then initiated for 16 s, followed by dual channel imaging for further 10 s. The bleaching time was selected in such a way that the rate of decrease in fluorescence intensity was approx. 66 u/s (see data analysis section b). Under the experimental conditions, the rate of change in fluorescence intensity post-bleaching can be followed accurately (Figure 2).

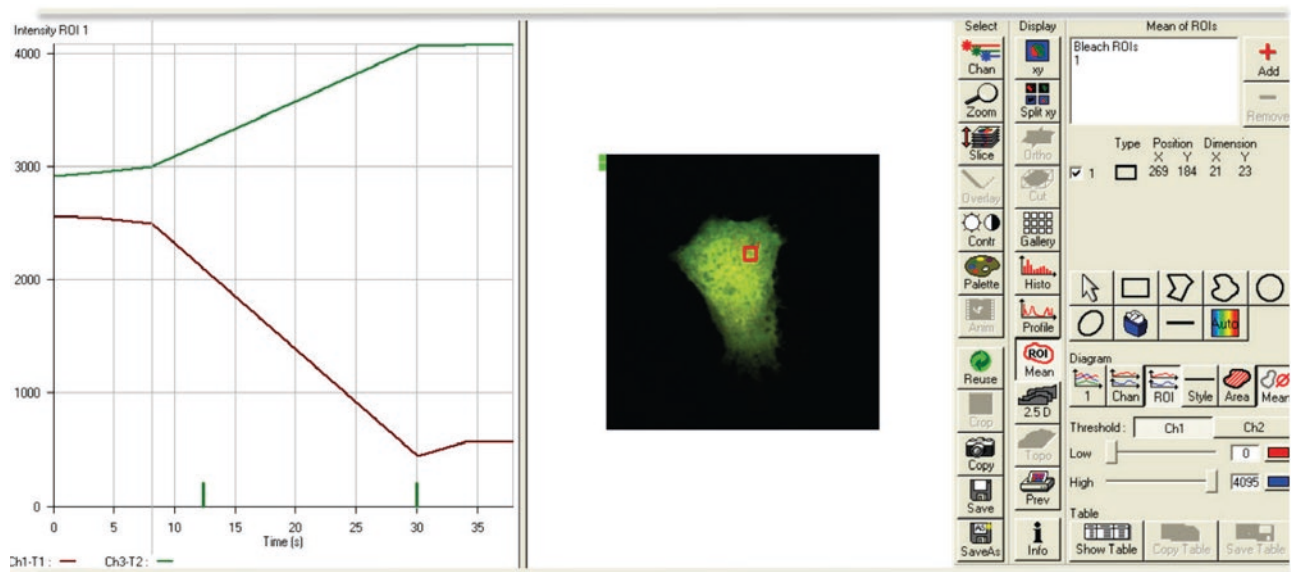


**Figure 3** A positive FRET control (GFP-mRFP) tandem fusion sample expressed in CHO-1 cells is undergoing FRET measurement. The sample was prepared as described in the method by co fusing GFP and mRFP and fixing after gene expression.

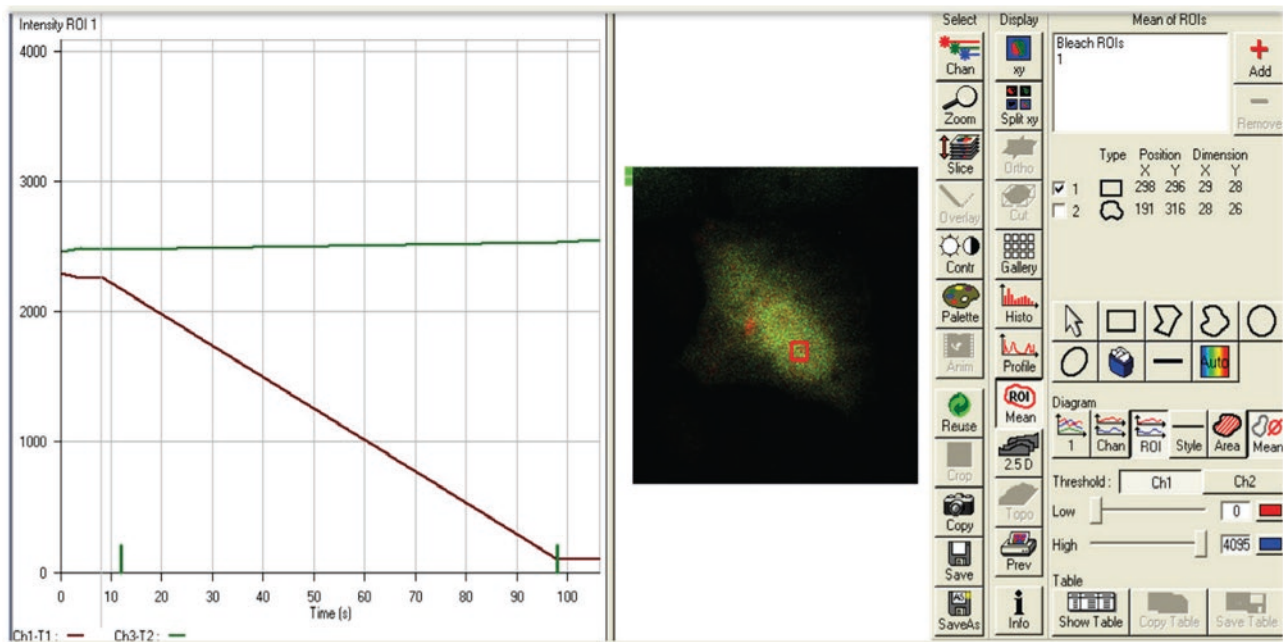


**Figure 4** A negative FRET control (free GFP and mRFP) sample expressed in CHO-1 cells is undergoing FRET measurement. The sample was prepared as described in the method by co-expressing free GFP and mRFP and fixing after gene expression.

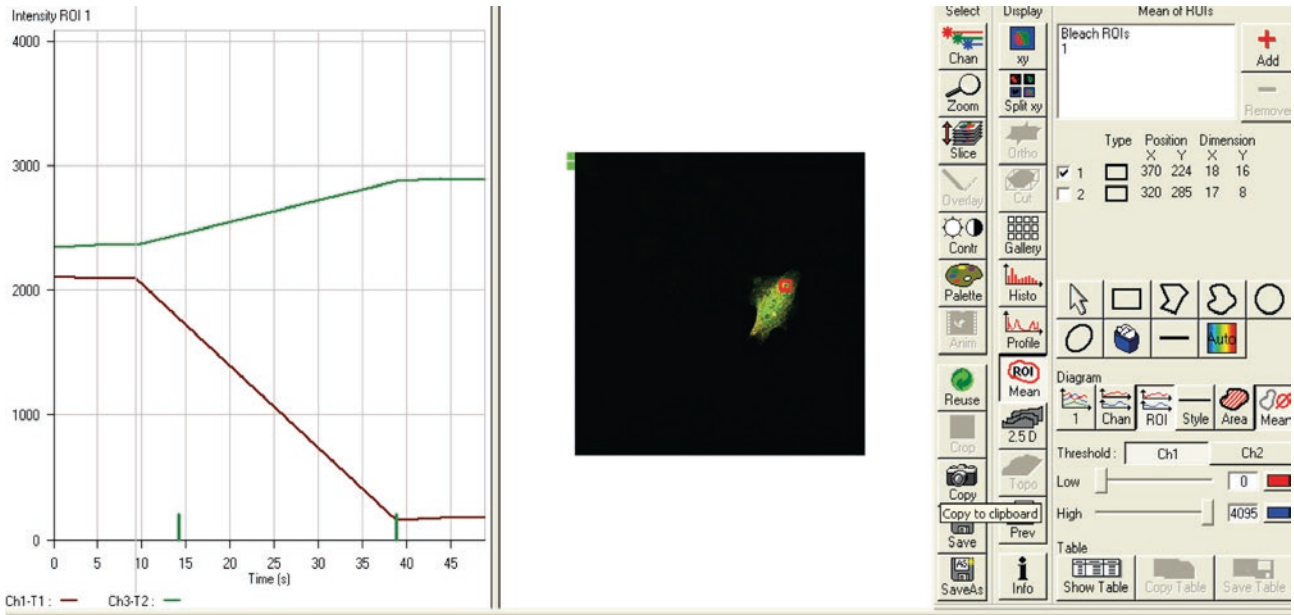


**Figure 5** Experimental FRET sample co-expressing GFP-Cdc42 and mRFP-CRIB in CHO-1 cells. The CRIB domain is a Cdc42 binding domain of N-WASP protein that binds Cdc42 with high affinity and is fused to mRFP.

In the control FRET negative scenario, there is little change in GFP intensity post-bleaching. In contrast, the positive FRET scenario exhibits significant change in GFP fluorescence intensity post-bleaching. The following four steps are used in order to collect the images and data.

- (i) Start the microscope, software, and laser. Switch on the microscope and open the software window. Create a new folder to save image data in order to carry out the experiment.
- (ii) Select an objective and focus the microscope. Select C-Apochromat 63 x 1.2 W objective by using Vis and Micro buttons in the expert mode. Click on Vis and Micro buttons in the software to focus on the sample using white light. Look for cells featuring fluorescence tags by using the mercury lamp and focus on them. Excite the GFP/mRFP fusion proteins of with the 488 and 561 nm laser lines as excitation source, while selecting [405/488/561] as dichoric mirror and [490,565] as secondary dichoric mirrors.
- (iii) Configure laser scanning and detection for confocal image acquisition. Monitor the emission by selecting GFP (BP 505-550) and mRFP (LP 575) emission filters to record the fluorescence intensity. Select ROI and photobleach by using 70% of the power of the 561 nm laser and select appropriate iterations so that at least 95% of the fluorescence intensity is bleached.
- (iv) Configure the bleaching and time lapse settings for acceptor photobleaching. Perform bleaching by running three pre-scan images and three post-bleach scans.

Figure 3 shows an experiment with GFP-mRFP

tandem fusion protein expression in CHO-1 cells. The tandem GFP-mRFP protein is generated from a cDNA construct where GFP encoding DNA is linked to mRFP encoding DNA directly. This tandem fusion protein is predicted to give maximum FRET and serves as positive control. For the negative control, we use free GFP and mRFP protein expression in CHO-1 cells (Figure 4). The experiment uses the small GTPase of the Rho family, Cdc42, as a GFP fusion protein. The CRIB domain is a Cdc42 binding domain that binds Cdc42 with high affinity and is fused to mRFP. An AP-FRET experiment using GFP-Cdc42 and mRFP-CRIB is shown in Figure 5.

## 5. Data Analysis

### A. FRET Efficiency

Background intensity data should be obtained by marking three ROIs outside the cell area for both GFP and mRFP channels and computing the average value. The respective background average value should then be subtracted from the GFP and mRFP fluorescence intensity values for each time frame. To calculate the FRET efficiency in percentage, E (%), the background subtracted values of GFP pre-bleaching and GFP post-bleaching should be used. These values can be obtained by using the “show table” function on the software and then by “exporting” the data as Excel files. The E (%) can be obtained using the following equation:

$$E(\%) = \frac{I_{GFP(post\text{-}bleach)} - I_{GFP(pre\text{-}bleach)}}{I_{GFP(post\text{-}bleach)}} \times 100$$

### B. Pearson Product Moment Correlation Coefficient – “r”

A very important parameter that can be extracted from the AP-FRET experiments is the Pearson product moment correlation coefficient “r”, a dimensionless index that ranges from -1.0 to 1.0. “r” can be determined by comparing rates of change in GFP fluorescence intensity with those in mRFP post bleaching. Thus a time series is performed on bleaching mRFP whereby GFP and mRFP intensities are recorded. An “r” value of -1.0 indicates a perfect fit with the linear relation and suggests that the increase in one parameter correlated with the decrease in the other parameter. “r” is calculated using the following equation;

$$r = \frac{\sum (x-\bar{x})(y-\bar{y})}{\sqrt{\sum (x-\bar{x})^2 \sum (y-\bar{y})^2}}$$

Where x and y are the sample means average (array1, GFP intensity) and average (array2, mRFP intensity), respectively.

## 6. Data Verification

The AP-FRET experiment generates two data types, (i) E (% FRET efficiency) and (ii) “r” (Pearson product moment correlation coefficient). The E and “r” values for the two controls (tandem GFP-mRFP fusion and free GFP/mRFP) can be used to define positive FRET. Positive FRET is defined as having a FRET efficiency value of > 3% and cross-correlation “r” values of between -0.7 to -1.0. Data from a minimum of about 10-12 cells should be collected for the calculation of “r”.

## 7. Applications and Limitations

By choosing different ROIs, it is possible to gain spatial and conformational information about protein-protein interactions. In our own work on the actin cytoskeleton and cell morphology, we have used AP-FRET to examine protein-protein interactions. In particular, we have examined the protein-protein interactions involved in Cdc42 and Rif induced filopodia. Small GTPases of the Rho family are well known to reorganize the actin cytoskeleton downstream of Ras and growth factor receptors. These signaling pathways involve recruitment of protein complexes to sites in the plasma membrane to remodel actin-membrane structures. Filopodia are small actin rich protrusions that are dynamic with a turnover every 1-2 min. Cdc42 is known to bind

**Table 1** Typical FRET data table complete with necessary controls showing FRET efficiency and correlation coefficient with standard deviation.

Protein	% FRET E ( $\pm$ SD)	r ( $\pm$ SD)
<b>Controls</b>		
GFP-mRFP (tandem fusion)	28.64 $\pm$ 3.69	-0.99 $\pm$ 0.01
Cyto-mRFP / GFP	1.91 $\pm$ 1.49	-0.17 $\pm$ 0.63
mRFP -IRSP53 + Cytp-GFP	2.12 $\pm$ 1.49	-0.16 $\pm$ 0.55
GFP-N-WASP + Cyto mRFP	2.73 $\pm$ 1.90	-0.63 $\pm$ 0.42
<b>Experimental</b>		
mRFP-Cdc42V12 + GFP-CRIB (domain)	18.40 $\pm$ 3.56	-0.99 $\pm$ 0.01
mRFP-Cdc42N17 + GFP-CRIB (domain)	2.34 $\pm$ 2.26	-0.09 $\pm$ 0.75
mRFP-N-WASP + GFP-Cdc42V12	10.17 $\pm$ 2.42	-0.97 $\pm$ 0.02
mRFP-N-WASP + GFP-Cdc42N17	2.42 $\pm$ 1.66	-0.47 $\pm$ 0.49
mRFP-IRSp53 + GFP-Cdc42V12	9.79 $\pm$ 3.47	-0.94 $\pm$ 0.06
mRFP-IRSp53 + GFP-Cdc42N17	2.69 $\pm$ 2.68	-0.1 $\pm$ 0.69

IRSp53, Toca1, and N-WASP. In turn, IRSp53 interacts with F-actin and actin modulators. The latter group includes Mena, Eps8, mDia1/2, and Dynamin. An example of such an AP-FRET analysis is shown in Table 1. Controls are critical in this analysis for the definition of a positive FRET. The first control is using the free protein pairs, GFP/mRFP versus a tandem fusion GFP-mRFP protein. This control defines minimum and maximum FRET, respectively. Second control experiment consists in using the experimental proteins with free GFP/mRFP as pairs. In this case FRET should not be observable. A last control uses point mutants (N17 in the case of Cdc42) in which protein-protein interactions are prevented. The data in Table 1, which compares controls with experiments, clearly show that Cdc42V12 interacts with CRIB, N-WASP and IRSp53 in vivo, but Cdc42N17 does not. We have used AP-FRET to examine spatial interactions of Cdc42, Rif, and IRSp53 with target proteins<sup>[14]</sup>. More specifically, we have examined if these proteins interact with filopodia. Interestingly, we have been able to show by AP-FRET that IRSp53 interacts with Mena, Eps8, mDia1, and Dynamin but not with mDia2 in filopodia<sup>[17]</sup>.

Limitations of AP-FRET include:

- (i) The need for samples to be fixed.
- (ii) The expression levels of donor and acceptor have to be carefully selected to aim for a 1:1 ratio.
- (iii) Several control measurements are needed to determine non-specific FRET.

## 8. Conclusions

AP-FRET is the most straightforward and intuitive method for measuring FRET. On one hand, if two fusion proteins, such as GFP-Cdc42 and mRFP-CRIB, are not interacting with each other, then there is no reason why bleaching of mRFP-CRIB should increase the fluorescence intensity of GFP. On the other hand, if the two fusion proteins are interacting and their dipole moments are in the correct orientation, while being 10 nm or less apart, then FRET should occur. In the positive FRET case, bleaching of mRFP-CRIB should affect the fluorescence of GFP-Cdc42 (a de-quenching process). Further, the rate of decrease in mRFP-CRIB fluorescence intensity should correlate with the rate of increase of GFP-Cdc42 intensity. By the use of two simple equations, the values for E and "r" can be determined and positive FRET identified.

## References

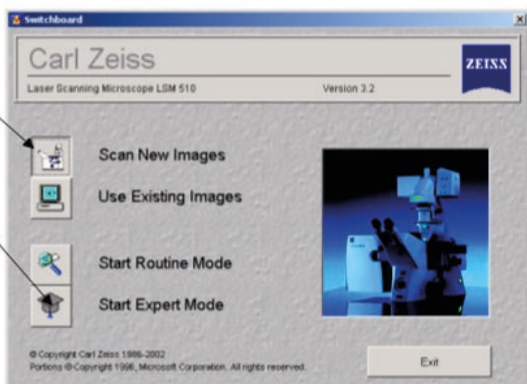
- [1] Microscopic imaging tracks the intracellular processing of a signal transduction protein: fluorescent labeled protein kinase C  $\beta$ I. Bastiaens, P.I.H. and Jovin T.M. Proc.Natl.Acad.Sci.USA, 1996,93, 8407-8412.
- [2] Imaging the intracellular trafficking and state of the AB5 quaternary structure of cholera toxin. Bastiaens, P.I.H., Majoul I.V., Verveer P.J., Soling H-D and Jovin T.M. The EMBO Journal 1996, 15. 4246-4253.
- [3] Serotonin 5-HT<sub>2C</sub> receptor homodimer biogenesis in the endoplasmic reticulum: real-time visualization with confocal fluorescence resonance energy transfer. Herrick-Davis K, Weaver BA, Grinde E, and Mazurkiewicz, JE, J. Biol Chem, 2006, 281, 27109-16.
- [4] Development of probes for cellular functions using fluorescent proteins and fluorescence energy transfer. Miyawaki A. Annu. Rev. Biochem, 2011, 80, 31.1-31.17.
- [5] Visualization of molecular activities inside living cells with fluorescent labels. Bunt G. and Wouters FG. International Review of Cytology, 2004, 237, 205-277.
- [6] FRET imaging. Jares-Erijman EA and Jovin TM. Nature Biotechnology, 2003, 21, 1387-1395.
- [7] Fluorescence resonance energy transfer microscopy of localized protein interactions in the living cell nucleus. Day RN, Periasamy A. and Schaufele F. Methods, 2001, 25, 4-18.
- [8] Fluorescence resonance energy transfer (FRET) measurement by gradual acceptor photo-bleaching: Van Munster E.B, Kremers GJ, Adjobo-Hermans M J, and Gadella TW, Jr. J Microsc., 2005, 218, 253-62.
- [9] APPL proteins FRET at the BAR: direct observation of APPL1 and APPL2 BAR domain-mediated interactions on cell membranes using FRET microscopy. Chial, H. J., Lenart, P., and Chen, Y. Q., PLoS One, 2010, 5, e12471.
- [10] Fluorescence resonance energy transfer (FRET) analysis demonstrates dimer/oligomer formation of the human breast cancer resistance protein (BCRP/ABCG2) in intact cells. Ni Z, Mark ME, Cai X, and Mao Q. Int J Biochem Mol Biol, 2010, 1, 1-11.
- [11] FRET with multiply labeled HERG K(+) channels as a reporter of the in vivo coarse architecture of the cytoplasmic domains. Miranda P, Manso DG, Barros F, Carretero L, Hughes TE, Alonso-Ron C, Dominguez P, and de la Pena P. Biochim Biophys Acta, 2008, 1783, 1681-99.
- [12] Determination of in vivo dissociation constant, KD, of Cdc42-effector complexes in live mammalian cells using single wavelength fluorescence cross-correlation spectroscopy. Sudhaharan, T, Liu, P, Foo, YH, Bu, W, Lim, KB, Wohland, T, and Ahmed, S., J Biol Chem, 2009, 284, 13602-9.
- [13] The Toca-1-N-WASP complex links filopodial formation to endocytosis. Bu W, Chou AM, Lim KB, Sudhaharan T and Ahmed S. J Biol Chem, 2009, 284, 11622-36.
- [14] The Cdc42 effector IRSp53 generates filopodia by coupling membrane protrusion with actin dynamics. J Lim KB, Bu W, Goh WI, Koh E, Ong SH, Pawson T, Sudhaharan T, and Ahmed S. J. Biol Chem, 2008, 283, 20454-72.
- [15] Cdc42 interaction with N-WASP and Toca-1 regulates membrane tubulation, vesicle formation and vesicle motility: implications for endocytosis Bu W, Lim KB, Yu YH, Chou AM, Sudhaharan T, and Ahmed S. PLoS One, 2010, 5, e12153.
- [16] Rho GTPase Cdc42 is a direct interacting partner of Adenomatous Polyposis Coli protein and can alter its cellular localization. Sudhaharan T, Goh WI, Sem KP, Lim KB, B, W, and Ahmed S. PLoS One, 2010, 6, e16603.
- [17] Rif-mDia1interaction is involved in filopodium formation independent of Cdc42 and Rac effectors. Goh WI, Sudhaharan T, Lim, KB, Sem, KP, Lau, CL, and Ahmed, S., J Biol Chem, 2011, 286, 13681-94.

Applications	FRET Pairs	References
<b>Reviews on FRET</b>		(Miyawaki, 2011) <sup>[4]</sup> (Bunt and Wouters, 2004) <sup>[5]</sup> (Jares-Erijman and Jovin, 2003) <sup>[6]</sup> (Day et al, 2001) <sup>[7]</sup>
<b>Selected Recent Applications</b>		
Gradual acceptor photobleaching method.	CFP and YFP	(Van Munster et al, 2005) <sup>[8]</sup>
APPL1 and APPL2 BAR domain-mediated interactions on cell membranes.	CFP and YFP	(Chial et al, 2011) <sup>[9]</sup>
Dimer/oligomer formation of the human breast cancer resistance protein (BCRP/ABCG2) in intact cells.	CFP and YFP	(Ni et al, 2011) <sup>[10]</sup>
HERG K (+) channels as a reporter of the <i>in vivo</i> coarse architecture of the cytoplasmic domains.	CFP and YFP	(Miranda et al, 2008) <sup>[11]</sup>
Determination of <i>in vivo</i> dissociation constant, Kd, of Cdc42-effector complexes in live mammalian cells.	GFP and mRFP	(Sudhaharan et al, 2009) <sup>[12]</sup>
The Toca-1-N-WASP complex links filopodial formation to endocytosis.	GFP and mRFP	(Bu et al, 2009) <sup>[13]</sup>
The Cdc42 effector IRSp53 generates filopodia by coupling membrane protrusion with actin dynamics.	GFP and mRFP	(Lim et al, 2008) <sup>[14]</sup>
Cdc42 interaction with N-WASP and Toca-1 regulates membrane tubulation, vesicle formation and vesicle motility.	GFP and mRFP	(Bu et al, 2010) <sup>[15]</sup>
Rho GTPase Cdc42 is a direct interacting partner of Adenomatous Polyposis Coli protein and can alter its cellular localization.	GFP and mRFP	(Sudhaharan et al, 2011) <sup>[16]</sup>
Rif-mDia1 interaction is involved in filopodium formation	YFP and mRFP	(Goh and others, 2011) <sup>[17]</sup>

## Appendix

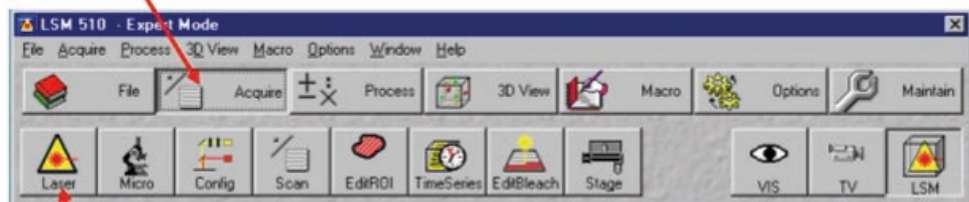
### Starting the LSM 510 Software

- Double click the LSM 510 icon
- Select “Scan New Images”
- Select “Start Expert Mode”



### Turning on the Lasers

1) Select Acquire

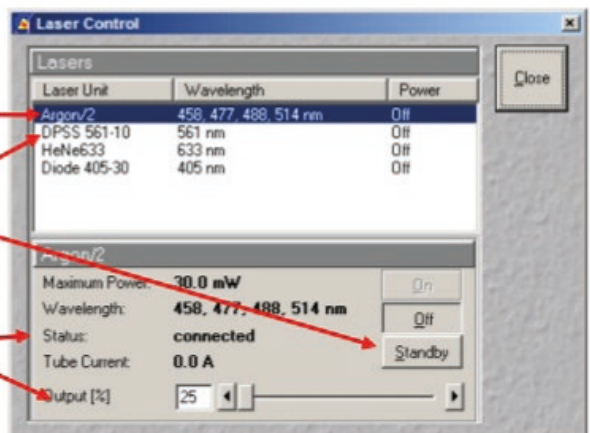


2) Select Laser

3) Click Standby for Argon Laser and wait for it to warm up. Once the status says "READY" switch it ON.

4) Set Output(%) so that tube current is in between 5.5A to 6.5A

5) Click on DPSS 561 Laser and switch it ON.



### Change Between Direct Observation and Laser Scanning



To view the sample through the eyepiece, click on "VIS". Toggle between VIS and LSM button in main menu to automatically switch between direct observation and laser scanning

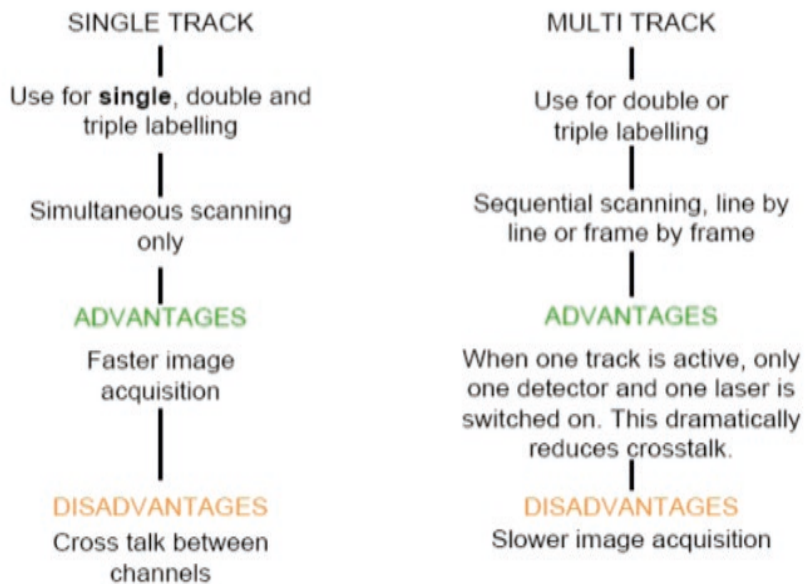
### Selecting an Objective and Focusing the Sample

- 1) Select "Micro" (Main menu Acquire)

The screenshot shows the LSM 510 Expert Mode software window with the 'Micro' button highlighted in the toolbar. To the right, a 'Microscope Control' dialog box is open, showing the 'Microscope Settings' tab with 'Blue' selected. Red arrows point from the numbered steps to the corresponding controls in the software interface.

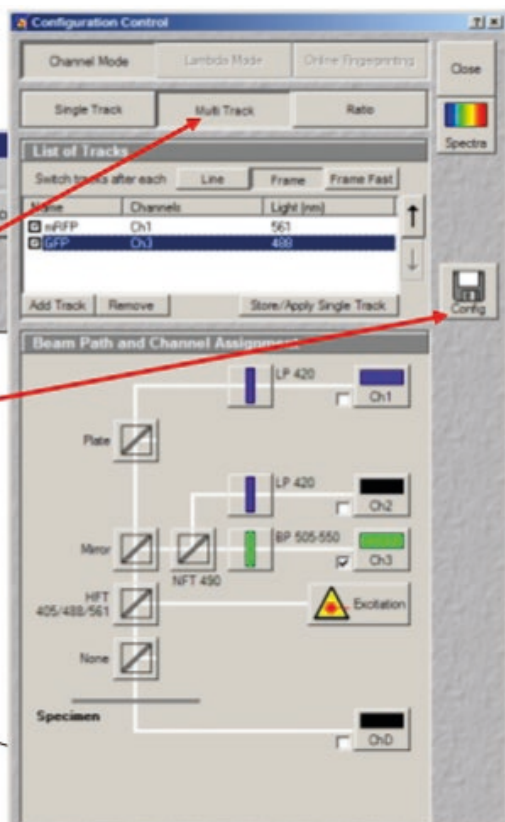
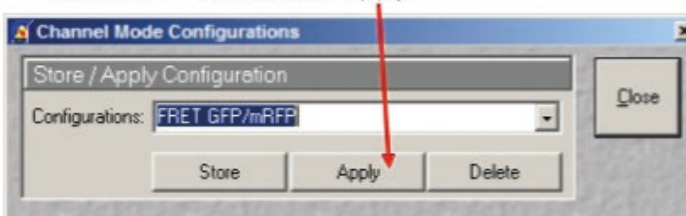
- 2) Click on Green or Red to visualize GFP or mRFP through eyepiece
- 3) Objective lens can be selected from a pull down menu by clicking onto the objective button. Click on 63x lens. Please note all the 4 lenses are water immersion lenses. You need to place a drop of water provided on the 63x lens and then place the sample with the coverslip facing the objective lens.
- 4) Use the focusing knob on the microscope to focus the sample

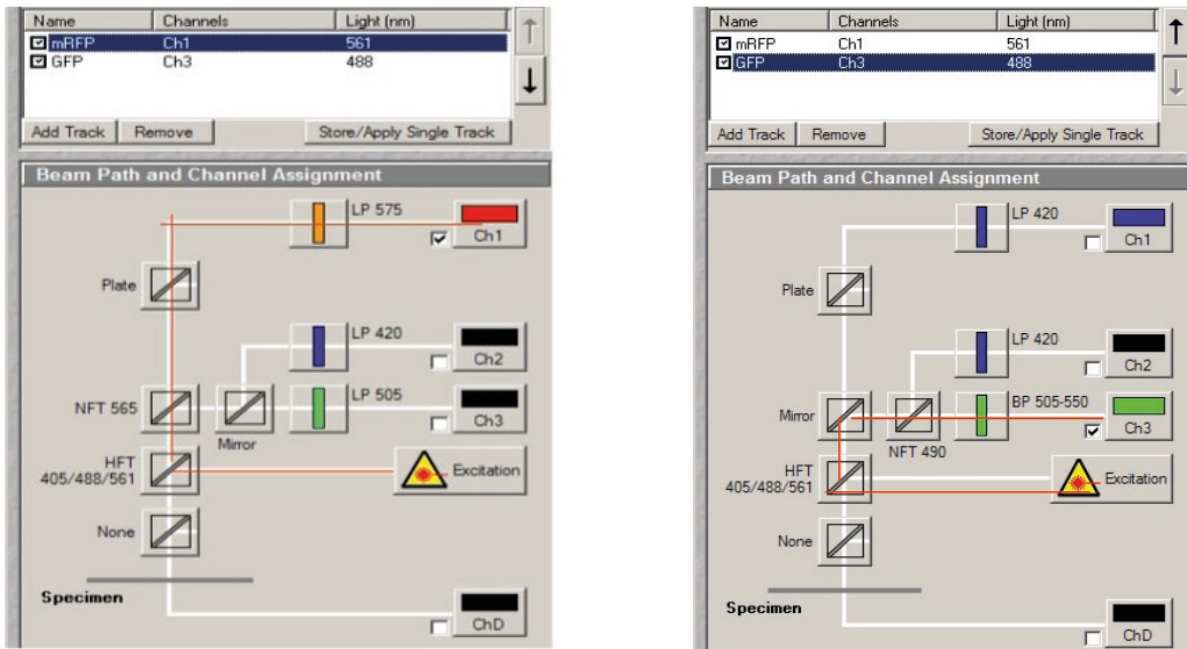
## The Right Way to Scan the Sample



## Apply a Stored Configuration

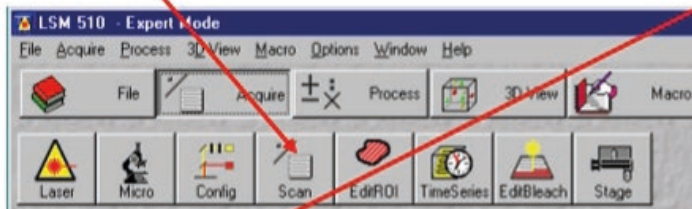
- 1) Select Config
- 2) Select "Multitrack" for sequential scanning
- 3) Select "Config"
- 4) Select the stored config: "FRET GFP/mRFP" and click on "Apply"





### Set the Parameters for Scanning

1) Select Scan

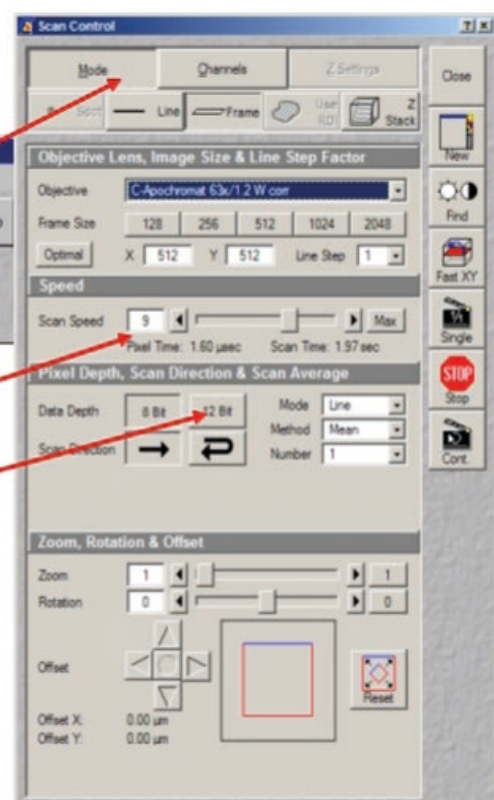


2) Select Mode

3) Select Frame Size as "512x512"

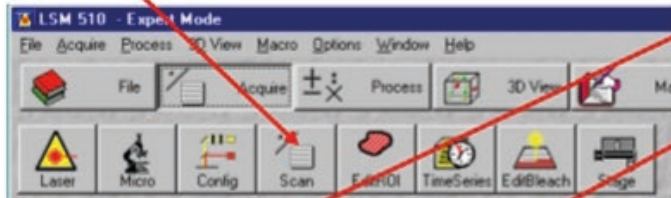
4) Set Scan speed as "9"

5) Choose a bit depth as 12bit.  
Publication quality images should be acquired using 12bits. 12 Bit is also recommended when doing quantitative measurements or when imaging low fluorescence intensities.



### Channel Settings – Adjust the Pinhole

- 1) Select Scan



- 2) Select Channel

- 3) Click on the Red channel and then click "1" (1 Airy Unit)

- 4) Set the 561nm Laser intensity to around 10-11%

- 5) Click on the Green Channel and then click "1" (1 Airy Unit)

- 6) Set the 488nm Laser intensity to around 5-6%

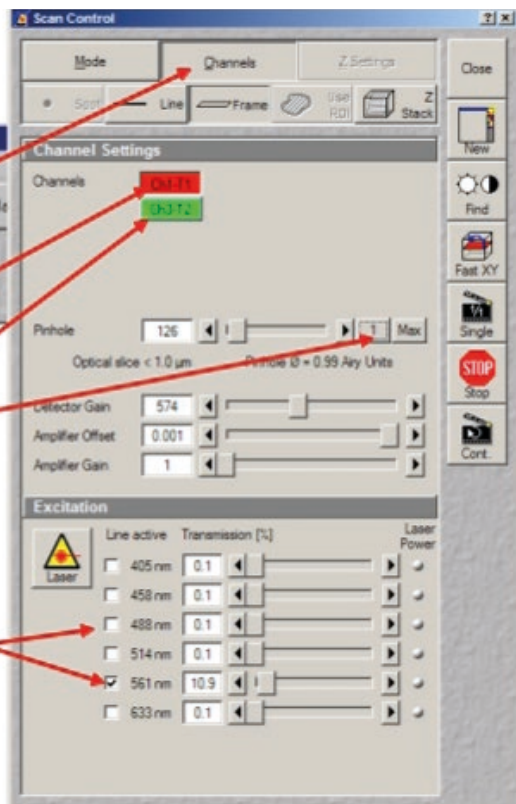


### Image Acquisition – Fast Scanning



- 1) Select "Fast XY" for continuous fast scanning - useful for finding and changing the focus

- 2) "Stop" blanks the laser beam and stops the scanning mirrors. Click on "Stop" after one scan.

- 3) Click on Split XY

- 4) Click on Palette and choose Range indicator

- 5) "Stop" the scanning.

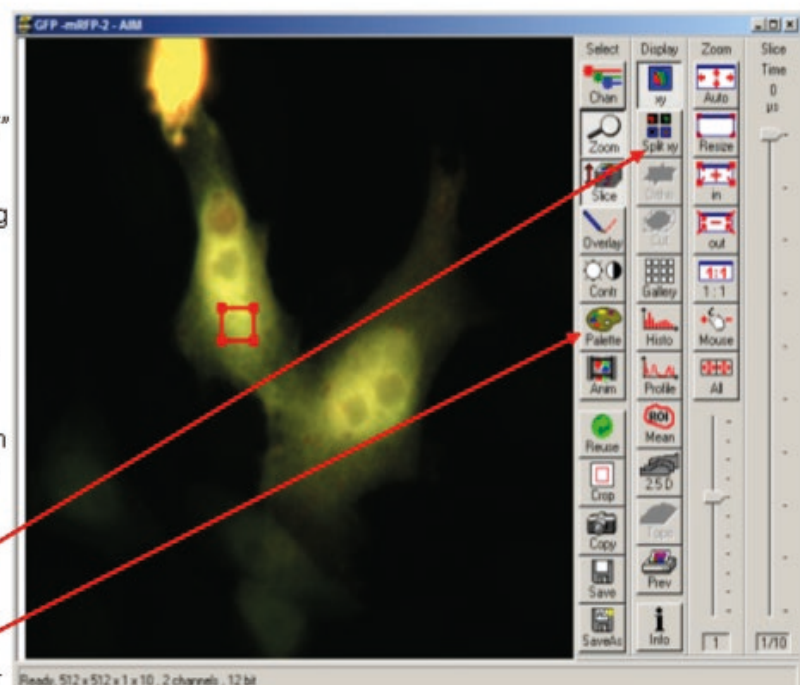


### Image Acquisition – Adjusting Gain and Offset

1) Go back to the config window and untick mRFP. Click on Fast XY again.

2) Adjust the Detector Gain just till you see some red pixels in the image

3) Adjust the Amplifier Offset just till you see some blue pixels in the image. Click "Stop".

4) Now go back to the Config window and untick GFP and tick mRFP

5) Click FastXY and repeat steps 2 and 3.

6) Once this is done tick both the channels in the config window

### Setting up Bleaching Parameters (Acceptor Photobleaching)

1) Select Edit Bleach

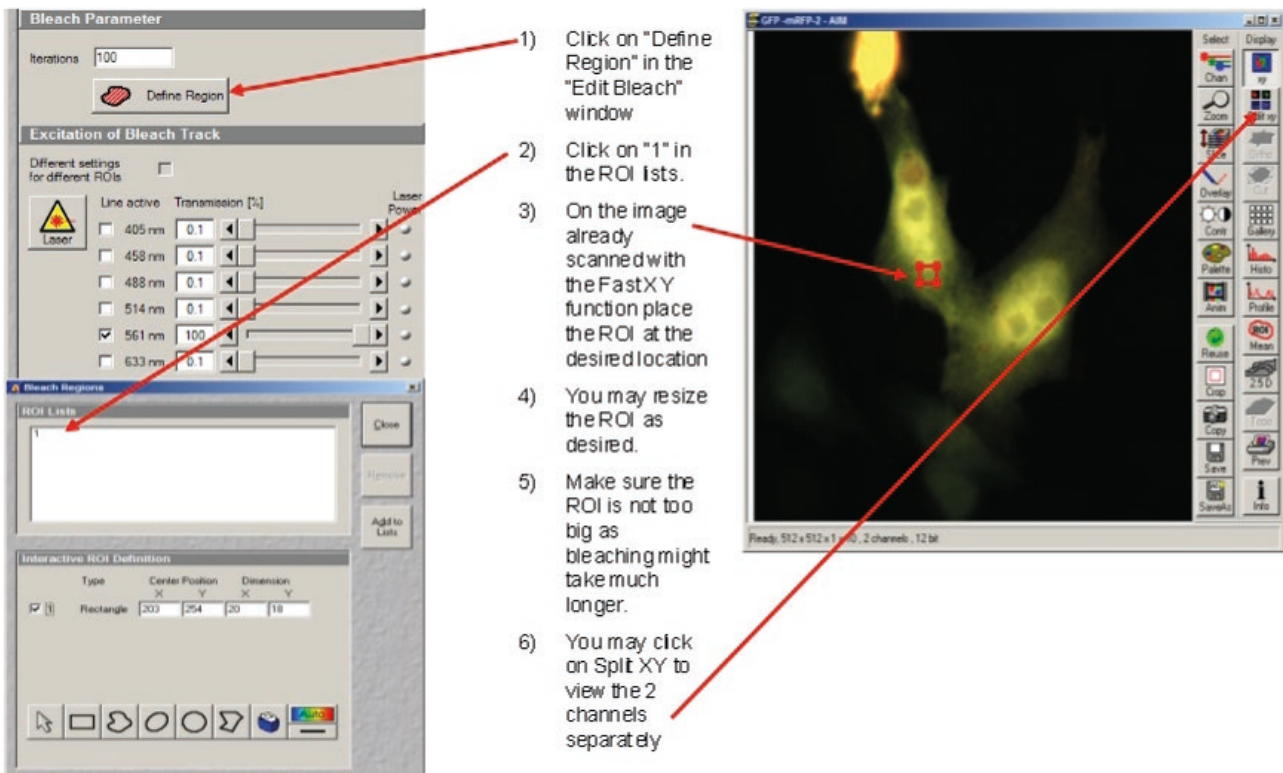
2) Select the setting "FRET GFP/mRFP" and click Apply

3) Select "bleach after number of scans" and type in 2 or 3 for the "Scan Number"

4) Select "Different Scan Speed" and set it to "4"

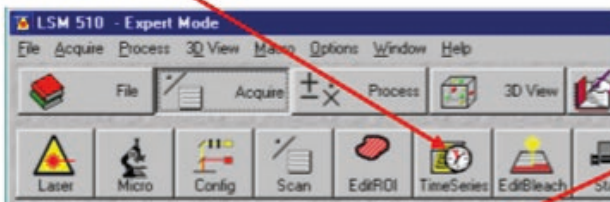
5) Set the 561 nm Laser transmission to 100%.

## Define the ROI for Bleaching

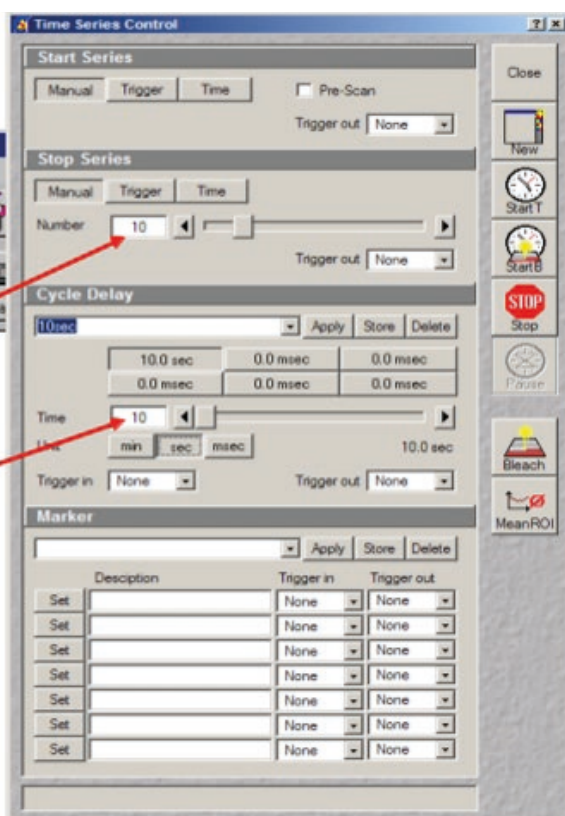


## Set the Time Series to Perform Experiment

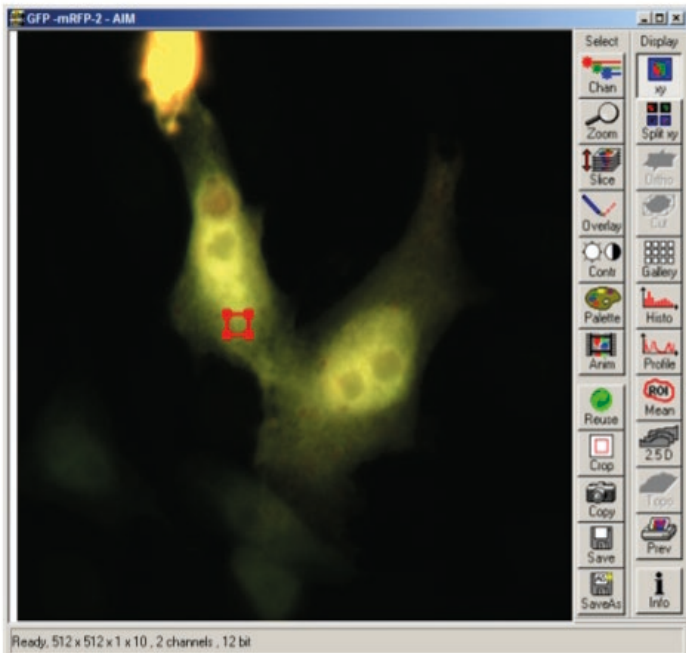
- ### 1) Select Time Series



- 2) We will take a total of 10 images per slide. Hence type in 10 at the Stop series slot.
  - 3) We shall continuously capture images and thus set the cycle delay to 0.
  - 4) Click on "Start B". This will start the time lapse and the bleaching process. Since we set 3 scans before bleaching, we will have 3 images before bleaching and 7 after bleaching.

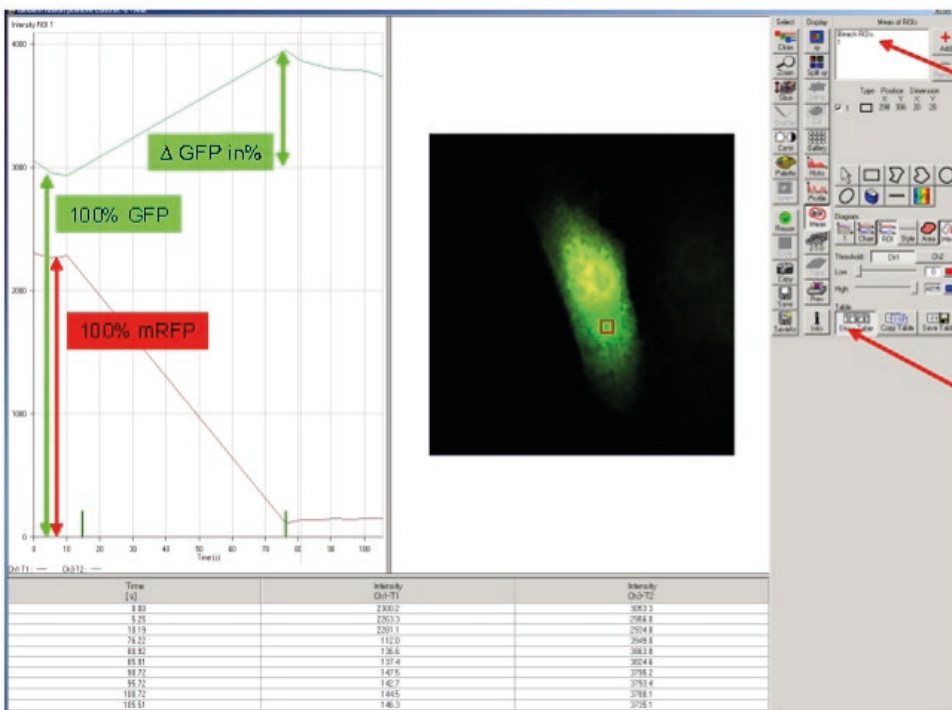


## FRET Result – Mean ROI



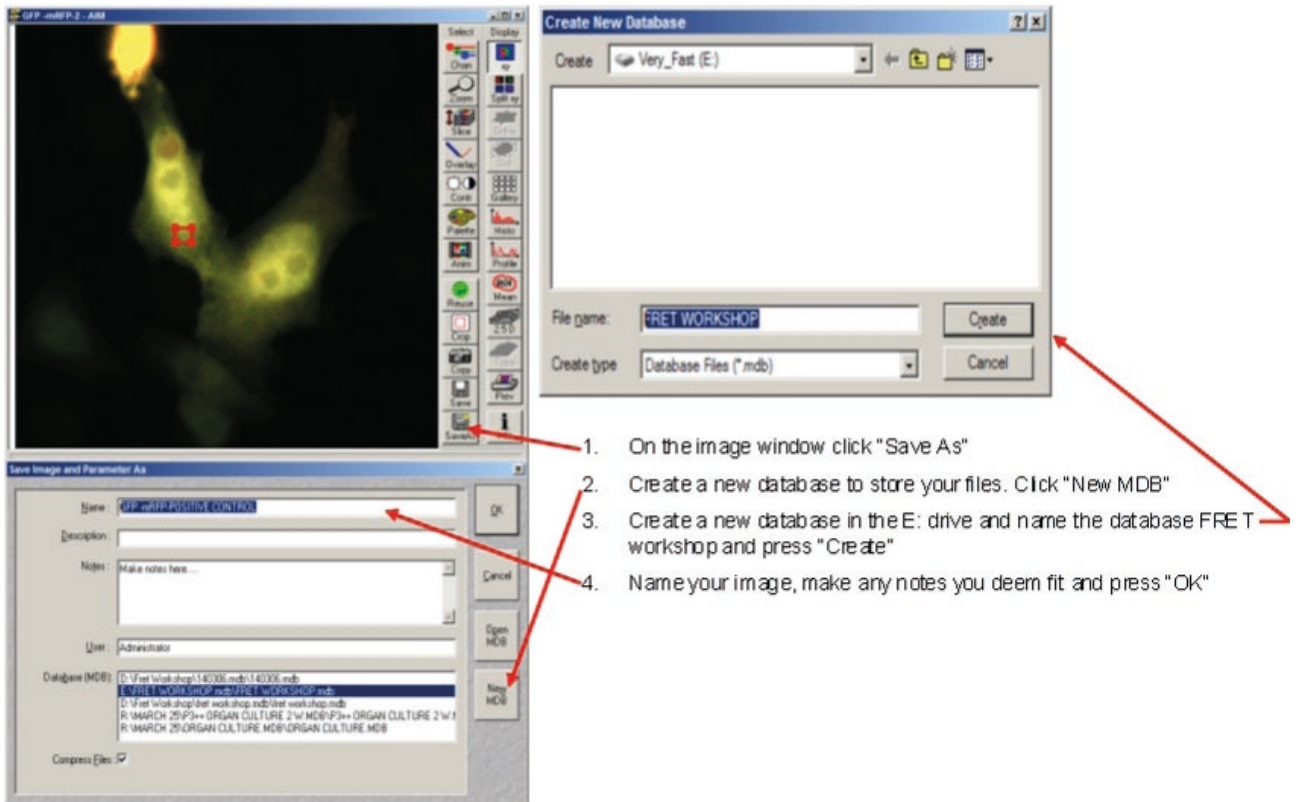
- 1) As the images are being captured, you might want to see how the average intensity of your ROI changes before bleaching and especially after the bleaching of the Acceptor (mRFP) changes. Click on "Mean ROI" in the image window.

## FRET Result – Mean ROI

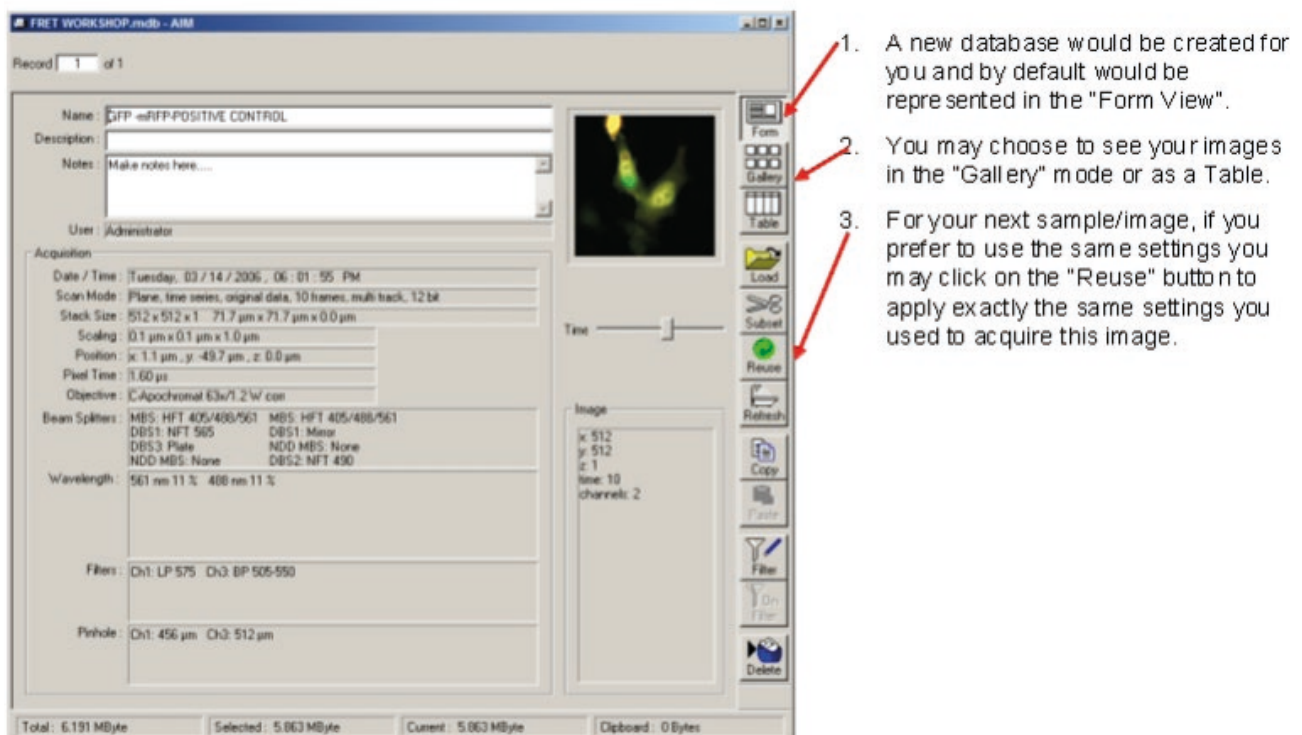


- 1) Click on Bleach ROI to see the ROI you had selected for bleaching.
- 2) The bleaching might take a while.
- 3) At the point bleaching starts note the increase in the intensity of Donor (GFP)
- 4) Click on "Show Table" to see the average intensity of your ROI in numbers.

## Saving Data – Database



## Saving Data – Database – Form View





# Chapter



# **Fluorescence Sensitized Emission FRET (SE-FRET)**

***Thankiah Sudhaharan and Sohail Ahmed***

*Institute of Medical Biology, Singapore*

*Contact details of corresponding author: Thankiah Sudhaharan,  
sudhaharan.thankiah@imb.a-star.edu.sg*

## **Index**

Abstract .....	3
1. Principle and Theory.....	3
Theory of Sensitized Emission (SE).....	4
2. Instrumentation.....	4
3. Methods.....	4
3.1 Materials Required .....	4
3.2 Sample Preparation.....	4
4. Data Acquisition.....	6
5. Data Analysis.....	6
6. Data Verification .....	6
7. Limitations .....	6
8. Conclusion.....	7
References and Further Reading .....	9
Appendix .....	10

## Abstract

Sensitised Emission (SE)-FRET is an fluorescence intensity based method that uses changes in fluorophore spectra to measure FRET. In the FRET scenario donor emission is decreased while acceptor emission is increased. CFP/YPF and GFP/mRFP pairs can be used to generate data with essential control experiments giving background corrections. When background data is subtracted from experimental data the degree of FRET (FRETc) can be determined.

We describe here a filter based setup to perform SE-FRET on a widefield microscope. SE-FRET is useful for measuring rapid changes protein-protein interaction in cells under live conditions where spatial information can also be followed – the classical

example is the measurement of cellular Ca<sup>2+</sup> fluxes. The concentration of CFP (GFP) and YFP (mRFP) in transfected cells needs to be controlled with similar levels of both fluorophores being optimal. The ideal SE-FRET probe is where a single protein contains both CFP/YFP or mRFP/GFP thereby bypassing the requirement for controlling individual protein concentrations.

## 1. Principle and Theory

Here we use the GFP/mRFP pair. When there is no protein-protein interaction between GFP/mRFP fusion protein pairs, FRET is not observed, and donor (GFP) excitation does not lead to excitation of the acceptor (mRFP). In contrast, when there is protein-protein interaction, FRET is observed, and

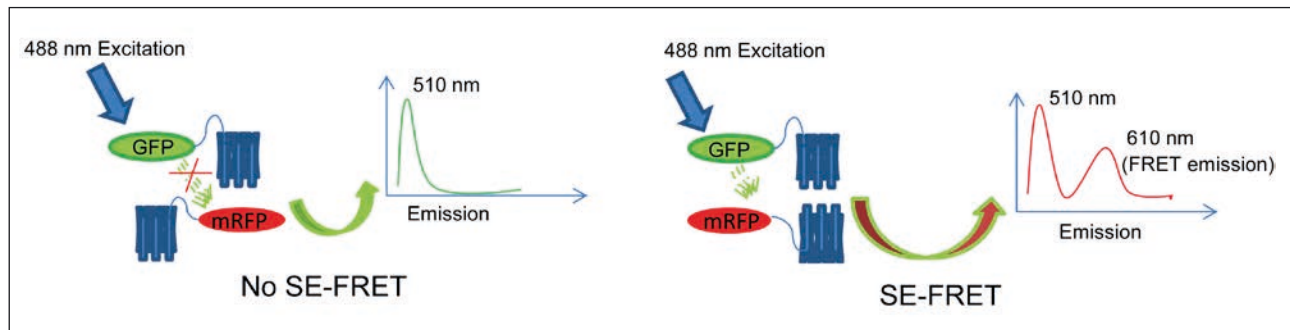


**Figure 1** Shown is the schematic representation of SE-FRET occurrence.

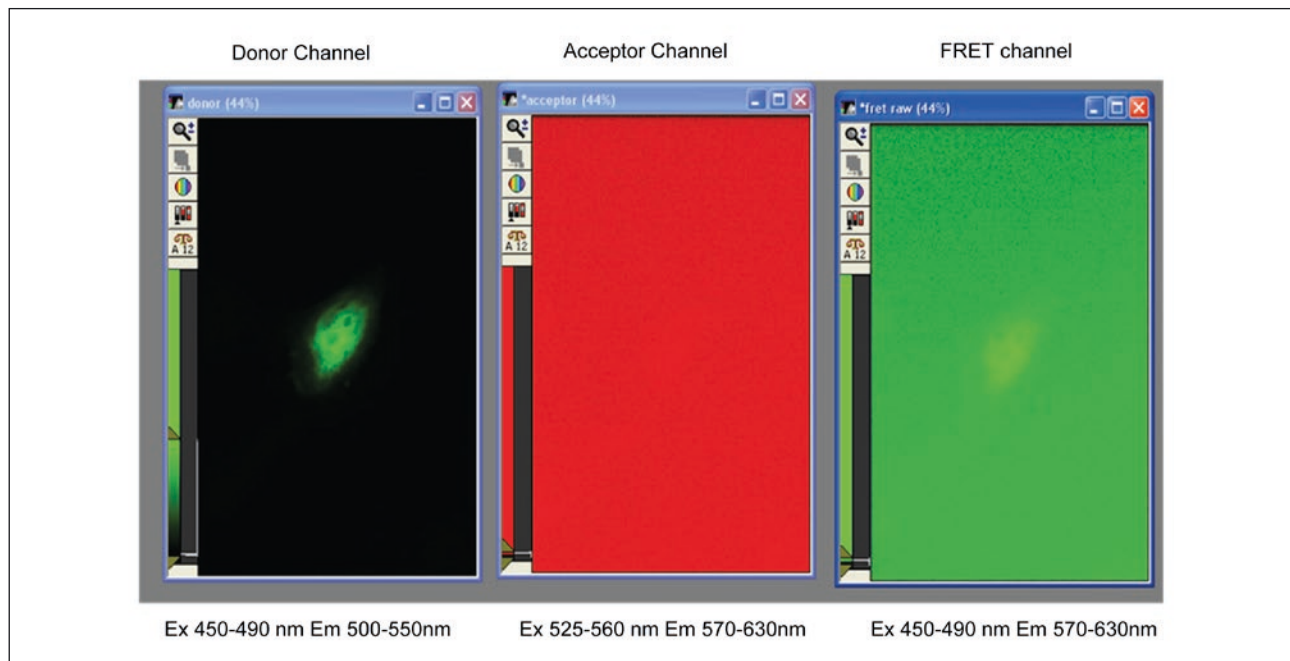


**Figure 2** Shown is the image representation of donor channel emission and its cross-talk in FRET channel (Cross-talk coefficient  $B = 0.087$ ) of donor alone (GFP) sample during donor excitation.

the excitation of the donor leads to excitation of the acceptor. In the FRET scenario the donor emission is decreased and the acceptor emission is increased (Figure 1).

### Theory of Sensitized Emission (SE)

SE-FRET is an fluorescence intensity based method where in widefield implementation filters are used to separate donor/acceptor (GFP/mRFP signals). In SE-FRET the fluorescence emission of the acceptor (mRFP) that results from the radiatiolness energy transfer from an excited donor (GFP) is measured. Thus controls are critically important to correct data for; (i) Cross talk between donor to acceptor channels and (ii) Direct excitation of acceptor when donor is being excited (Figures 2 and 3). For controls, four samples are analysed. GFP (donor only), mRFP (acceptor only) and a pair of fusions which do not interact as a negative control. For the fourth sample, the positive control, we use of a tandem GFP-mRFP fusion protein.

A range of mathematical equations have be used to analyse SE-FRET data. We use here Youvan's method (equation 1; see Data analysis in section 5). Two coefficients, A and B, need to be determined. The coefficient B ( $F_d/D_d$ ) is measured with donor (GFP) only (Figure 2) and represents the ratio of the signal obtained ( $F_d$ ) in the FRET channel over the signal obtained in the donor ( $D_d$ ) channel (Figure 2). The coefficient A ( $F_a/A_a$ ) is measured with acceptor (mRFP) only (Figure 3) and is the ratio of the signal

obtained in the FRET channel ( $F_a$ ) over the signal obtained in the acceptor channel ( $A_a$ ; Figure 3). Both A and B coefficients are constant for any one set of experimental conditions.

## 2. Instrumentation

Here we use a dual view set-up on an Olympus widefield microscope with a 60x oil with appropriate GFP and mRFP excitation/emission filters and corresponding dichroic mirrors; a Xenon lamp for excitation, a CCD camera as detector and Metamorph software for image acquisition.

## 3. Methods

### 3.1 Materials Required

Any mammalian cell line of interest could be used. We chose here CHO-1 cells as they are easy to transfect and culture in 37°C CO<sub>2</sub> incubators. Fetal bovine serum (FBS), Antibiotics (penicillin and streptomycin), Trypsin, cDNA encoding GFP and mRFP acceptor and donor pairs, F-12K nutrient mixture [Kaighn's modification] media and transfection reagent (Turbofect). Glass bottom Matek dishes.

### 3.2 Sample Preparation

1. CHO-1 cells were grown in a 75 cm<sup>2</sup> tissue culture flask up to 90% confluence in the complete growth media (1 x F-12 nutrient mixture [Kaighn's

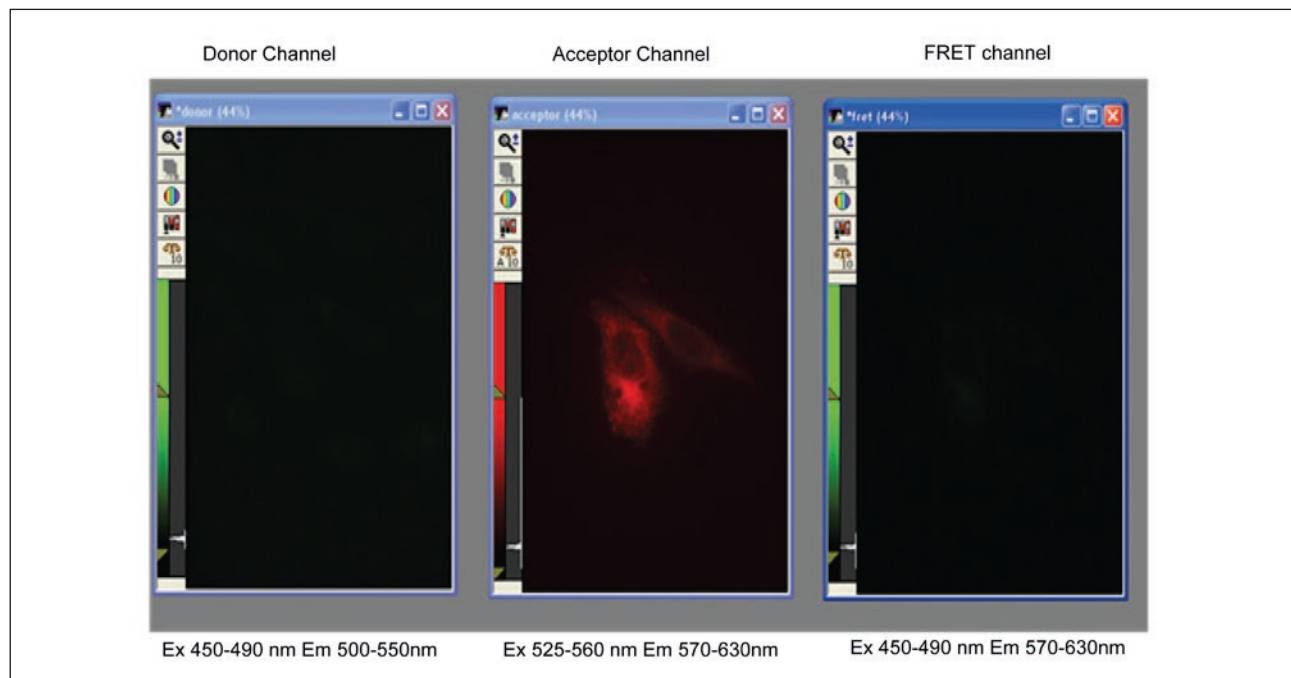


**Figure 3** Shown is the image representation of acceptor channel emission and its cross-talk in FRET channel (cross-talk coefficient  $A = 0.043$ ) of acceptor only (mRFP) sample during acceptor excitation.

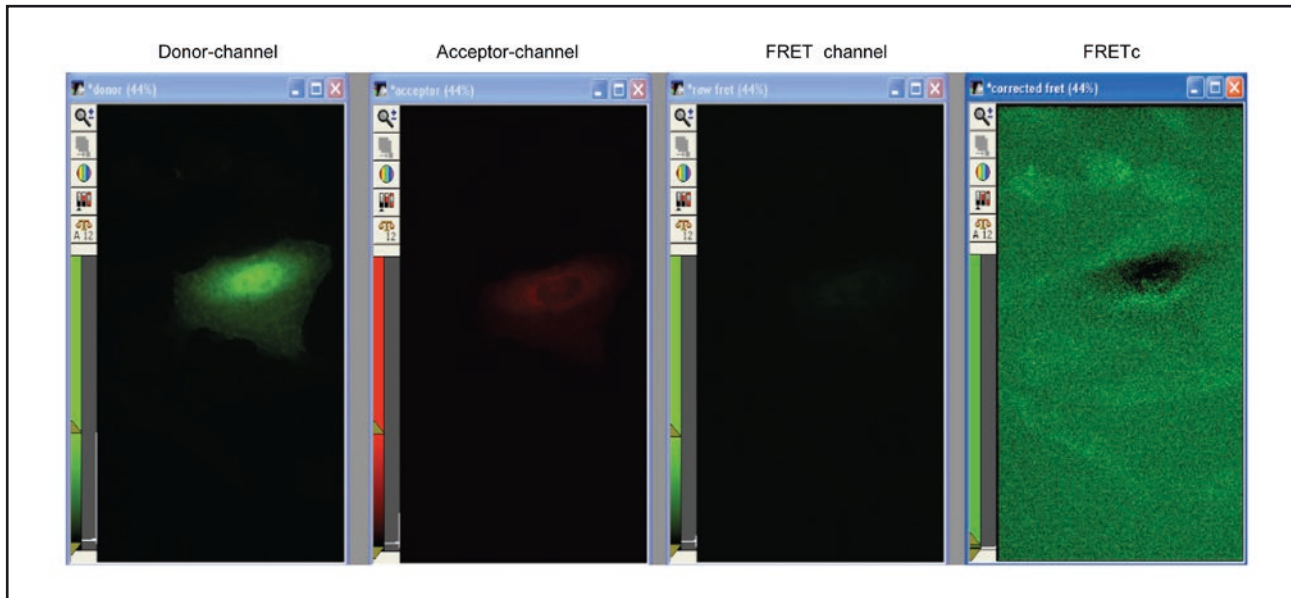


**Figure 4** A negative FRET control sample [GFP-NWASP and mRFP-Toca (non-interacting mutant)] expressed in CHO-1 cells upon 488 nm excitation during FRET measurement. FRETc image was obtained by performing the cross-talk correction on FRET channel image.

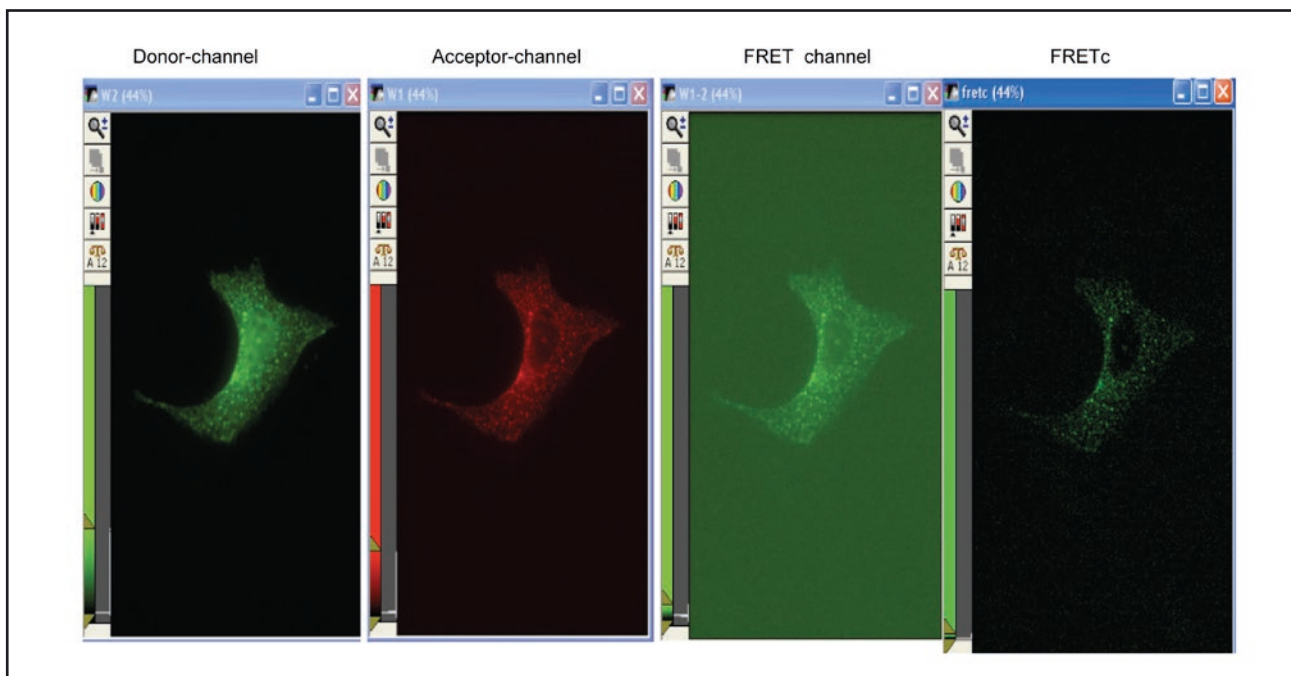


**Figure 5** Shown is the CHO-1 cell expressing positive control (GFP-mRFP) tandem fusion image in donor, acceptor and FRET channel respectively obtained using 488 nm excitation. FRETc image was obtained by performing the cross-talk correction on FRET channel image.

- modification] media) containing 10% FBS and 1% antibiotics [penicillin and streptomycin].
2. Cells were detached from the flask, using 2 ml trypsin and incubating at 37°C for 5 min. Cells were counted using a hemacytometer.
  3. For transfection, cells were seeded with a cell density of  $1.5 \times 10^4$  cells in a tissue culture Matek glass bottom dish and left for 24 hours.
  4. CHO-1 cells were transfected using Turbofect transient transfection reagent as per the following protocol; Mix 3  $\mu$ l of Turbofect with 1.5  $\mu$ g of plasmid (1:2 (w/v), DNA/Turbofect) and 150  $\mu$ l of serum free media in a tube and allow it to stand for 25 min at room temperature. Transfection mixes of different plasmids were transferred into different wells of a 6 well plate containing

cells. The transfected cells in 6 well plates were incubated in 37°C for 24 hours to allow protein expression to occur. Typically 5 transfections were carried out in parallel:

- a) GFP-mRFP tandem fusion (positive control)
  - b) Experimental sample (coexpression of mRFP-Toca + GFP-NWASP). Protein pairs that are known to interact be independent methods.
  - c) Coexpression of mRFP-Toca (mutant) + GFP-NWASP (negative control)
  - d) GFP alone expressing sample and
  - e) mRFP alone expressing sample.
5. On the day of fluorescence measurements, cells were harvested and rinsed 2 times with PBS containing 2.0 ml of Hank's Balanced salt media (Gibco).

## 4. Data Acquisition

Switch on microscope Olympus IX81 live cell system and accessories and allow microscope to warm up (Screen shot prints are given in Appendix). Briefly, the following four steps were used to collect images.

- (i) Switch-on the microscope. Switch on the microscope with dual view setup and start Metamorph software. Create a new folder to save image data in order to carry out the experiment.
- (ii) Select an objective and focus the microscope. Select 60X oil objective and focusing the sample open software window. To focus the sample use white light then look for cells having fluorescence signal using Xenon lamp.
- (iii) Configure the software for acquisition and calculating crosstalk coefficients A and B
- (iv) Capture FRET images for data analysis.

## 5. Data Analysis

After determining the coefficients A and B, equation 1 is used to determine FRET and is called FRETc for corrected data.

$$Fc = Ff - \left[ \frac{Fd}{Dd} \cdot Df \right] - \left[ \frac{Fa}{Aa} \cdot Af \right] \quad (1)$$

This data analysis protocol has been automated in the Metamorph FRET module.

## 6. Data Verification

It is important to use negative and positive controls in the experiments to eliminate possible artifacts.

For negative control we use GFP and mRFP fusion protein pairs that we know do no interact. For the positive control we use a tandem GFP-mRFP fusion that will give maximum FRET.

To validate the data obtained with the widefield protocol the samples can be analysed using spectral imaging on a confocal microscope. In the present case an FV1000 Olympus microscope was used. The data was collected in the lambda scan mode by exciting the FRET (tandem fusion GFP-mRFP) sample with donor excitation (GFP, 488 laser line). The emission was scanned through by adjusting the filter range in the lambda mode from 475-675 nm. Basically the emission scan covers the donor emission (490-550nm) along with FRET emission (575-675 nm) using single donor excitation. Figure 6 shows a typical example of spectral imaging data of FRET sample obtained in the region of interest (ROI) in lambda scan mode. The GFP-mRFP expressing cell used for spectral imaging before and after acceptor photobleaching is shown in figure 6 (a). The spectral data in the ROI of the cell which is subjected to pre and post acceptor photobleach (using 559 nm laser line) to abolish FRET in the ROI is shown in figure 6 (b and c, respectively). From the data it can be observed that the FRET emission peak seen in the ROI of GFP-mRFP sample is lost upon photobleaching the acceptor, simultaneously the donor (GFP) intensity increased due to de-quenching effect of acceptor bleaching (Figure 6b and c).

## 7. Limitations

SE-FRET is an indirect method to measure FRET. In SE-FRET images and data need to be corrected and analysed before the presence or absence of FRET can be determined. Critically important in the SE-FRET method described here is to look for cells that have similar levels of donor and acceptor protein concentration. The SE-FRET experiments can be optimised by insuring the expression levels of donor and acceptor are similar to endogenous levels. Also one should check that protein localization of the GFP/mRFP fusion proteins is similar to that found for the endogenous protein. If protein concentration of the fusion protein pairs are different then protein concentration normalisation can be carried, However, this approach is not preferred. Normalisation can be achieved by determining A and B coefficients with protein concentrations of donor and acceptor as for the experimental condition. In SE-FRET specific controls should be considered in advance and are essential for assessing the presence or absence of protein-protein interactions. With regard to controls, point mutants of fusion proteins that do not change

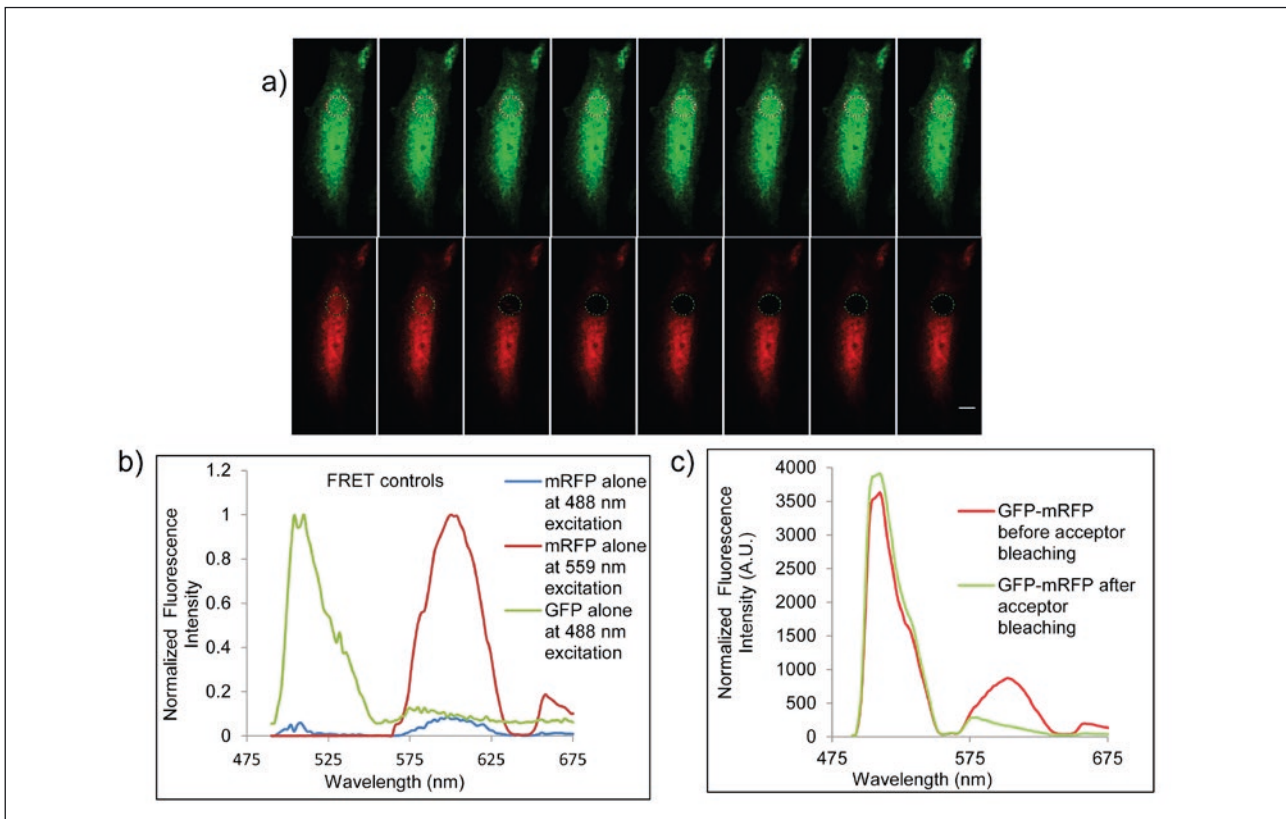


**Figure 6** Shown is the spectral imaging (SE-FRET) mode data (a) positive control sample (GFP-mRFP) tandem fusion expressed in CHO-1 cells image in donor and acceptor channel respectively upon 488 nm excitation. The ROI was photo bleached using 561 nm laser and used for spectral image FRET measurement. (b) Spectral image measurement data from control cells. (c) Spectral image measurement data of (a) before and after acceptor bleaching.

the overall size or structure but affect protein-protein interaction, are powerful negative controls.

## 8. Conclusion

Controls and validation in SE-FRET are key for obtaining accurate data. The SE-FRET allows event occurring in the msec range to be followed with good spatial resolution (see range of uses for SE-FRET in Table 1). Thus SE-FRET is the FRET method of choice for monitoring rapid events in live cells.

**Table 1** Table describing the publication list of SE-FRET method applications used in cells with various fluorescent proteins FRET pairs.

Application	FRET-PAIR	References
Reviews on Sensitized emission FRET		(Padilla-Parra and Tramier, 2012) <sup>[1]</sup> (Periasamy et al, 2008) <sup>[2]</sup> (Miyawaki, 2011) <sup>[3]</sup> (Jares-Erijman and Jovin, 2003) <sup>[4]</sup>
<b>Selected Recent Applications</b>		
Observing distinct micro domains	mCFP-mCitrine	(Abankwa and Vogel, 2007) <sup>[5]</sup>
FRET efficiency measurement in live cells	CFP-YFP	(Chen et al, 2006) <sup>[6]</sup>
Homo- and heterodimerization of two human peroxisomal ABC transporters	CFP-YFP	(Hillebrand et al, 2007) <sup>[7]</sup>
Structure and localization of functional neurokinin-1 receptors	CY3-CY5	(Meyer et al, 2006) <sup>[8]</sup>
Homodimerization and internalization of galanin type 1 receptor	CFP-YFP	(Wirz et al, 2005) <sup>[9]</sup>
Role of calmodulin in MAPK signaling	CFP-YFP	(Moreto et al, 2009) <sup>[10]</sup>
Serotonin transporter oligomerization documented in RN46A cells and neurons	GFP-mCherry	(Fjorback et al, 2009) <sup>[11]</sup>
Dynamic but not constitutive association of calmodulin with rat TRPV6 channels	CFP-YFP	(Derler et al, 2006) <sup>[12]</sup>
AKAP79-mediated targeting of the cyclic AMP-dependent protein kinase	CFP-YFP	(Gardner et al, 2006) <sup>[13]</sup>
Identification of plasma membrane macro- and microdomains	CFP-YFP	(Kobrinsky et al, 2005) <sup>[14]</sup>
Investigation of the dimerization of proteins from the epidermal growth factor receptor family	CFP-YFP	(Liu et al, 2007) <sup>[15]</sup>

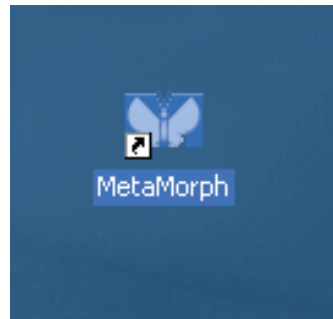
## References and Further Reading

- [1] Padilla-Parra, G. and Traimer, M. FRET microscopy in the living cells: Different approaches, strengths and weaknesses: *Bioessays*, 34, 2012,369-376.
- [2] Periasamy,A., Wallrabe, H., Chen, Y. and Barroso,M. Quantitation of Protein-protein interaction interactions: Confocal FRET Microcopy. *Methods in Cell biology*,89,2008,569-598.
- [3] Miyawaki. A. Development of probes for cellular functions using fluorescent proteins and fluorescence energy transfer: *Annu.Rev.Biochem*, 80, 2011,31.1-31.17.
- [4] Jares-Erijman, E.A. and Jovin,T.M. FRET imaging, *Nature Biotechnology*,21,2003,1387-1395.
- [5] Abankwa, D., and Vogel, H., 2007, A FRET map of membrane anchors suggests distinct microdomains of heterotrimeric G proteins: *J Cell Sci*, 120, 2953-62.
- [6] Chen, H., Puhl, H. L., 3rd, Koushik, S. V., Vogel, S. S., and Ikeda, S. R., 2006, Measurement of FRET efficiency and ratio of donor to acceptor concentration in living cells: *Biophys J*, 91, L39-41.
- [7] Hillebrand, M., Verrier, S. E., Ohlenbusch, A., Schafer, A., Soling, H. D., Wouters, F. S., and Gartner, J., 2007, Live cell FRET microscopy: homo- and heterodimerization of two human peroxisomal ABC transporters, the adrenoleukodystrophy protein (ALDP, ABCD1) and PMP70 (ABCD3): *J Biol Chem*, 282, 26997-7005.
- [8] Meyer, B. H., Segura, J. M., Martinez, K. L., Hovius, R., George, N., Johnsson, K., and Vogel, H., 2006, FRET imaging reveals that functional neurokinin-1 receptors are monomeric and reside in membrane microdomains of live cells: *Proc Natl Acad Sci U S A*, 103, 2138-43.
- [9] Wirz, S. A., Davis, C. N., Lu, X., Zal, T., and Bartfai, T., 2005, Homodimerization and internalization of galanin type 1 receptor in living CHO cells: *Neuropeptides*, 39, 535-46.
- [10] Moreto, J., Vidal-Quadras, M., Pol, A., Santos, E., Grewal, T., Enrich, C., and Tebar, F., 2009, Differential involvement of H- and K-Ras in Raf-1 activation determines the role of calmodulin in MAPK signaling: *Cell Signal*, 21, 1827-36.
- [11] Fjorback, A. W., Pla, P., Muller, H. K., Wiborg, O., Saudou, F., and Nyengaard, J. R., 2009, Serotonin transporter oligomerization documented in RN46A cells and neurons by sensitized acceptor emission FRET and fluorescence lifetime imaging microscopy: *Biochem Biophys Res Commun*, 380, 724-8.
- [12] Derler, I., Hofbauer, M., Kahr, H., Fritsch, R., Muik, M., Kepplinger, K., Hack, M. E., Moritz, S., Schindl, R., Groschner, K., and Romanin, C., 2006, Dynamic but not constitutive association of calmodulin with rat TRPV6 channels enables fine tuning of Ca<sup>2+</sup>-dependent inactivation: *J Physiol*, 577, 31-44.
- [13] Gardner, L. A., Tavalin, S. J., Goehring, A. S., Scott, J. D., and Bahouth, S. W., 2006, AKAP79-mediated targeting of the cyclic AMP-dependent protein kinase to the beta1-adrenergic receptor promotes recycling and functional resensitization of the receptor: *J Biol Chem*, 281,33537-53.
- [14] Koprinsky, E., Mager, D. E., Bentil, S. A., Murata, S., Abernethy, D. R., and Soldatov, N. M., 2005, Identification of plasma membrane macro- and microdomains from wavelet analysis of FRET microscopy: *Biophys J*, 88, 3625-34.
- [15] Liu, P., Sudhaharan, T., Koh, R. M., Hwang, L. C., Ahmed, S., Maruyama, I. N., and Wohland, T., 2007, Investigation of the dimerization of proteins from the epidermal growth factor receptor family by single wavelength fluorescence cross-correlation spectroscopy: *Biophys J*, 93, 684-98.

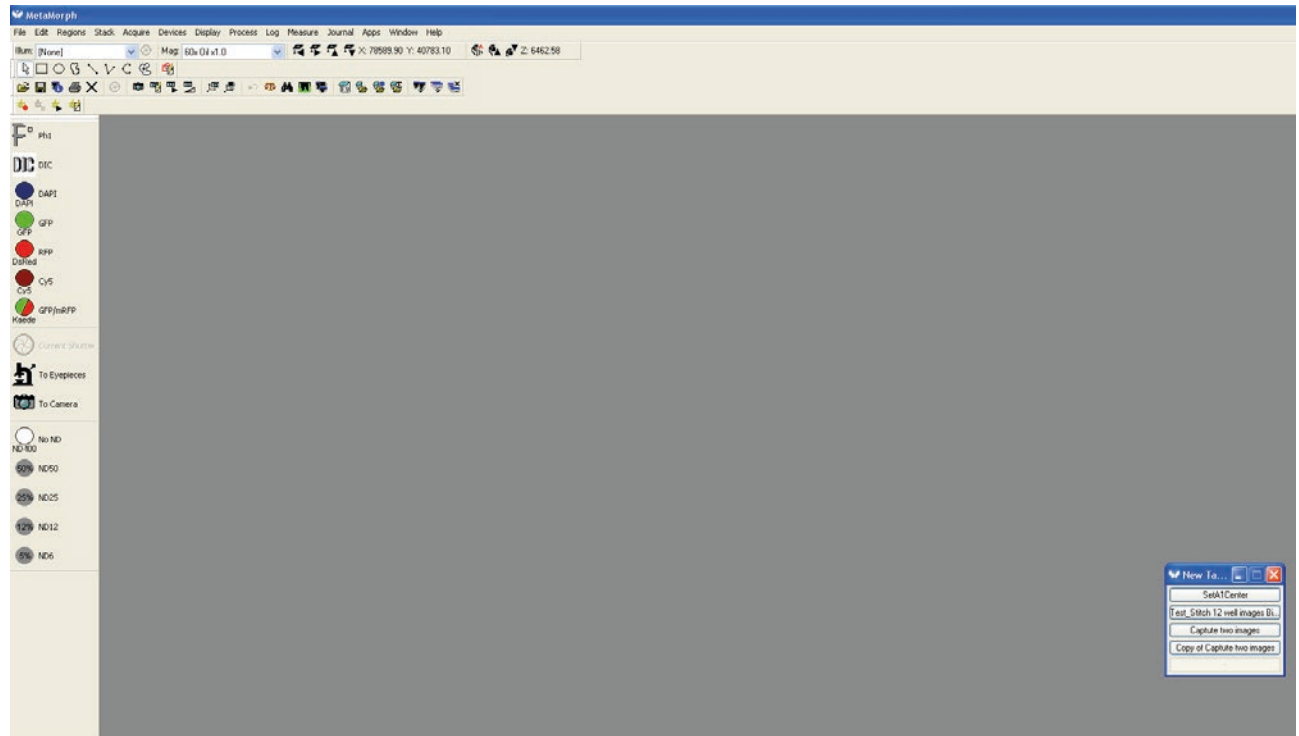
## Appendix

### Image Acquisition Using Metamorph

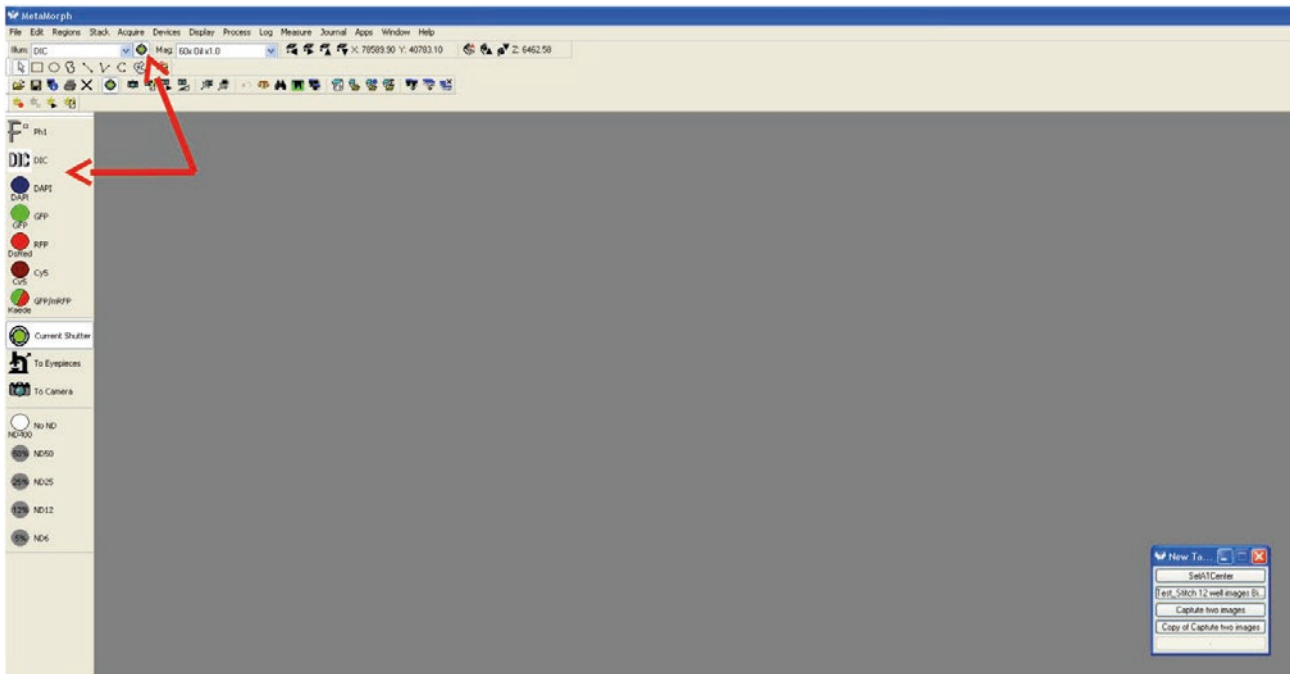
→ Click on Metamorph software



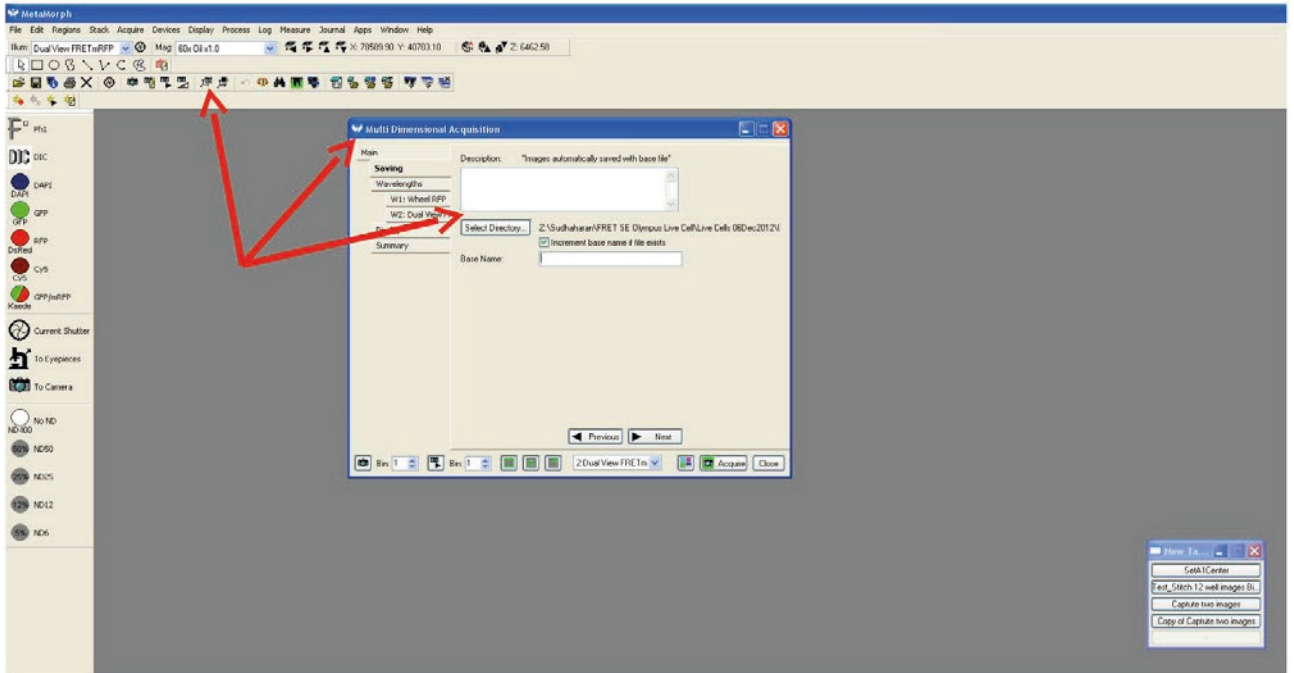
→ Metamorph opens with the following window



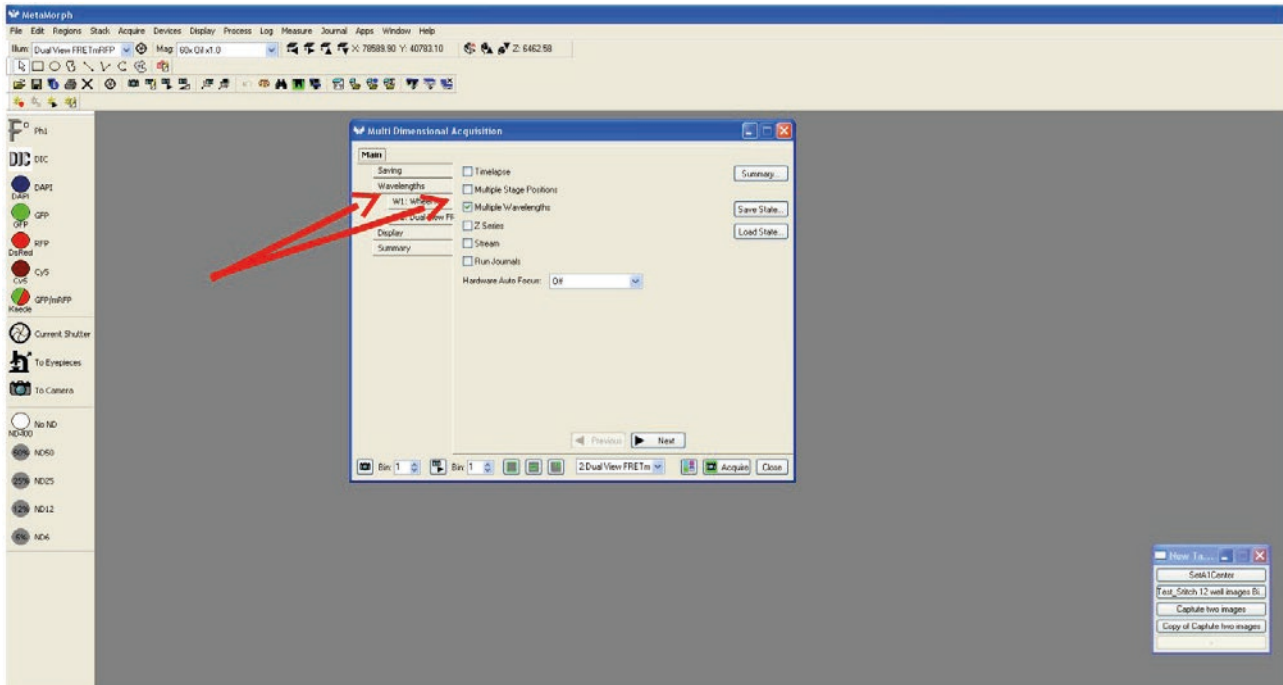
→ Click on DIC and shutter to open to view the cells through eyepiece



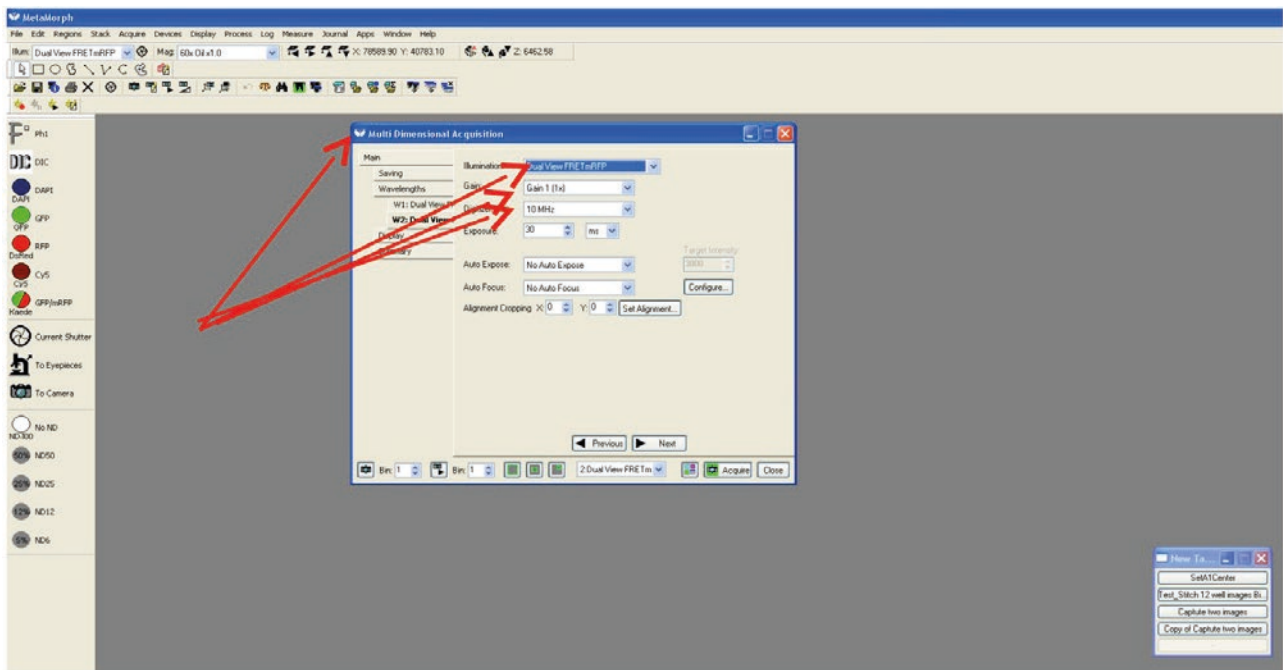
- Click on Multidimensional button
- The window opens up a new page
- In the new window create a folder to save images by clicking select directory



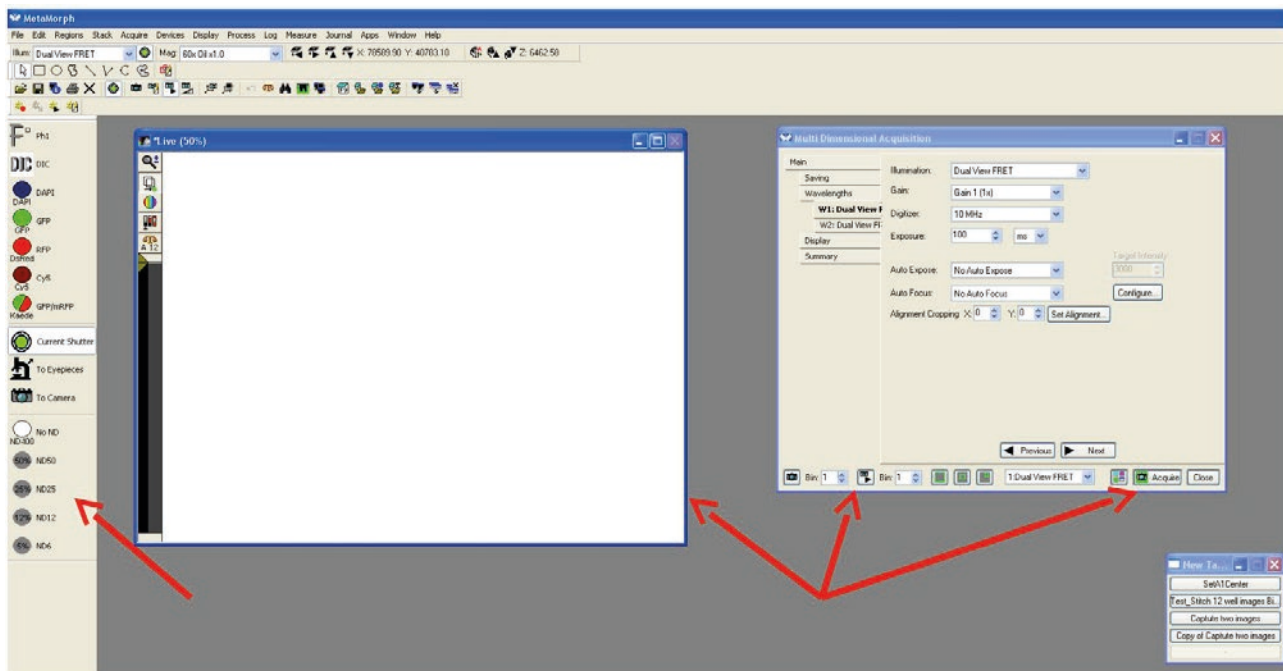
→ Click on wavelength and multiple wavelengths to select different channels



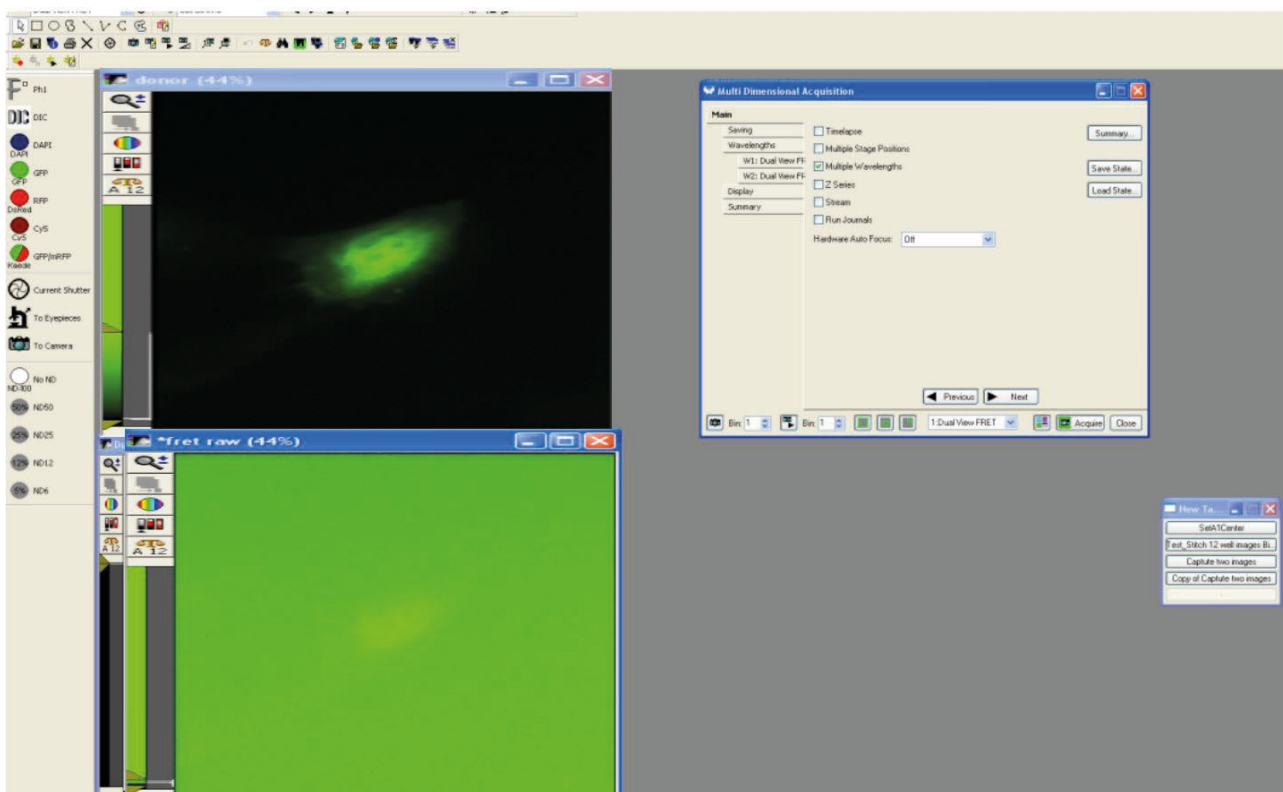
- Now select the required wavelengths using illumination button
- Keep the Gain at 1 and Digitizer at 10 MHz
- Adjust the exposure time to the desired levels



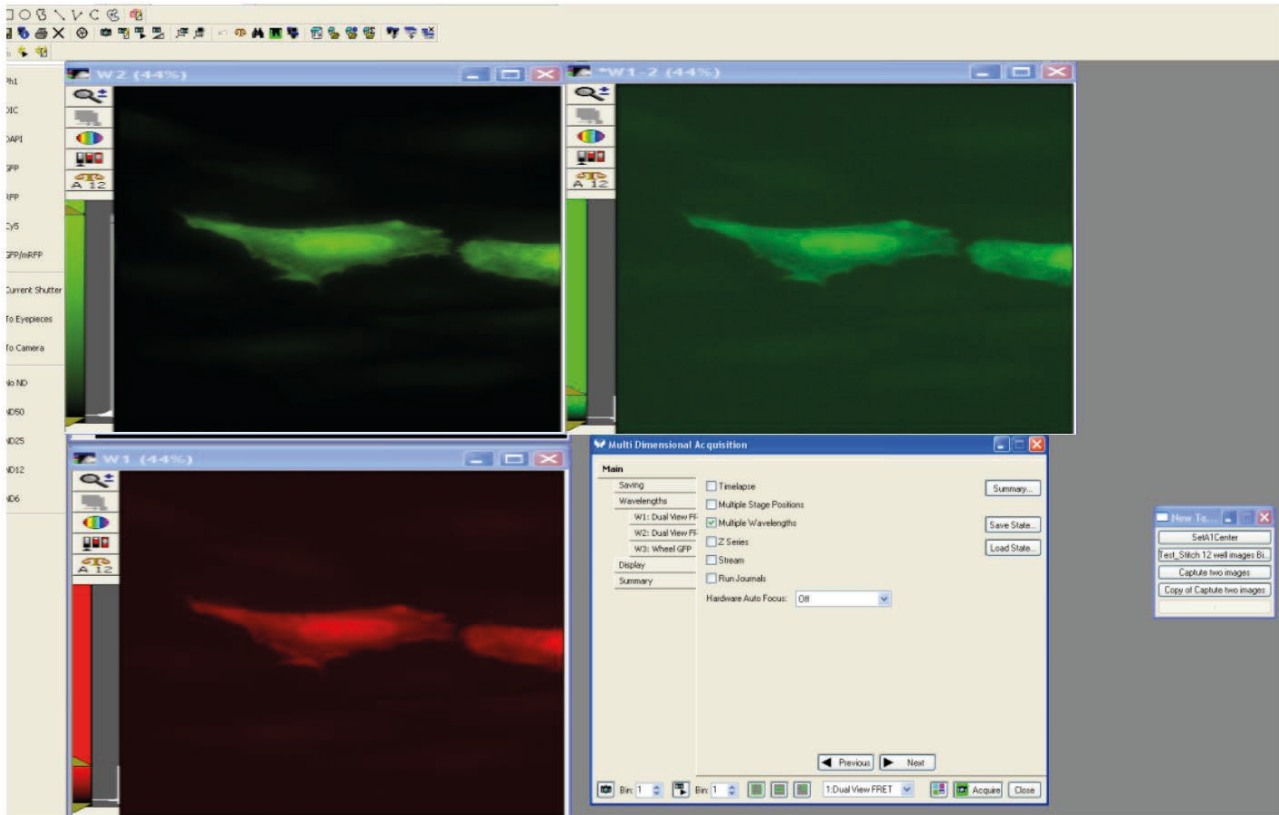
- Click on live to open a new window for selecting right cells for imaging
- Also select the required ND filter to reduce bleaching while imaging



- The following window shows two channel image collected for crosstalk correction of GFP
- Repeat the same for RFP correction factor using RFP wavelength

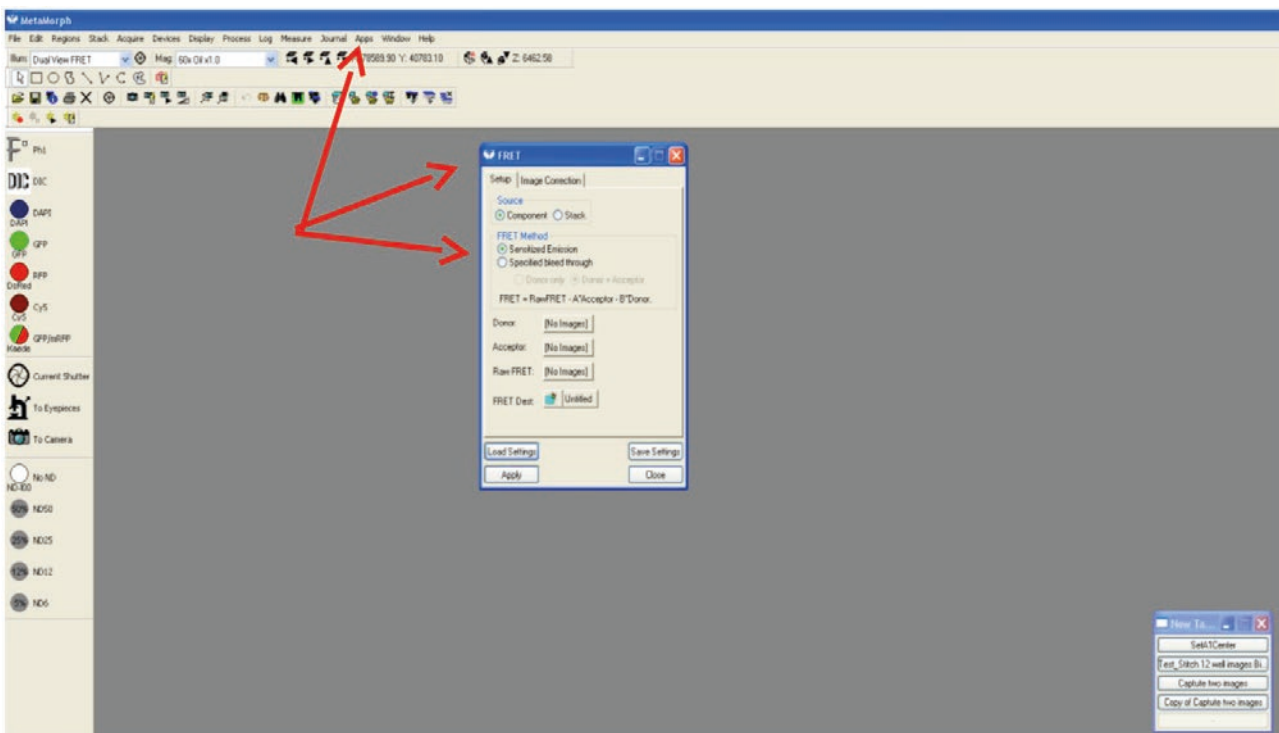


→ Finally select acquire to get three channel image for experimental sample to perform corrected FRET

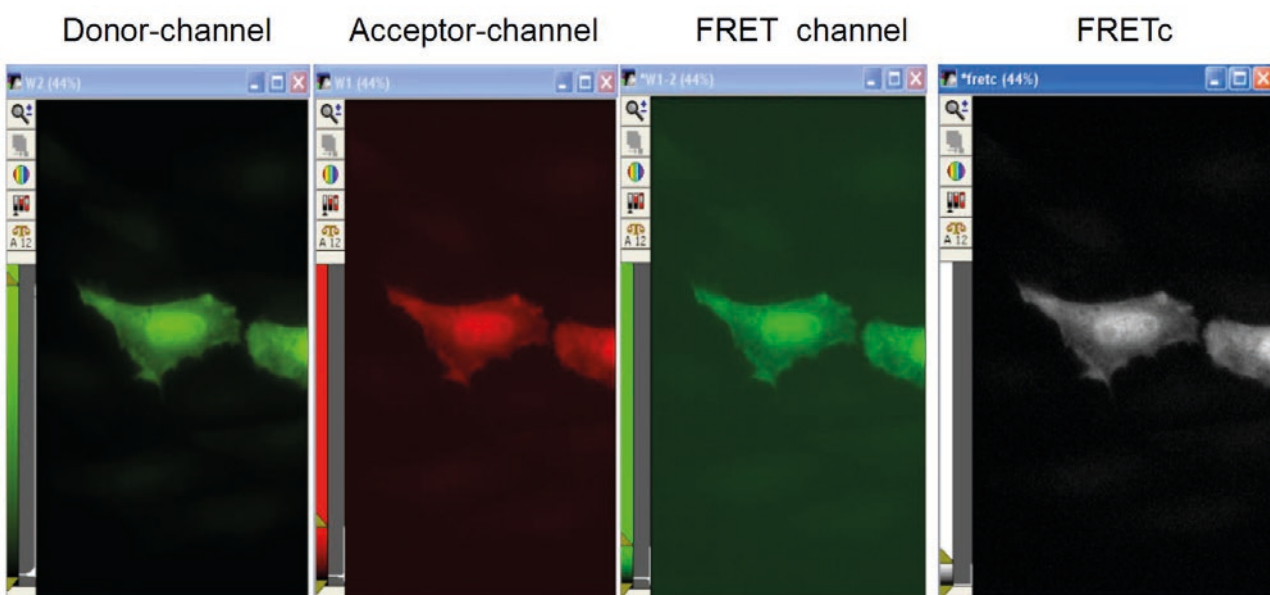
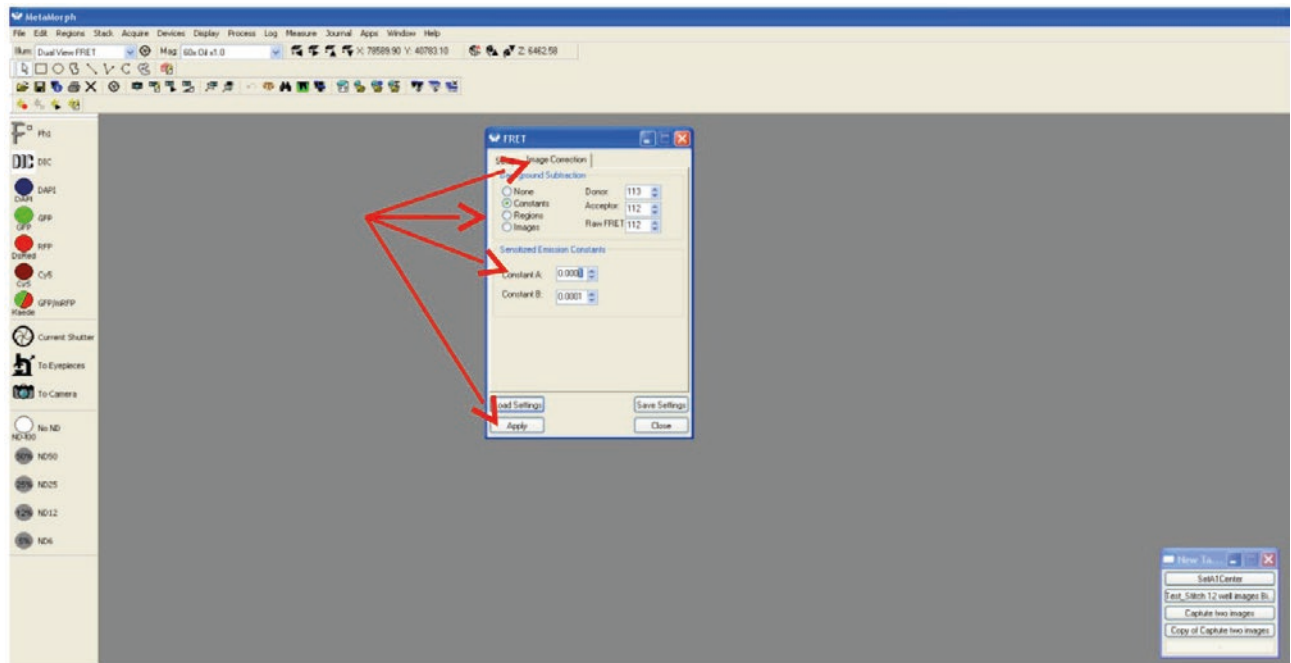


→ The collected images could be used for obtain FRETc

→ Click on Apps and select FRET from Metamorph software and select sensitized emission method



- Feed in the correction factor coefficient values by selecting image correction button in FRET window  
 → Draw a ROI outside the image and select regions in background subtraction and click apply to get FRETc





# Chapter 3

# Frequency-domain Fluorescence Lifetime Imaging Microscopy (FD-FLIM)

*Andrew H.A. Clayton*

*Centre for Micro-Photonics, Faculty of Science,  
Engineering and Technology, Swinburne University of Technology,  
Hawthorn, Victoria, Australia*

## Index

1. Principle and Theory.....	3
How is the Fluorescence Waveform Detected? .....	4
2. Instrumentation.....	4
Light Sources .....	5
Detectors .....	5
Microscope .....	5
Software .....	6
3. Method.....	8
Sample: General Considerations .....	8
Sample: Specific Examples.....	8
4. Image Acquisition .....	9
5. Data Analysis.....	9
Histogram Analysis of Regions of Interest.....	9
Polar Plot Analysis.....	9
Interpretation of Results .....	9
Artefacts and Trouble shooting .....	10
4. Technique Overview .....	11
Applications .....	11
Limitations .....	12
References and Further Reading .....	13
Appendix: Lifetime Acquisition and Analysis from Lambert Manual .....	15

## 1. Principle and Theory

The excited-state lifetime is defined as the mean time a molecule spends in the excited-state. The excited-state lifetime of a fluorescent probe provides a robust and sensitive measure of the probe's environment. It can change in response to environmental changes such as micro-polarity and pH. It can also change when a suitable molecule in nearby by a process called fluorescence resonance energy transfer (FRET). In the latter case the excited-state lifetime of the fluorophore decreases in a characteristic fashion with distance between the two molecules. The excited-state lifetime, unlike intensity, is a kinetic quantity and as such largely independent of factors such as concentration or optical path length. When the lifetime is resolved spatially and presented as an image we refer to this as a fluorescence lifetime image. The technology used to collect and interpret a fluorescence lifetime image is called fluorescence lifetime imaging microscopy (FLIM).

The principle behind measuring excited-state lifetimes is to excite the molecule of interest and measure the response of that molecule to that excitation. In the time-domain the excitation is pulsed and the response is a convolution of that pulse with the excited-state decay of the molecule-usually for short pulses the emission appears as an exponentially-decaying signal, see Figure 1.

The frequency-domain technique is less intuitive

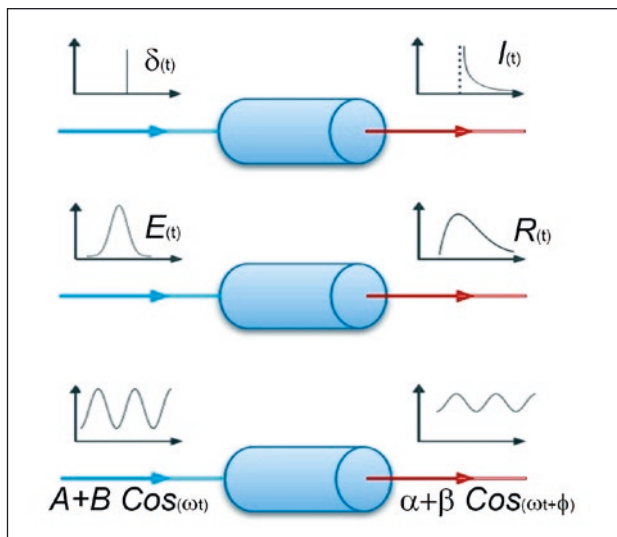


**Figure 1** Schematic representation of the principle behind time-resolved fluorescence measurement techniques. Top: Delta excitation pulse (blue line) excites a fluorescent sample (cylinder) and this sample emits fluorescence with exponential time decay (red line). Middle: If the excitation pulse (blue line) is broad, the response to the excitation appears as broadened emission decay (red-line). Bottom: Sinusoidal-modulated excitation (blue line) and resulting sinusoidal emission (red line). Note the change in shape of the fluorescence due to the finite excited state decay of the fluorophore.

than the time-domain analogue because we are often used to thinking of decay processes in time. But in fact our circadian rhythms operate in the frequency-domain. We are used to waking and sleeping with a given period or frequency which is controlled by the periodicity of night and day. We can also excite a collection of molecules with light that is continuous but intensity modulated with a given frequency. If the molecules emit photons immediately after excitation, then the emission will appear with the same frequency as the excitation and the shape of the emitted waveform will be identical to the shape of the excitation waveform. This is the situation of zero-lifetime. However, if there is a delay between excitation and emission, due to a finite excited-state lifetime, then the emitted waveform will be shifted in phase. We call this a phase shift or a phase lag. A human analogy is jet lag. The light and day cycle is shifted in phase due to air travel from different time zones and this is out of phase with our internal circadian clock. In the frequency-domain two parameters are obtained from the detected waveforms that relate to the lifetime or lifetime distribution. Not surprisingly, the phase shift, is related to the lifetime of the excited state. As implied from the above discussion, the smaller the phase difference between excitation and emission, the shorter the lifetime of the excited state. Another property of a waveform is the modulation. A time-delay between excitation and emission causes a loss of modulation or demodulation of the fluorescence signal. That is the longer the excited-state lifetime the greater the demodulation.

Figure 2 contains a schematic that illustrates and defines modulation and phase-shift.

For a single exponential decaying system characterised by a lifetime,  $\tau$ , the intensity remaining,  $I(t)$ , after time,  $t$  is given by the expression.

$$I(t) = \exp(-t/\tau) \quad (1)$$

The corresponding phase ( $\phi$ ) in FD-FLIM is given by the expression,

$$\phi = \text{Arctan}(\omega\tau) \quad (2)$$

And the modulation is given by the expression,

$$M^2 = 1/(1+(\omega\tau)^2) \quad (3)$$

In equations (2) and (3)  $\omega$  is the modulation frequency. The lifetime determined from the phase (equation 2) is often referred to as the "phase lifetime" and the corresponding lifetime determined from the modulation (equation 3) is called the "modulation lifetime". For single exponential processes the phase lifetime is equal to the modulation lifetimes. For non-exponential decay processes (those involving sums of

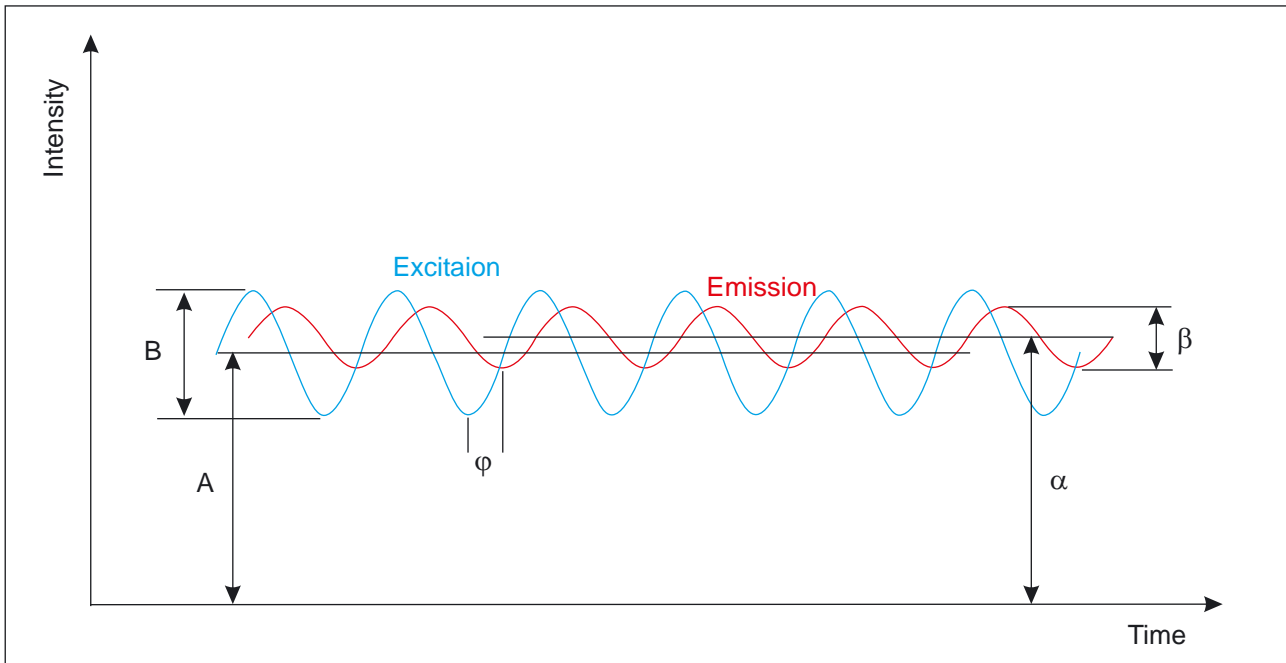


**Figure 2** Schematic representation of excitation and emission waveforms in FD-FLIM. Blue line represents the excitation waveform with average signal intensity  $A$  and waveform amplitude  $B$ . The red-line represents the waveform of the emission. Due to the finite lifetime of the excited-state, the emission waveform is shifted in phase ( $\phi$ ) and de-modulated, that is the amplitude of the emission waveform ( $\beta$ ) divided by the average signal ( $\alpha$ ) is reduced compared to the modulation of the excitation ( $B/A$ ).

exponential functions) the phase lifetime and modulation lifetimes are not equal. Expressions for more complex decaying systems (non-exponential time decays or sums of exponential decays) are given elsewhere. Although determination of these more complex models is possible using multi-frequency methods, in practise measurements of FLIM on biological samples are performed at a single modulation frequency. For questions of biological importance one is usually more interested in a change in the emission decay of a sample through FRET or changes in microenvironment. Importantly, changes in the excited-state lifetime of the fluorophore are inferred through a change in the phase and modulation of the emission. Later we will see a representation of this phase and modulation that is particularly convenient and useful for interpretation of FLIM experiments.

### How is the Fluorescence Waveform Detected?

Before we go into the “nuts and bolts” of the instrumentation, it is important to consider how the sinusoidal fluorescent waveform is detected. As can be gleaned from equations 2 and 3, to measure lifetimes on the order of nanoseconds requires modulation frequencies of the order of reciprocal lifetimes, i.e. 10-100 MHz. The excitation must be modulated at high frequency and we require the phase and modulation of the emitted high-frequency signal. The determination of the emitted fluorescence signal waveform can be achieved using heterodyne or homodyne detection. In heterodyne detection a high-frequence-

cy signal is transformed into a low frequency signal. In homodyne detection the high frequency signal is transformed into a static phase-dependent signal. In both techniques the fluorescence signal is multiplied with a reference waveform derived from a common modulation source.

In the heterodyne technique the gain of the detector is modulated at a slightly different frequency to the frequency of the excitation source. The result of mixing the emission at one frequency with the gain at a slightly different frequency is a new waveform with low frequency and identical phase and modulation to the original (high-frequency) emitted waveform. Time-sampling of this low frequency waveform and subsequent Fourier analysis recovers the phase and modulation information.

In the homodyne method the gain of the detector is modulated at exactly the same frequency as the excitation. This gives a filtered signal that depends only on the phase difference between the emission and the reference waveform. This signal may be sampled by shifting the phase between the detector and the excitation. Repeating this process generates a waveform at each pixel of the image which contains the phase and modulation information.

## 2. Instrumentation

A schematic of a typical wide-field FD-FLIM is shown in Figure 3. This system is built around a research grade microscope with the light source directed

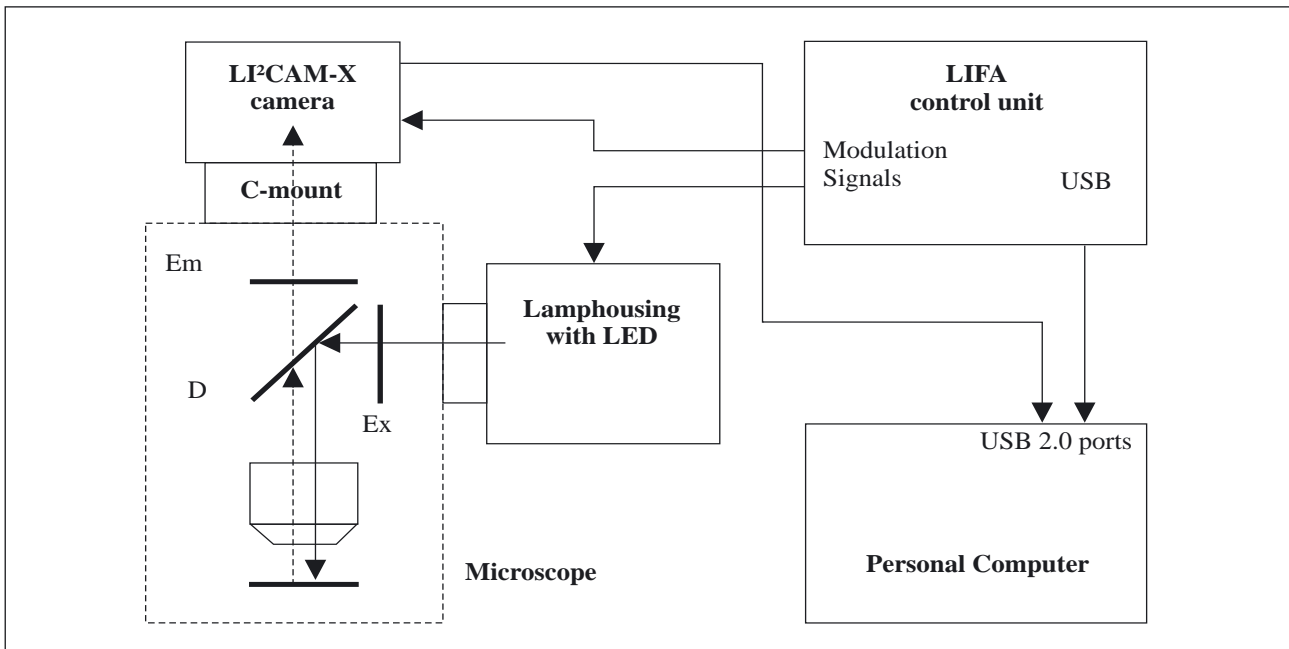


**Figure 3** Schematic representation of the LIFA wide-field FD-FLIM. Components are discussed in the main text. (Diagram from the Lambert Instruments LIFA manual).

through the back of the microscope and the detector mounted onto an emission side-port (microscope not shown). The difference between a conventional microscope and an FD-FLIM microscope lies in the detector. The heart of this system is the micro-channel plate image intensifier which serves as the mixing device in homo-dyne or heterodyne detection. The gain of the intensifier is modulated at high-frequency under control of the signal generator and this waveform is essentially mixed in the detector with the emission signal waveform that emerges from the microscope. The signal generator sends an identical frequency signal to the light source which provides the modulated excitation waveform. The CCD camera is a detector that provides a digital 2D representation of the image that impinges on the MCP phosphor. The computer contains software that controls the frequency of modulation and shifts the phase between the MCP and light source, reads the images from the CCD camera, and computes lifetime images.

### Light Sources

In FD-FLIM any repetitive waveform that excites the molecule of interest is required. For typical lifetimes of 1-10 ns one requires 10-100 MHz frequencies (see equation (2)). Continuous lasers can be used in combination with acousto-optic or electro-optic modulators to provide the periodic, modulated excitation waveform. Pulsed laser systems such as Ti-Sa lasers, have also been used and provide the added advantage of two-photon excitation. Direct electrical modulation of light-emitting diodes and

laser diodes has been demonstrated. For example, in the Lambert Instruments LIFA system modulated LEDs or modulated laser diodes are used as the excitation source.

### Detectors

The detection of the emitted fluorescence signal waveform can be carried out in a number of ways depending on the configuration of the microscope (scanning or wide-field) or whether the detection is homo-dyne or heterodyne. When scanning is used (either stage scanning with fixed laser or laser scanning with fixed stage) the emission is focussed onto a single detector, usually a photomultiplier tube, an avalanche photodiode or a micro-channel plate detector and the signal is timed with the position of the scanning stage or laser to extract an image. In wide-field FD-FLIM instruments the whole field is illuminated and the image focussed onto an area detector such as a micro-channel plate image intensifier and a charge-coupled device camera.

### Microscope

Most FLIM systems are built on a research grade fluorescence microscope. The objective lens is an essential optical element that provides the magnification needed to see objects on the (sub) micron scale. The delivery of the excitation light and the handling of the fluorescence emission differ depending on the type of microscope and the desired imaging modality but most systems employ a dichroic mirror to reflect emitted light to the detector and excitation

and emission filters to select excitation and emission wavelengths.

In confocal systems, hardware is needed to deliver and raster scan a laser beam to the sample and a pin-hole between the emission and the detector is utilised to reject out of focus light. In wide-field systems, no extra hardware is needed aside from the excitation source, signal generator and image intensifier and charge-coupled device camera.

### Software

The output of a FD-FLIM experiment is a stack of images that represents a sinusoidal function at every pixel. There are a number of steps required before the raw data stacks can be converted into a lifetime image. These steps include;

1. Background correction. This can be performed in a number of ways. A small region outside the sample is interactively selected and the average intensity value from that region in each phase image is subtracted. Alternatively, an image is collected with the excitation source blocked and this image is subtracted from each phase-dependent image. In-cell background correction is more challenging but can be done in some circumstances as a post processing step (see details later).
2. Correction for photobleaching. All fluorophores photobleach to some extent and if not taken into account FD-FLIM values can be distorted. The traditional photobleaching correction is to record

phase images in one sequence then re-record the phase images in reverse sequence. Averaging the two sequences of images corrects for linear photobleaching. A more recent innovation utilised permuting the recording order so that the phase steps are not sequentially increasing but rather pseudo-random in recording order. This second method is advantageous because it obviates the requirement of recording two series of phase stacks.

3. Correction for instrumental phase shift and demodulation. The instrument has an intrinsic phase bias and a demodulation. In the time-domain this is called the instrument response function and represents the finite width of the laser pulse and the timing jitter in the detector and the electronics. In the frequency domain, the light source, electronics and detector all contributed to a finite demodulation and phase of the instrument. This is readily corrected by recording a phase stack of images with a reference of known lifetime (fluorescein, rhodamine 6G are good examples). Because the reference stacks are from solutions with no microscopic detail spatial averaging is usually performed on these solution images before the phase and modulation images are extracted.
4. Calculation of phase and modulation images of sample and reference. Once the image stacks representing corrected images are stored in memory, the phase and modulation images are required because they contain information about

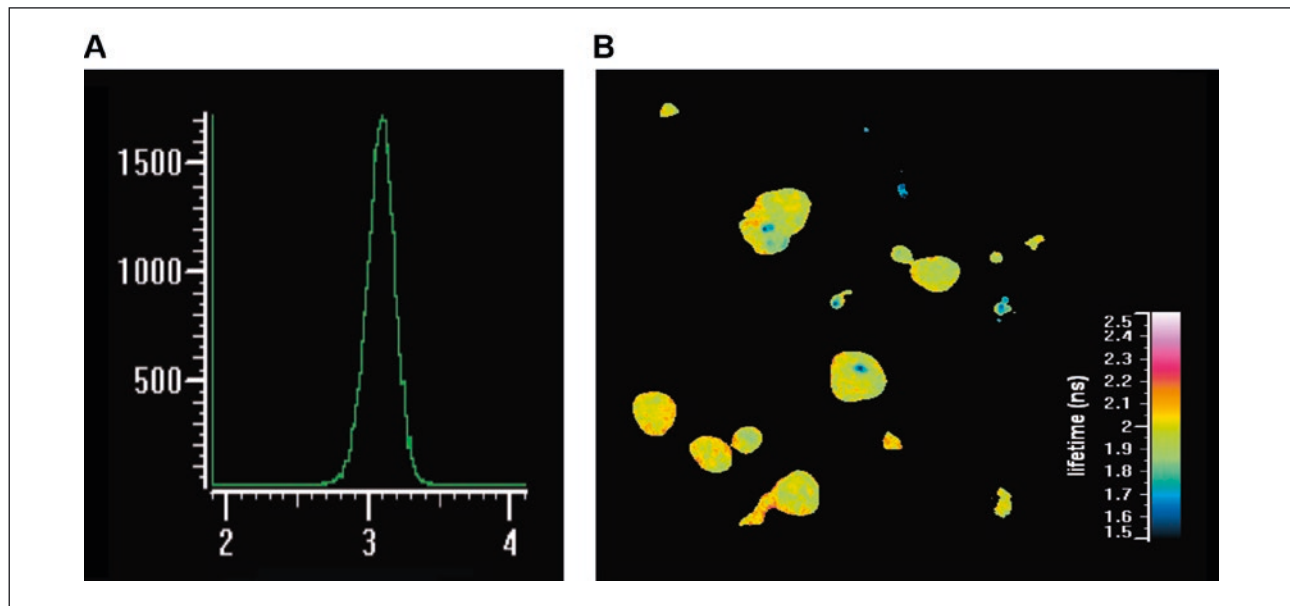


**Figure 4** **A** Representative lifetime histogram. Plot of the number of pixels versus fluorescence lifetime (in nanoseconds). The large number of pixels in an FD-FLIM image leads to large sample sizes and consequently well-defined lifetime distributions. Even small lifetime shifts of the order of 100ps or less can be readily discerned. **B** Representative lifetime image. Note the regions in blue that denote very short lifetimes (1.6 ns) compared with the yellow-orange regions (2-2.1 ns).

the excited-state decay processes at hand. The phase-stacks can be processed efficiently using Fourier Transform methods, namely discrete sine and cosine transformations, which in turn can be manipulated to deliver the required phase and modulations at every pixel location in an image. Direct fitting to a sinusoidal function is also a possibility, which yields the required phase and modulation.

Once the phase and modulation are known then phase lifetime and modulation lifetime images are created (see equations 2 and 3). The lifetime images can be color-coded to aid visualisation of regions with different lifetime. An alternative representation is in terms of histograms. The lifetime is binned into different values on the horizontal axis and the number of pixels in each bin is plotted on the vertical axis. An example of a lifetime histogram is displayed in Figure 4A and an example of a color-coded FLIM image is shown in Figure 4B.

A very useful and convenient visualisation of data is achieved with a plot called the polar plot (or phasor or AB-plot). The phase and modulation is transformed into point on a 2D plot. For a given phase,  $\phi$ , and modulation,  $M$ , the coordinates of the point on the polar plot are;

$$x\text{-axis}=B=M\cos\phi \quad (4)$$

$$y\text{-axis}=A=M\sin\phi \quad (5)$$

For a single species the time-decay of the fluorescence emission is represented by a single point on the polar plot at location  $(M\cos\phi, M\sin\phi)$ . If the emission decay is single exponential, the phasor will be located somewhere on a semi-circle circumscribed by the points  $(0,0)$ ,  $(1/2, 1/2)$  and  $(1,0)$  and the position on that semi-circle reveals the actual lifetime value. For more complex heterogenous decays the phasor will be located inside the semi-circle. For excited-state reactions involving sensitised acceptor emission or solvent relaxation, the phasor will be located outside the semi-circle.

The polar plot can also reveal data from different experiments (different samples, or same sample different conditions) or data as a function of image location or time or any other hidden variable. The resulting spread of data is often referred to as a polar plot trajectory. The use of the polar plot has many advantages.

- (a) Irrespective of the complexity of the fluorescence decay, any fluorophore can be represented as a single point in the polar plot.
- (b) Mixtures between different species are represented by the vector sum of the phasors of the

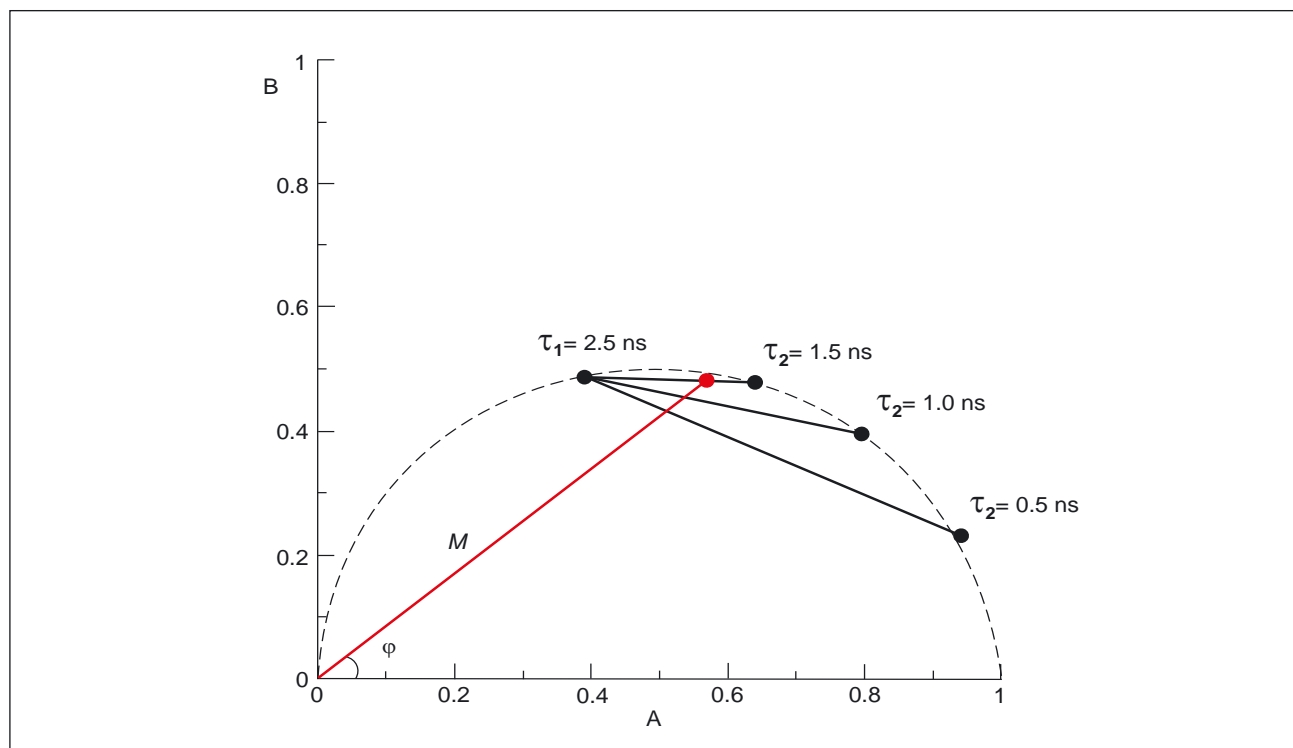


**Figure 5** Polar plot or AB-plot. The red dot represents one fluorescent species with a given fluorescence decay profile. The length of the red-line is the modulation of the emission and angle subtended by the red-line is the phase. Selected single-exponential lifetimes are denoted by the black dots on the dashed semi-circle. Binary mixtures of different lifetime species are denoted by the chords linking the dots.  $A, B, M$  and  $\phi$  are defined in the text.

individual species. All possible mixing combinations fall on a line connecting the individual species. For the mixture of three species the mixture falls inside a triangle. For N-species this will be a polygon with N-vertexes.

- (c) FRET experiments can also be simulated taking into account background fluorescence and contributions from non-FRET states.
- (d) Data from only one modulation frequency is required.
- (e) Analysis of a potentially complex multi-exponential decay problem is reduced to simple rules of vector algebra and trigonometry.

### 3. Method

#### Sample: General Considerations

The most important sample in FD-FLIM is the reference solution! The reference must have a defined, single exponential lifetime that is spatially-invariant. If these conditions are not met then the lifetime measurements of the sample will be in error. We have found that a dilute ( $1\text{-}5 \mu\text{M}$ ) solution of rhodamine 6G in distilled water provides an excellent and robust reference solution with a lifetime of 4.1 ns. A few drops ( $100\text{-}200 \mu\text{L}$ ) of this solution applied to a coverslip. Other standards in use include fluorescein (4 ns), rhodamine B (lifetime 1.7 ns), erythrosin (0.080 ns). Scattered light (0 ns) in principle can also be used but care is needed to avoid spurious multiple reflections can cause artefacts.

The sample for FD-FLIM should be prepared in the same way as for standard fluorescence microscopy. That is the cells should be live or fixed, as appropriate, and the molecules or cellular structures of interest need to be specifically tagged with a fluorescent probe. FD-FLIM is compatible with standard dyes (the Alexa dyes, fluorescein, rhodamine) and genetically-encoded probes (GFP, CFP, YFP, and other flavours). One has to be mindful that experimental conditions such as pH, temperature, fixation and mounting can all affect lifetimes. This needs to be taken into account in the experimental design and also when comparing results from different datasets or different laboratories.

For FRET studies one normally compares the lifetime of the donor with the lifetime of the donor in the presence of an energy transfer acceptor. In these cases more samples need to be prepared. One sample with donor-only, one with donor and acceptor, one with acceptor only and an unlabelled set of cells.

#### Sample: Specific Examples

##### *GFP-fusion construct transfection into cells*

A procedure we routinely use for transfecting epider-

mal growth factor receptor-GFP into HEK293 cells is given below.

1. Sub-confluent HEK293 cells ( $2.5 \times 10^5$  cells) were seeded onto sterilized coverslips housed in 6-well plates in 5 mls DMEM + 10% foetal calf serum and cultured at  $37^\circ\text{C}$  in 5% CO<sub>2</sub>. After 6 hours, the media volume was brought up to 5 mls with DMEM + 10% fetal calf serum.
2. Immediately prior to transfecting the cells, the media volume was reduced by aspiration to 1 ml.
3. EGFR-eGFP cDNA was complexed to the non-liposomal transfection reagent FuGENE 6, at a ratio of 1:6, in serum-free DMEM, incubated for 30 mins at room temperature, then aliquoted dropwise onto the cells.
4. After 6 hours, the media volume was brought up to 5 mls with DMEM + 10% fetal calf serum.
5. The cells are left for at least 24 hours to allow transfection.

#### *Immuno-staining protocol*

The protocol for antibody-staining and imaging is shown below.

1. Seed A431 cells on sterile round cover slips, washed with PBS.
2. Grow to ~80% confluence.
3. 1x wash with warm ( $37^\circ\text{C}$ ) PBS – aspirate fluids.
4. Fix cells – add 4% PFA to each well to cover the cells (0.5-1.0ml). Incubate 25min @ RT.
5. Wash 2x PBS
6. Incubate with mAb528 – 50µg/ml in FACS buffer (PBS/5% FCS). 18µl of 11.7mg/ml in 4.2ml FACS buffer, allowing 0.7ml/well for total of 6 wells. Incubate 15-30 min RT.
7. Wash 1-2 x PBS
8. Incubate with anti-mouse-IgG FITC-secondary mAb (sheep anti-mouse IgG (Fc gamma chain) FITC conjugate from Jackson Immunoresearch #515-095-071) – 50µl of 1.5mg/ml in 3.8ml FACS buffer, allowing ~0.7ml/well for total of 5 wells (final concentration of ~20µg/ml). Incubate 15-30 min @ RT in the dark.
9. Wash 1-2 x PBS
10. Mount cells on slide (no glycerol between the coverslip)

#### *Protocols for FRET studies*

For FRET studies one needs ideally four samples;

1. Donor-only sample
2. Acceptor-only sample
3. Donor-Acceptor sample
4. Cell background-sample with no transfection or labelled molecules introduced.

Samples 1 and 2 are needed to compare lifetime of donor with lifetime of the donor in the presence of acceptor (see below).

Samples 2 and 3 can be used to determine FRET through sensitized emission (see below).

For donor-detected FRET studies sample 2 ensures no spectral bleed-through from acceptor into the donor channel.

Sample 4 is to correct the data for background fluorescence signal.

## 4. Image Acquisition

The reader is directed to the Appendix provided by Lambert Instruments on the operation of the LIFA instrument and obtaining a lifetime image.

## 5. Data Analysis

The lifetime image takes a bit of getting used to. It is a map of kinetic processes not the intensity or concentration of species as in normal fluorescence microscopy. As a consequence lifetime images can sometimes appear to have less contrast than a fluorescence intensity image. Careful analysis and display of lifetime images can provide improved interpretation.

### Histogram Analysis of Regions of Interest

Spectroscopists are used to measuring absorption or emission spectra and measuring shifts in spectra. Lifetimes can be displayed in a similar fashion using histograms- a plot of the no. of pixels versus lifetime. Differences in lifetime between different regions of interest of the same image can be revealed by plotting the lifetime histograms of these regions of interest. Using the ROI tools one can select successive regions, which will be numbered 1,2,3 etc. Then going to the statistics tab tick the boxes corresponding to the lifetime histogram and the ROI number. A color-coded histogram will appear in the window. The statistics function also provides information on the mean, standard deviation and the number of pixels in the ROI. The histogram analysis can also be applied to different experiments. For example in FRET one compares the lifetime of cells containing a donor with cells containing a donor and acceptor. A shift in the donor histogram to lower lifetime values in the presence of acceptor indicates FRET from the donor to the acceptor.

### Polar Plot Analysis

Another way of visualising a FLIM experiment is to use the polar plot. This can be accessed using the polar plot tab in the LIFA software or alternatively one can use Enrico Gratton's Globals for Images software. As mentioned before the polar plot represents the phase and modulation values of an

image on a two-dimensional graph. For images the polar plots usually appear as a cloud of points instead of a single point. A selection tool is used to point to specific regions of the polar plot and pixels with these phase and modulation characteristics are highlighted onto the intensity image.

### Interpretation of Results

#### *Tests of statistical significance*

For cell biophysical studies, where biological variability is the rule, statistical tests are an important way of testing whether two sets of observations are significant or insignificant. The simplest implementation is to analyse 20-50 cells (number of observations,  $N_1$ ) from one treatment and 20-50 cells (number of observations,  $N_2$ ) from another treatment and compute the corresponding mean phase lifetimes ( $x_1$  and  $x_2$ ) and variances ( $\sigma_1^2$  and  $\sigma_2^2$ ) in the phase lifetime from each treatment dataset.

The t-value, which provides a measure of whether the mean values from each dataset are significantly different, is given by the expression,

$$t = (x_1 - x_2) / \sqrt{(\sigma_1^2/N_1) + (\sigma_2^2/N_2)}^{0.5} \quad (6)$$

The number of degrees of freedom is given by  $N_1+N_2-2$ . Using the number of degrees of freedom and the t-value, a t-table can be examined to determine the significance level of the t-value. For example if 10 cells per treatment condition is measured, the number of degrees of freedom is 18. Inspection of a t-table reveals that for t-values greater than 2.1 the means of the two datasets are significantly different at the 95% significance level.

### *Background Mixing*

For cells containing a high level of fluorescence label background fluorescence is usually ignored in FD-FLIM. However as meaningful, biologically-relevant studies demand protein expression at physiological levels background fluorescence can become an inevitable component of the detected emission. There are generally two types of background. Off-cell background arises from camera offset, room lights, immersion oil, buffers and cover-slips. This type of background can be examined by selection of regions that do not contain cells and subtracted or taken into account in analysis. Cellular autofluorescence is the other source of background and arises from native (not extrinsically-labelled) molecules contained within the cell eg flavins, collagen etc. This type of fluorescence must be measured in unstained cells before it can be subtracted.

The effect of background mixing into the (desired) sample is given by the simple equations,

$$A \text{ total} = \alpha A \text{ sample} + (1-\alpha) A \text{ background} \quad (7)$$

$$B \text{ total} = \alpha B \text{ sample} + (1-\alpha) B \text{ background} \quad (8)$$

Where A and B are the sine and cosine components of the phasor (defined above), and  $\alpha$  is the fractional fluorescence contribution of the sample emission to the total emission. Equations (7) and (8) can be applied to cell populations, single cells, or at the pixel level. Significant background mixing can be visualised in an FD-FLIM image from the polar plot as an elongated cloud of points that begins at (B,A) *sample* and stretches out to (B,A) *background*.

#### *FRET or no-FRET?*

Arguably FD-FLIM is of greatest use in FRET applications for detecting interactions (or conformational changes) between labelled biological macromolecules. In FRET excitation of the donor molecule results in non-radiative transfer of energy to the acceptor molecule. If the acceptor is fluorescent it can emit a fluorescence photon. The requirements for FRET are restrictive. The spectral properties of the fluorophores, the orientation between the fluorophores and the distance are important determinants on the efficiency of the FRET process. These aspects are discussed in detail elsewhere.

Detection and measurement of FRET by FD-FLIM is relatively straightforward but depends on the experimental design. The measurement method is a consequence of the photo-physics of the FRET process itself.

*FRET induced donor lifetime quenching in FD-FLIM*  
FRET adds a non-radiative decay channel to the excited state of the donor. As a consequence FRET decreases the lifetime of the donor molecule in the presence of the acceptor. To detect FRET one measures the lifetime of the donor in the absence of the acceptor ( $\tau_d$ ) and then measures the donor lifetime in the presence of the acceptor ( $\tau_{da}$ ). The FRET Efficiency, E, can be computed with the relation,

$$E = 1 - (\tau_{da}/\tau_d) \quad (9)$$

The donor lifetime can be determined from a sample containing the donor-only (with no acceptor). Alternatively, the donor-only sample can be prepared from the donor-acceptor sample photo-chemically by photobleaching the acceptor (see acceptor photobleaching chapter). It is very important that in the donor lifetime method the donor is uniquely excited and the emission represents the emission from the donor only. In FD-FLIM lifetime is often the phase lifetime or modulation lifetime. The FRET can also

be calculated using the polar plot and is visualised as a movement of the donor phasor in a clockwise direction along the universal-circle.

Methods exist for using the polar plot to analyse FRET in the presence of background emission or in the situation of variable amounts of FRET and non-FRET states. The reader is referred to the publications for more detailed accounts.

#### *Sensitized Emission*

FRET results in a delayed emission from the acceptor fluorophore because the initially excited donor transfer energy is transferred (albeit invisible, non-radiatively) to the acceptor. This delay gives an additional phase shift to the acceptor emission (over that associated with the normal excitation and emission from the acceptor). This extra phase can cause an effect known as lifetime inversion, that is the lifetime calculated from the modulation becomes less than the lifetime calculated from the phase. This effect also causes the phasor of the acceptor to move in a counter-clockwise movement outside the semi-circle of the polar plot.

#### **Artifacts and Trouble shooting**

##### *Photobleaching*

Photobleaching can dramatically distort lifetime measurements and in some cases cause an inversion of modulation and phase lifetimes even for simple fluorophores. Reducing the excitation intensity and measurement times can reduce photobleaching. When photobleaching is unavoidable, pseudo-random phase recording can help reduce the effects of photobleaching on lifetime measurements. Consideration of background is needed if photobleaching deteriorates signal to background levels.

##### *Roomlight*

Roomlight adds a DC signal to the data. This systematically causes a demodulation of the signal and will distort the lifetime computed from the modulation (i.e. the modulation lifetime will increase). The phase lifetime will not be effected for pure DC signal background. This can be visualised in the polar plot as a line that connects the origin (0,0) to the fluorescence signal. This can be eliminated by turning off the light, covering the sample, or ensuring a background correction image is recorded and subtracted from the phase stacks.

##### *Sample Movement*

An FD-FLIM image is a single image derived from several individual images obtained at different times (or different phase steps). An implicit assumption is that there is no movement during image acquisition or perhaps more precisely that the concentration distribution of fluorophores in the image is time invariant.

ant during the FLIM acquisition. This is often a good assumption (where fluxes in the cell ensure pseudo-steady-state) or cells are fixed. However, in some cases “comets” can appear in the lifetime images and correspondingly, streaks in the polar plot. These are due to motion of a small number of particles in the image. Whole cell motion will give the effect of shadowing whereby there is a distinctive gradient of high to low lifetime. Motions of a large number of particles will broaden lifetime histograms and cause a blooming of polar plots. In some selected cases this is useful for determining translational diffusion coefficients<sup>23</sup>. Stabilising the sample and decreasing exposure times is the best way to reduce these effects.

#### *Instrument Drift*

Drift can sometimes occur due to lack of temperature stabilisation on LEDs or AOMs or electronics. If left unchecked, drift can give erroneous impressions of time-dependent biological phenomena or give erratic results. The simplest way of diagnosing and correcting drift is to measure a lifetime standard or any stable sample periodically. Small lifetime fluctuations (<0.1 ns) are probably due to random fluctuations. However, any monotonic change in the lifetime of the standard is evidence for drift.

A good way to avoid drift is to carry out drift tests during instrument warm up until stability is confirmed. We have found drift to be a rare problem with our set-up with stability of better than 50 ps over a period of hours. Another way of safe-guarding against drift is by permuting sample collection order so that the same sample or reference is collected at several different times.

#### *Fixation, Antifade*

We have found that fixation can alter the lifetime of a YFP-tagged cell surface receptor and more anecdotal evidence suggests it can effect lifetimes of GFP-tagged proteins. The exact reason for this phenomenon is not currently known but it is important to understand that the lifetime of a fluorophore in living cells is not necessarily the same as in fixed cells. Antifade has also been anecdotally attributed to lifetime changes. Because the composition and quantity of antifade may vary from batch to batch or sample to sample it is not recommended to use this with FLIM experiments.

#### *Temperature*

Most cell studies are carried out at 4 degrees centigrade, 37 degrees centigrade or ambient temperature (often undefined). The excited-state lifetimes of nearly all organic fluorophores depend on temperature with a decrease in lifetime with increasing temperature. Where possible it is preferable to control

the temperature or at least note the ambient temperature at the time of the measurements.

#### *Polarisation Effects*

For molecules excited with polarised light, the time-dependent detected emission depends on the excited-state lifetime, the rotational motion of the fluorophore and the emission collection geometry. This can be useful for measuring rotational dynamics of fluorophores. However this effect can also perturb lifetime measurements. Use of a polariser in the excitation (or a laser which is polarised) and an analyser in the emission path oriented at the magic angle (54.7 degrees) is the traditional way to exclude polarisation artefacts in time-resolved spectroscopy. This approach is rarely employed in FLIM probably because of the reduction in attendant signal. Instead, lasers are sent through polarisation scrambling fibres to produce excitation light that is not linearly-polarised. Unpolarised light sources from lamps or LEDs also reduces but does not guarantee complete removal of the effects of polarisation on FLIM measurements.

#### *Noise*

Noise is not really an artefact but a reality of the measurement process. Clearly a trade-off exists between reducing photo-bleaching and reducing effects of movement, which requires use of low excitation and fast acquisition, and collection of enough emission photons to ensure nicely resolved FLIM images. The signal to noise ratio can be increased by using averaging or increasing the exposure time. Increasing the averaging or exposure time by a factor of  $N$  will increase the signal to noise ratio by a factor of  $\sqrt{N}$ . An alternative approach, for advanced users, is to use de-noising routines as a post-acquisition step in cleaning up FLIM images. A very detailed and excellent account of such an approach has been published by Professor Clegg's laboratory.

*Optical Elements in the Excitation or Emission Path*  
Optical elements such as ND filters can add to the optical path length and consequently cause a phase delay in excitation or emission. Consequently care should be taken in ensuring that when extra optical elements are introduced into a sample measurement they are preserved in the measurement of the reference as well.

## 4. Technique Overview

#### **Applications**

A selection of applications is collected in Table 1. The list of FLIM applications is growing rapidly. FLIM is popular in biophysics and cell biology as a means

to measure interactions between biological macromolecules in the cellular environment. Not only is it useful for detecting the presence of these interactions but also is highly quantitative allowing detection of stoichiometry of these interactions as well. FD-FLIM has the distinct advantage of rapid acquisition (up to video rate) making it favourable for detecting dynamics on cellular timescales. FLIM can provide a robust readout of fluorescent biosensors because it is independent of signal intensity and biosensor concentration. FLIM has also been proposed as an alternative tool to biopsies in the clinical setting because autofluorescent lifetimes have been shown to be a function of metabolic state or pathological state of cells and tissues.

### **Limitations**

FD-FLIM requires specialised instrumentation but commercial options are available.

## References and Further Reading

**Table 1 Selected FD-FLIM applications and artefact corrections**

Application	Labels	Comment	References
Reviews on FLIM			Berezin et al <sup>[1]</sup> Wouters et al <sup>[2],[3],[4]</sup>
Ligand-ligand interactions	Fluorescein/rhodamine	FRET	Gadella et al <sup>[5]</sup>
Receptor phosphorylation	GFP, Cy3-antibody	FRET, Global analysis	Verveer et al <sup>[6]</sup>
Sub-unit assembly	Cy3 and Cy5 direct	FRET	Bastiaens et al <sup>[7]</sup>
Rotational dynamics	GFP	- FLIM+polarisation	Clayton et al <sup>[8]</sup>
Spectral FLIM		Prism-based spectrograph	Hanley et al <sup>[9]</sup>
FLIM with ICS	AlexaFluor488/546 GFP/Alexa555 GFP/mRFP		Clayton et al <sup>[10]</sup> Clayton et al <sup>[24]</sup> Kozer et al <sup>[25]</sup>
Biosensor Application(s)		Phase-suppression, pH gradient <sup>11</sup> , Ca concentration	Eichorst et al <sup>[12]</sup> Hansen et al <sup>[11]</sup>
Pre-clinical applications Graphical representation/ analysis	Unstained tissue Unstained tissue	TD-FLIM,Cancer TD-FLIM,Cardio	Lakowicz et al <sup>[13]</sup> McGinty et al <sup>[14]</sup> Marcu <sup>[15]</sup> Clayton et al <sup>[16]</sup> Redford et al <sup>[17]</sup> Digman et al <sup>[18]</sup>
Photo-bleach correction	YFP		Van Munster et al <sup>[19]</sup>
De-noising routines			Spring et al <sup>[20]</sup>
Fixation effects Lifetime calibration Movement	YFP Rhodamine 6G Beads		Ganguly <sup>[21]</sup> Hanley et al <sup>[22]</sup> Lajevardipour et al <sup>[23]</sup>

- [1] Berezin, M. Y.; Achilefu, S. *Chem Rev* 2010, 110, 2641.
- [2] Wouters, F. S.; Bastiaens, P. I. *Curr Protoc Cell Biol* 2001, Chapter 17, Unit 17 1.
- [3] Wouters, F. S.; Bastiaens, P. I. *Curr Protoc Neurosci* 2006, Chapter 5, Unit 5 22.
- [4] Wouters, F. S.; Bastiaens, P. I. *Curr Protoc Protein Sci* 2001, Chapter 19, Unit 19 5.
- [5] Gadella, T. W., Jr.; Jovin, T. M. *J Cell Biol* 1995, 129, 1543.
- [6] Verveer, P. J.; Wouters, F. S.; Reynolds, A. R.; Bastiaens, P. I. *Science* 2000, 290, 1567.
- [7] Bastiaens, P. I.; Jovin, T. M. *Proc Natl Acad Sci U S A* 1996, 93, 8407.
- [8] Clayton, A. H.; Hanley, Q. S.; Arndt-Jovin, D. J.; Subramaniam, V.; Jovin, T. M. *Biophys J* 2002, 83, 1631.
- [9] Hanley, Q. S.; Murray, P. I.; Forde, T. S. *Cytometry A* 2006, 69, 759.
- [10] Clayton, A. H.; Tavarnesi, M. L.; Johns, T. G.

- Biochemistry 2007, 46, 4589.
- [11] Hanson, K. M.; Behne, M. J.; Barry, N. P.; Mauro, T. M.; Gratton, E.; Clegg, R. M. *Biophys J* 2002, 83, 1682.
- [12] Eichorst, J. P.; Huang, H.; Clegg, R. M.; Wang, Y. *J Fluoresc* 2011, 21, 1763.
- [13] Lakowicz, J. R.; Szmacinski, H.; Nowaczyk, K.; Johnson, M. L. *Cell Calcium* 1992, 13, 131.
- [14] McGinty, J.; Galletly, N. P.; Dunsby, C.; Munro, I.; Elson, D. S.; Requejo-Isidro, J.; Cohen, P.; Ahmad, R.; Forsyth, A.; Thillainayagam, A. V.; Neil, M. A.; French, P. M.; Stamp, G. W. *Biomed Opt Express* 2010, 1, 627.
- [15] Marcu, L. *J Biomed Opt* 2010, 15, 011106.
- [16] Clayton, A. H.; Hanley, Q. S.; Verveer, P. J. *J Microsc* 2004, 213, 1.
- [17] Redford, G. I.; Clegg, R. M. *J Fluoresc* 2005, 15, 805.
- [18] Digman, M. A.; Caiolfa, V. R.; Zamai, M.; Gratton, E. *Biophys J* 2008, 94, L14.

- [19] van Munster, E. B.; Gadella, T. W., Jr. Cytometry A 2004, 58, 185.
- [20] Spring, B. Q.; Clegg, R. M. J Microsc 2009, 235, 221.
- [21] Ganguly, S.; Clayton, A. H.; Chattopadhyay, A. Biochem Biophys Res Commun 2011, 405, 234.
- [22] Hanley, Q. S.; Subramaniam, V.; Arndt-Jovin, D. J.; Jovin, T. M. Cytometry 2001, 43, 248.
- [23] Lajevardipour, A. and Clayton, A.H.A, J. Fluoresc 2013, 23(4):671-9.
- [24] Clayton AH, Orchard SG, Nice EC, Posner RG, Burgess AW. Growth Factors 2008, 26(6):316-24..
- [25] Kozer N, Barua D, Henderson C, Nice EC, Burgess AW, Hlavacek WS, Clayton AH Biochemistry 2014, 53(16):2594-604

## Appendix: Lifetime Acquisition and Analysis from Lambert Manual

*Reproduced from Lambert Instruments manual with permission.*

### 4 System Setup guide

This tour will guide you through the process of recording lifetime images with LI-FLIM. The purpose of this chapter is to get you up and running, and to lead you through the most common tasks that you will do with LI-FLIM. It does not try to optimise your experiment in any way. If you want to start doing real lifetime measurements, then you should read chapter about "Analysis", to get a more detailed description of the effects of different hardware settings and parameters on the measurement speed and accuracy. Likewise, if you come across some menu options or toolbar buttons in LI-FLIM, that are not explained in this guide, please refer to "Reference guide" chapter for a complete reference of all options, features and functionality of LI-FLIM.

Last but not least is the LIFA system and camera, and possibly other hardware correctly connected to the computer (via USB and possibly other cables) and the widefield fluorescence microscope (camera, lamp housing with adjusted LED) and that all drivers are installed and are working correctly. Such that the system is set-up in such a way that by pressing 'Reference' and 'Sample' subsequently, LI-FLIM is capable of taking correct lifetime measurements.



#### Warning!

The fiber-optically coupled image intensifier to the CCD camera is a relatively expensive device. Therefore it is important to take all the warnings mentioned in the [Hardware](#) manual into account. Although the software detects potential damaging levels, it remains important to be aware of possible harm to this device.

#### 4.1 Preparations

Before one can obtain a lifetime measurement one should take care of the following:

##### Filter cube

Select the proper filter cube with the excitation filter that matches the wavelength of the LED excitation and the emission filter that matches the wavelength of the emitted fluorescence light of the specimen. It is important that the LED emission is completely blocked by the dichroic and the emission filters.

Be aware that for fluorescence resonance energy transfer (FRET) experiments, a band pass emission filter cube is required for the emission of the donor fluorophore only. The emission of the acceptor fluorophore should be eliminated from this signal completely in order ONLY to measure the lifetime of the donor fluorophore and to calculate the difference in donor lifetime before and after FRET. Some examples are given below. For more information on the FLIM FRET theory, see the "Reference guide" chapter and the referenced literature.

##### Objective

In principle every objective is fine for doing FLIM. However, the higher numerical aperture (NA), the more light is coming to the sample, the less intensification is required and the better lifetime value will be obtained.

##### Light path of microscope

All ND filters should be eliminated from the light path and the field diaphragm and aperture should be opened as much as possible. The more light is coming to the sample, the less intensification is required and the better lifetime value will be obtained.

During measurements, 100% of the light has to be directed to the camera port. When starting up and between experiments, all the light should be directed to the eyepieces of the microscope.

##### Reference solution

For the frequency domain method a reference solution is required. The ideal reference is a material or solution with a uniformly distributed concentration of fluorescent molecules and a known single lifetime component that can be used with the same filter cube as the sample. It is not necessary that the reference has the same lifetime as the sample. Advisable is to have comparable brightness for reference and sample. Some possible references are listed below:

**HPTS**

Sigma Aldrich: "Fluka 56360". HPTS (8-hydroxypyrene-1,3,6-trisulfonate) has an excitation maximum at 460 nm and an emission maximum at 510 nm and thus can be used for e.g. GFP transfected cells (use 1  $\mu\text{M}$ ) as well as for CFP transfected cells by using a more concentrated solution. HPTS has a single lifetime component of 5.3 ns and is pH insensitive.

**Fluorescein**

Sigma Aldrich: "Fluka 46955". Fluorescein has an excitation maximum at 490 nm and an emission maximum at 514 nm and can thus be used for e.g. GFP transfected cells (use 1  $\mu\text{M}$ ) as well as for CFP transfected cells by using a more concentrated solution (use 10  $\mu\text{M}$  fluorescein). This fluorescein solution has a single lifetime component of 4.00 ns at pH above 10. A disadvantage is that the solution is prone to bleaching.

**Rhodamine 6G**

Sigma Aldrich: "Fluka 83697". Rhodamine 6G has an excitation maximum at 528 nm and an emission maximum at 547 nm and thus can be used for GFP transfected cells (use 50  $\mu\text{M}$  in saline??). Rhodamine 6G saline solution has a single lifetime component of 4.11 ns.

**FluorRef slides**

The advantage of FluorRef slides (<http://www.microscopyeducation.com/fluorrefslides.html>) is that each slide has a stable lifetime value and is not prone to bleaching. These slides can be used for evaluation of the LIFA system after some doubts of correctness in lifetime calculations. Note that the slides are very bright; extra ND (neutral density) filters should be used, not to damage the photocathode (see hardware manual for explanation).

**Object glass with cavity**

The reference solution can best be used with an object glass with cavity. E.g. from Fisher Scientific: Object glass with cavity; Menzel; Glass thickness 1.2 - 1.5 mm. Diam. Cavity 15 - 18 mm with depth of 0.6 - 0.8 mm.

**Erythrosin B:**

The lifetime is 86 ps. this gives better (more accurate) results because its lifetime is closer to zero (i.e. the measured phase and modulation are close to the phase and modulation of the excitation light). one need 1 mg dissolved in 1 ml of pure water, fresh (one day it can not be saved). This gives a deep pink solution. One should focus clearly within the drop, preferably far away from the glass. For example, for a YFP emission filter. The excitation can be anything up to 532 nm.

A schematic drawing of the setup with a standard LIFA system, and an upright wide field fluorescence microscope is given in figure 4.1.

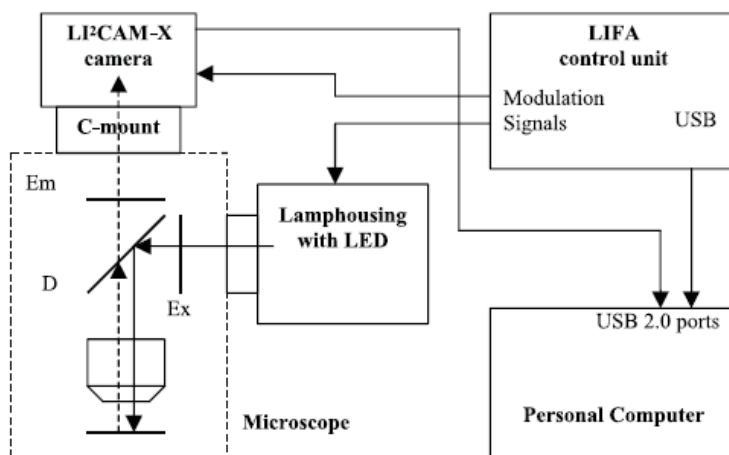


Figure 4.1: Schematic overview of the LIFA setup in \*\*Modulation\*\* mode with wide field microscope. The filter cube is represented as an excitation (Ex) and emission (Em) filter, and a dichroic mirror (D).

The excitation light from the LED first passes an excitation filter (Ex). Then it is reflected into the objective lens by the dichroic mirror (D). The sample is excited by the incoming photons, and emits light of a longer wavelength: we have fluorescence. This emission signal passes through the dichroic mirror and is filtered by an emission filter (Em). It then reaches the photocathode of the TRiCAM, to be intensified by the built-in image intensifier tube. You should select the filtercube that matches the wavelength of the LED (excitation), and the wavelength of the emitted fluorescence light of the specimen and the reference material figure 4.2. It is important that the LED emission is completely blocked by the dichroic and the emission filters.

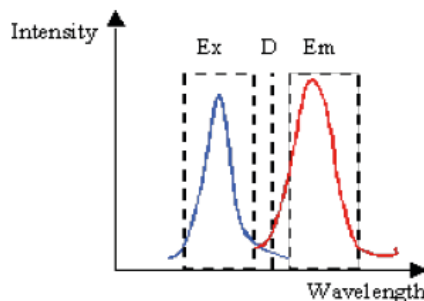


Figure 4.2: Selecting the filter cube to match the excitation (blue line) and emission wavelengths (red line).

In the case of FRET detection by FLIM, the LED and filtercube should match the excitation and emission wavelengths of the Donor fluorophore. The emission filter should be a bandpass filter that blocks the emission of the Acceptor fluorophore. See for example the following two FRET pairs:

*CFP-YFP FRET pair:*

- LED of around 440 nm,
- Filter cube with EX: 436/20 nm, DM: 455 nm, BA: 480/30 nm,
- CFP (Donor): Excitation peak = 439 nm, Emission peak = 476 nm,
- YFP (Acceptor): Excitation peak = 514 nm, Emission peak = 527 nm.

*GFP-mCherry FRET pair:*

- LED of around 480 nm,
- Filter cube with EX: 480/30 nm, DM: 505 nm, BA: 535/40 nm,
- GFP (Donor): Excitation peak = 484 nm, Emission peak = 507 nm,
- mCherry (Acceptor): Excitation peak = 587 nm, Emission peak = 610 nm.

The fluorescence lifetime is determined on a per-pixel basis, by modulating the LED light source and the gain of the camera at different phase shifts with respect to each other. This process is automated by LI-FLIM to easily acquire all data needed to calculate the spatial distribution of the lifetime(s) of a specimen. Recording a lifetime image usually takes only a few seconds. For a more detailed description of the theory behind frequency-domain FLIM, please refer to chapter "Theory", and the referenced literature.

## 4.2 Startup

Before you power up the LIFA system, make sure that the microscope is set up to direct all the light to the eyepiece. This ensures that no light can reach the intensified camera by accident. Switch on the LIFA system, and then launch LI-FLIM by clicking on the LI-FLIM 1.2.19 icon on the desktop, or the LI-FLIM 1.2.19 entry in the Windows Start menu, under the Lambert Instruments section.

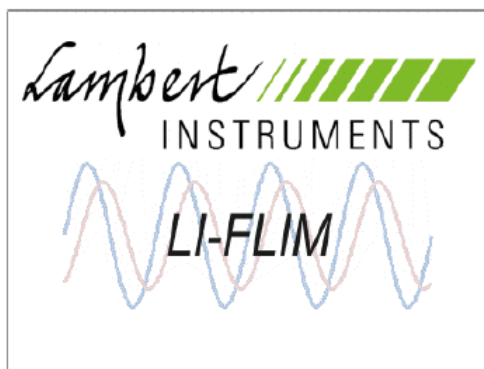


Figure 4.3: *Splash screen of LI-FLIM.*

When LI-FLIM is starting up, it will show a splash screen (figure 4.3). During this time, the software is trying to detect all connected hardware. If the LIFA control unit and the TRiCAM camera are correctly connected, and powered, then the software should detect the presence of these two devices. You can also use LI-FLIM without any hardware connected, but then you will not be able to do lifetime measurements, but only analysis of data that was recorded earlier.

### 4.3 Layout of the main window

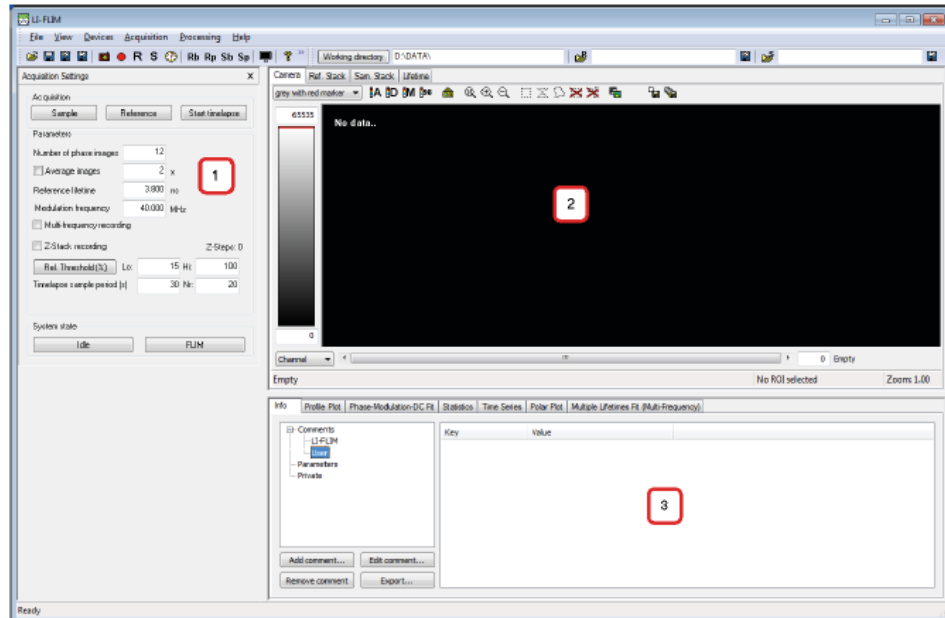


Figure 4.4: Layout of the main window of LI-FLIM. 1. Hardware view, 2. Data view, 3. Info view.

LI-FLIM's main window consists of three parts (figure 4.4). At the left, there is the *Hardware view* section. It contains the Acquisition Settings window, and the hardware control windows. In the displayed image there are no control windows present, standard there is one for the LIFA and for the TRiCAM. If your system has other hardware that is controlled by LI-FLIM, the corresponding control windows should show up in this part of the main window. You may need to use the scrollbar at the right side of the *Hardware view* section to see all device control windows. If not all devices show up in this section, then you should close LI-FLIM and check if all systems are connected correctly and are powered. If the missing devices still do not show up after restarting LI-FLIM, please contact Lambert Instruments for support. At the top right we have the *Data view* section. The recorded images and the calculated lifetime data will show up in this part of the main window. You can select which data you want to see by clicking on one of the tabs at the top of this section. We will see how this works when we record a Reference. At the bottom right part of the main window, we have the *Info view* section. By selecting one of the tabs at the top of this section, you can see various types of information about the recorded data. For example: you can see the statistics of all defined regions of interest on the lifetime data. Or you can inspect the sine that was fitted through the recorded phase-images in a single pixel. To summarize: at the left side, the *Hardware view*, you control the hardware and the acquisition of images. At the top right side, the *Data view*, you can see the recorded images, and the calculated lifetime data. At the lower right, the *Info view*, you can see various types of information about the recorded and calculated data. Note: this layout is set as default when LI-FLIM is started for the first time. You can change the layout to suit your needs by using the *View -> Options* menu. Please refer to "Reference guide" chapter for more detailed information on changing the layout. Recently a 'basic' and 'expert' view have been added to LI-FLIM since version 1.2.10. As a standard LI-FLIM is used in basic view, where only a limited number of settings can be used in the Acquisition Settings, the Lifa Settings and the TRiCAM settings. For less experienced users, the LI-FLIM software will be easier to use.

## 4.4 Recording a Reference

Before LI-FLIM can determine the lifetime of a specimen, it must know the "system phase" and "system modulation" of the entire setup. The fluorescence lifetime for a single pixel is calculated by recording the phase shift and decrease in modulation depth of the emitted fluorescence light coming from the sample (see chapter "Theory"). By recording a Reference, the software knows the system's phase and modulation for a lifetime of  $t=0\text{ns}$ . Every deviation in phase and modulation of the sample's emitted fluorescence corresponds to a certain lifetime. In this guide, we will first record a Reference, and then a Sample. Often, you will want to do this the other way around. The specimen of which you want to determine the lifetime may emit very little fluorescence. In that case you would want to optimise the measurement of the Sample, and afterwards record the Reference. Most of the time it is easier to change the amount of fluorescence coming from the reference material (by changing the concentration for example), than from the sample of which the lifetime is to be determined. If you start with a very bright Reference material, you may find that you have to use inconveniently long exposure times or very high intensifier gain settings for recording the sample. It is generally best to keep the intensifier gain setting the same between a reference and a sample recording for getting the most accurate lifetime measurements.

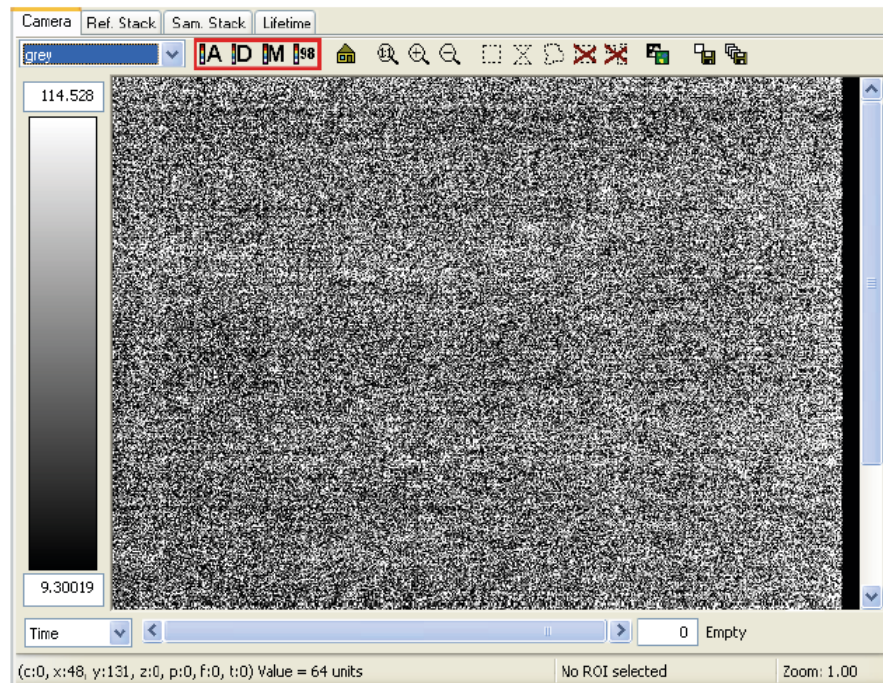
We start by placing the reference material (in our case a piece of fluorescent plastic) under the microscope. We make sure that all light is directed towards the eyepiece of the microscope, and then switch on the LED by clicking FLIM (figure 4.5) The Green box "Gated Closed" should become yellow "Gating active" to signify that the camera is active and the LED is indeed "on".



Figure 4.5: Switching on the LED by pressing "FLIM" in the Hardware view section.

Now try to bring the reference into focus by looking through the ocular of the microscope. This is often not an easy thing to do, because for example a fluorescein solution or fluorescent plastic does not have any structures on which you can focus. You can focus by finding the position that results in the brightest image. You could also try to set the field diaphragm half-open, and then try to focus on the projected diaphragm shadow.

We are ready to start the Live video mode, by pressing "FLIM" an image appears in the Camera tab of the Data view section. The intensity values from the camera images are mapped to displayed image colors using the colormap shown at the left side of the Camera window. In our case, intensity values below 9.3 are set to black, values above 114.5 are set to white, and values in between will get their corresponding level of grey (figure 4.6). Because the emission light is directed to the eyepiece of the microscope, and not to the camera, we should see noise only. If you see a completely black or completely white image, you should adjust the color limits. To change these limits, you can either enter new values by hand, or click one of the four toolbar buttons (figure 4.6)



**Figure 4.6:** Toolbar buttons to change the colormap limits. A - Scale to Absolute minimum and maximum. D - Scale to minimum and maximum data value. M - Scale to average plus and minus one standard deviation of the entire image data. 98 - Scale to fit 98% of the image data. Only camera noise is visible and displayed with the Grey Colormap

To see the noise, you would click the "98" toolbar button, to fit the colormap limits to the minimum and maximum values in the camera image, ignoring outliers (dead or hot pixels). Now we can direct the emitted fluorescence light to the camera port of the microscope. Although the gain of the intensifier is low (usually 400V, 450V after starting LI-FLIM), you should already start seeing the image become brighter. You may need to click the "98" toolbar button again to see a dim image appear instead of pure white. As a side note: if your microscope has an 80/20 camera port, and not a preferred 100/0 port, then the sample or reference is partly illuminated by ambient or background light from the environment (e.g. sunlight) that enters the oculars. If this is the case, make sure that the oculars are covered with black cloth to avoid any unexpected background light influencing the measurements. At this point, it is best to select the "grey with red marker" colormap (figure 4.7). This map has a clear indication for overexposed areas of the camera. We are going to increase the MCP voltage to increase the gain of the image intensifier until we have an image on screen that makes use of the full dynamic range of the camera. To do this easily, we want to see overexposed parts of the image clearly.

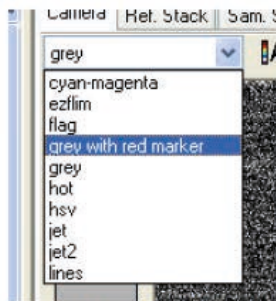


Figure 4.7: Select the "grey with red marker" colormap from the drop-down list in the toolbar.

Now click the "A" button in the toolbar to set the colormap limits to Absolute (0 - 65535). Before we can take a reference we first need to make sure that we setup the right MCP value and therefore we need to find the phase setting that results in the brightest image on screen. The emission and detector signal will go in and out of phase with respect to each other while stepping through the 0 - 360 degrees, resulting in a sinusoidal variation in intensity. Keep the phase setting at the position that results in the brightest image, to make use of the full dynamic range of the camera start increasing the MCP voltage until you have an image that is as bright as possible, without overexposing any part of it. If needed, you can zoom the image in and out quickly by using the scrollwheel of the mouse while the pointer is over the image. You may have to click once inside the image area to make it "active" before the scrollwheel works.

We are now set to record the reference phase stack. Click the "Idle" button in the Acquisition Settings window, and fill in the correct lifetime of the reference material (figure 4.8). In our example, this is 3.8ns for a fluorescent plastic. Then enter the number of phase steps taken during recording, in our example, we use 12 phase steps. This is normally a good compromise between measurement speed (less phase steps is faster) and accuracy (taking more phase steps results in more accurate measurements). If everything is set, click the Reference button (figure 4.8). The system will now be set to record a background image first while the lightsource is off, and then the 12 phase images using the "FLIM" settings we stored earlier. After the recording is finished, the system will return to Idle state automatically. During a measurement, a progress indicator is displayed along with a "Cancel" button. If you want to cancel the measurement for some reason, you can click this button. The system may need some time to react. After cancelling a measurement, the system will return to the Idle state.

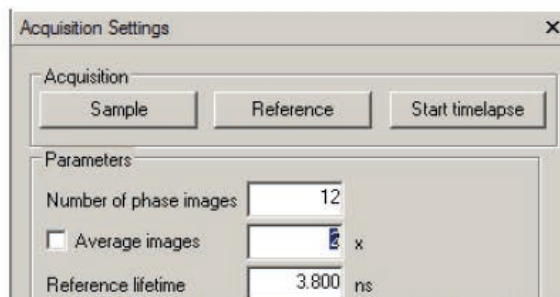


Figure 4.8: Fill in the reference lifetime and the number of phases. Then click the "Reference" button to start recording the reference.

The "Ref. Stack" data tab has been filled with new data it contains the recorded phase images. Let's look at the "Ref. Stack" by clicking on the corresponding tab. We can walk through the phases by selecting the

"Phase" dimension and moving the scrollbar at the bottom of the Data view section. We can have a look at the intensities of a single pixel and the sine that is fitted through those intensities, by selecting the "Phase-Modulation-DC fit" tab in the Info view section. You can move the cursor by clicking somewhere in the phase stack image with the left mouse button (figure 4.9).

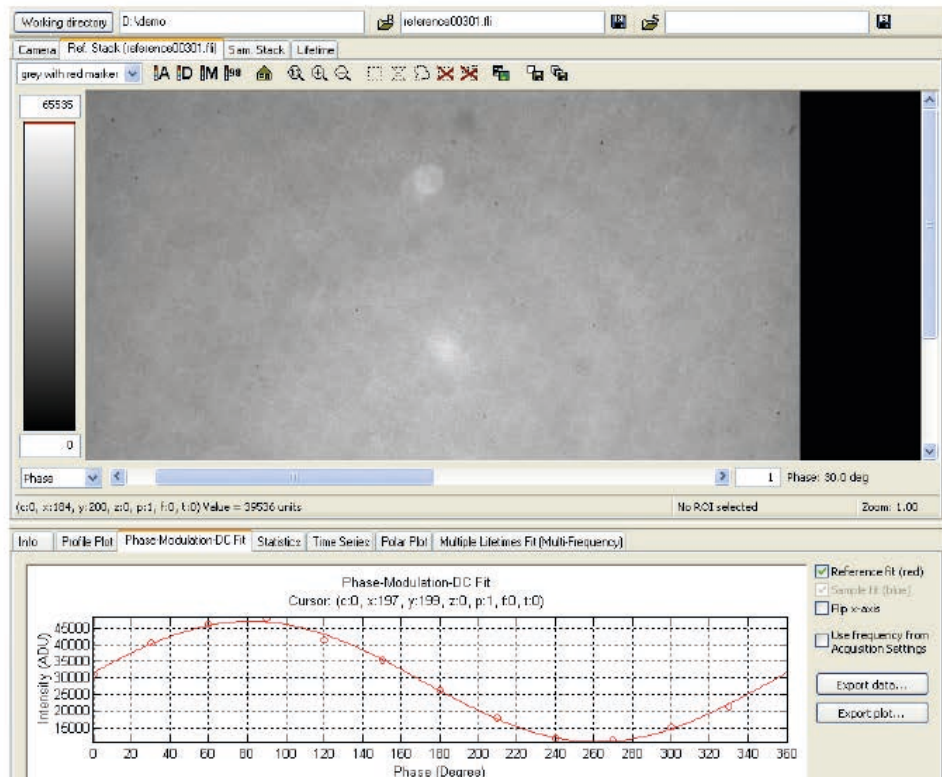


Figure 4.9: Viewing the sine fitted through the phase intensities of a single pixel in the reference stack. First select the Ref. Stack tab , then walk through the phase images by selecting the Phase channel (Dropdown below the colormap) and using the horizontal scrollbar to see the images that we recorded. In the Info View section, you can see the sine fit through the phase intensities by selecting the Phase-Modulation-DC Fit tab.

The reference phase stack has automatically been given a new (file)name, in our case it is reference00301.fli. By default, the auto-saving option is off (see Chapter "Reference Guide", the LI-FLIM Options window for more information on using auto-saving), so we will save the recorded data by hand. First, select a suitable folder in which we are going to save all our data by clicking the "Working directory" button. You can select an existing folder, and also create new folders in the window that pops up. Next, click the "Save Reference" button to save the Reference phase image data we have just recorded.

We are now done recording the Reference. It is time to place a specimen of which we want to determine the lifetime under the microscope.

## 4.5 Recording a Sample and calculating the lifetime

The specimen that we are going to measure in this example has different fluorescent properties than the reference material. Most notably, there is a lot less emission light coming from the sample. We can overcome this by increasing the exposure time of the camera, and changing the Neutral Density filters if

present. These two parameters are also the only two things you can safely adjust between recording a reference and a sample. The MCP voltage should ideally not be changed, in some case it is allowed to change but ideally not more than about 5 to 15 Volt, the amount of allowed voltages can be found in the Testsheet, there is a special lookup table. All other parameters should be kept the same, otherwise the reference will be invalid, and as a result the calculated lifetimes too. Note that changing the setup of the microscope, by selecting another filter cube, changing the diaphragm or selecting another objective lens, can also invalidate the reference. Let's start by placing the specimen under the microscope and focussing it using the eyepiece. We set the LED to 200 mA to get a bit more light. When the specimen is in focus, we turn off the LED and switch the microscope to output 100% of the light to the camera port.

We will now take three steps in one to get a brighter image. We will increase the exposure time of the camera to catch more photons per image than we do now with 100 ms exposure time. We will also increase intensify of the excitation light by removing an ND filter. And, while in the process of adjusting these two parameters we will switch to FLIM mode, and find the brightest phase, and finetune the exposure time further, in the same way as we did when recording the reference. By increasing the exposure time, you catch more "primary photons" and reduce the relative photon noise, at a cost of longer acquisition times. By increasing the MCP voltage, you also intensify the photon noise, but you can do faster acquisitions on an image that uses the full dynamic range of the camera, decreasing the relative contribution of (digitisation) noise from the camera itself.

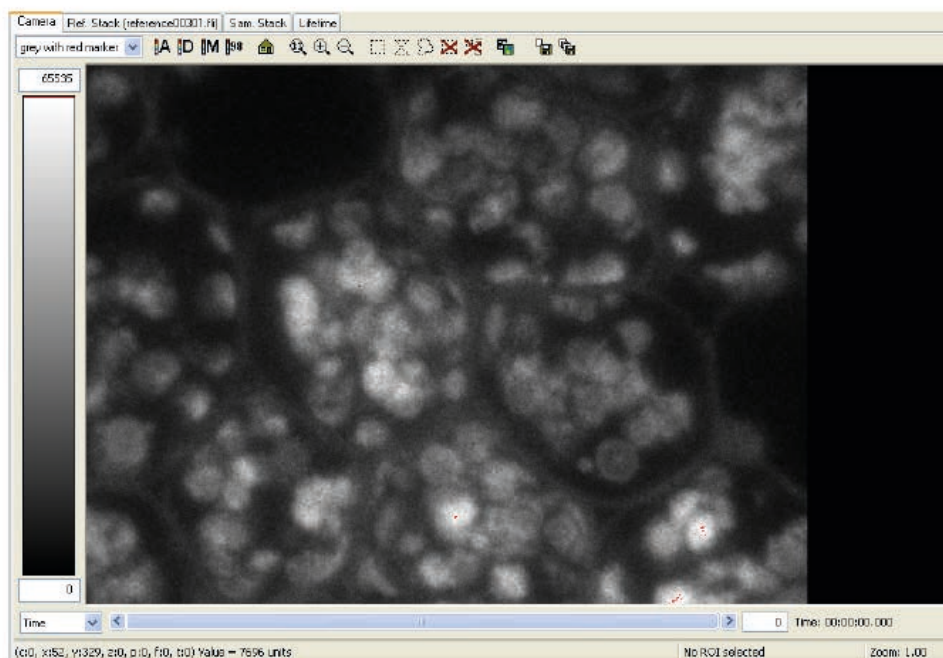


Figure 4.10: The system is in the FLIM state (modulation signals are on), and the MCP voltage and exposure time have been adjusted to make use of the full dynamic range of the camera at the brightest phase.

Now we can record a Sample by clicking the "Sample" button in the Acquisition Settings window. A new background image is recorded, and stored in the (invisible) "Sam. Back" tab. Then the phase images are recorded, and stored in the "Sam. Stack" tab. Finally, the phase, modulation and DC data (the invisible "Sam. PMD" tab) and the lifetime image are calculated ("Lifetime" tab). The system is switched to Idle state automatically (figure 4.11).

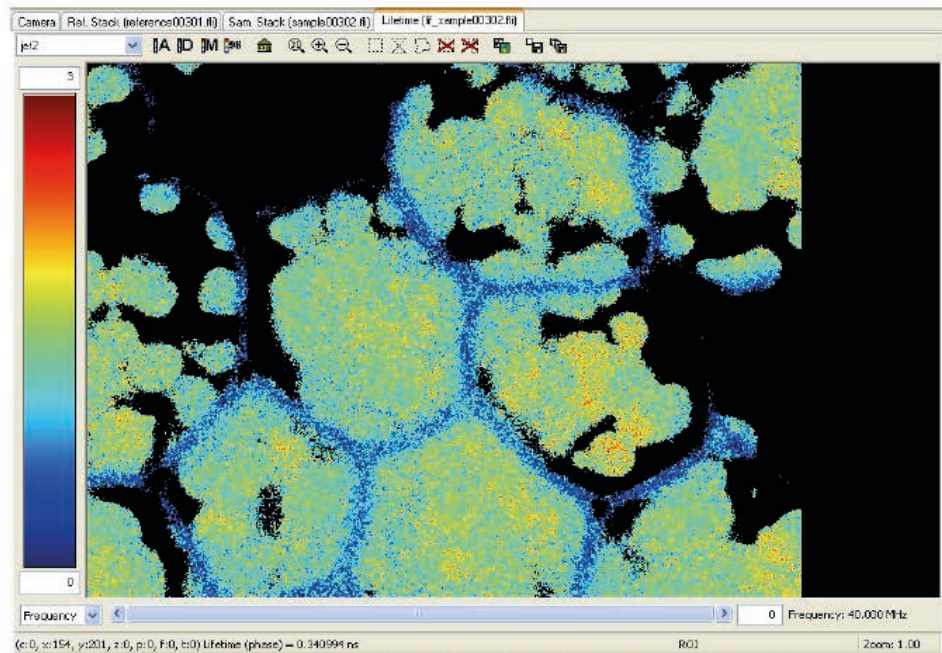


Figure 4.11: The resulting lifetime image. We selected the "jet2" colormap, and set the lower limit to 0 ns (blue) and the upper limit to 3 ns (red). Because the "Threshold" was set to 15%, some parts of the lifetime image contain no data (black).

The resulting lifetime image shows the per-pixel lifetime calculated from the phase shift of the Sample's fluorescent emission. The lifetime data has three channels: Lifetime from phase, Lifetime from modulation and DC intensity. The DC intensity channel is the average of the 12 phase images in the Sample stack. Because the "Threshold" value in the Acquisition Settings window of the Hardware View part was set to 15%, some parts of the image will have no lifetime data. At those pixels, the DC intensity was below the value of 15% of the maximum DC intensity in the image. If you want to change this value, you will have to select *Processing -> Recalculate Sample* in the main menu to let this change have any effect on the lifetime image. At this point we want to make sure that we save all data needed for analysis afterwards (see Chapter "Analysis"). An experiment is completely described with the Reference phase stack and the Sample phase stack. All other data (Phase-Modulation-DC and lifetime image) can be recalculated exactly from these two datasets. We already saved the Reference phase stack (as reference00301.fli), so we now have to save the Sample phase stack. Click the "Save Sample" button on the toolbar. In our case, it is saved as sample00302.fli. The FLI file format in which the files are saved by default is described in detail in Appendix B. Saving all these stacks can become cumbersome. LI-FLIM has an autosave option, that will automatically save every new Reference and Sample stack. See "Reference Guide" for more information on this subject. It is good to note that if you had first recorded the Sample, and afterwards the Reference, the lifetime image will not have been calculated automatically: that only happens after a new Sample is recorded, and not after recording a Reference. To calculate the lifetime image after recording a new Reference, you would click *Processing -> Recalculate Sample* in the main menu. See figures figure 4.12, figure 4.13 and figure 4.14, on how to do some simple statistical analysis on the data, and how to combine the intensity image with the lifetime image. The Reference and Sample that we recorded will be used in Chapter "Analysis" as basis for a more detailed description on how to analyse the results. We have now recorded our first lifetime image (time for some coffee?). The next two sections show two acquisition modes that we have not mentioned yet: Time lapse recordings and Multi-frequency recordings.

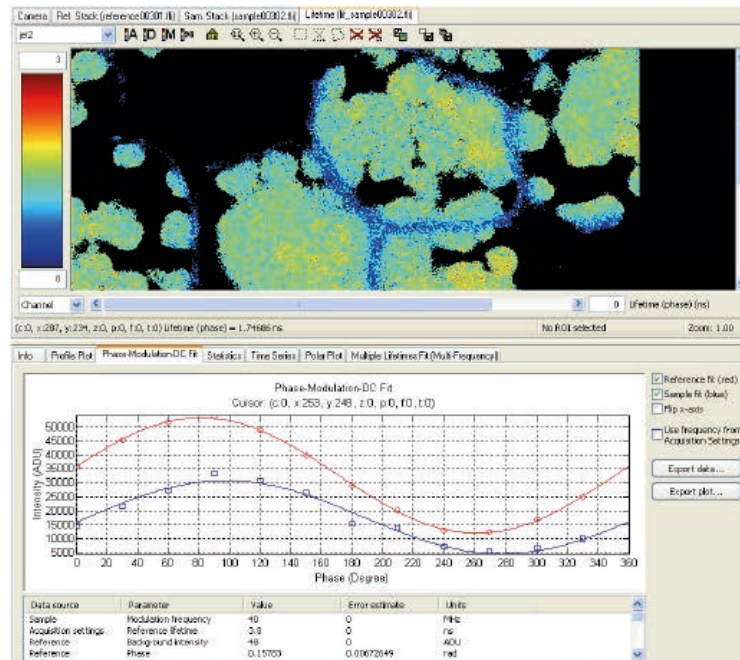


Figure 4.12: Showing the two sine fits through the phase intensities of a single pixel: the red line is the reference and the blue line is the sample at the same (X, Y) location. The blue line (sample) is shifted in phase and has a different modulation depth than the red line reference.

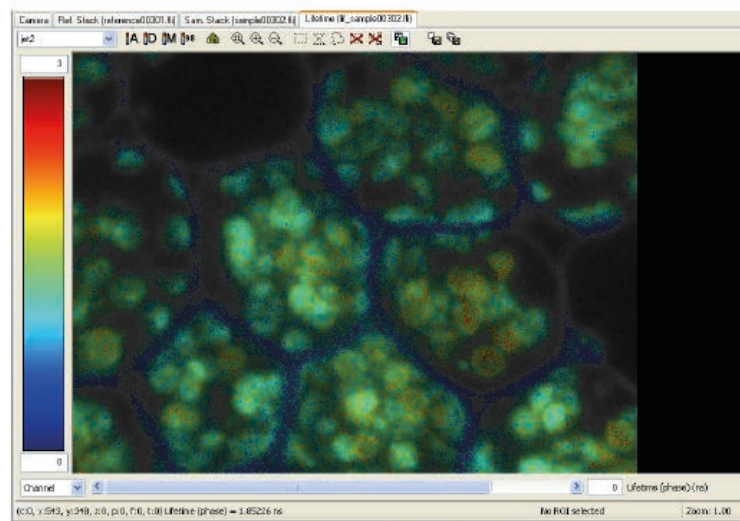


Figure 4.13: Combination of intensity values from the DC channel with the colormapped lifetime values of the lifetime channel. To do this, first go to the DC Intensity channel using the horizontal scrollbar, then adjust the colormap limits to get a nice image, then go back to the lifetime channel and select a colormap. Finally click the "Combine color" toolbar button.

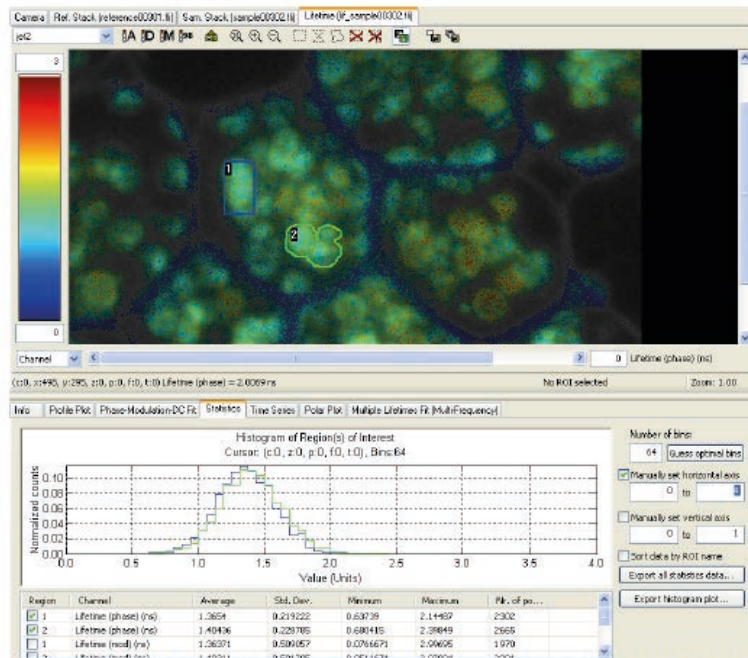


Figure 4.14: You can draw Regions of Interest using the encircled toolbar buttons, and see statistics in the Statistics tab in the Info View section. You can move regions of interest around by holding the SHIFT key, and click + drag the ROI to a new location.

## 4.6 Timelapse recordings

You can record samples at regular intervals to see changes in lifetime over time. To do this, we need a valid Reference, and a single Sample phase stack recording. In fact, only a sample background is enough: the system will record only phase-image stacks during a timelapse recording and uses the current background image for background subtraction. The easiest way to begin with a timelapse experiment, is to first record a normal Sample, to see if everything (intensifier gain, number of phase images you want to use, etc.) is set up OK, and then start the timelapse measurement. In this way, you will automatically have a valid sample-background image, and you have an idea about how long it takes to record a single sample stack.

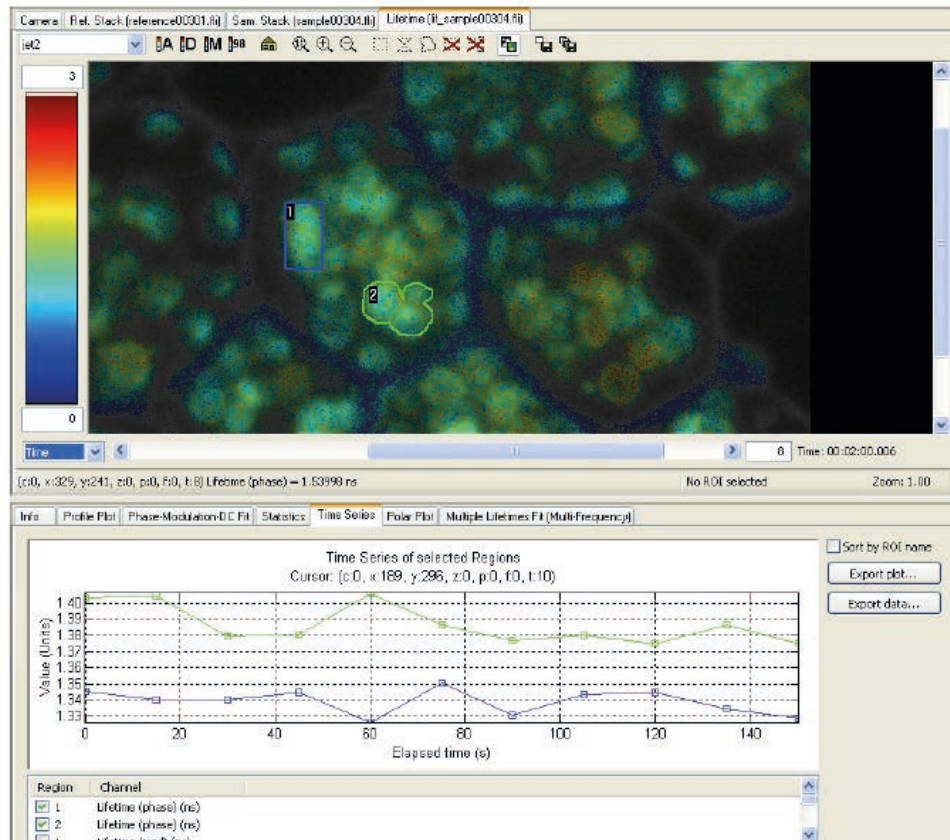


Figure 4.15: A time series measurement with 11 time-frames. 1. Enter the sampling period. 2. Enter the number of samples to record. 3. Enable, or disable, the Idle state between recordings (only in expert view). 4. Select the Time Series tab and select the regions of interest you want to follow. 5. Start the timelapse recording 6. Scroll back and forth through the data in the time dimension after the timelapse recording has completed.

To start a timeseries experiment, enter the sample-period, the number of samples you want to record, and decide if you want the system to return to "Idle" state between samples (figure 4.15). If you want to measure as fast as possible, then you can set the period to 0 seconds, and disable the "return to idle state" option. You should enable the "Always return to Idle" option if you are planning to measure for longer periods (say more than 10 minutes). Modulating the image intensifier for long periods of time has a negative effect on its lifespan. You should also create some ROIs on interesting locations, and select the data you want to follow during the timelapse by selecting the checkboxes in the "Time Series" tab. You cannot do this once the timelapse recording has started. Click "Start Timelapse" to begin the measurement. A progress indicator window pops up which shows you the number of timeframes that were already recorded, and an estimated time left to finish the entire recording. Click "Cancel" to prematurely stop the recording. Note that in this case, the sample is *not* automatically saved if you have enabled the autosave option of LI-FLIM. With the "Time Series" tab in the Info view section, you can plot the average values of the selected ROIs over time. This plot is continuously updated while recording a time series experiment. You can also scroll back and forth in the time dimension in the Data View tabs. All data collected (and calculated) for the "Sam. Stack", "Sam. PMD" and "Lifetime" tabs are available. However, LI-FLIM may feel a bit sluggish if you scroll through big time-series files. All data is stored in temporary files, and the time frame that you are viewing is loaded into the computer's RAM memory for fast access. If you scroll through the time dimension, new data must be loaded from these temporary files, which takes some small amount of time. Similarly, if you have a timelapse

experiment with a lot of timeframes, it will be difficult to move around ROIs (by holding the SHIFT key and dragging them with the mouse). Every time the ROI is displaced, all timeframes must be revisited to recalculate the ROI's statistics. The best way to move ROIs in the case of a large number of timeframes is to first select the "Info" tab, then move the ROI(s), and then select the "Time Series" tab again.

## 4.7 Multi-frequency recordings

Instead of recording a Reference and a Sample at a single modulation frequency, you can also choose to record at multiple frequencies. This has the advantage that, in theory, you will be able to determine multiple lifetime components per pixel and their relative fractions. However, this method is very sensitive to noise, so in practice we will not be looking at multiple lifetimes in single pixels, but instead we will take an entire ROI at once and find the lifetime components that are present in, for example, a single cell. There is one difficulty in recording a multi-frequency phase stack: the modulation depth of the LED varies greatly with the frequency, so you may find that at lower frequencies your Reference or Sample stack is overexposed at some parts of the image, while at higher frequencies you are not using the camera's dynamic range fully. With this version of LI-FLIM it is difficult to prevent this from happening. You will have to experiment with the exposure time setting of the camera or the MCP voltage setting of the LIFA to find reasonable values for the entire frequency range. In this example we will record phase stacks in the 10 – 80 MHz range, and we will use the settings that were found to be OK in the 40 MHz single frequency case. We will ignore a little amount of overexposure in the lower frequency phase stacks. Click the "Setup" button next to the "Multi frequency recording" checkbox in the "Acquisition Settings" window. The window shown in figure (figure 4.16) will pop up. We enter 10 MHz for the lowest frequency, 80 MHz for the highest frequency, and 7 for the number of frequencies. Next, click the "Generate logarithmically distributed list" button to update the frequency list at the bottom of the window. This exact list of frequencies will be used during the Sample and Reference recording. You can edit the list by hand if needed. Make sure that the "Number of exponentials to fit" (= number of lifetimes) is set to 1. This will speed up the per-pixel lifetime calculation, and we can always re-calculate the lifetime image using another number of exponentials. The other settings can be left at their default values. They are discussed in more detail in section 5.8.

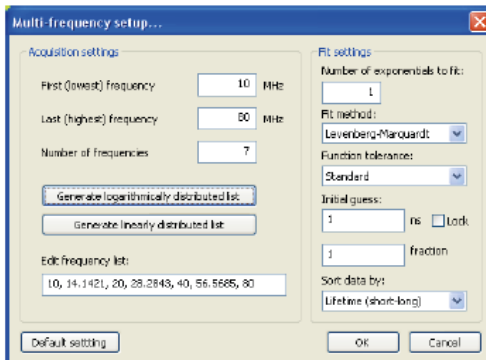


Figure 4.16: Multi-frequency setup window. Enter the lowest and highest frequencies to be used, and the number of frequencies. Then click the "Generate logarithmically distributed list"-button to update the frequency list at the bottom. Also make sure the "Number of exponentials to fit" is set to 1 for now.

After clicking "OK", we enable the "Multi frequency recording" checkbox in the Acquisition Settings window. As we have our Sample still under the microscope, we click the "Sample" button. The system will start with taking a background image at every frequency, and continue with recording an entire phase stack of twelve images at every frequency in the list. When the sample is recorded, we save it to disk, resulting in a ~45 MB file, which contains 7 background images and  $7 \times 12 = 84$  phase images, all loss-less compressed into a single file. Next we place the Reference material under the microscope and find the optimum settings for 40

MHz. Then, we make sure the "Multi frequency recording" checkbox is still enabled and click the "Reference" button to record a multi-frequency Reference. In this case, the lifetime image is not automatically recalculated after recording the Reference (that is done only after recording a new Sample), so we will do that by hand: select *Processing ->Recalculate Sample* from the main menu. Note: The frequency will not automatically be reset to the single frequency value it had before.

If we look at the Statistics tab we see that the lifetime image now has four channels: A *Lifetime 1, Fraction 1*, *Chi-square* and *DC intensity* channel. If you had entered more than one exponential in the multi-frequency setup window (figure 4.16), then you would find more channels here: every extra exponential adds a lifetime and fraction channel. In this single-lifetime-fit case, the lifetime image looks fine. But when fitting multiple lifetimes per pixel, the data will usually look very noisy, having pixels with lifetime components of billions of nanoseconds, with a very tiny fraction for example. In that case, the Statistics tab does not help very much in the analysis of the results. Instead we will select the "Multiple Lifetimes Fit" tab in the Info View section for analysis (figure 4.17).

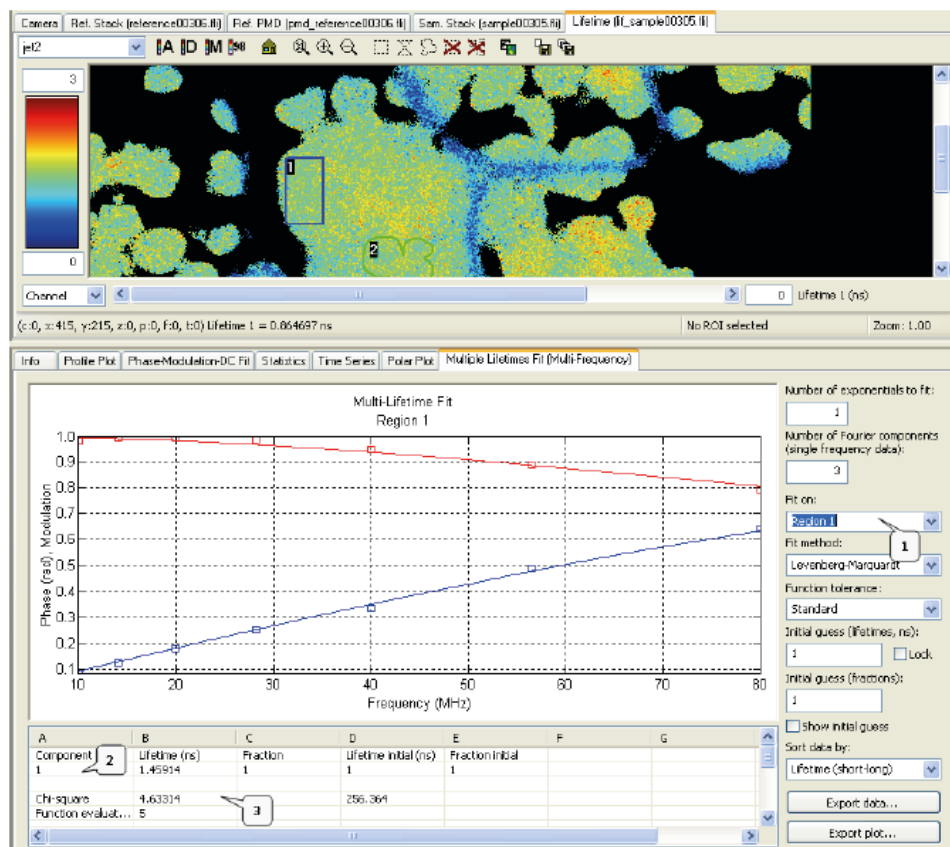


Figure 4.17: The Multiple Lifetimes Fit tab. In this tab, the Phase (blue line) and Modulation (red line) are plotted for a single pixel, or region(s) of interest. In this case, Region 1 is selected (1). The table (2) lists the Lifetime and Fraction for every lifetime component found by trying to find the best fit for the selected number of exponentials through the phase and modulation data. Chi-square is a measure of the goodness-of-fit (3).

In the Multiple Lifetimes Fit tab (figure 4.17), we can extract multiple lifetime components from a single pixel, a region of interest, all regions combined, or the entire image. In our case, we want to look at region 1. If you know the number of lifetime components present beforehand, you can enter them in the "Number of

exponentials to fit" edit box at the top left of the Multiple Lifetimes Fit tab. In this example, we do not know how many lifetime components should be present. In that case, we start with fitting for a single component, and note the value of Chi-square. Then we start increasing the number of components and see if Chi-square gets smaller by a significant amount (say 2x smaller). If Chi-square hardly gets any smaller, or increases, then we know that our new "model" is wrong.

Table 3-1. Chi-square values for different number of exponentials to fit. This shows that the single-exponential model is the best one for our sample.

Number of exponentials to fit	Chi-square
1	4.6
2	5.5
3	6.8 (figure 4.18)

Table 3-1 shows the results in our case. The single-exponential model is the best one for our sample (at least for the data in region 1). When fitting more exponentials, we get an increasing Chi-square. What you will generally see in the list of lifetime components when you are fitting too many exponentials, is that several components have almost exactly the same lifetime, or wildly different lifetimes (say thousands of nanoseconds) with tiny fractions (0.00001 for example, see also figure 4.18). This is also a sign that the model is a bad one, and the number of exponentials to fit should be reduced.

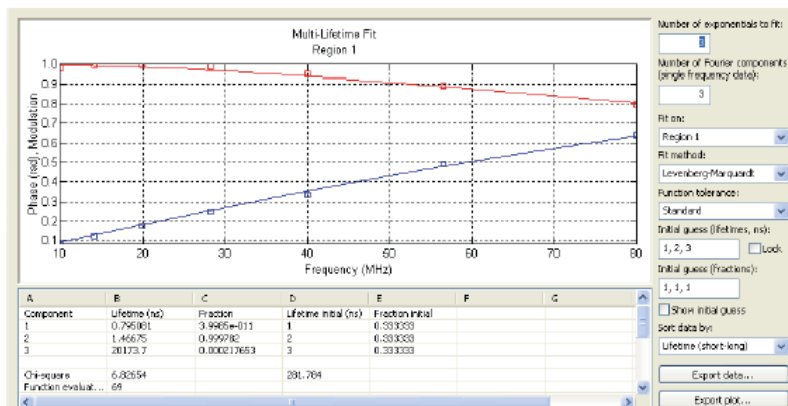


Figure 4.18: Three component fit. Two lifetime components (1 and 3) have very small fractions: a sign that there are less than three lifetime components present in the sample.

We now have seen the three basic measurement types: a single Reference and Sample, a Timelapse sample, and a Multi-frequency Reference and Sample. The next chapter will go into more detail about how to optimise your measurements. Chapter "Analysis" shows you how to analyse the samples you recorded in more depth: the buttons, edit fields, check boxes etc. that we did not discuss in this chapter will be explained there.

## 4.8 Summary

### 1. Recording the Reference

- I. Start LI-FLIM software
- II. Place reference material with known mono-exponential lifetime under the microscope
- III. Switch the light beam to the eye port of the microscope
- IV. Set the LED current to 100 mA or laser to 10 mW
- V. Switch the LED/laser on by clicking the LED DC/MOD. DC checkbox

- VI. Focus using the eyepiece
- VII. Click "Idle" to switch off the LED/laser
- VIII. Switch the light beam to the camera port of the microscope
- IX. Set the MCP voltage to minimum (400 V) and the Exposure time to 100 ms
- X. Click "FLIM" to switch on the LED/laser and the image intensifier in modulation mode
- XI. Draw a region of interest in the middle of the camera image
- XII. Enable the Statistics tab and find the average ADU value
- XIII. Determine the brightest phase (= highest average ADU) by sliding the phase control from 0 to 359 (if you do not see a difference between phases incrementally increase the MCP voltage by 10 V)
- XIV. To make use of the whole dynamic range of the camera, increase the MCP voltage until the maximum ADU in the statistics reaches 55.000-65.000 (anything above 65.000 means overexposure and thus possible damage to the camera). You might also want to adjust the Exposure time
- XV. Click "Reference" to record a reference phase image stack
- XVI. Click "Save Reference" to store the stack on disk (obsolete if Autosave is enabled)
- XVII. Remove the reference material
- XVIII. Switch the light beam to the eye port of the microscope

## 2. Recording the Sample

- I. Unless noted here do not change any parameter of the system between reference and sample!
- II. Place specimen under the microscope
- III. Switch the LED/laser on by clicking the LED DC/MOD. DC checkbox
- IV. Focus using the eyepiece
- V. Click "Idle" to switch off the LED/laser
- VI. Select "Edit comment" on the Info tab and give a description of your sample (very useful afterwards)
- VII. Set the MCP voltage to minimum (400 V) to prevent overexposure
- VIII. Switch the light beam to the camera port of the microscope
- IX. Click "FLIM" and determine the brightest phase and optimal MCP and Exposure time settings. Best results are obtained with approximately the same MCP voltage ( $\pm 15$  V) as used for the reference. Exposure time may be increased
- X. Refocus the microscope using the camera image if necessary
- XI. Click the "Sample" button to record the sample phase stack and get a lifetime image
- XII. Don't forget to save your data!

Note that you can safely change the

- Exposure time of the camera
- ND filters

between recording a reference and a sample. Every other parameter should be kept at the same value. You should also *not* change the filter cube, objective lens of the microscope or diaphragm between reference and sample. Changing one of these things may result in inaccurate or invalid lifetimes. If you exit LI-FLIM, all acquisition settings and hardware parameters will be stored. The next time LI-FLIM is started, these values will be restored, except for the MCP voltage (to prevent accidental overexposures).

## 6 Analysis

---

This chapter will explain how to analyse the samples you record. Either directly after recording them, or afterwards after loading previously stored samples. You can also run LI-FLIM on a computer with no hardware attached to analyse stored data.

We will load the files that were stored while performing the steps in Chapter "Optimising lifetime measurements". The results are completely uninteresting from a biological point of view. Instead, we will focus on how to do the analysis and not on the results we get.

The currently selected Info tab generally shows information about the currently selected data tab: if you have selected the Statistics tab and the Lifetime tab, then you are watching the statistical data of the Lifetime image.

Most Info Tab windows will update themselves "live". For instance, the Statistics tab can show live histograms and statistical data while the camera is running. This means that the computer may become a bit sluggish if you have drawn many regions of interest, and are displaying the statistics and histograms during live video mode. Similarly, if you select the Time Series tab, and you have a Sample with many timeframes, it will take some time before the tab is displayed: all time frames stored in a temporary file on the hard disk are visited, to update the statistics of all ROIs before the data can be displayed.

Note that the "Reference Guide" refers to this chapter for a detailed description of the various Info View tabs.

### 6.1 Preparation

---

Before we begin describing the different Info View tabs, make sure that you have a Reference and a Sample file ready. Either by recording a new Reference and Sample, or by loading them from disk using the File menu or the Working Directory toolbar. When loading a Reference or Sample directly after starting LI-FLIM, or when loading a Reference or Sample phase stack that has a different number of pixels, you may see the window in figure 6.1 being displayed. LI-FLIM was not able to calculate a lifetime image using the Reference and Sample data that are currently loaded. Once both Reference and Sample tabs contain compatible phase stacks, then a Lifetime image can be calculated automatically.



Figure 6.1: An error is displayed when LI-FLIM cannot recalculate the lifetime image after loading a new Reference or Sample stack. You can turn off automatic recalculation of the lifetime image in the LI-FLIM Options to prevent this error message from being displayed.

Make sure that you now have a valid lifetime image. Check if the entered Reference lifetime is OK. If not, enter a new value and select *Processing -> Recalculate reference* and *Processing -> Recalculate sample* if needed.

## 6.2 The Info tab

The “Info” tab (figure 6.2) shows data in text format that is stored with the image data currently selected.

The screenshot shows the 'Info' tab of a software interface. On the left, there is a tree view of comments and parameters. Under 'Comments', 'LI-FLIM' and 'Polar Plot' are listed, with 'User' expanded to show 'LI-FLIM' again. Under 'Parameters', 'ACQUISITION SETTINGS' is expanded to show 'LICAM 45504' and 'LIFA 06010'. At the bottom are buttons for 'Add comment...', 'Edit comment...', 'Remove comment...', and 'Export...'. On the right is a table titled 'Key' and 'value' with one entry: 'Objective' = '60x, Oil'.

Key	value
Objective	60x, Oil

Figure 6.2: The Info tab showing data of the Sample stack.

You can add, edit and remove comments. They take the form “Key = value”. In this example, a user comment “Objective = 60x, Oil” has been added. Every Data view tab has its associated Info. When you enter a new comment for the Sample stack, it will not show up in the Reference stack. When the data (i.e. the Sample stack) is saved, this info, including the user comments, are stored with it.

LI-FLIM remembers the last entered user comments for every Data View tab. When LI-FLIM is restarted, those comments will already be present, even if no data is loaded/recorded yet.

For every new Sample, the Parameters section (figure 6.3) is updated with the parameters used for recording it. Here you can see which settings were used for a specific sample.

The screenshot shows the 'Info' tab with a more detailed view of parameters. The tree view on the left shows 'Comments' and 'Parameters' expanded. Under 'Parameters', 'ACQUISITION SETTINGS' is expanded to show 'LICAM 45504' and 'LIFA 06010'. At the bottom are buttons for 'Add comment...', 'Edit comment...', 'Remove comment...', and 'Export...'. On the right is a table titled 'Key' and 'Value' with multiple entries, including CathodeAC, CathodeDC, CathodeDC-FLIM, CathodeDC-Focus, EdgeType, Frequency, LEDAC, LEDDC, LEDDC-FLIM, LEDDC-Focus, MCP, Phase, and UseTrigger.

Key	Value
CathodeAC	-12.0 dBm
CathodeDC	-0.2 V
CathodeDC-FLIM	-0.2 V
CathodeDC-Focus	-10.0 V
EdgeType	1
Frequency	40.000 MHz
LEDAC	2.0 V
LEDDC	100 mA
LEDDC-FLIM	100 mA
LEDDC-Focus	100 mA
MCP	700 V
Phase	90 deg
UseTrigger	0

Figure 6.3: Parameters of the LIFA during recording of the Sample stack.

With the “Export” button you can store all Info data as a text file. Note however that this text file cannot be used to set all connected hardware back to the state that it was in at the time the image stack or lifetime image was recorded/calculated.

### 6.3 The Profile Plot tab

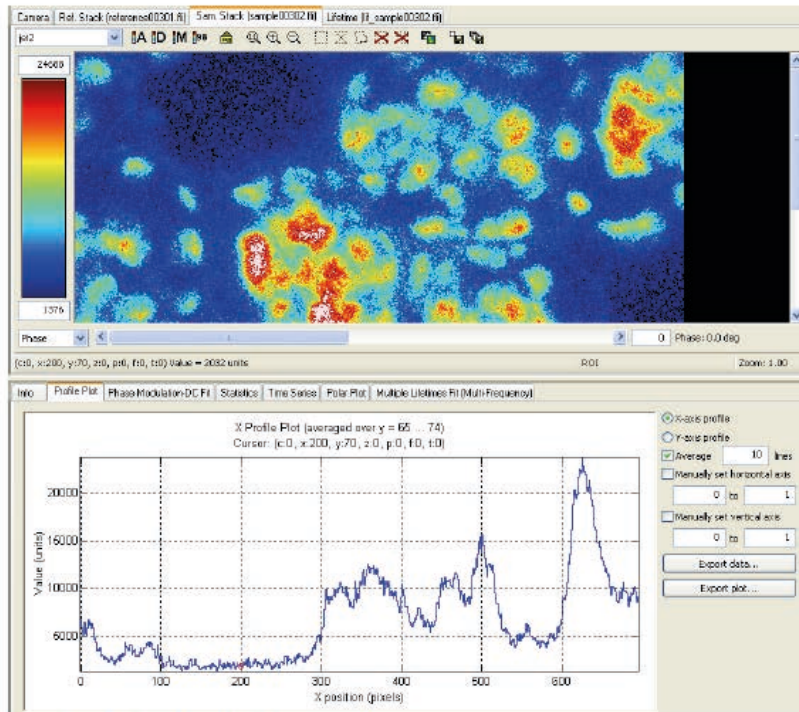


Figure 6.4: Profile plot of the Sample stack.

The profile plot shows the pixel values of the selected Data tab (figure 6.4) along the X or Y direction at the current cursor location. You can change the cursor location by left-clicking in the image in the Data View section.

You can select an X or Y axis profile (see right hand side of figure 6.4), and the number of lines to average. In this example, we have set averaging to 10, to smoothen the plot. The ranges of the horizontal and vertical axes of the plot can be set to fixed values, to prevent auto-scaling.

The data of the plot can be exported ("Export data" button) as a Comma Separated Value file, or an Excel sheet. The plot itself can be exported as a bitmap image ("Export plot" button).

A small red circle in the plot shows the actual cursor location along the selected axis (in this example it is displayed at x = 200).

## 6.4 The Phase-Modulation-DC Fit tab

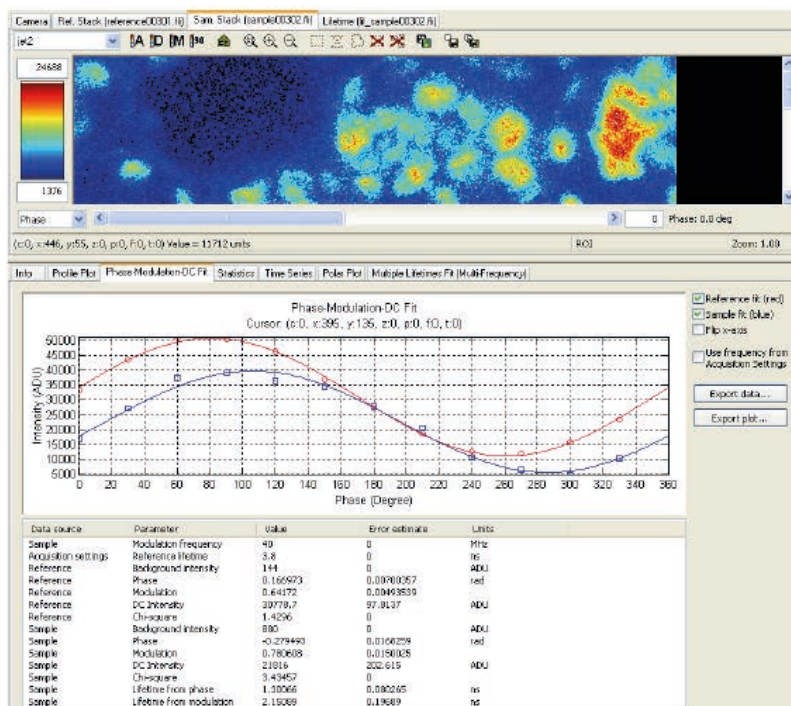


Figure 6.5: The Phase Modulation DC Fit tab shows the phase intensities of a single pixel in the Sample and Reference phase stack.

The Phase-Modulation-DC Fit tab (figure 6.5) shows the phase intensities of a single pixel of the Reference and Sample phase image stack. You can change the cursor location by left-clicking inside the image displayed by the currently selected Data tab. It is not important which Data tab is currently selected, because the data from the Reference Stack and Sample Stack tabs is always used. You may want to select the Lifetime tab, and set the cursor to interesting locations in the image, for instance.

The red line is the sine fit through the Reference phase stack intensities. The blue line is the fit through the Sample phase stack data. The hollow squares are the actual measured intensities at the cursor location.

You can export the data ("Export data" button) as a Comma Separated Values text file, or an Excel sheet. The plot itself can be exported ("Export plot" button) as a bitmap image.

The table below the plot shows the calculated values for Phase, Modulation, DC Intensity and lifetime along with an error estimate. These error estimates, (and the Chi-square), are really just that: estimates. Li-FLIM does not directly fit a lifetime for a pixel: it fits sine waves through the Reference and Sample data, using a Fourier transform, and from those sines, the lifetime is calculated. Because the image intensifier gain and the LED lightsource are not modulated with a pure sine wave, there will be higher order components present. Li-FLIM cannot determine easily if deviations from the fitted first order sine are due to noise, or to higher order components. For the error estimates, all deviations from the fit are assumed to be caused by noise. This usually gives an error estimate that is higher than the actual value, but still gives an indication about the accuracy of the measurement.

In practice, you can use this Info tab to quickly determine if something went wrong during a Sample or

Reference recording. You can see at a glance if there is very noisy data, invalid data (e.g. half of the sine is OK, but for the last part all phase intensities are equal), overexposure (if the actual phase intensities do not follow the sine at its top, but are clamped to the maximum intensity value of 65535), etc.

## 6.5 The Statistics tab

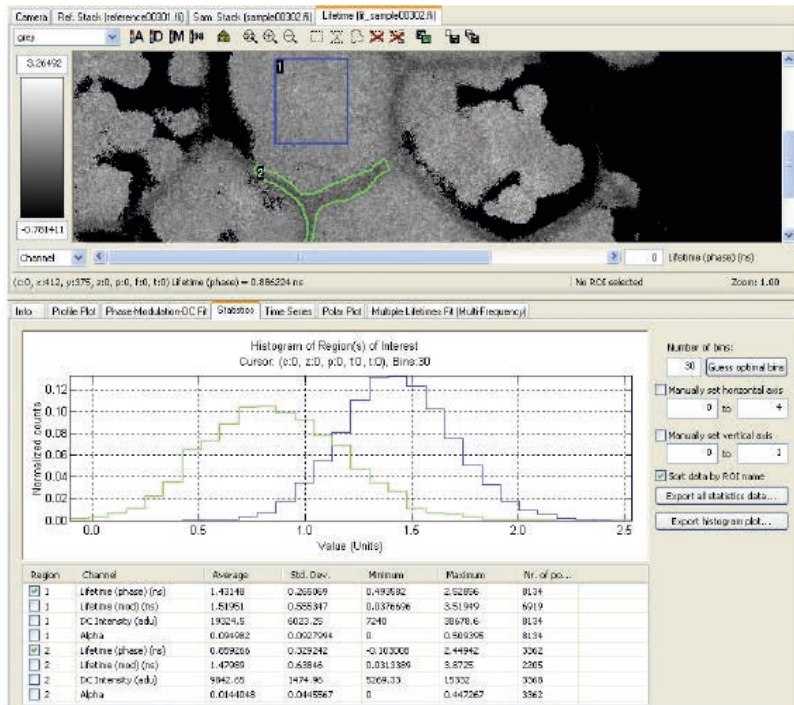


Figure 6.6: The Statistics tab showing histograms of both ROIs.

With the Statistics tab (figure 6.6), you can see statistical data of the pixels within the defined regions of interest. The statistics of the currently selected Data tab are shown, at the currently selected cursor location (phase, Z, frequency, time) of every channel present. In (figure 6.6), the Lifetime image is selected, and the four channels Lifetime (phase) (ns), Lifetime (mod) (ns), DC Intensity (adu) and Alpha are listed in the table for every region of interest.

Every line in the table shows the Average, Standard Deviation, minimum value, maximum value and number of valid pixel values of the ROI. Different channels within the same Region of Interest may show a different value for "Nr. of points". In this example, the "Lifetime (phase)" channel contains a different number of "not a value" pixels, which are ignored for the statistics, than the "Lifetime (mod)" channel.

To display a histogram of the pixel values of an ROI, select the checkboxes in front of the data that you want to see. The displayed lines have the same color as the ROI that they belong to.

When viewing the statistics of intensity images, you can click the "Guess optimal bins" button to change the number of bins for the histogram to such a value that no "gaps" occur. The TRICAM produces 16 bit intensities, with a 12 bit resolution. This means that some values will never occur, and this could result in the histogram showing gaps, which may be annoying.

When looking at the Phase/Modulation/DC data, the phase may have a value close to  $+\pi$  or  $-\pi$ . If the actual

phase is near one of these values, then because of the noise, some of the pixel values will have "wrapped around" to the other end of the  $[-\pi, +\pi]$  interval. This will result in unexpected values for the average phase (it may end up close to 0.0!).

When looking at lifetime images, you may want to create a small region of interest, and move it around with SHIFT + left mouse button, to see the histogram changing as the ROI moves. In that case, it could be useful to enable the "Manually set axis" checkboxes, to fix the horizontal and vertical axes of the histogram plot.

If you select the lifetime channel of a multi-exponential lifetime image, you may get unexpected results for the average value of some ROIs: because single pixel data is often too noisy to get accurate lifetime results, there is a chance that one or more pixels in a region have extremely long lifetimes (say  $10^{15}$  ns). Such a pixel immediately pulls the average up to a nonsense number.

For calculating the lifetime from modulation of a ROI, two methods exist in LI-FLIM. Standard LI-FLIM takes the averages of the calculated Lifetimes and displays it in the Statistics table, but when one enable the "Use average Modulation" checkbox, LI-FLIM first calculates the average of the modulation and secondly calculates with that the Lifetime value.

Finally, you can export the statistics data and the plot as a Comma Separated Values text file, or an Excel sheet. The histogram plot itself can be exported as a bitmap image.

## 6.6 The Time Series tab

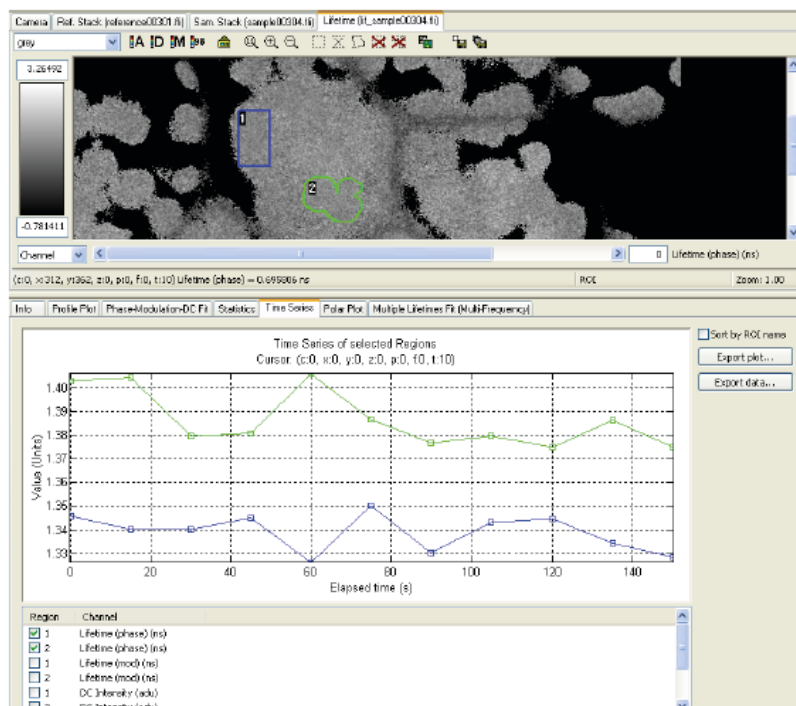


Figure 6.7: The Time Series tab, showing the average value of the Lifetime from phase of regions 1 and 2 plotted against the elapsed time in seconds.

With the Time Series tab you can see changes in the average value of a Region of Interest over time. In figure 6.7, the Lifetime tab is selected, and the average lifetime from phase is plotted for regions 1 and 2.

Note that when you have a large number of timeframes, then the Sample Stack, Sample PMD and Lifetime data will have their timeframes stored in temporary files that are several gigabytes in size. That means that every time you switch to the Time Series tab, or switch between the Sample's phase stack, PMD or Lifetime tab, LI-FLIM has to reprocess all timeframes and recalculate the statistics. This may take several seconds. The same applies when you move ROIs. In that case, it is best to first switch to another Info view tab, and then move the ROI.

You can export the displayed plots as a Comma Separated Values text file, or an Excel sheet. For every selected ROI and every point in time, the average, standard deviation and number of pixels is written to the file. The plot itself can be exported as a bitmap image.

To determine if a change in measured lifetime is due to noise or to some biological effect, you can use the following rule of thumb: the standard deviation of the average value of the ROI, is equal to the standard deviation of the pixel values in the ROI divided by the square root of the number of data points. If you see a change in average lifetime that is larger than 2 of those standard-deviations-of-the-average, you are approximately 95% certain that this change in lifetime is not due to noise, but due to a change in the actual lifetime of the sample. Note that this is only valid if the lifetime inside the region of interest is supposed be homogeneous, and all variations between pixels are caused by noise with a Gaussian distribution.

## 6.7 The Polar Plot tab

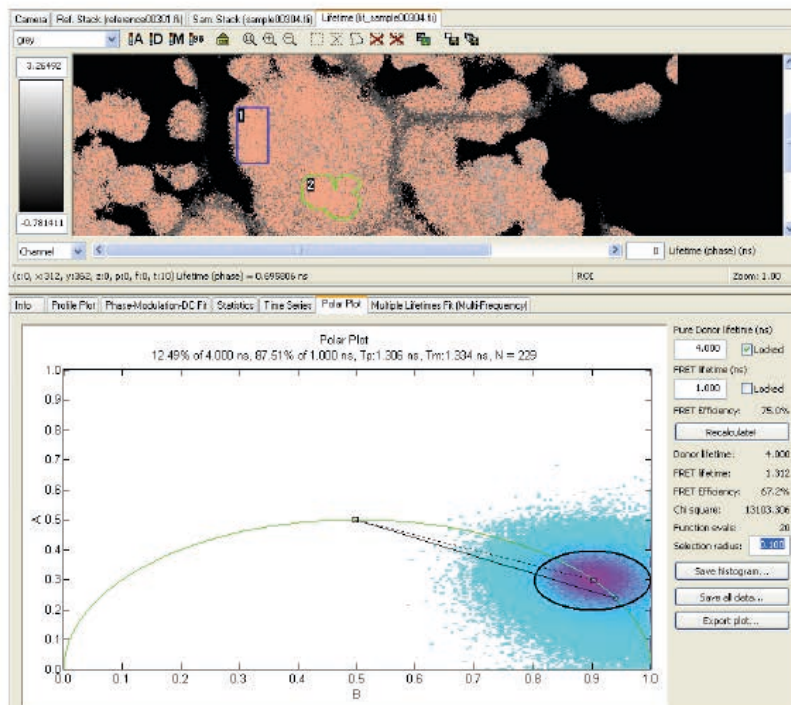


Figure 6.8: The Polar Plot tab. The left mouse button is being held down in the center of the black circle. All pixels that fall within the circle (depending on their phase and modulation) are highlighted in the Lifetime tab.

The Polar Plot tab performs a Global Analysis on the entire image. For details on the theory behind this, please refer to section 7.4.

The Polar Plot analysis can be used if the following two statements are true:

- 1. The sample contains exactly two different lifetimes.**
- 2. The lifetime components appear in different relative concentrations throughout the sample.**

An example would be two cells, one of which has 100% donor molecules, while the other one next to it contains donor and acceptor molecules, and exhibits FRET at a well defined donor-acceptor separation distance. In this case we have two cells in our phase stack images, with a total of two lifetimes (requirement 1): the donor lifetime and the shorter FRET lifetime. The second requirement is also met: inside one cell we have 100% donor molecules, while in the other, the concentration might be 25% non-FRETting donor molecules and 75% FRETting molecules.

The Polar Plot of a sample is represented as a two dimensional histogram. Every pixel in the sample phase stack (or lifetime image) corresponds to a location on the polar plot. You can picture this as a pixel having a relative phase shift and a relative modulation decrease. You can draw a line with an angle equal to the phase shift, and length equal to the modulation decrease to arrive at the correct location in the plot. The plot is divided in 200 x 200 bins, and all pixels of the lifetime image end up in one of the bins depending on their phase and modulation. Bins with little pixels are blue-ish, bins with many pixels are bright purple.

The green half-circle represents locations of 100% pure lifetime components. Mixtures of multiple lifetimes end up somewhere inside the circle. In figure 6.8, a single dot (more like a cloud actually) shows up at a lifetime of 1.3 ns, because the vast majority of the pixels have this lifetime.

LI-FLIM tries to fit a straight line through the histogram. This is shown as the dotted line in figure 6.8. The line starts at the pure Donor lifetime and ends at the pure FRET lifetime. You can lock one or both lifetimes to prevent them from being fitted to another value. All points in between the two fitted lifetimes represent a mixture of both lifetime components. All pixels in the lifetime image are then projected perpendicularly onto this line to find the relative Donor concentration in that pixel. These values are stored for every pixel in the Alpha channel of the lifetime image. In figure 6.8, the Donor lifetime was locked to 4.0 ns, and you can see in the plot that most pixels would have a low value of alpha (nearly 0% donor concentration, near 100% "FRET" concentration).

The solid line is the line between the two entered lifetimes under "Pure Donor Lifetime" and "FRET lifetime" (in this case 4.0 and 1.0 ns). This can be used to play around with the location of the line and see the values for alpha displayed in the title of the plot as you move the mouse cursor around. When you click inside the plot, a circle is displayed, and all pixels that fall within the circle are highlighted in the currently active Data tab (i.e. the lifetime image). This allows you to quickly identify Donor and FRET cells. The selection radius can be adjusted by entering a new value at the right hand side of the plot.

By clicking the "Recalculate!" button, a new fit is made, and the lifetime image, including the Alpha channel is recalculated. Note that the lifetimes that were found can also be viewed in the Info tab, under the "Polar Plot" item in the "Comments" section.

With the three buttons at the lower right side of the Polar Plot tab, you can save the histogram data (the number of pixels that fall inside the bins), a list of all data (as sets of [B, A, X, Y] values where B and A are polar plot coordinates and X, Y are pixel coordinates), and a bitmap image of the polar plot.

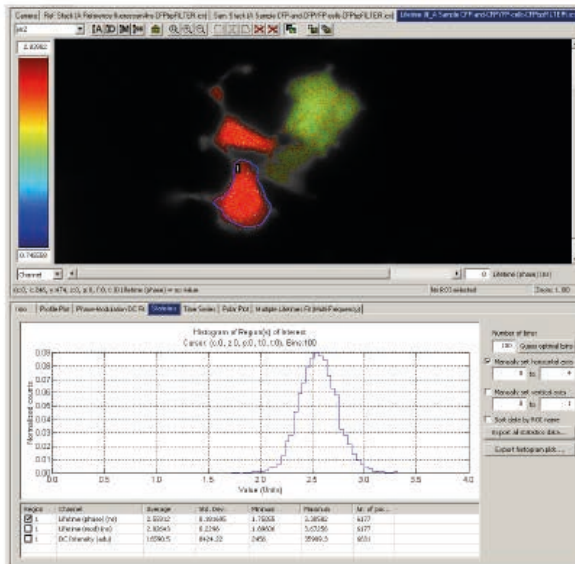
## 6.8 The Polar Plot tab - FRET Efficiency map

---

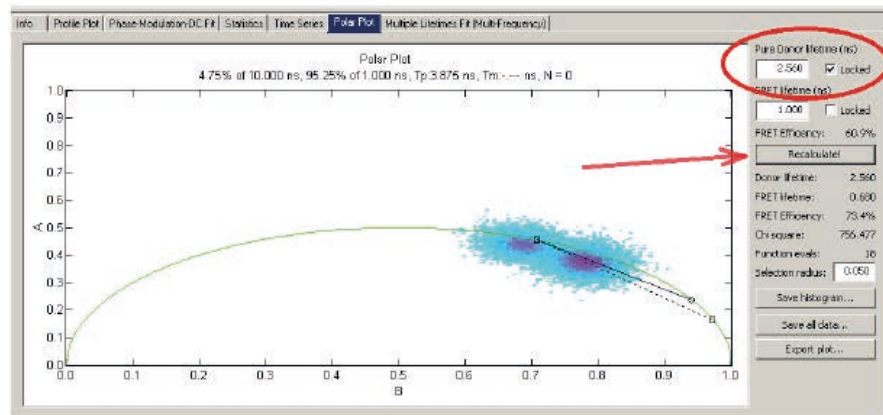
This adds a new channel to the Lifetime image, showing a per-pixel FRET efficiency value calculated from the decrease of lifetime-from-phase with respect to a given pure donor lifetime value.

Short how-to on how to start using this feature:

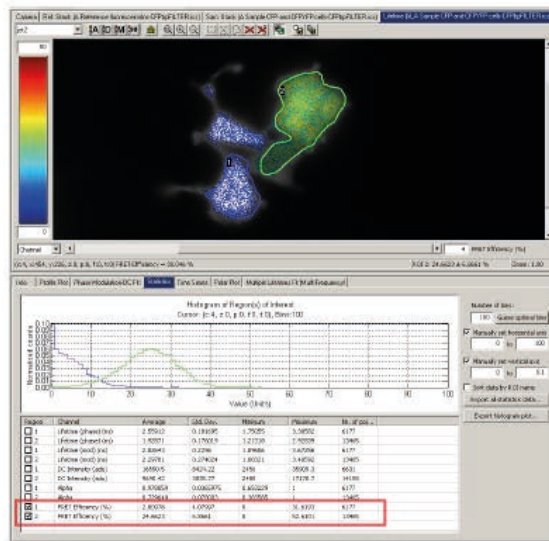
- 1) Record a lifetime image of a sample that contains pure Donor cells. Determine the lifetime-from-phase of the pure Donor. In this example, it is 2.56 ns:



2) Enter that value in the *Pure Donor lifetime* edit box of the *Polar Plot* tab. Lock this lifetime by clicking the *Locked* checkbox next to it. Then click the *Recalculate!* button.



3) The FRET Efficiency map is now enabled, and will be recalculated/updated automatically every time a new sample is recorded, relating the measured lifetime-from-phase to a per-pixel FRET efficiency based on the value given for the Pure Donor lifetime.



## 6.9 The Multiple Lifetimes Fit (Multi-Frequency) tab

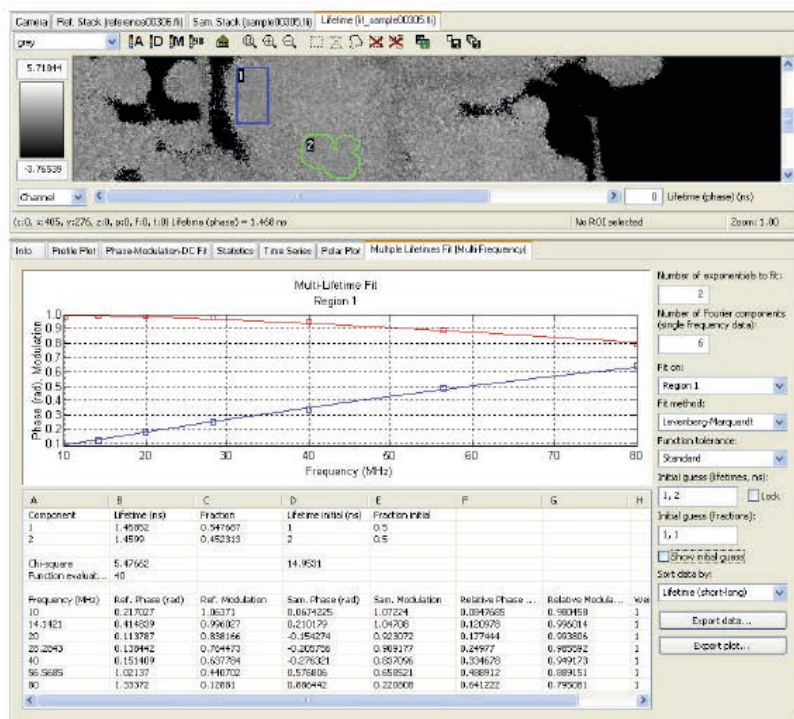


Figure 6.9: The Multiple Lifetimes Fit (Multi-Frequency) tab. The fit for Region 1 is shown.

The Multiple Lifetimes Fit (Multi-Frequency) tab shows a plot of the relative modulation (red line) and phase

shift (blue line) of the sample at different frequencies. The solid line is the result of the fit through the actual data points (hollow squares). If the sample has been recorded at multiple frequencies, then those frequencies are shown, while in the case of a single-frequency sample, the value entered in the "Number of Fourier components" box determines the number of higher-order components that are shown. If you recorded a single frequency sample at 40 **MHz**, and entered "5" as the number of components, then the phase and modulation data are plotted for 40, 80, 120, 160 and 200 **MHz**.

The "Number of exponentials to fit" at the upper right side determines the number of lifetimes that the fit procedure should find. It will always find that number of lifetimes, but some of them may be bogus. The table below the plot shows the results. In our case, two lifetime components that are nearly the same were found. This is a clear indication that there is actually only one lifetime present.

You should carefully watch the value of Chi-square: if that does not improve by a factor of 2, after changing the number of exponentials to fit, then the new model is not better than the one you had. In our case, 1 exponential is a better model than 2 exponentials, the Chi-square was larger in the latter case.

Below the found components and the Chi square, a table displays the phase and modulation data used for the fit, and the plot.

At the right hand side of the tab, you can select on what data you want to fit the lifetime(s): a single pixel (can be selected by clicking the left mouse button inside the Data view tab), a region, all regions combined, or the entire image combined. Single pixel data is usually very noisy. When you select a region, the phase image intensities are combined, and a single phase and modulation is calculated from the combined data. This results in much more accurate exponential fits.

The "Fit Method" lets you choose the type of fit. The "Levenberg-Marquardt" method is usually the most stable. You can use the "Simplex Weighted" in the case of single-frequency data, when the higher order components have a low modulation and hence result in noisy phase and modulation data. A weighting factor is applied in that case.

The "Function tolerance" determines at what accuracy level the fitting procedure decides that it is close enough to the best fit. A low tolerance (for fit errors) means that the resulting lifetimes will generally be the best possible fit, but many iterations may be needed to reach that result, taking a relatively long time. A high tolerance produces less accurate results, but is faster. The "Standard" setting is the best compromise in most cases.

The initial guesses for lifetimes and fractions provide a starting point for the fit. You can display the phase and modulation curves that correspond to the initial guess by clicking "Show initial guess". The fractions that you enter are internally normalised to 1. This means that if you enter 1, 2, 2 as fractions for three lifetime components, the actual relative fractions used for a starting point of the fit are 0.2, 0.4, and 0.4. This adds up to 1.0.

As the fit does not necessarily give the correct answer (it is a trial-and-error process), choosing your initial guess can make a significant difference to the resulting lifetime components. You should always visually check if the fit (solid curves) is following the data points. If that is not the case, you can change the lifetimes and fractions for the initial guess and see if it improves the fit.

Next, you can choose the order in which the results are presented (lifetimes sorted from long to short or the other way around, etc.). The data can be exported to Comma Separated Value text files, or Excel sheets. The plot itself can be exported as a bitmap image.

As a final note: experience shows that you will need a very good (little noise) reference and sample phase stack before you can get sensible lifetimes out of the data, especially when looking for more than 2 exponentials. If the lifetimes are very close together (say 2.0 and 2.2 ns), it will be difficult to reliably find those two components. However, if you know beforehand which lifetimes are present, you can enter them as initial guess and "lock" them. In that case, only the fractions will be fitted for, which may give more accurate results than fitting both lifetimes and fractions.



# Chapter

# 4

# Fluorescence Lifetime Imaging Microscopy by TCSPC (TD-FLIM)

Thomas Korte<sup>1</sup> and Andreas Herrmann<sup>2</sup>

Humboldt-University Berlin, Institute of Biology,

Group of Molecular Biophysics, Berlin, Germany

Contact details: <sup>1</sup>thomas.korte@rz.hu-berlin.de,

<sup>2</sup>andreas.herrmann@rz.hu-berlin.de

## Index

1. Principle and Theory.....	3
Principle of TCSPC .....	3
Characterization of Lipid Organization and Membrane Structures of Model	
Systems and Biological Membranes by FLIM .....	4
Measurement of FRET via FLIM .....	5
2. Instrumentation.....	6
3. Method .....	6
Characterization of the Lateral Distribution of the Transmembrane Domain of	
the Fusion Protein of Influenza Virus in CHO-K1 Cells .....	6
Materials Required .....	7
Sample Preparation.....	7
4. Data Acquisition .....	7
5. Data Analysis.....	8
6. Results and Data Verification .....	10
7. Limitations and Trouble Shooting .....	10
8. Conclusions and Applications.....	10
Acknowledgments .....	11
References and Further Reading .....	12
Appendix.....	14
(A) Step-by-step guide for the mesurement of CFP/YFP FLIM-FRET using an	
Olympus FV1000 CLSM with PicoQuant LSM FLIM and FCS upgrade kit .....	14
(B) Video links for FLIM data acquisition.....	17
(C) SPT64 links for FLIM data analysis.....	17
(D) Tipps/Tricks .....	17

## 1. Principle and Theory

Fluorescence Lifetime Imaging is a single molecule technique which uses the detection of fluorescence lifetime instead of fluorescence intensities to obtain information on the environment of the fluorophore or the interaction of molecules labelled with a donor-acceptor pair via FRET. There are two ways for the acquisition of lifetime data, measurements in the frequency domain (see chapter FD-FLIM by Andrew H.A. Clayton) or in the time domain as introduced here (TD-FLIM). Both techniques use different equipment and have individual advantages. The frequency method is mainly used on wide field fluorescence microscopes. It can be directly performed with fast imaging detectors like CCD cameras with additional time-gating equipment and it often requires a shorter time for data acquisition. Measurements in the time domain are single point measurements

combined with a scanning method using for instance Confocal Laser Scanning Microscopes (CLSM). This intuitive method provides a higher sensitivity since single photon counting detectors are used, a better time resolution can be obtained and it provides more options for the analysis of multi-exponential fluorescence decays.

### Principle of TCSPC

After absorption of light, a fluorophore molecule remains for a certain time (usually several nanoseconds) in the excited state before returning to the ground state, either by emitting a photon or by non-radiative energy transfer. The transition from the excited state to the ground state is a statistical process and therefore the emission of fluorescence photons follows an exponential decay law. The average time between excitation and the emission of fluorescence light for a large number of cycles

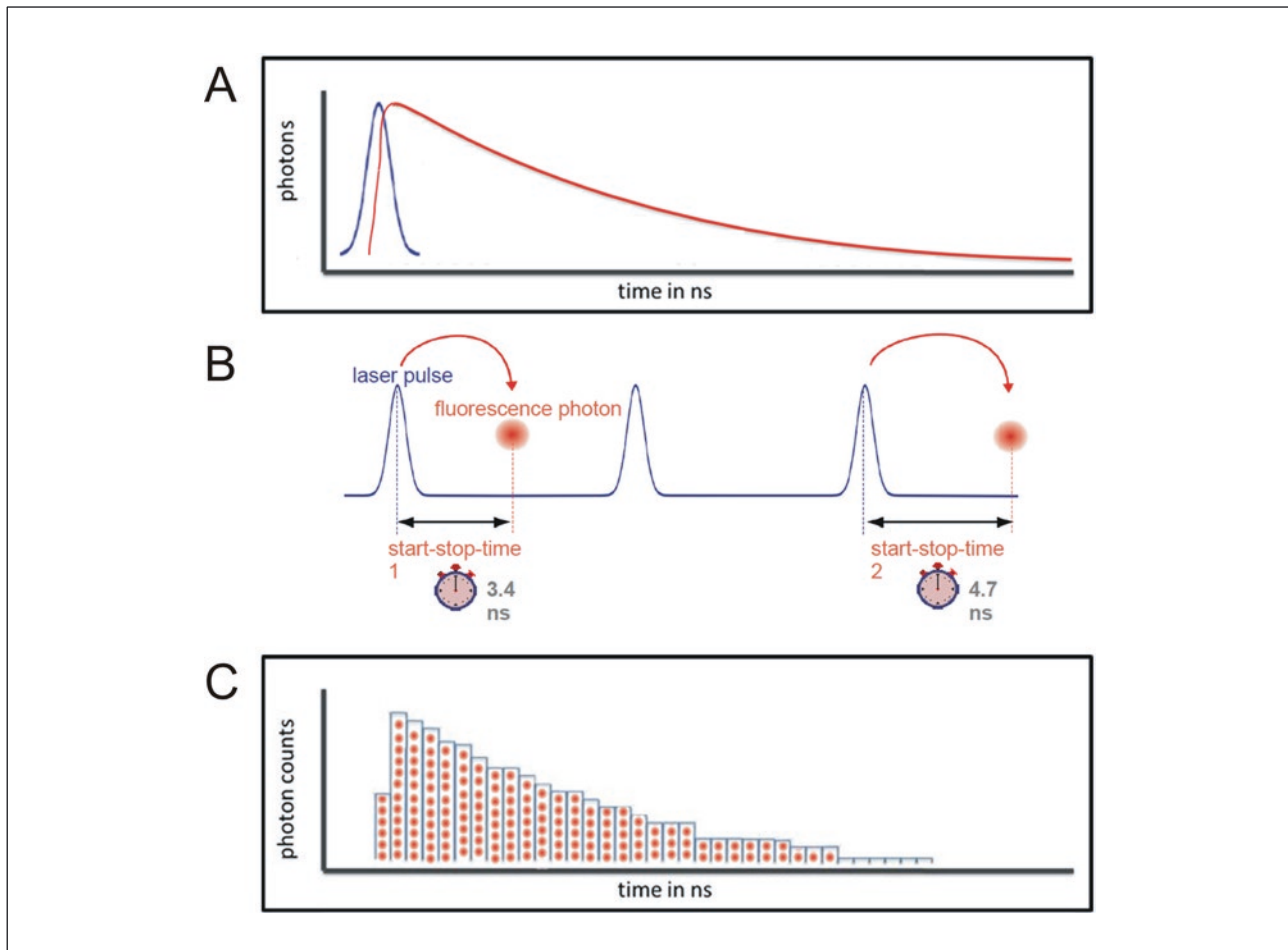


**Figure 1** Principle of TCSPC. **A** Excitation of a large number of fluorophore molecules with a short flash of light results in an exponential decay of emitted photons. **B** Instead of detecting the complete time dependent emission profile from one excitation – emission cycle, periodic excitation by a pulsed laser is used and a large number of single photons are recorded, at maximum one per excitation pulse. The difference between the start (trigger of laser) and the stop (signal from the detector) is measured by electronics that acts like a stopwatch. **C** The arrival times are grouped into bins ("channels") with picosecond time resolution and a histogram of their distribution is build up.

is called the fluorescence lifetime of a fluorescent molecule. The lifetime is an intrinsic property of a fluorophore based on the stability of the excited state. However, since it depends on its local environment it can be used to monitor changes in the immediate surrounding or to detect conformational changes within molecules as well as molecular interactions with other molecules via FRET (see Figure 1). Lifetime measurements in the time domain require recording of lifetimes of a large number of molecules. After excitation with a short flash of light, commonly a laser pulse, the time dependent intensity profile of emitted light is detected. Since it is physically impossible to detect the required number of photons from one excitation – emission cycle, periodic excitation by a pulsed laser is used and a large number of single photons are recorded. This method is called Time-Correlated Single Photon Counting (TCSPC). After excitation by a short laser pulse the precise time of the detection of single photon is registered, the reference for the timing is the corresponding excitation pulse. The difference between the start (trigger pulse of laser) and the stop (arrival of electronic pulse from the detector) is measured by electronics that acts like a stop watch. With periodic excitation and the detection of a large number of individual photons, arrival times are grouped into bins (often called time channels) with picosecond time resolution and a histogram of their distribution is build up. By adjusting laser power and repetition rate, the probability of registering more than one photon per cycle is kept low to avoid the pile-up effect. The typical result is a TCSPC histogram with an exponential drop of counts at increasing times. This histogram reflects the fluorescence decay and is analyzed by fitting to

exponential decay function(s) to extract the fluorescence lifetime(s) and the amplitude(s).

### Characterization of Lipid Organization and Membrane Structures of Model Systems and Biological Membranes by FLIM

As mentioned above, the fluorescence lifetime of a fluorophore depends on its local environment, which can be influenced by factors like temperature, pH and interactions with other fluorescent and non-fluorescent molecules. The fluorescence lifetime is thereby more sensitive to these influences than other spectral parameters, like the steady state fluorescence emission intensity or wavelength, and since it is a single molecule method it is less dependent on measurement artefacts like varying (local) concentrations and bleaching. One application of TD-FLIM measurements in our lab is the characterization of the lateral organization of artificial and biological membranes using fluorescently labelled phospholipids.

For many biological processes domains enriched in cholesterol, phospholipids and/or (glyco)sphingolipids with long saturated acyl and alkyl chains - so called "rafts" - have been discussed to play an important role for instance as reactions platforms or sites of protein interaction. However, presumably due to their small size and their short lifetime detailed knowledge about them, especially in live cells under physiological conditions, is elusive. It has been shown, that distinct liquid-ordered (lo) and -disordered (ld) domains can be induced in model membranes by the variation of the lipid composition. Giant Unilamellar Vesicles (GUVs) have been established as valuable tool to visualize lipid domain formation using various

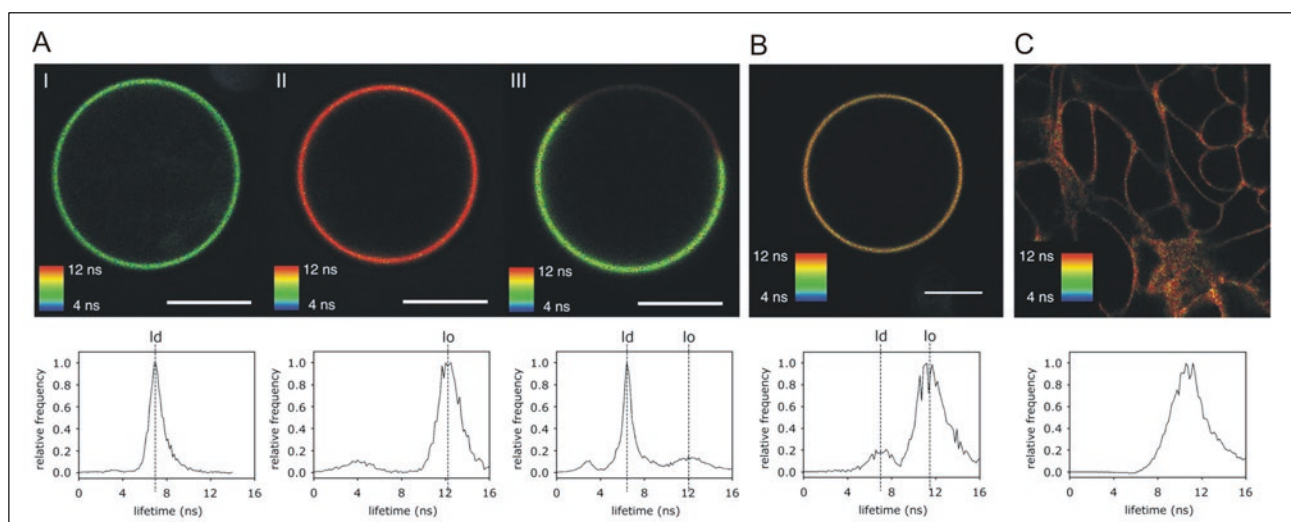


**Figure 2** Fluorescence lifetimes of C6-NBD-PC in different membranes. **A** C6-NBD-PC in GUV prepared from DOPC (I, pure ld phase), DOPC/SSM/Chol=1/1/8 (II; pure lo phase) and DOPC/SSM/Chol=1/1/1 (III; ld and lo phase) at 25 °C. (Scale bars 10 µm). **B** GUV prepared from POPC/PSM/Chol=4/2/4 (no visible domains). **C** HepG2-cells. Top row: average lifetime (see scale), Bottom row: respective lifetime histograms. (maximum normalized to 1) From [23].

lipid-like fluorophors, which enrich either in the Id or in the Io domain (see Figure 2).

We have employed phospholipid analogues labelled with the fluorophore NBD to characterize lipid domains in GUVs and the plasma membrane of mammalian cells by TD-FLIM<sup>[1],[2]</sup>. C6-NBD-phosphatidylcholine incorporates into both phases, the fluorescence decay of the NBD fluorophore is characterized by a short and long lifetime. The latter was found to be strongly dependent on the lipid environment: a large difference in the fluorescence lifetime was found for lipid mixtures forming pure Io or Id vesicles, we measured fluorescence lifetimes of about 12 ns (Io) and 7 ns (Id), respectively. The same localization-dependent lifetimes were obtained for GUVs forming microscopically visible lipid domains (Figure 2A). Moreover, even at a lipid composition showing no visible lateral lipid segregation (POPC/PSM/Chol=4/2/4) the lifetime diagram indicated the coexistence of submicroscopic domains in GUV (Figure 2B), which is in agreement with a previous study based on FRET measurements on LUV<sup>[3],[4]</sup>. NBD-labelled phospholipid analogues can easily be incorporated into the plasma membrane of mammalian cells, they have been previously established as marker for phospholipid transport. HepG2- cells were labeled with C6-NBD-PC and the distribution of fluorescence lifetimes was studied. For plasma membrane and intracellular membrane compartments different average lifetimes were observed, reflecting the differences in membrane composition. No microscopically visible domains could be resolved when analyzing the plasma membranes of HepG2 cells labelled with C6-NBD-PC, however, a broad distribution of the fluorescence lifetime around 10-11ns was observed (see Figure 2C) suggesting the coexistence of various submicroscopic domains. These results show, the TD-FLIM studies are a valuable tool for the investigation of lipid organization and membrane structures, but also protein localization and protein-lipid-interaction in model systems and biological membranes.

### Measurement of FRET via FLIM

The principle and theory of Förster Resonance Energy Transfer (FRET) is given elsewhere in great detail<sup>[13]</sup>, here only a short summary: In essence, FRET is the transfer of energy from an excited donor molecule to an acceptor fluorophore in close vicinity by non-radiative dipole-dipole coupling. This results in quenching of the donor indicated by its lower fluorescence intensity and shorter fluorescence lifetime as well as increasing of the acceptor fluorescence intensity. The efficiency of the transfer depends mainly on (a) the spectral overlap of donor emission and acceptor excitation, (b) the distance of donor and acceptor molecule (<10nm) and (c) the orientation of the flu-

rophore dipoles. Commonly, FRET can be detected by imaging of the acceptor fluorescence after donor excitation (sensitized emission) or by comparing the donor emission in the presence and the absence of the acceptor. The latter is usually achieved by photobleaching of the acceptor (see chapter AP-FRET). However, these methods are based on the intensity and therefore can be influenced by fluorophore concentration (e.g. the expression level for genetically encoded fluorescent proteins), background fluorescence, spectral cross-talk, and bleaching of the donor as well as the acceptor.

Another method to determine the presence of FRET is measurement of the donor excited state lifetime (FLIM-FRET). For measurements in the time domain (td-FLIM) the quenching of the donor fluorescence lifetime detected by the TCSPC method is analyzed. Because in the presence of FRET the donor molecule has an additional non-radiative pathway to return to the ground state, its fluorescence lifetime is shortened, resulting in a faster drop of the fluorescence decay. Since the fluorescence lifetime is independent of the fluorophore concentration, FLIM-FRET enables quantitative measurements and straightforward comparison of different samples (e.g. cells) with varying fluorophore amount. It is notable, that due to the very steep distance dependence of the FRET efficiency, especially in cells with typical protein concentrations in the micro molar range, the average distance between molecules is too large for false positive FRET, even at high molecular concentrations.

The fluorescence decay curve is analyzed by fitting it to a mono or multi exponential function and the parameters fluorescence lifetime and fractional amplitude can be extracted. As a unique feature, FLIM-FRET allows to resolve subpopulations if only a fraction of donor-labeled molecules is bound in a complex. The prerequisite is a mono-exponentially decaying donor fluorophore. In case of FRET, the decay curve exhibits a bi-exponential behavior consisting of a short lifetime corresponding to the FRET quenched donor molecules and a longer lifetime of unquenched donors. Based on the amplitudes of these two lifetime components, the fraction of free and associated molecules can be determined. This procedure can be applied to every image pixel and the differences in the lifetime distribution can be visualized by a color-coded FLIM image. This enables to visualize e.g. the presence or absence of FRET as well as the localization of the subpopulations along the sample.

## 2. Instrumentation

Fluorescence lifetime imaging in the time domain based on Time-Correlated Single Photon Counting (TCSPC) as introduced here is a single point excitation / single photon detection method. A laser beam is focussed on one point of the sample, the image is generated by point-by-point scan. Therefore commercial Confocal Laser Scanning Microscopes (CLSM) are in most cases the basis for such a FLIM system.

### *Light sources:*

A short pulsed laser with a high repetition rate is required for FLIM measurements. Most commonly picosecond diode lasers controlled by a laser driver unit are used, these systems have the advantage of a variable repetition rate up to 80 MHz and adjustable output power. Therefore they can be easily used for fluorophores with a wide range of lifetimes. Alternatively a multi-photon Titanium:Sapphire can be applied for time-resolved two photon excitation.

### *Detectors:*

While the standard detectors of a laser scanning microscope are photomultipliers operated in an analogue mode, specially designed detectors with single photon counting sensitivity and high time resolution are needed for TCSPC measurements. Detectors suitable for this purpose are photon counting Photomultiplier Tubes (PMTs), Single Photon Avalanche Diodes (SPADs) and recently developed Hybrid-Photomultiplier Tubes. In some multi-photon excitation systems the Non-Descanned

Detectors (NDDs) can be operated in a photon counting mode and therefore these systems can be upgraded for FLIM imaging.

A FLIM system is completed by electronics for recording of TCSPC data (to measure the time between triggering of the laser pulse and arrival of the signal at the detector) and additional timing tags for the correct reconstruction of the image from the data stream. Specific software is needed for data display, acquisition and analysis (see Figure 3).

We are using a Confocal laser scanning microscope Olympus FV1000 with appropriate filter sets and corresponding dichroic mirrors and an 60X oil objective with NA=1.35. For FLIM-Imaging the system is equipped with an external FLIM/FCS upgrade kit from PicoQuant with excitation by pulsed picosecond diode laser(s), detection by single photon counting SPADs, a TCSPC module PicoHarp 300 and a separate computer for FLIM / FCS data acquisition and processing along with the FLIM/FCS software SymPhoTime.

## 3. Method

### **Characterization of the Lateral Distribution of the Transmembrane Domain of the Fusion Protein of Influenza Virus in CHO-K1 Cells**

Hemagglutinin (HA), the fusion protein of Influenza virus, has been suggested to be enriched in liquid-ordered lipid domains – so-called rafts<sup>[5-7]</sup>. In the following experiment based on a study of Scolari et al. (2009)<sup>[8]</sup> we are using FLIM-FRET measurements

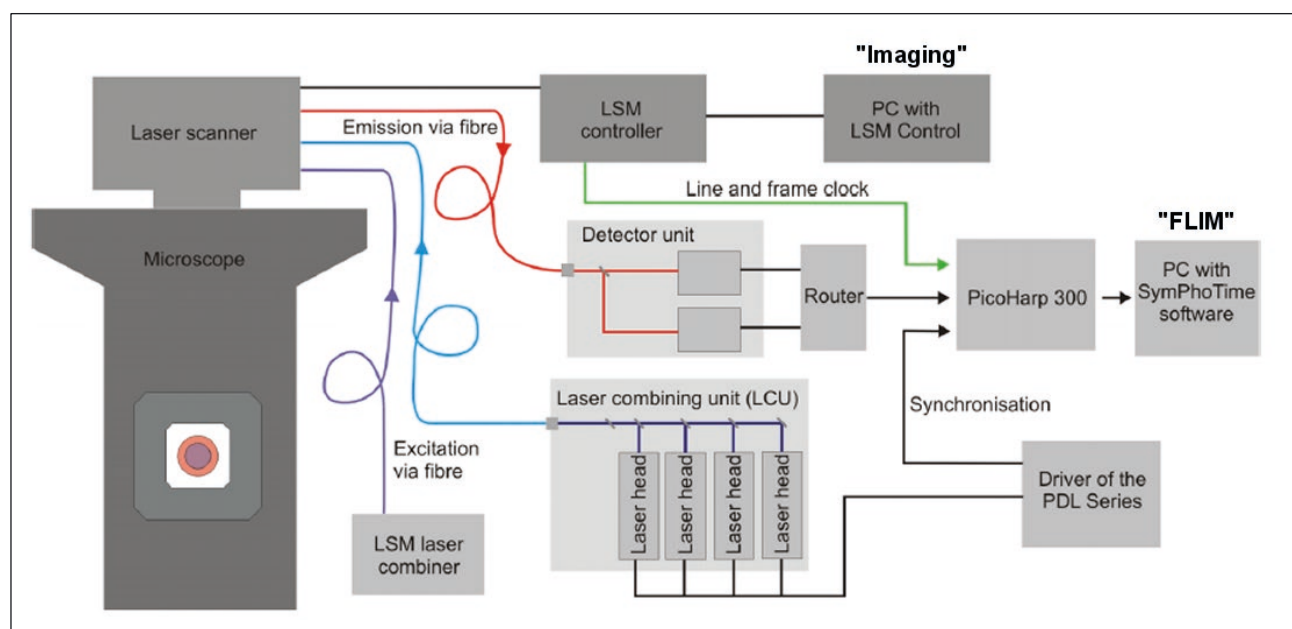


Figure 3 Sketch of the general layout of the PicoQuant FLIM & FCS Upgrade Kit.

between GPI-CFP as raft marker and the YFP-tagged transmembrane domain (TMD) of HA to characterize the mechanism of the lateral organization of the viral fusion protein in the plasma membrane of eukaryotic cells, in particular its recruitment to raft domains. This recruitment has been associated with specific properties of the transmembrane domain (TMD) and the cytoplasmatic tail of HA<sup>[9-11]</sup>. GPI stands for Glycosylphosphatidylinositol which is a lipid anchored structure. Its localization to raft domains has been demonstrated previously<sup>[12],[13]</sup>.

### Materials Required

Chinese hamster ovary cells (CHO-K1, American Type Culture Collection), for which the presence of cholesterol-sensitive lipid nanodomains and their dimension in the plasma membrane have been described<sup>[12]</sup>. FBS, Antibiotics (penicillin and streptomycin), Trypsin, plasmids for GPI and TMD-HA tagged with CFP and YFP, respectively, DMEM media and transfection reagent (Lipofectamine 2000). 35mm glass-bottom-dishes (MatTek, Ashland, MA), T75 flasks and pipettes and other cell culture supplies.

### Sample Preparation

1. CHO-K1 cells (ATCC) are maintained in T75 flasks in DMEM with 10%FBS and 1% Penicillin-Streptomycin at 37°C and 5% CO<sub>2</sub> .
2. Cells were detached from the flask using 1,5 ml trypsin-EDTA by incubating at 37oC for 5 min.
3. Cells were seeded in 35mm glass-bottom-dishes and grown to ~80% confluence, transfection was carried out using Lipofectamine 2000 following the manufacturer's protocol (Invitrogen).
4. 20-24 h post transfection cells are washed, analyzed for expression of the fluorescent proteins and FLIM-FRET measurements are carried out in DMEM without phenol red.

In general, the following protein expressions would be ideal to provide sample and additional controls:

- a) Co-expression of x-donor and y-acceptor as experimental model where x and y are the proteins/molecules of interest
- b) Expression of x-donor alone (or even better co-expression of x-donor and non-tagged y) as negative control
- c) Co-expression of x-donor and y-acceptor where interaction is blocked or inactivated
- d) Tandem-fusion of donor and acceptor to one protein or sample with both proteins x-donor and y-acceptor expressed and cross-linked as positive control

In our case x-donor corresponds to the raft marker GPI-CFP and y-acceptor to TMD-HA-YFP. We are investigating the FRET caused by co-localization

of GPI-CFP and TMD-HA-YFP in raft domains, as control with an abandoned interaction (c) we are using cells depleted of cholesterol since this treatment has been shown to result in the disruption of rafts<sup>[14]</sup>. As positive control (d) GPI-CFP and GPI-YFP were co-expressed, both should be incorporated into raft domains.

## 4. Data Acquisition

We are using an Olympus FV1000 confocal microscope equipped with a PicoQuant LSM upgrade kit for FLIM / FCS and the Software SympoTime for acquisition and analysis of fluorescence lifetime data. A step-by-step guide for the acquisition of the data required for FLIM-FRET measurements is given in the Appendix. The PicoQuant LSM upgrade kit is available for CLSMs of all major manufacturers, with the help of the guide it should be easy to perform the measurements on suitable instrumentation of other suppliers.

The following data sets have to be acquired for the data analysis and the evaluation of the results:

1. Confocal Images of CFP and YFP expression in the sequential mode to monitor the expression of the individual proteins. Note: While the signal in Channel 2 shows the expression of YFP, the signal in Channel 1 reflects only CFP molecules not affected by FRET.
2. Confocal "Intensity" FRET image of the YFP fluorescence (excitation with 458nm) Channel 1 shows the CFP fluorescence intensity without FRET, channel 2 the YFP intensity due to FRET but also spill-over of CFP, acceptor emission due to direct excitation at 458 nm and eventually background-fluorescence. Therefore additional measurements like FLIM-FRET or acceptor photobleaching are necessary to obtain conclusive results.
3. FLIM image of CFP fluorescence (excitation with pulsed 440nm diode) recorded on the FLIM computer.
4. Measurement of the Internal response function (IRF)  
The overall timing precision of a complete TCSPC system is characterized by its Instrument Response Function (IRF). For an ideal system with an infinitely sharp excitation pulse and infinitely accurate detectors and electronics, the IRF should be infinitely narrow. Due to the properties of light source, detector and electronics, the IRF is broadened. Thus, to precisely analyze decay curves with short lifetimes the IRF has to be determined for the method of "n-Exponential Deconvolution" (see "Data analysis" below).

The best way to measure the IRF is to use a solution of a fluorophore with similar fluorescence properties as the sample but with a very short lifetime, which can be induced by a quencher at saturating concentration (for instance KJ).

If such a fluorophore is not available, one can alternatively record the scattering of the excitation light. In that case a narrow-band filter for the wavelength of the excitation light is placed in front of the detector. Since the IRF of some detectors is dependent on the wavelength, measurement at the excitation wavelength might not be useful for numerical deconvolution. The solution is to acquire the IRF at the emission wavelength, or at least spectrally closer to the fluorescence emission.

## 5. Data Analysis

In SymphoTime select regions of interest (ROI) of the images either by hand or using the magic wand tool. In our case, the plasma membrane of an individual cell is selected. First, all measured photons of the ROI are combined into a global histogram. This global decay curve is used to obtain the fitting parameters, which are afterwards used for the pixel by pixel fit and the generation of the fluorescence lifetime image (see Figure 4).

The SymPhoTime software allows to analyze the data either by “n-Exponential Tailfit” or by “n-Exponential Deconvolution”. Tail fitting can only be used when the fitted lifetimes are significantly longer than the IRF. It is not sufficient for a detailed analysis of the individual components of a multi-exponential decay. Therefore, for deconvolution the correspond-

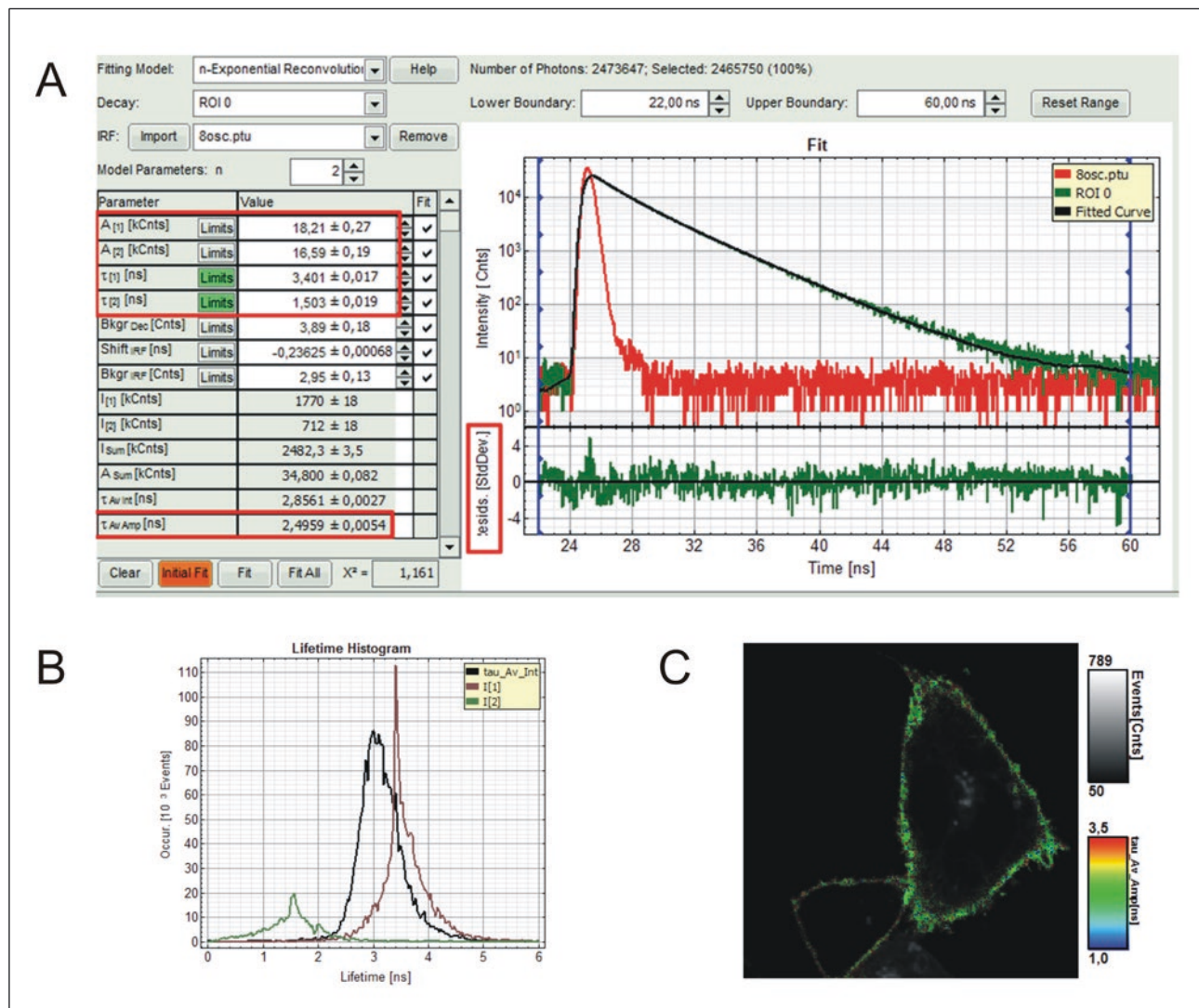


**Figure 4** Analysis of fluorescence lifetime data using SymphoTime 64. **A** Decay curve for a ROI (green), imported IRF (red), biexponential curve fit (black). Important parameters are highlighted with red boxes. **B** Lifetime histogram with distribution of lifetimes. **C** Color-coded fluorescence lifetime image.

ing IRF has to be imported. Alternatively, the IRF is reconstructed in the software by directly evaluating the onset of the fluorescence decay. Afterwards, the decay curve is analyzed by fitting it using a nonlinear least squares iterative procedure to a mono or multi-exponential function. First the control sample (GPI-CFP only) is processed. Our constructs contain ECFP as donor, which has been shown to express an intrinsic biexponential fluorescence decay with lifetimes of about 1.3 and 3.8 ns<sup>[15],[16]</sup>. Therefore, the fitting procedure is started with two exponential components, the quality of the fit is judged by the distribution of the residuals and the goodness of fit parameter ( $\chi^2$ ). The  $\chi^2$  value should be close to 1, the fitted curve should overlay well with the decay curve, the calculated fitting values must be reasonable and the residuals representing the deviation of the fit from the measured decay curve should be small and randomly distributed. An exemplary fit with the highlighted parameters is shown in Figure 4A. If the fit is not satisfying, especially if a tendency can be seen in the distribution of the residuals, an additional exponential should be added, all parameters have to be cleared and the fit has to be repeated. An additional exponential is for instance needed if different populations of the donor occur (FRET and non-FRET, different local environment) or to correct for deviations in the beginning of the curve due to a not perfectly fitting IRF.

Parameters obtained from the SymphoTime software are the lifetime  $\tau_i$  and amplitude  $A_i$  of the individual exponential component. The quantification of the individual exponential terms is complicated by the bi-exponential decay of CFP. Therefore, for every ROI the amplitude-weighted average lifetime of CFP is calculated using the following equation<sup>[17]</sup>:

$$\tau_{\text{Av Amp}} = \frac{\sum_{k=0}^{n-1} A[k] \tau[k]}{A_{\text{Sum}}}$$

SymPhoTime uses two ways of calculating the average lifetime ( $\tau_{\text{AV int}}$  and  $\tau_{\text{AV amp}}$ ) differing in the way the single decay times are weighted,  $\tau_{\text{AV amp}}$  is proportional to the steady state intensity and therefore applicable for the calculation of the FRET efficiency based on the donor lifetimes.

The FRET efficiency (E) is defined as the proportion of the donor molecules that have transferred excitation state energy to the acceptor molecules. It is calculated for each ROI using the equation

$$E = \left[ 1 - \frac{\tau_{\text{Av Amp}}}{\tau_D} \right]$$

where  $\tau_{\text{DA}}$  is the amplitude-weighted average lifetime of the donor in the presence of the acceptor and  $\tau_D$  is the one of 10 control cells (donor GPI-CFP expressed alone). To generate lifetime images (for instance in order to compare lifetimes in different compartments), afterwards each pixel of the selection is analyzed based on the parameters obtained with a maximum likelihood estimation and a color coded FLIM image and a lifetime distribution histogram are generated (see Figure 4B and C). A sufficient number of cells have to be analyzed, the mean and standard error have to be calculated to compare the different samples and measured differences have to be verified by statistical tests and appropriate controls.

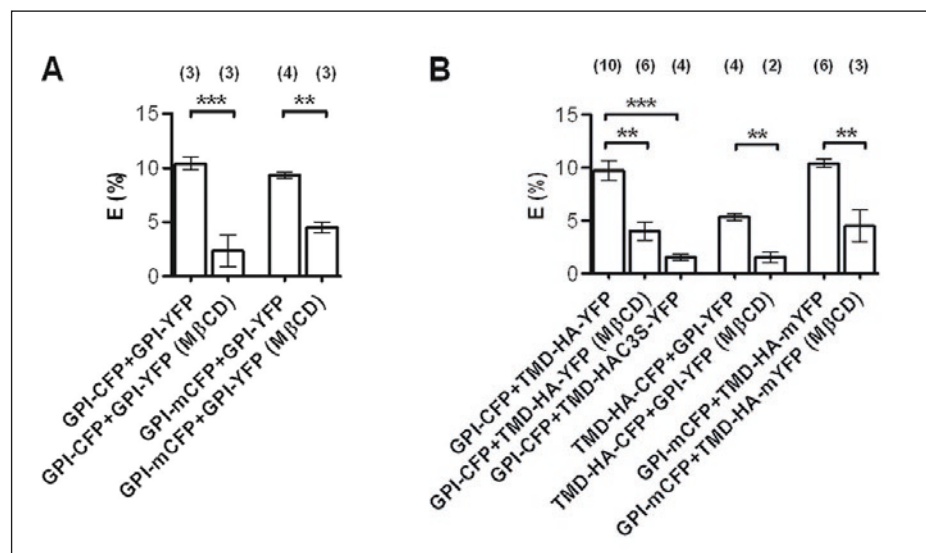


**Figure 5** Interaction between GPI and TMD-HA constructs measured by FLIM-FRET. FRET efficiency between raft markers (A), between raft marker and different TMD-HA variants (B), MβCD, after pretreatment with MβCD to disrupt liquid ordered domains in the plasma membrane. Above the bars, n refers to the number of independent experiments is given. Each experiment is based on 10 cells. Data represent the mean  $\pm$  S.E. \*\*,  $p < 0.0001$ , \*\*  $p < 0.005$ . Experiments were carried out at 25 °C. (from Scolari et al., 2009)

## 6. Results and Data Verification

We have used this method to characterize the lateral distribution of the TMD of HA in CHO-K1 cells and purified plasma membranes<sup>[8]</sup>. Co-expression of the raft-marker GPI-CFP with TMD-HA-YFP led to a significant shortening of donor lifetime in comparison to cells expressing GPI-CFP only. This could be attributed to FRET indicating sorting of TMD-HA-YFP into raft domains in the plasma membrane, FRET efficiency was calculated to about 10% (Figure 5). Cholesterol depletion using methyl-β-cyclodextrin (MβCD) has been shown to result in the disruption of ordered domains in biological membranes<sup>[14]</sup>. This treatment of the plasma membrane resulted in a decrease of FRET between GPI-CFP and TMD-HA-YFP, while CFP lifetime in cells expressing only the donor GPI-CFP was not affected. As positive control, co-expression of GPI-CFP and GPI-YFP, which both should be enriched in raft domains, resulted also in a shortening of CFP lifetime and a FRET efficiency of about 10%, which was significantly reduced by MβCD treatment.

## 7. Limitations and Trouble Shooting

While genetic labeling with fluorescent proteins has become a valuable tool for live-cell imaging and the detection of protein-protein interaction by FRET, there are also several limitations. Due to the large size of the fluorescent proteins, which are 4.2nm long with a 2.4 nm barrel<sup>[18],[19]</sup>, a large part of the usable FRET is occupied resulting in a maximum FRET efficiency of about 40%. If two proteins are labeled on opposite sites or in case the dipole moments of donor and acceptor are not properly aligned, FRET might not be measurable even if the proteins of interest are bound to each other. Also, tagging of proteins with these large markers might change the folding, transport or localization of the proteins which are investigated. Some of the fluorescent proteins (also ECFP) have the tendency to form homodimers by themselves, which can reduce the fluorescence lifetime and therefore could lead to false-positive results<sup>[20]</sup>. Therefore CFP variants shown to be monomeric should be used<sup>[13],[16]</sup>, also the ratio donor : acceptor should be kept low in order to prevent dimerization of the donor and to improve the signal-to-noise ratio. To obtain the full content of information allowing to quantify the FRET results, it is crucial to use a donor fluorophore with a mono-exponential decay. FLIM-FRET measurements are based on a statistical analysis of a sufficient number of photons, therefore image acquisition is in most cases longer than for Intensity-FRET or FLIM-FRET in the frequency domain, for dynamic processes this might require fixation of the sample.

## 8. Conclusions and Applications

Measurement of FRET by FLIM is a highly sensitive method that can be used to detect protein-protein interactions *in vivo*. Since only the donor fluorescence lifetime is detected and analyzed, it is not dependent on variations in the protein expression level, a problem often occurring in cellular systems – especially if more than one protein is expressed by transfection. Compared to intensity-based FRET measurements, FLIM-FRET leads to quantitative results and, if the donor fluorescence can be described by a mono-exponential decay, allows to identify sub-populations that undergo FRET. Another advantage of measurements in the time domain (td-FLIM) is that this is a single molecule method and therefore performed on a very low illumination level, which prevents photo damage and bleaching. Also, since this is a point scanning method, illumination can be restricted to the area of interest and time for data acquisition can be reduced by selecting a smaller area or scanning resolution.

Finally, the whole decay curve is recorded and therefore more sophisticated analysis can be performed, also it is possible to detect two (or more) fluorescence channels at the same time and to use the information from the second channel to gate or correlate the data analyzed.

Over the last years, the td-FLIM has been established as valuable tool not only to measure protein-protein interaction but also protein localization in membranes and protein-ligand binding. The table below shows a selection of recent publications using td-FLIM and FLIM-FRET measurements for *in vivo* studies.

Applications	Method / FRET-Pair	Ref.
Receptor phosphorylation / dephosphorylation	td-FLIM (FLIM-FRET)	[21], [22]
Receptor localization (IgE-FcεRI) in microdomains	td-FLIM	[23]
Characterization of membrane properties in model and biological membranes	td-FLIM	[24], [1], [25], [2], [26], [27]
Phospholipid traffic in cells	td-FLIM	[28], [29]
Influence of ABC transporters on membrane composition	td-FLIM	[30]
NAD(P)H to visualize pathogen-host interactions	td-FLIM	[31]
In Vivo imaging of specific probes to cancer biomarkers	td-FLIM	[32]
Interaction site of cellular actin with the plasma membrane	GFP and RFP	[33]
Interaction of chemokine receptor CXCR4 and protein kinase C	GFP and RFP	[34]
Membrane localization of viral proteins	CFP and YFP Cer and YFP	[8], [11], [35]
Interaction of poxvirus proteins with kinesin	GFP and DsRed	[36]
Interaction of proteins in yeast	Cer and YFP	[37]
Complexes of t- and v-SNARE in fungi	Cer and Ven	[38]
Interaction of plasma membrane proteins in maize	CFP and YFP	[39]
Interaction of serotonin receptors in different cell lines	GFP and mCherry	[40]
Cell division multi-protein complex in Streptomyces	GFP and mCherry	[41]
Interaction of Golgi tethering factors and small GTPases	GFP and mRFP	[42]
Interactions of proteins related to Alzheimer's disease	GFP and mRFP	[43]
Receptor-Ligand interaction in endocytosis and trafficking	YFP and Cy3.5 GFP and mRFP	[44] [45]
Characterization of membrane fusion	lipid markers	[46]

## Acknowledgments

We are thankful to Dr. Sandra Orthaus (PicoQuant GmbH, Germany) for helpful comments and editing of this manuscript.

## References and Further Reading

- [1] Stöckl, M., et al., Detection of lipid domains in model and cell membranes by fluorescence lifetime imaging microscopy of fluorescent lipid analogues. *J Biol Chem*, 2008. 283(45): p. 30828-37.
- [2] Stöckl, M. and A. Herrmann, Detection of lipid domains in model and cell membranes by fluorescence lifetime imaging microscopy. *Biochim Biophys Acta*, 2010. 1798(7): p. 1444-56.
- [3] de Almeida, R.F., A. Fedorov, and M. Prieto, Sphingomyelin/phosphatidylcholine/cholesterol phase diagram: boundaries and composition of lipid rafts. *Biophys J*, 2003. 85(4): p. 2406-16.
- [4] de Almeida, R.F., et al., Lipid rafts have different sizes depending on membrane composition: a time-resolved fluorescence resonance energy transfer study. *J Mol Biol*, 2005. 346(4): p. 1109-20.
- [5] Scheiffele, P., et al., Influenza viruses select ordered lipid domains during budding from the plasma membrane. *J Biol Chem*, 1999. 274(4): p. 2038-44.
- [6] Takeda, M., et al., Influenza virus hemagglutinin concentrates in lipid raft microdomains for efficient viral fusion. *Proc Natl Acad Sci U S A*, 2003. 100(25): p. 14610-7.
- [7] Wagner, A.J., S. Loew, and S. May, Influence of Monolayer-Monolayer Coupling on the Phase Behavior of a Fluid Lipid Bilayer. *Biophys J*, 2007.
- [8] Scolari, S., et al., Lateral distribution of the transmembrane domain of influenza virus hemagglutinin revealed by time-resolved fluorescence imaging. *J Biol Chem*, 2009. 284(23): p. 15708-16.
- [9] Scheiffele, P., M.G. Roth, and K. Simons, Interaction of influenza virus haemagglutinin with sphingolipid-cholesterol membrane domains via its transmembrane domain. *Embo J*, 1997. 16(18): p. 5501-8.
- [10] Melkonian, K.A., et al., Role of lipid modifications in targeting proteins to detergent-resistant membrane rafts. Many raft proteins are acylated, while few are prenylated. *J Biol Chem*, 1999. 274(6): p. 3910-7.
- [11] Engel, S., et al., FLIM-FRET and FRAP reveal association of influenza virus haemagglutinin with membrane rafts. *Biochem J*, 2010. 425(3): p. 567-73.
- [12] Sharma, P., et al., Nanoscale organization of multiple GPI-anchored proteins in living cell membranes. *Cell*, 2004. 116(4): p. 577-89.
- [13] Zacharias, D.A., et al., Partitioning of lipid-modified monomeric GFPs into membrane micro-domains of live cells. *Science*, 2002. 296(5569): p. 913-6.
- [14] Hao, M., S. Mukherjee, and F.R. Maxfield, Cholesterol depletion induces large scale domain segregation in living cell membranes. *Proc Natl Acad Sci U S A*, 2001. 98(23): p. 13072-7.
- [15] Tramier, M., et al., Picosecond-hetero-FRET microscopy to probe protein-protein interactions in live cells. *Biophys J*, 2002. 83(6): p. 3570-7.
- [16] Rizzo, M.A., et al., An improved cyan fluorescent protein variant useful for FRET. *Nat Biotechnol*, 2004. 22(4): p. 445-9.
- [17] Lackowicz, J.R., *Principles of Fluorescence Spectroscopy*. 2006, New York.: Springer Science+Business Media.
- [18] Ormo, M., et al., Crystal structure of the *Aequorea victoria* green fluorescent protein. *Science*, 1996. 273(5280): p. 1392-5.
- [19] Yang, F., L.G. Moss, and G.N. Phillips, Jr., The molecular structure of green fluorescent protein. *Nat Biotechnol*, 1996. 14(10): p. 1246-51.
- [20] Piston, D.W. and G.J. Kremers, Fluorescent protein FRET: the good, the bad and the ugly. *Trends Biochem Sci*, 2007. 32(9): p. 407-14.
- [21] Peltan, I.D., et al., Fluorescence lifetime imaging microscopy (FLIM) detects stimulus-dependent phosphorylation of the low density lipoprotein receptor-related protein (LRP) in primary neurons. *Biochem Biophys Res Commun*, 2006. 349(1): p. 24-30.
- [22] Treanor, B., et al., Microclusters of inhibitory killer immunoglobulin-like receptor signaling at natural killer cell immunological synapses. *J Cell Biol*, 2006. 174(1): p. 153-61.
- [23] Davey, A.M., et al., Membrane order and molecular dynamics associated with IgE receptor cross-linking in mast cells. *Biophys J*, 2007. 92(1): p. 343-55.
- [24] Margineanu, A., et al., Visualization of membrane rafts using a perylene monoimide derivative and fluorescence lifetime imaging. *Biophys J*, 2007. 93(8): p. 2877-91.
- [25] de Almeida, R.F., L.M. Loura, and M. Prieto, Membrane lipid domains and rafts: current applications of fluorescence lifetime spectroscopy and imaging. *Chem Phys Lipids*, 2009. 157(2): p. 61-77.
- [26] Bastos, A.E., et al., Applications of fluorescence lifetime spectroscopy and imaging to lipid domains *in vivo*. *Methods Enzymol*, 2012. 504: p. 57-81.
- [27] Sezgin, E., et al., Partitioning, diffusion, and ligand binding of raft lipid analogs in model and cellular plasma membranes. *Biochim Biophys Acta*, 2012. 1818(7): p. 1777-1784.
- [28] Wustner, D., Fluorescent sterols as tools in membrane biophysics and cell biology. *Chem Phys Lipids*, 2007. 146(1): p. 1-25.
- [29] Wustner, D., et al., Quantitative assessment of sterol traffic in living cells by dual labeling with dehydroergosterol and BODIPY-cholesterol. *Chem Phys Lipids*, 2011. 164(3): p. 221-35.

- [30] Zarubica, A., et al., Functional implications of the influence of ABCA1 on lipid microenvironment at the plasma membrane: a biophysical study. *FASEB J*, 2009. 23(6): p. 1775-85.
- [31] Szaszak, M., et al., Fluorescence lifetime imaging unravels *C. trachomatis* metabolism and its crosstalk with the host cell. *PLoS Pathog*, 2011. 7(7): p. e1002108.
- [32] Ardest Shirpour, Y., et al., In vivo fluorescence lifetime imaging monitors binding of specific probes to cancer biomarkers. *PLoS One*, 2012. 7(2): p. e31881.
- [33] Konig, I., J.P. Schwarz, and K.I. Anderson, Fluorescence lifetime imaging: association of cortical actin with a PIP3-rich membrane compartment. *Eur J Cell Biol*, 2008. 87(8-9): p. 735-41.
- [34] Peter, M., et al., Multiphoton-FLIM quantification of the EGFP-mRFP1 FRET pair for localization of membrane receptor-kinase interactions. *Biophys J*, 2005. 88(2): p. 1224-37.
- [35] Thaa, B., et al., Intrinsic membrane association of the cytoplasmic tail of influenza virus M2 protein and lateral membrane sorting regulated by cholesterol binding and palmitoylation. *Biochem J*, 2011. 437(3): p. 389-97.
- [36] Jeshtadi, A., et al., Interaction of poxvirus intracellular mature virion proteins with the TPR domain of kinesin light chain in live infected cells revealed by two-photon-induced fluorescence resonance energy transfer fluorescence lifetime imaging microscopy. *J Virol*, 2010. 84(24): p. 12886-94.
- [37] Schreiber, G., et al., Unraveling interactions of cell cycle-regulating proteins Sic1 and B-type cyclins in living yeast cells: a FLIM-FRET approach. *FASEB J*, 2012. 26(2): p. 546-54.
- [38] Valkonen, M., et al., Spatially segregated SNARE protein interactions in living fungal cells. *J Biol Chem*, 2007. 282(31): p. 22775-85.
- [39] Zelazny, E., et al., FRET imaging in living maize cells reveals that plasma membrane aquaporins interact to regulate their subcellular localization. *Proc Natl Acad Sci U S A*, 2007. 104(30): p. 12359-64.
- [40] Fjorback, A.W., et al., Serotonin transporter oligomerization documented in RN46A cells and neurons by sensitized acceptor emission FRET and fluorescence lifetime imaging microscopy. *Biochem Biophys Res Commun*, 2009. 380(4): p. 724-8.
- [41] Willemse, J., et al., Positive control of cell division: FtsZ is recruited by SsgB during sporulation of *Streptomyces*. *Genes Dev*, 2011. 25(1): p. 89-99.
- [42] Osterrieder, A., et al., Fluorescence lifetime imaging of interactions between Golgi tethering factors and small GTPases in plants. *Traffic*, 2009. 10(8): p. 1034-46.
- [43] Herl, L., et al., Mutations in amyloid precursor protein affect its interactions with presenilin/gamma-secretase. *Mol Cell Neurosci*, 2009. 41(2): p. 166-74.
- [44] Nievergall, E., et al., PTP1B regulates Eph receptor function and trafficking. *J Cell Biol*, 2010. 191(6): p. 1189-203.
- [45] Bu, W., et al., Cdc42 interaction with N-WASP and Toca-1 regulates membrane tubulation, vesicle formation and vesicle motility: implications for endocytosis. *PLoS One*, 2010. 5(8): p. e12153.
- [46] Dumas, F., et al., Spatial regulation of membrane fusion controlled by modification of phosphoinositides. *PLoS One*, 2010. 5(8): p. e12208.

## Appendix

### (A) Step-by-step guide for the measurement of CFP/YFP FLIM-FRET using an Olympus FV1000 CLSM with PicoQuant LSM FLIM and FCS upgrade kit

The Olympus Fluoview software on one computer (Imaging) is used to control the confocal microscope while the PicoQuant SymPhoTime software on a second computer (FLIM) is used for FLIM data acquisition and analysis. Both computers are connected by a network cable and the small tool SymPhoTime\_RC can be used to remote-control the image acquisition of the SymPhoTime software from the Imaging computer.

#### 1. Starting of the microscope and the software

Switch on the microscope, the appropriate lasers, the Imaging computer and the FLIM computer.

On the Imaging computer, start SymPhoTime\_RC and Fluoview software. On the FLIM computer, start SymPhoTime and open a new workspace.

#### 2. Selecting an objective, focussing the microscope and configuring the laser scanning and detection for confocal image acquisition.

Select 60x/1.35 Oil UPlanSApo objective and focus the sample using white light then search for cells having fluorescence tags using mercury lamp and focus them. Load the predefined settings for eCFP/eYFP. This will excite fusion proteins of CFP/YFP using the 458 nm and the 515 nm laser line as excitation source for confocal imaging, the primary dichroic mirror should be set to DM405-458/515/561/633 and the secondary dichroic mirror to SMD510. Activate the TD-channel to get an additional DIC image.

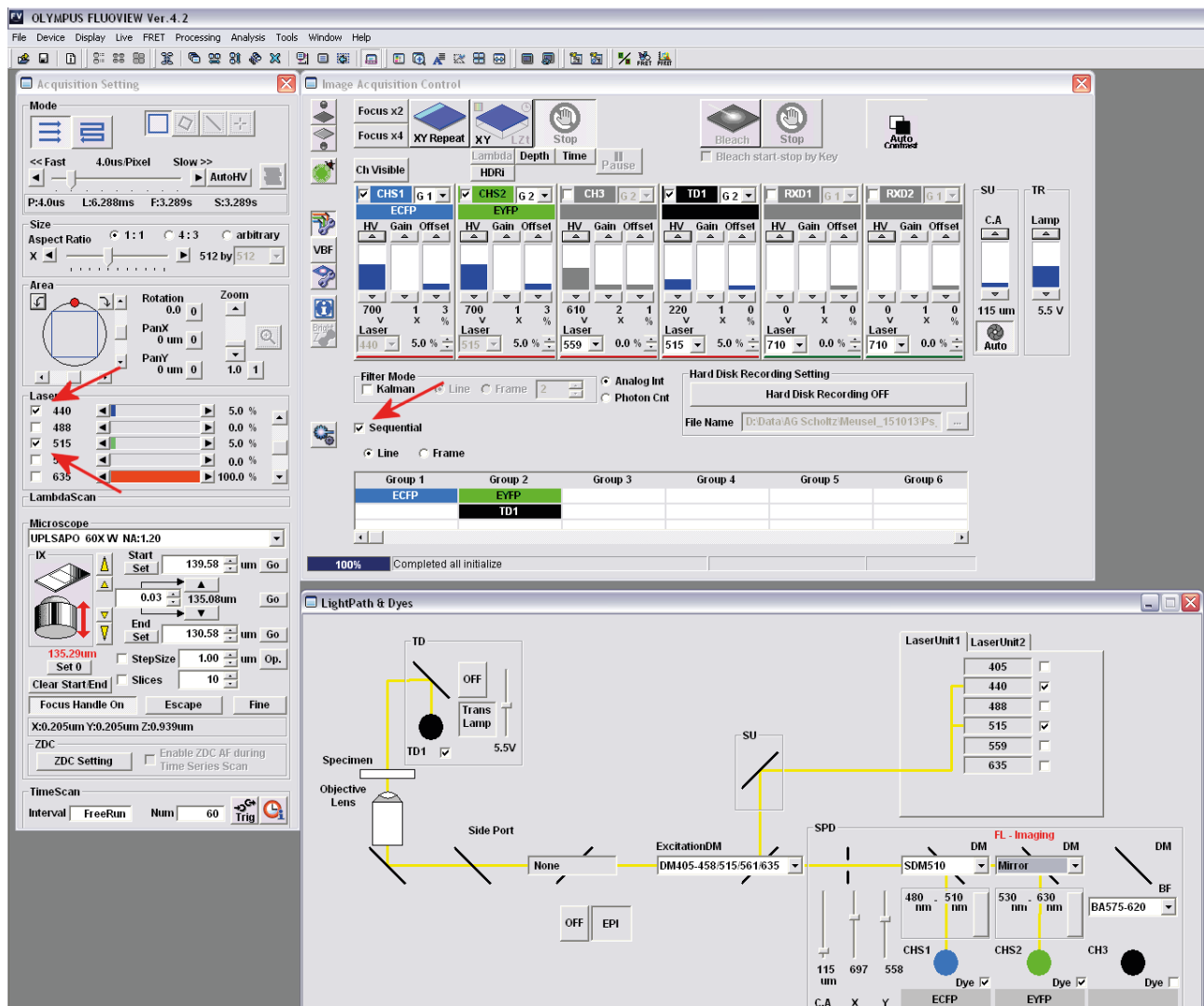


**Figure A1** Settings of FV-1000 software for confocal imaging of CFP and YFP expression individually. Sequential scan with 458 nm and 515 nm laser lines.

### 3. Acquisition of confocal images

To Monitor the expression of the individual proteins, take an image in the sequential mode. Under those conditions CFP and YFP are excited and detected alternately. (Figure A1) Deactivate the 515nm excitation and the sequential mode and take an "Intensity" FRET image. (Figure A2) Channel 1 shows the CFP fluorescence intensity, channel 2 the YFP intensity due to FRET but also spill-over of CFP, acceptor emission due to direct excitation at 458 nm and eventually background-fluorescence. Therefore additional measurements like FLIM-FRET or acceptor photo-bleaching are necessary to obtain conclusive results.

### 4. Configuring the microscope and laser settings for FLIM imaging

For FLIM-FRET Imaging, only CFP is excited using a pulsed 440nm diode laser, images are recorded with the PicoQuant Detector Unit, in our case equipped with SPAD detectors and connected to the output port of the FV1000 scanner unit by fiber optics. Therefore all cw-lasers have to be deactivated and the light path has to be changed so the signal is routed to the output port. (see Figure A3)

The pulsed laser diodes have to be switched on and off either by hand or with additional hardware via the *FluoView* software like in our setup. Therefore all pulsed diode lasers are handled as 635nm laser independent of the wavelength

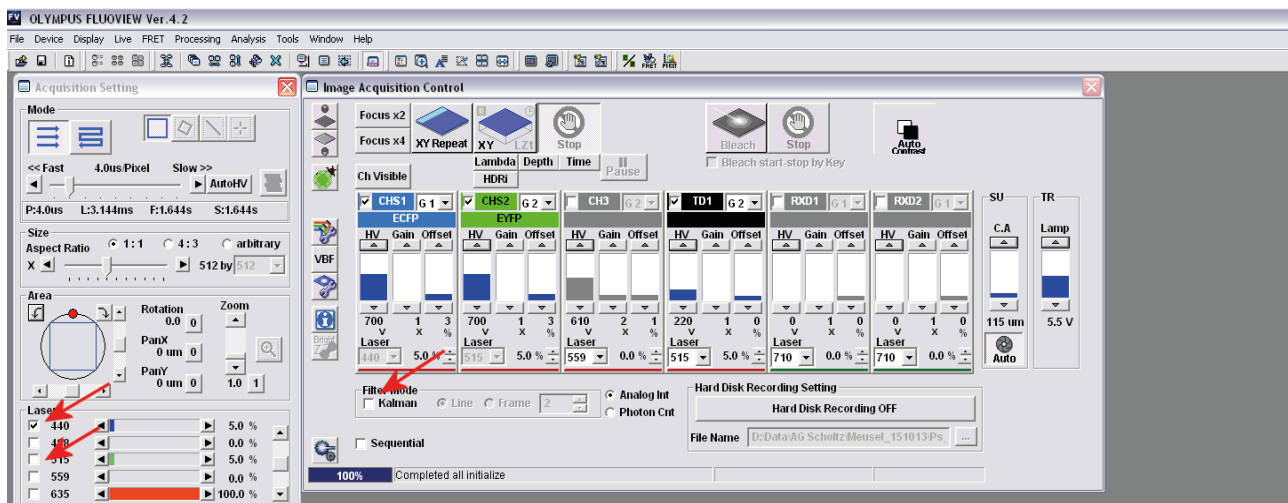


**Figure A2** Settings of FV-1000 software for confocal imaging of CFP-YFP intensity FRET. Only 458 nm laser line is activated, CFP and YFP emission are detected in parallel.

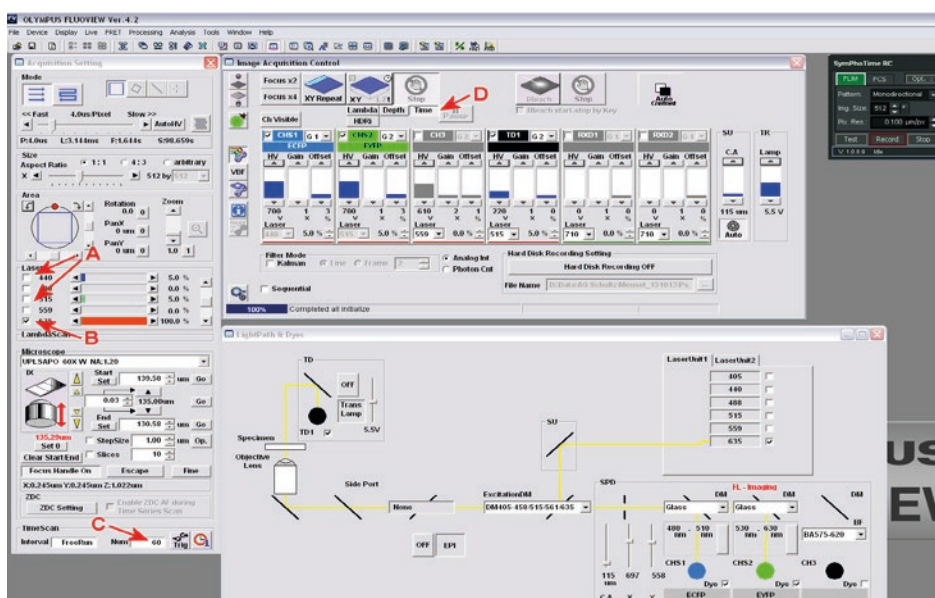


**Figure A3** Settings of FV-1000 software for FLIM imaging of CFP fluorescence. Cw lasers lines are deactivated (A), pulsed diode laser on/off is controlled FV1000 software (B), TimeScan is set to free run, 60 frames and Time toggle is activated (C) and emission signal is routed to output port (D). SymphoTime on the FLIM computer can be controlled via SymphoTime\_Rc from the IMAGING computer.

used. The intensity has to be set to 100% enabling the on/off software control of the pulsed lasers, whereas power adjustment of the pulsed lasers has to be done manually at the Laser Combining Unit (LCU) or via the pulsed diode laser driver unit (PDL).

##### 5. Acquisition of FLIM images

Adjust equal image size in *FluoView* and *SymphoTime* software (e.g. 512 x 512 pixel). Reduce scan speed (pixel dwell time) to enable proper calculation of the average photon counts per pixel. Start scanning in the XY Repeat mode and activate “Test” with *SymphoTime\_RC*. Adjust laser power to a maximum <105 counts/second. When all adjustments are done, stop “Test” mode. You can set the filename, resolution (can be obtained from the “info” button of *FluoView*) and additional comments for the FLIM file using

##### *SymPhoTime\_RC*.

For the acquisition of the FLIM image, activate the “Time” toggle button and set time settings to “Free run” and 60 scans, this will result in a FLIM acquisition time of about 90 seconds. Start FLIM recording with *SymPhoTime\_RC* (“Record”) and then start x-y-t acquisition in the *FluoView* software. After scanning has finished stop FLIM acquisition with *SymPhoTime\_RC* (“Stop”).

##### 6. Measurement of the internal response function (IRF)

If there is no fluorophore solution with the spectral properties of CFP and a very short lifetime available, scattering of the excitation light is used to record the IRF. Put a drop of buffer on a cover slip and place a narrow-band laser-line filter in front of the detector. Set the scanning mode to point-scan

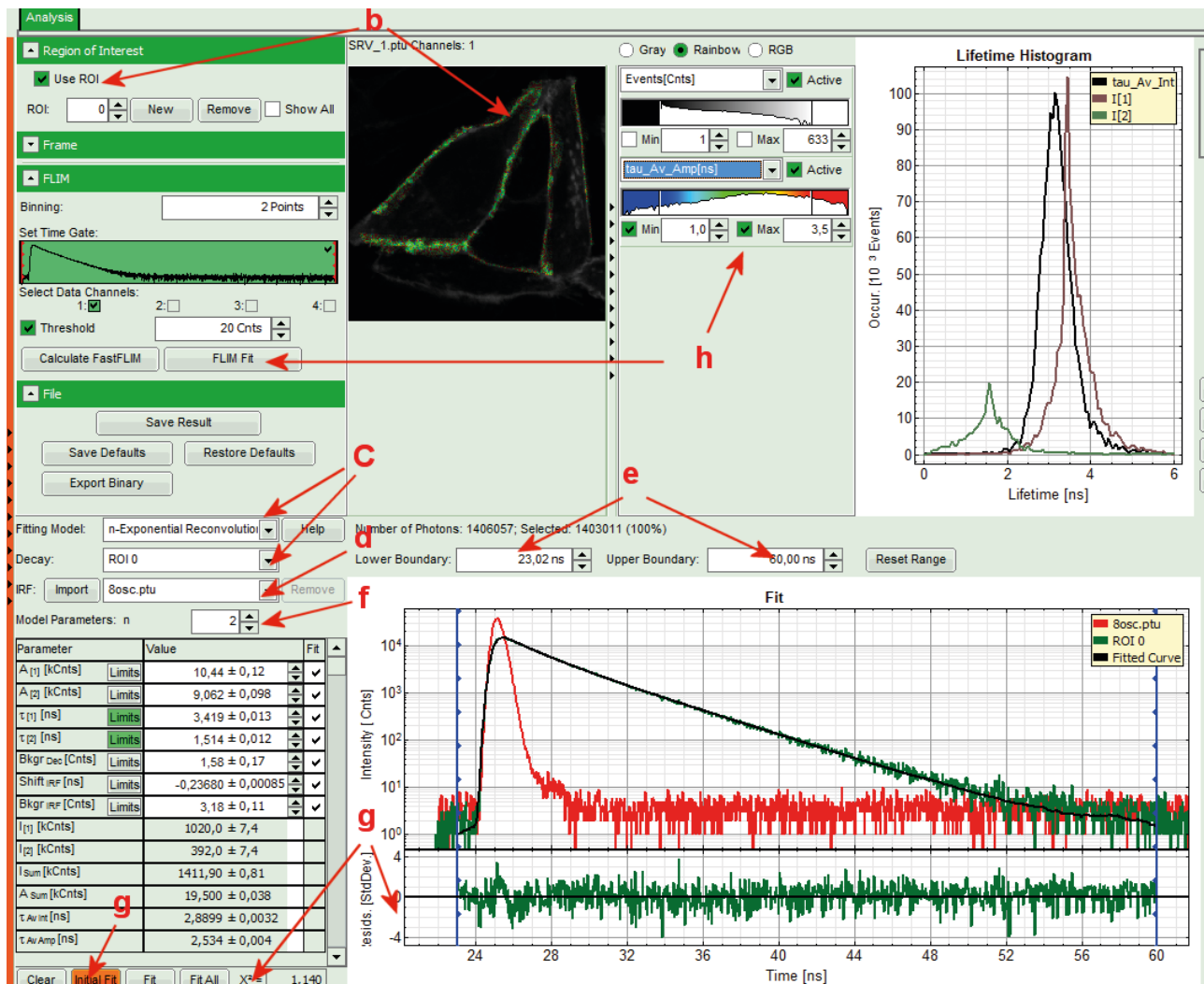


**Figure A4** FLIM Image analysis with PicoQuant SymPhoTime 64 software. (b) Selection of ROIs, (c) setting of fitting model and ROI, (d) loading of the IRF, (e) selection of range of channels, (f) selecting the number of exponentials for the fit, (g) fitting of the decay curve and analysis of the results and (h) finally lifetime fit for each individual point, generation of the lifetime image and the Lifetime histogram).

and the number of scans to 32.000. Start scanning in the XY Repeat mode and activate "Test" with *SymPhoTime\_RC*. Attenuated the signal down to about 104 counts / second. Afterwards measure the decay curve as described for the FLIM images above for about 60 seconds.

## 7. Data Analysis

- a) In *SymphoTime*, select the data set to be analyzed. With the latest version, *SymphoTime 64*, choose "Analysis – Imaging – FLIM analysis". The following steps are similar for the 32 and the 64 bit version of *SymphoTime* (see Figure A4)
- b) Activate "Use ROI" and mark one or more Regions of Interest (ROI) on the FLIM image using the selection tools (available by right-click on the image). We are interested in the interaction of TMD-HA-YFP with the raft-marker GPI-CFP, so we are selecting the plasma membrane of cells expressing both CFP and YFP (based on the confocal image data set 1)
- c) Set "Fitting Modell" to "n-Exponential Reconstruction" and select in "Decay" to the ROI you want to measure.
- d) Import the IRF measured and activate it (in the screenshot "8osc.ptu") instead of the "Calculated IRF"
- e) Set the "Lower Boundary" and the "Upper Boundary" for the range of the fitted interval according to the measured decay curve.
- f) Set "Model Parameters: n" to the number of exponentials you want to fit your decay with. In our case, CFP is known to have a biexponential decay so we are starting with "2".
- g) Do an "Initial Fit", afterwards "Fit". The fitted curve (black) should overlay well with the decay curve measured (green), quality of the fit is judged by the goodness of fit parameter  $\chi^2$  (should be close to 1) and the distribution of the residuals. The residuals representing the deviation of the fit from the measured decay curve should be small and randomly distributed. If the fit is not satisfying, especially if a tendency can be seen in the distribution of the residuals, an additional exponential should be added, all parameters have to be cleared and the fit has to be repeated.  
The number parameters should be kept as low as possible and the parameters obtained have to be reasonable (for instance no lifetime below the resolution of the instrument, no negative amplitudes).
- h) When a satisfying fit has been obtained, the lifetime fit for each individual point of the selected ROI and the Lifetime histogram can be calculated with "FLIM Fit". Calculation time can be reduced by Binning, but by doing so

resolution will be reduced. The color coding of can be adopted to optimize the contrast of the lifetime image.

## (B) Video links for FLIM data acquisition

- Zeiss LSM 710 with a PicoQuant LSM Upgrade Kit (FLIM Demo)
- Nikon A1R with a PicoQuant LSM Upgrade Kit (FLIM and FCS Demo)
- Measuring a FLIM image with an LSM Upgrade Kit (Nikon A1)
- Recording a FLIM stack with an LSM Upgrade Kit on a Nikon A1
- Performing a FLIM-FRET Measurement with an LSM Upgrade Kit (Olympus FV 1200)
- Measure an Instrumental Response Function (IRF) with an LSM Upgrade Kit

## (C) SPT64 links for FLIM data analysis

- SymPhoTime Lifetime Fitting
- Lifetime Fitting Using the FLIM Analysis
- FLIM ROI Fitting
- FLIM-FRET Calculation for Single Exponential Donors
- FLIM FRET Calculation for Multi Exponential Donors
- Pattern Matching
- Visualizing Dynamics with the Multi Frame FLIM Analysis
- Phasor Analysis

## (D) Tipps/Tricks

- How to Measure the Instrument Response Function (IRF)
- How to Avoid the Pile-up Effect in FLIM Measurements





# Chapter

# Fluorescence Correlation Spectroscopy (FCS)

**Radek Macháň<sup>1,2</sup> and Martin Hof<sup>1</sup>**

<sup>1</sup> J. Heyrovský Institute of Physical Chemistry of ASCR, Prague, Czech Republic

<sup>2</sup> Department of Biological Sciences and Centre for BioImaging Sciences,  
National University of Singapore, Singapore

Contact details of corresponding author: Martin Hof, martin.hof@jh-inst.cas.cz

## Index

1. Principle and Theory.....	3
2. Instrumentation.....	4
3. Sample Preparation.....	5
4. Data Acquisition.....	6
5. Data Analysis.....	7
Calibration of the Detection Volume .....	8
Models for Fitting of Autocorrelation Curves.....	9
Choice of an Appropriate Model of Autocorrelation function .....	10
6. Artefacts in FCS.....	11
7. Technique Overview .....	13
Applications and Limitations of FCS .....	13
Selected References .....	13
8. Conclusion.....	13
References and Further Reading .....	15
Appendix.....	17
FCS with SymPhoTime 64.....	17
Test Mode .....	17
Measurement Mode.....	17
Analysis Mode.....	17

## 1. Principle and Theory

FCS is a technique which utilizes statistical analysis of fluctuations in fluorescence intensity to extract information on equilibrium processes in the sample (such as molecular diffusion or reversible chemical reactions), which are the cause of the intensity fluctuations. Low concentrations of fluorescent particles (fluorophores, fluorescently labelled molecules or supramolecular complexes) and small effective detection volumes ( $1 \mu\text{m}^3$  or smaller, typically defined by the point spread function of a confocal laser scanning microscope – CLSM) are used in FCS to obtain pronounced fluorescence intensity fluctuations<sup>[1-3]</sup>. For that reason, FCS is sometimes considered a single-molecule technique.

In an FCS measurement, time-trace of fluorescence intensity  $I(t)$  originating from the small effective detection volume  $V_0$  is recorded and its autocorrelation function  $G(\tau)$ , defined by equation (1), is calculated (pointed brackets represent averaging over all values of time  $t$ ). The shape of the autocorrelation function reflects the time-scales of the fluorescence intensity fluctuations.

$$G(\tau) = \frac{\langle I(t)I(t+\tau) \rangle}{\langle I(t) \rangle^2} \quad (1)$$

$G(\tau)$  rises steeply to its maximum value on nanosecond time-scale; the effect (called photon antibunching) is caused by a non-zero delay between two consecutive photons emitted by a single fluorophore and is related to the fluorescence lifetime and number of individual fluorescence emitters within the detection volume<sup>[4],[5]</sup>. The rise of  $G(\tau)$  is below temporal resolution of typical FCS experiments which capture only the subsequent decay of autocorrelation. Fluorescence intensity fluctuations caused by fast photophysical and photochemical processes (such as intersystem crossing to non-fluorescent triplet states or excited-state reactions) and by rotational diffusion of molecules (in the case of polarized detection) dominate the decay of  $G(\tau)$  on microsecond and sub-microsecond time-scale<sup>[6],[7]</sup>. Decay on longer time-scales is related to translational diffusion or flow of molecules in and out of the detection volume. If several processes in the sample are happening on similar time-scales, their contributions to  $G(\tau)$  are difficult to distinguish.

Theoretical models have been developed, which describe the relation between characteristics of the processes underlying fluorescence fluctuations (such as kinetic constants in the case of chemical reactions or diffusion coefficients in the case of diffusion) and the shape of the autocorrelation function calculated according to (1). Fitting  $G(\tau)$  with an ap-

propriate model yields information on equilibrium dynamics in the sample.

Investigation of diffusion of molecules and supramolecular complexes belongs among the most common applications of FCS and is, therefore, dealt with in most detail in the following text. The principle of FCS is schematically illustrated in Figure 1. Diffusion or flow causes fluctuations in the number of fluorescent particles present in the effective detection volume resulting in fluctuations in detected fluorescence intensity. Let us consider a value  $\tau_1$  of the lag time in formula (1), which is small with respect to the average residence time  $\tau_D$  of a fluorescent particle within the effective detection volume. The number of particles  $N$  present within the effective detection volume is not likely to change significantly within a time interval of the length  $\tau_1$ ;  $I(t)$  and  $I(t + \tau_1)$  are, therefore, most likely very similar to each other and the autocorrelation  $G(\tau_1)$  is close to its maximal value. The situation is analogous for other sources of fluorescence intensity fluctuations. When the fluctuations are caused by reversible transitions of the fluorophore to a dark state, the number of fluorophores in their bright state is not likely to change significantly within a lag time short with respect to the reciprocal value of the transition rate constant.

The autocorrelation function reaches its maximum at  $\tau = 0$  (disregarding the initial increase in autocorrelation caused by photon antibunching, which is below the temporal resolution of typical FCS experiments). If we consider only fluctuations caused by movement of fluorescent particles, the amplitude  $G(0)$  is inversely proportional to the average number of fluorescent particles within the detection volume<sup>[8]</sup>. FCS, apart from providing kinetic information (diffusion coefficients, kinetic constants), provides also independent estimate of concentration of fluorescent particles in the sample. Note that by the term fluorescent particle, we describe any fluorescent molecule, aggregate or complex containing at least one fluorophore which is moving as a single entity and is entering and exiting the effective detection volume at once. In the case of very large molecules (larger than the dimensions of  $V_0$ ; for example large DNA chains) labelled at multiple sites, individual segments of the molecule can behave like independent fluorescent particles and enter and exit effective detection volume at different instants<sup>[9]</sup>.

When we consider a value of lag time  $\tau_2$ , which is long with respect to  $\tau_D$ , the particle numbers  $N(t)$  and  $N(t + \tau_2)$  and, therefore, also the fluorescence intensities  $I(t)$  and  $I(t + \tau_2)$  are no more correlated and the autocorrelation  $G(\tau_2)$  is close to zero – its asymptotic value  $G(\infty)$ . The average residence time  $\tau_D$  of a fluorescent particle in the detection volume corresponds (in common models) to the lag time at which  $G(\tau)$  decays to the half of its maximal value.

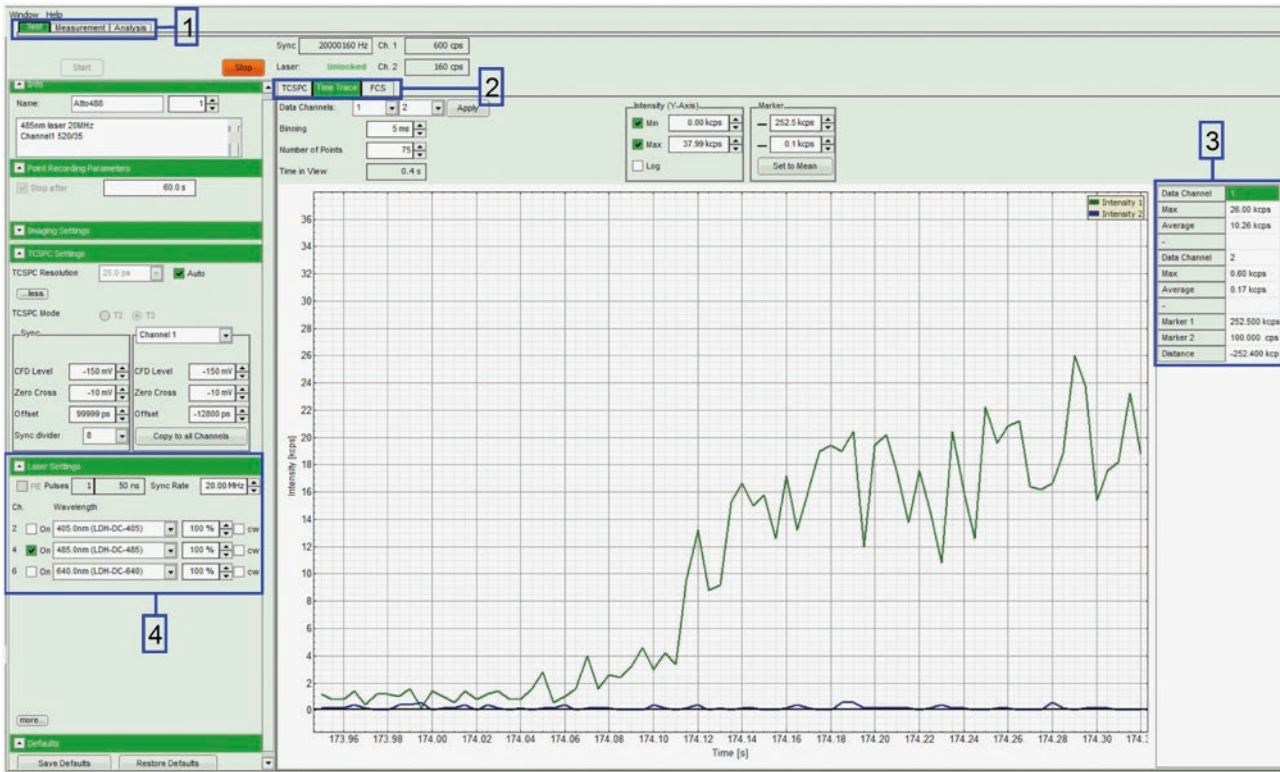


**Figure 1** Illustration of the principle of FCS. Fluorescence intensity is collected from a small effective detection volume (usually the point spread function of a confocal laser scanning microscope) (A). Recorded fluorescence intensity exhibits fluctuations (B) caused by movement of fluorescent particles out and into the detection volume (by diffusion or flow) or by reversible chemical reactions of the fluorophore. Autocorrelation function  $G(\tau)$  reflects the time-scale of the fluctuations; average residence time  $\tau_D$  of a fluorescent particle in the effective detection volume can be found by analysis of the decay of  $G(\tau)$ .

$\tau_D$  and particle number  $N$  are found by analysis of the experimentally obtained autocorrelation function. If the volume  $V_0$  is known,  $\tau_D$  and  $N$  can be used to calculate diffusion coefficient  $D$  and concentration of the fluorescent particles  $c$ .  $V_0$  is usually determined by a calibration measurement; more details on calibration in FCS and its pitfalls can be found in the section Method.

## 2. Instrumentation

As has been said in the Introduction, a CLSM is the most common instrument for FCS. The essential features of an FCS setup comprise a small effective detection volume  $V_0$  and highly efficient detection of fluorescence intensity.

The effective detection volume is defined by diffraction limited focusing of the excitation laser beam via a high numerical aperture (usually larger than 1) objective and by spatial efficiency of collecting fluorescence emission from the sample (defined by adjustment of the confocal pinhole).  $V_0$ , thus, corresponds to the point spread function (PSF) of the microscope [2],[10].

Photomultiplier tubes (PMTs) or single photon av-

alanche diodes (SPADs) are used as photo-detectors for FCS, the latter ones being preferred for their higher detection efficiency [2].

An FCS setup can be, therefore, based on most commercially available CLSMs without a need for any extensive modifications. The only modification, which is often necessary, is the addition of more sensitive photo-detectors. CLSMs designed for performing FCS and upgrades of other types of CLSMs are commercially available.

A hardware correlator used to be a common part of FCS setups. Software calculation of autocorrelation functions is, however, preferred nowadays, because it is more versatile [2],[11]. The measured time-trace of fluorescence intensity  $I(t)$  is directly stored in the computer and used to calculate  $G(\tau)$  either during the measurement or after the end of data acquisition. Software calculation of  $G(\tau)$  from stored intensity time-trace allows  $I(t)$  to be processed by application of numerical filters (which is the principle of some advanced FCS variants described in specialized chapters) or by removing sections of  $I(t)$  during which large fluorescent aggregates resided in effective detection volume. Since autocorrelation  $G(\tau)$  depends on square of fluorescence intensity, contribution of each particle to the autocorrelation function

is weighted by the square of its brightness. Large aggregates, several times brighter than the average fluorescent particle in the sample, have a significant impact on  $G(\tau)$ . A rare event such as diffusion of a single bright aggregate through the detection volume can, therefore, considerably distort the whole autocorrelation function (see Figure 2).

A 2-photon microscope is also suitable for performing FCS thanks to its small PSF (which is even smaller than in the case of a CLSM)<sup>[12],[13]</sup>. The principle of 2-photon FCS is identical to 1-photon FCS and is, therefore, not discussed separately.

Alternatively any other instrumental setup can be used, which allows selective detection of fluorescence from a sufficiently small volume element within the sample. Very promising are imaging FCS modalities in which fluorescence is collected in parallel from many effective detection volumes; those are defined in the lateral plane by pixels of an imaging detector (typically an electron multiplying charge coupled device – EMCCD) and by illumination by a thin light sheet in the axial direction. The illumination light sheet can be created by total internal reflection (TIR)<sup>[14],[15]</sup> or by a cylindrical lens such as it is done in selective plane illumination microscopy (SPIM)<sup>[16]</sup>. Imaging FCS approaches possess the advantage of performing FCS measurements in parallel in many

points in the sample, in which way a statistically significant dataset can be obtained in a single measurement. This is particularly beneficial for FCS studies of intrinsically heterogeneous samples such as a living cell or even multicellular structures.

### 3. Sample Preparation

Fluorescent labelling is a crucial step in preparation of samples for FCS. It has been shown that signal to noise ratio in FCS reaches the highest values when the average number  $N$  of fluorescent particles in the effective detection volume is approximately 1. The lower the particle number  $N$  is, the longer the measurement time needed to observe statistically significant number of molecules diffusing through the detection volume. On the other hand, high values of  $N$  result in smaller relative fluctuations and lower amplitude of autocorrelation function  $G(0)$ . Values of  $N$  in the range between 0.1 and  $10^2$  are considered well suited for FCS<sup>[3],[18]</sup>. The optimal particle numbers around 1 correspond in the case of standard confocal FCS to concentrations of fluorescent particles in nM range. Higher concentrations are used in the cases of special experimental setups with reduced effective detection volumes<sup>[19],[20]</sup>.

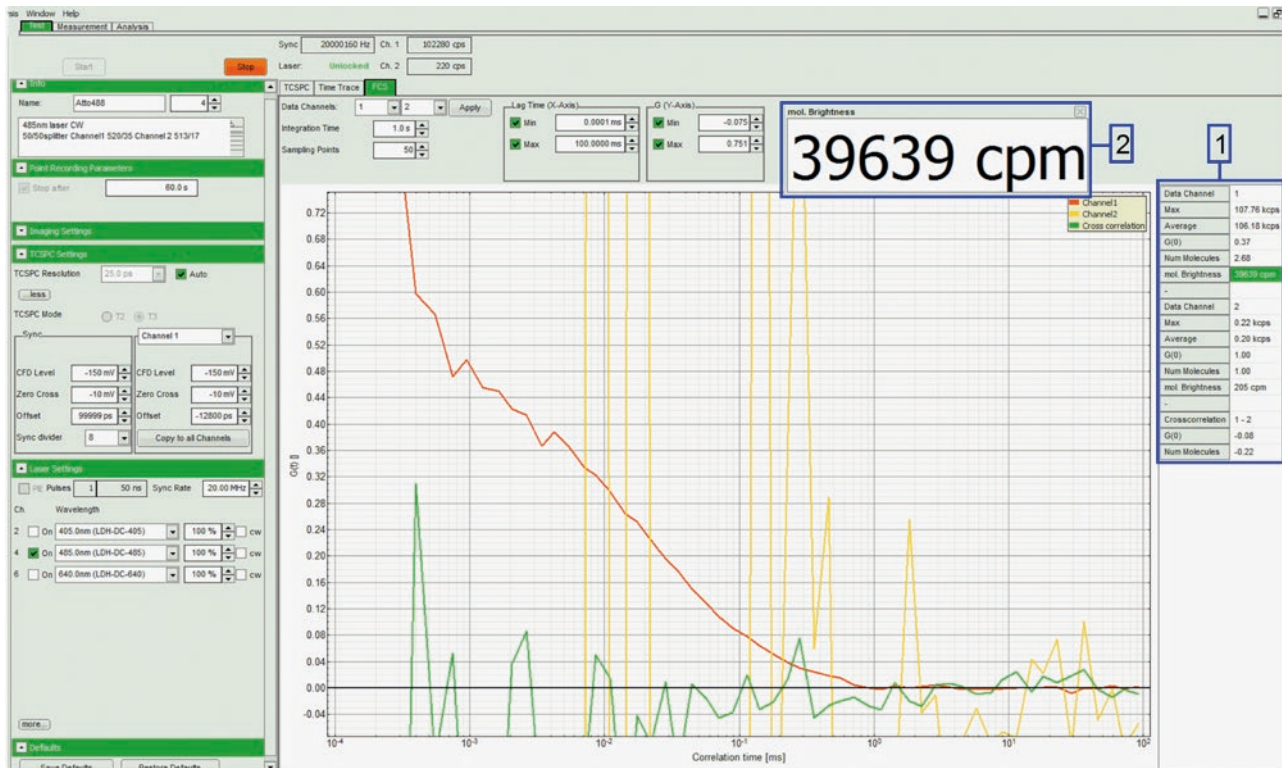


**Figure 2** Illustration of calculation of FCS autocorrelation curves. Passage of a large aggregate through the effective detection volume (manifested by a large peak in intensity time-trace – upper panel) distorts the shape of the autocorrelation function in the region of longer lag times  $\tau$ . Selecting only a part of the intensity time-trace (which is not influenced by the aggregate) results in an improvement of the shape of  $G(\tau)$ , which can be, then, fitted with model (3).

The choice of the fluorophore is also of considerable importance. High brightness (photon count-rate per molecule) is needed in order to acquire sufficiently high signal from each individual fluorescent particle diffusing through the detection volume. High photo-stability of the dye is also important to reduce artefacts caused by photobleaching. Photo-stability is important especially in samples where the investigated kinetics are slow and fluorophores are, therefore, undergoing excitation for prolonged periods of time. Apart from synthetic organic fluorophores, fluorescent proteins such as GFP and its mutants are frequently used in biological applications of FCS<sup>[21],[22],[23]</sup>. In this case it is crucial to find the conditions under which the fluorescent protein is expressed at concentrations suitable for FCS measurements. Quantum dots are also sometimes used for their high photo-stability<sup>[22],[24]</sup>.

Large aggregates of fluorescent particles can, due to their very high brightness, considerably distort the autocorrelation function and should be, therefore, avoided when possible. If they are present in low numbers with respect to the non-aggregated particles, the data can be cleaned from their influence, provided software correlation is used (see Figure 2).

## 4. Data Acquisition

Prior to acquiring FCS data, the instrument should be carefully aligned. FCS measurements are very sensitive to the actual shape of the effective detection volume. Proper alignment is, therefore, more critical than in the case of confocal imaging. The alignment ensures optimal photon collection efficiency through optimizing the emission light pathway of the microscope (such as mirrors and lenses directing the fluorescence emission to the detectors) in order that the maximum number of photons from the effective detection volume reaches the detector. Critical is the alignment of the confocal pinhole which has a large impact on the shape of the effective detection volume. Besides that, the correction collar of the objective needs to be adjusted to compensate correctly for the thickness and refractive index of the cover-glass.

The easiest way to optimize the pinhole position is to measure fluorescence intensity originating from a solution of a reference fluorophore and adjust the pinhole position to reach maximal intensity at the detector. It is advisable to use higher fluorophore concentration than for FCS (for example in the  $\mu\text{M}$  range). The optimal setting of the objective correction collar can be found by searching for maximum of fluorescence intensity in a solution of a reference fluorophore, like in the case of pinhole position optimization. A more rigorous way of adjusting confocal

pinhole and correction collar is via measuring FCS in a solution of a reference fluorophore and searching for the maximum of molecular brightness (total photon count-rate divided by particle number  $N$ ) of the fluorophore<sup>[25]</sup>. It is usually sufficient to perform such measurement at the end of the alignment procedure; if such a measurement is performed each time under the same experimental conditions, it serves as a good control whether the microscope is correctly aligned. Besides serving as a proof of a correct alignment of the microscope, the FCS measurement in a solution of a reference fluorophore is usually also used for calibration of the effective detection volume (discussed in more detail later).

After focusing (placing the effective detection volume) to the place of interest within the sample, fluorescence intensity  $I(t)$  is recorded. The detection volume should be ideally placed close to the centre of the CLSM field of view. Further from the centre, the dimensions and shape of the effective detection volume change due to optical aberrations. However, the deviations are relatively small within the majority of the field of view of a well-aligned CLSM (excluding the regions closest to the edges of the field of view)<sup>[26]</sup>. The acquisition time should be at least  $10^3 - 10^4$  times longer than the characteristic time-scale of the slowest investigated processes<sup>[27],[28]</sup>. When focusing into small structures (e. g. biological membranes, thickness of which is much smaller than dimensions of  $V_0$ ), long measurements may suffer from artefacts caused by movements of the structure of interest with respect to the microscope focus (e. g. membrane undulations). Such movements may result in additional apparent slow kinetics in the autocorrelation function. The optimal excitation intensity in FCS is a compromise between the requirement of high number of fluorescence photons needed for statistical accuracy of  $G(\tau)$  (a tenfold reduction of excitation intensity means approximately a hundred times longer measurement needed to reach a comparable statistical accuracy<sup>[29],[30],[31]</sup>) and the need to minimize artefacts caused by photobleaching and optical saturation (nonlinearity in the dependence of fluorescence intensity on excitation intensity resulting from depletion of the ground-state fluorophore population caused by high excitation rate). The maximal excitation intensity at which no photobleaching and saturation artefacts appear depends on the photophysics of the fluorophore under given conditions and on the average time it undergoes excitation (which depends on the effective detection volume dimensions and on  $D$ )<sup>[32]</sup>. For typical organic fluorophores, excitation intensities should be sufficiently lower than  $30 \text{ kW cm}^{-2}$ , a value which corresponds for usual microscope objectives to excitation powers of approximately  $100 \mu\text{W}$  (at back aperture of the objective)<sup>[2],[30]</sup>. The excitation intensity at which optical saturation starts to play a sig-

nificant role can be directly determined for each type of samples (for a particular fluorophore in a particular environment) by measuring the dependence of fluorescence intensity on the excitation intensity (a saturation curve). A linear dependence is observed at low excitation intensities; increasing deviations from linearity appear at higher intensities, until saturation is reached. Further increase of excitation intensity does not lead to any increase in the intensity of fluorescence. FCS measurements should be performed with excitation intensities corresponding to the linear region of the curve.

The influence of photobleaching and optical saturation (as well as other possible sources of artefacts in FCS such as confocal pinhole misalignment or mismatch in refractive indices between the sample and the immersion liquid on the objective) on the shape of  $G(\tau)$  have been extensively studied by the group of Enderlein<sup>[2],[30],[33]</sup>.

## 5. Data Analysis

Data analysis in FCS can be divided into two steps: the first step is the calculation of the autocorrelation function  $G(\tau)$  from the measured fluorescence intensity time-trace  $I(t)$ ; the second step is the analysis of the autocorrelation function. If a hardware correlator is used, only the second step is present, because  $G(\tau)$  represents the direct instrumental readout. If software correlation is used, only a part of the intensity time-trace  $I(t)$  can be chosen to avoid distortion of  $G(\tau)$  by large fluctuations of fluorescence intensity caused for example by the passage of a large fluorescent aggregate through the detection volume (see Figure 2).

The first step is not problematic since it follows a straightforward algorithm. Many implementation of the algorithm are readily available for the users. For example FCS software packages QuickFit (Deutsches Krebsforschungs Zentrum, Heidelberg, Germany) or FFS Data Processor (Scientific Software Technologies Center, Minsk, Belarus) can correlate data recorded by various instruments. Dedicated FCS instruments are usually supplied with software allowing correlating time-traces recorded by the respective instrument.

Let us focus in more detail on the second step, which involves more input from the user, because an appropriate model for interpretation of  $G(\tau)$  has to be chosen. Analysis of autocorrelation functions can be performed in most FCS software packages such as the above mentioned QuickFit or FFS Data Processor. Alternatively, any data processing software allowing non-linear curve fitting can be used to fit  $G(\tau)$  with a theoretical model.

The theoretical models, which describe the shape of

the autocorrelation function  $G(\tau)$  are usually derived by approximating the effective detection volume by a 3-dimensional Gaussian profile (2) describing the probability  $W(R,Z)$  of detecting a photon emitted by a fluorophore located at a given position  $(R,Z)$ .  $R$  is the radial distance from the optical axis and  $Z$  is the axial coordinate ( $Z = 0$  corresponds to the focal plane);  $\omega_0$  and  $\omega_z$  are parameters describing the extent of the effective detection volume in the focal plane and along the optical axis respectively.

$$W(R,Z) = \exp\left(-2\frac{R^2}{\omega_0^2}\right) \exp\left(-2\frac{Z^2}{\omega_z^2}\right) \quad (2)$$

Some authors have derived models for more realistic shapes of effective detection volumes<sup>[10],[34]</sup>; however, the resulting models are much more complicated and not commonly used in practice. We will, therefore, mention only models derived for the 3-dimensional Gaussian approximation (2). The most basic situation is the free diffusion of a single type of particles in all 3 dimensions.  $G(\tau)$  is, in that case, described by the model (3). A detailed derivation of the model can be found in the original works on theory of FCS<sup>[8],[35]</sup>. Models applicable in other frequently encountered situations are summarized in one of the following sections.

$$G(\tau) = \frac{1}{N} \frac{1}{1+(\tau/\tau_D)} \sqrt{\frac{1}{1+(\tau/\tau_D)(\omega_0/\omega_z)^2}} \quad (3)$$

(3) can be rewritten in terms of diffusion coefficient  $D$  and concentration of fluorescent particles  $c$  (4) using their relationship to the dimensions of the effective detection volume (5) and (6) respectively<sup>[36]</sup>.

$$G(\tau) = \frac{1}{c N_A V_0} \left(1 + \frac{4D_\tau}{\omega_0^2}\right)^{-1} \left(1 + \frac{4D_\tau}{\omega_z^2}\right)^{-1/2} \quad (4)$$

$$\tau_D = \frac{\omega_0^2}{4D} \quad (5)$$

$$N = c N_A V_0 = c N_A \pi^{\frac{3}{2}} \omega_0 \omega_z \quad (6)$$

The simple model (3) contains 3 fitting parameters:  $\tau_D$ ,  $N$  and the ratio  $\omega_z/\omega_0$  called structure parameter  $k$  and describing the shape of the effective detection volume. While  $\tau_D$  and  $N$  represent the readout parameters of the fit, structure parameter is determined by a calibration measurement and then used as a constant parameter when fitting the results of the subsequent series of measurements. Determination of the physically relevant parameters  $D$  and  $c$  requires the knowledge of  $V_0$ , which is also determined by the calibration measurement. Note, that at  $\tau = 0$ ,  $G(\tau)$  reaches its maximal value  $G(0)$ , which is inversely proportional to the number  $N$  (or concentration  $c$ ) of fluorescent particles.

### Calibration of the Detection Volume

Calibration of the detection volume is necessary for quantitative interpretation of FCS data. Calibration should be performed after any change to the experimental setup, which may affect the size and shape of the detection volume (change of excitation wavelength, of confocal pinhole, etc.); a calibration measurement is usually performed at least every day, if the identical setup is used for a longer time. There exist three approaches to the calibration in FCS<sup>[36],[37]</sup>:

1. Measurement of an FCS autocorrelation function in a solution of a reference fluorophore of exactly known concentration (or, optimally, a series of measurements with a series of concentrations);  $V_0$  is calculated from the amplitude of the autocorrelation  $G(0)$  according to (6). This calibration procedure is optimal for FCS experiments focusing on determination of concentrations via measuring  $G(0)$ , because  $V_0$  is, in this case, determined without making any assumptions concerning the shape of the effective detection volume. Deviations of the shape from the usually assumed Gaussian profile do not, therefore, affect the results. On the other hand, this calibration procedure is not sufficient for determination of diffusion coefficients, because it provides no information on  $k$  (or  $\omega_0$ ). That information can be supplemented by the second calibration procedure described below. Not all standard fluorescent dyes are suitable for concentration-based calibration; for example rhodamine 6G or some Alexa Fluor® dyes adsorb strongly to glass surface, which causes a large uncertainty in their concentration<sup>[36]</sup>. Uncorrelated background or scattered light can lead to overestimation of  $N$  (see the section Artefacts in FCS below), which would introduce an error in  $V_0$  calibration if the fluorescence intensity is not high enough to yield the relative contribution of the parasitic signal components negligible<sup>[38]</sup>.

2. Measurement of an FCS autocorrelation function in a solution of a reference fluorophore of exactly

known diffusion coefficient;  $\omega_0$  is determined from  $\tau_D$  using (5) while  $\tau_D$  is found by fitting  $G(\tau)$  with (3) or another appropriate model. Structure parameter  $k$  is also found from the fit of  $G(\tau)$  as another adjustable parameter. Increased number of free parameters naturally increases the risk of numerical instability of the fit and a good quality of autocorrelation function is important in the calibration measurement. Fortunately,  $\tau_D$  and  $k$  are not strongly correlated and the uncertainty in  $k$  affects only moderately the accuracy of  $\tau_D$  determination from the fit. The value of structure parameter for typical experimental setups ranges from 3 to 8 (depending on the magnification and numerical aperture of the objective)<sup>[37],[39]</sup> and varying  $k$  within this range has usually only minor influence on the fitted values of  $\tau_D$ .

Reference values of diffusion coefficients of standard fluorophores are for example summarized in one of the PicoQuant Application Notes<sup>[40]</sup>. Diffusion coefficient depends on temperature by Stokes-Einstein relation<sup>[40]</sup> and accurate knowledge of temperature by Stokes-Einstein relation<sup>[40]</sup> and accurate knowledge of temperature within the sample is indispensable for correct diffusion-based calibration. The reference value of diffusion coefficient must be corrected for the actual temperature in the sample for calibration purposes.

Diffusion-based calibration is optimal for FCS studies focusing on measuring diffusion coefficients, because it calibrates  $\omega_0$ , which is the crucial parameter for determination of  $D$ . However, the value of  $V_0$  calculated from  $\omega_0$  and  $k$  (6) is strongly influenced by any uncertainty in the value of  $k$  and may lead to considerable errors in the concentration determination.

3. CLSM scanning of a small fluorescent bead attached to a glass surface provides an FCS-independent determination of the dimensions and shape of the effective detection volume<sup>[37]</sup>. When a fluorescent bead of a size much smaller than the detection volume is scanned by CLSM, the resultant image shows the effective detection volume of the microscope. The accuracy of the calibration depends on the accuracy of the CLSM scanner. The image can also reveal any distortion or asymmetry of the effective detection volume, which may stem from any misalignment of the microscope and would affect the shape of  $G(\tau)$ . The shape of the detection volume in the scan can be, however, slightly different from the effective detection during the actual FCS experiment, because the scanned bead is located directly at glass surface (at the boundary between two media of different refractive indices), while the detection volume in the actual experiment is usually located in some distance (usually between 20 to 100  $\mu\text{m}$ ) from the glass surface (unless structures located at the glass surface, like membranes adhering to glass, are investigated).

Correct calibration is crucial for absolute determination of diffusion coefficients and concentrations. However, absolute values of  $D$  and  $c$  are not essential in many FCS studies and only their relative changes are of importance. Those are fully described by relative changes in  $N$  and  $\tau_D$ , which are determined by fitting  $G(\tau)$  with the model (3) (or any other appropriate model expressed in terms of  $N$  and  $\tau_D$  – see the next section). The model contains only one parameter describing the effective detection volume – the structure parameter  $k$ . Since error in  $k$  has usually only marginal effect on  $\tau_D$ , a simplified calibration procedure is sufficient if only relative changes are investigated. The calibration usually consists of an FCS measurement (long enough to obtain good quality of autocorrelation data) in a solution of a reference fluorophore.  $G(\tau)$  is fitted with model (3) or (7) (see the next section for the model and its use) and  $k$  is determined as a free parameter. If the values of  $k$  and  $\tau_D$  obtained by the fit are in reasonable agreement with values usually obtained with the given setup and the given reference fluorophore,  $k$  can be used as a fixed parameter in fitting data from subsequent measurements and the instrument can be considered properly aligned. FCS calibration and its problems are further discussed in the section Artefacts in FCS.

### Models for Fitting of Autocorrelation Curves

Model (3) was derived for the basic situation of a 3-dimensional free diffusion of one population of particles (all having identical  $D$ ). Here we summarize other frequently used models of  $G(\tau)$ .

Photophysical processes such as transition to a dark state (such as a triplet state) are frequently apparent in  $G(\tau)$  on microsecond time-scale. To account for that phenomenon, an average fraction  $T$  of molecules in the triplet state and a characteristic time-scale  $\tau_T$  of the transition are included in the model (7)<sup>[7]</sup>.

$$G(\tau)=\left[1-\tau+\tau e^{-\frac{\tau}{\tau_T}}\right]\frac{1}{N(1-\tau)}\frac{1}{1+(\tau/\tau_D)}\sqrt{\frac{1}{1+(\tau/\tau_D)(\omega_0/\omega_z)^2}} \quad (7)$$

Model (8) describes a more general case of a sample containing  $M$  populations of fluorescent particles; each population characterized by its diffusion time  $\tau_{D,i}$ , brightness  $Q_i$  and fraction of the particle number  $F_i$ <sup>[41]</sup>.

$$G(\tau)=\frac{\sum_{i=1}^M (Q_i)^2 F_i g_i(\tau)}{N \left(\sum_{i=1}^M Q_i F_i\right)^2}; g_i(\tau)=\frac{1}{1+(\tau/\tau_{D,i})}\sqrt{\frac{1}{1+(\tau/\tau_{D,i})(\omega_0/\omega_z)^2}} \quad (8)$$

To account for transitions to triplet state, model (7) with  $T_i$  and  $\tau_{T,i}$  can be used as  $g_i(\tau)$  in (8). Diffusion in biological systems is often far from the ideal Brownian free diffusion characterized by the simple diffusion law (9), according to which the mean square displacement of a diffusing particle within a time interval  $t$  is proportional to  $t$  (duration of the interval).

$$\langle r^2(t)\rangle=\langle(r(t)-r(0))^2\rangle=4Dt \quad (9)$$

Interaction of the diffusing particle with other molecules and supramolecular structures slows down the diffusion and may result in a nonlinear diffusion law, according to which the mean square displacement is proportional to  $t^\alpha$ . Such type of molecular motion is called anomalous diffusion (or anomalous subdiffusion) and  $\alpha$  ( $0 < \alpha < 1$ ) is called anomalous exponent. Anomalous exponent is present in model (10) of  $G(\tau)$  derived for anomalous diffusion<sup>[42],[43]</sup>.

$$G(\tau)=\left[1-\tau+\tau e^{-\frac{\tau}{\tau_T}}\right]\frac{1}{N(1-\tau)}\frac{1}{1+(\tau/\tau_D)^\alpha}\sqrt{\frac{1}{1+(\tau/\tau_D)^\alpha(\omega_0/\omega_z)^2}} \quad (10)$$

If the fluorescent particles are not only moving by diffusion, but also by an oriented flow of velocity  $v$ ,  $G(\tau)$  is described by the model (11)<sup>[21]</sup>.

$$G(\tau)=\frac{1}{N}\frac{1}{1+(\tau/\tau_D)}\sqrt{\frac{1}{1+(\tau/\tau_D)(\omega_0/\omega_z)^2}}\exp\left(\left(-\frac{\tau V}{\omega_0}\right)^2\frac{1}{1+(\tau/\tau_D)}\right) \quad (11)$$

So far we have discussed only the situation when the fluorescent particles are free to move in all three dimensions. However, in many biologically relevant samples such as biological membranes, movement of molecules is effectively restricted only to two dimensions (movement along the plane of the membrane; thickness of biological membranes is several orders of magnitude smaller than the dimensions of the effective detection volume and can be, therefore, neglected). The effective detection area is, then, defined by the intersection of the detection volume of the microscope (defined by the confocal optics)

and the planar structure along which molecules of interest are moving. It is, therefore, only a 2-dimensional area with Gaussian distribution of photon detection efficiency  $W(R)$ , described by the first exponential function in (2). The theoretical models of autocorrelation functions simplify considerably in the 2-dimensional case. (12) is the 2-dimensional counterpart of (3); 2-dimensional variants of other models (7, 8, 10, 11) are derived in an analogous manner<sup>[44]</sup>.

$$G(\tau) = \frac{1}{N} \frac{1}{1 + (\tau/\tau_D)} \quad (12)$$

Calibration procedure in the 2-dimensional case is apparently simpler, since there is no structure parameter  $k$  in (12). That is, however, a false impression, because calibration of effective detection volume is an important source of artefacts in FCS of planar samples (see Artefacts in FCS for further details). A slightly different definition of autocorrelation function  $G_A(\tau)$  is also frequently used.

$$G_A(\tau) = \frac{\langle I(t)I(t+\tau) \rangle}{\langle (t) \rangle^2} \quad (13)$$

The only difference between  $G_A(\tau)$  and  $G(\tau)$  defined by (1) is in the constant offset  $G_A(\infty) = 1$ ;  $G_A(\tau)$  converges to 1, while  $G(\tau)$  to 0. The necessary modification of the theoretical models of the autocorrelation function (3, 7, 8, 10-12) is, therefore, trivial:  $G_A(\tau) = G(\tau) + 1$ . Some authors also use a factor  $\gamma$  in the amplitude of the autocorrelation function. Introduction of factor  $\gamma$  into the theoretical models only changes the definition of the effective detection volume. There is, therefore, no need to be confused by slightly different formulas of autocorrelation functions in some works.

### Choice of an Appropriate Model of Autocorrelation function

The choice of the model for fitting of  $G(\tau)$  is a crucial step in the analysis of FCS data. The general guideline is to use as simple a model as possible. Increasing the number of free parameters always improves the agreement of the model with the experimental autocorrelation curve; on the other hand, it decreases numerical stability of the fit and increases the risk of obtaining parameter values which lack any physical meaning. The use of models with higher numbers of free parameters should be, therefore, supported either by a significant disagreement of the simpler models with the experimental curve or by an a priori knowledge of properties of the sample

(for example that the sample contains a population of free fluorophore and a population of fluorophore bound to a protein or that the fluorophore is known to undergo transition to a triplet state). Statistical approaches are being developed for unbiased selection of the optimal model based on the quality of fits with individual models from a set<sup>[45]</sup>. However, those methods have not been so far implemented in any software package for FCS analysis.

When using models with large numbers of parameters, the reliability of the analysis is considerably improved by reducing the number of free parameters or introducing constraints on the range, within which the values of parameters are searched. For example the characteristic time  $\tau_T$  of transition to triplet state in model (7) is known to be around 10-3 ms for most fluorophores<sup>[7],[21]</sup>; a value of  $\tau_T$  larger than 0.1 ms is most likely an artefact of the fitting procedure.

Reduction of number of free parameters can be achieved by determining values of as many parameters as possible by additional FCS experiments and then using them as fixed parameters in the fitting procedure. Let us, for example, consider a sample containing free fluorophore and fluorophore bound to a protein. Model (8) with  $M = 2$  is appropriate in such a case. An additional measurement in a sample containing only free fluorophore yields the diffusion time  $\tau_{Df}$  (and optionally also characteristics of transition to triplet state) of the free fluorophore. The fit of the autocorrelation curve measured in the mixture of free and bound fluorophore, then, determines the remaining parameters: diffusion time  $\tau_{Dp}$  of the fluorescently labelled protein and the amplitude  $A_p$  of its contribution to the autocorrelation function; according to (8)  $A_p$  is given by (14).

$$A_p = \frac{Q_p^2 N_p}{(Q_p N_p + Q_f N_f)^2} \quad (14)$$

(14) simplifies considerably if  $Q_p = Q_f$ , which means that not more than a single fluorophore is bound to each protein and that binding changes neither its absorption cross-section nor its fluorescence quantum yield. Under such conditions, particle numbers  $N_p$  and  $N_f$  of the labelled protein and free fluorophore respectively can be determined easily from the amplitudes ( $A_p$  and  $A_f$ ) of their respective contributions to the autocorrelation function (8). If the brightness of the free fluorophore is not equal to that of fluorescently labelled protein, more data are needed to determine particle numbers of free fluorophore and labelled protein<sup>[39]</sup>.

Constraints on the ranges within which values of free parameters are probed are of particular importance when the experimental autocorrelation function is

not perfectly described by the model used for fitting. Such systematic deviations of the experimental autocorrelation function from the theoretical model are caused by instrumental artefacts (see the section Artefacts in FCS) as well as by complexity of the sample itself, which is not sufficiently described by the model. A typical problem is polydispersity of the populations of fluorescent particles, which are characterised by continuous distributions of diffusion times instead of a single  $\tau_D$  value assumed in models (3, 7, 8, 10-12). Many supramolecular structures such as micelles or vesicles always display some degree of polydispersity and macromolecules such as DNA can adopt various conformations resulting in a distribution of diffusion coefficients. Simple models with (usually not more than 2) discrete values of  $\tau_D$  are commonly used even in such situations. If a continuous particle size distribution is present in the sample, only apparent mean values of  $\tau_D$  are extracted from the fits; if brightness of the particles depends on their size (such as in the case distribution of oligomers of various sizes), the obtained values of  $\tau_D$  tend to be biased towards the larger particles in the distribution, because the contribution to  $G(\tau)$  is weighted by the square of particle brightness (8). Maximum

entropy method (MEM) fitting of  $G(\tau)$  is more appropriate when systems of polydisperse particles are studied, because MEM can perform fitting with an arbitrary continuous distribution of the parameters<sup>[46],[47]</sup>. MEM fitting is for example implemented in the FCS software QuickFit.

In general it can be concluded that the more is a priori known about the sample, the higher is the probability that the parameters obtained by fitting of  $G(\tau)$  are physically relevant (see Figure 3).

## 6. Artefacts in FCS

Like any other experimental technique, FCS can suffer from a variety of artefacts, which may introduce significant errors to FCS results and lead to their misinterpretation. The artefacts in FCS can be divided into three main categories:

1. artefacts caused by limited validity of approximations used in derivation of the theoretical models (3, 7, 8, 10-12),
2. artefacts caused by detector background and parasitic signal components and
3. artefacts related to calibration of the effective

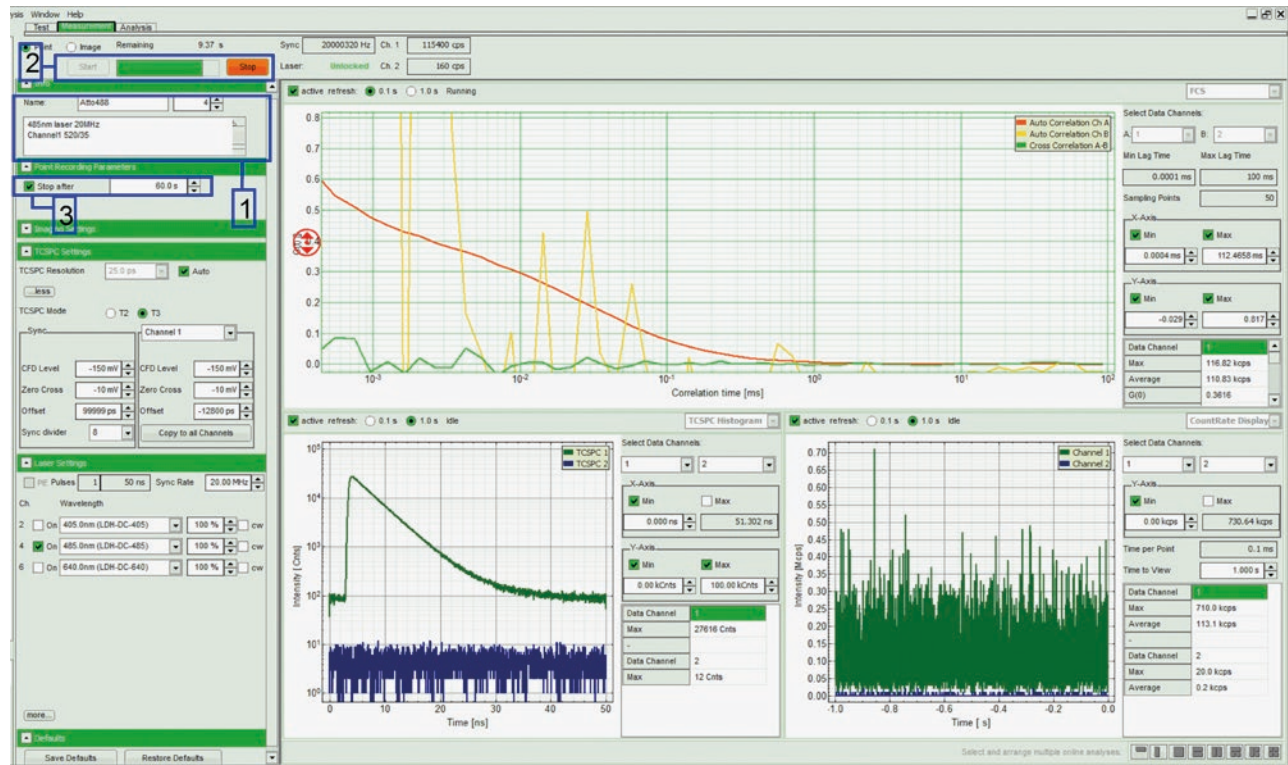


**Figure 3** Illustration of FCS fitting. The investigated sample was a suspension containing liposomes loaded with carboxyfluorescein and free carboxyfluorescein. The simple model with a single value of  $\tau_D$  (3) yields an unsatisfactory fit as can be also seen from the residues in the lower panel. A model with 2 values of diffusion time and a transition to triplet state yields a much closer fit with parameters  $\tau D1 = 6$  ms,  $A1 = 0.29$ ,  $\tau D2 = 0.076$  ms,  $A2 = 0.35$ ,  $\tau T = 0.017$  ms. A similar fit is obtained when 2 parameters are fixed using values found in an FCS measurement in a solution of pure carboxyfluorescein:  $\tau D2 = 0.048$  ms,  $\tau T = 0.001$  ms. The remaining free parameters obtained from the fit are:  $\tau D1 = 5.7$  ms,  $A1 = 0.30$ ,  $A2 = 0.42$ .

detection volume (leading to incorrect interpretation of values of  $\tau_D$  and  $N$  obtained by fitting).

Let us look at more detail on the individual types of artefacts and the ways to prevent or at least reduce their impact on the FCS data:

1. Since the theoretical models of autocorrelation function were derived assuming Gaussian profile (2) of the photon detection efficiency and mono-disperse point-like fluorescent particles, the artefacts of the first type are mainly manifested in those situations where the reality deviates significantly from the above mentioned assumptions. Deviations of the actual shape of the effective detection volume from (2) can be caused for example by optical aberrations of the microscope, optical saturation or misalignment of the confocal pinhole<sup>[2],[10],[33]</sup>. Although not all of the sources can be completely avoided, it is important to take precautions to minimize the risk of artefacts where possible. A careful alignment of the confocal pinhole as well as of the correction collar of the objective are essential for FCS. The excitation intensity should be low enough to minimize distortions of the effective detection volume caused by optical saturation and photobleaching (as has been see the section Data acquisition).

When dimensions  $r$  of the fluorescent particles are no more negligible with respect to effective detection volume dimensions, fits of  $G(\tau)$  yield inaccurate values of  $\tau_D$  and  $N$ <sup>[48]</sup>. It has been shown that for  $r/\omega_0 > 0.2$ , both  $\tau_D$  and  $N$  are overestimated<sup>[49],[50]</sup>.

2. The influence of background and various parasitic signal components on FCS data depends on whether the parasitic counts are correlated on timescales probed by the FCS experiment. A correlated parasitic signal component influences the correlation decay  $G(\tau)$ , while an uncorrelated one only affects the amplitude  $G(0)$ . The most commonly encountered example of correlated parasitic signal components are detector afterpulses<sup>[38],[51]</sup>. Those are false counts resulting from transient effects induced in the detector by a real photon detection event. Therefore, photon detection events and the subsequent afterpulses are correlated in time. For the commonly used detectors in FCS setups, afterpulses add to the correlation decay on  $\mu\text{s}$  and sub- $\mu\text{s}$  timescales and can be, therefore, misinterpreted as a result fluorophore transitions to a dark state or of other fast photophysical processes. A commonly used method to prevent afterpulses from distorting the correlation functions is to split the fluorescence signal onto two detectors and then obtain  $G(\tau)$  by cross-correlating signals from the two detectors instead of auto-correlating signal from each individual detector. Since afterpulses from one detector are uncorrelated to

counts from the other detector, they are not manifested in the cross-correlation function. Nevertheless the false afterpulse counts are still present in the overall signal as a non-correlated parasitic component and add to the artefacts caused by non-correlated parasitic components discussed in the following paragraph<sup>[51]</sup>.

The remaining sources of background and parasitic signal, such as detector background (thermal noise), scattered excitation photons or background fluorescence from the sample (e. g. weak fluorescence of the solvent) are typically not correlated and affect the correlation function only by lowering its amplitude  $G(0)$ , thus, leading to overestimation of the number of the fluorescent particles of interest. The effect is especially prominent in samples containing very low fluorophore concentrations. While it does not compromise the determination of  $D$ , it is a serious problem for concentration measurements by FCS. A corrected value of particle number  $N$  can be calculated from the autocorrelation amplitude  $G(0)$  using formula (15), where  $B$  denotes the average background intensity<sup>[37]</sup>.

$$N = \frac{1}{G(0)(1 + \langle B \rangle I \langle I \rangle)^2} \quad (15)$$

The correction formula (15), however, holds only when the fraction  $T$  of the fluorophores undergoing transition to a non-fluorescent state is small<sup>[37]</sup>. A more general method of eliminating both correlated and non-correlated parasitic signal components is offered by fluorescence lifetime correlation spectroscopy (FLCS)<sup>[38],[52]</sup>.

3. Calibration-related artefacts are caused by differences in effective detection volume  $V_0$  in the sample and in the reference solution. The differences are minimized by using identical experimental settings (identical temperature, identical excitation intensity, ...) during the measurement and the calibration; however they cannot be always completely avoided. Differences in refractive indices are a common cause for different effective detection volumes. That is especially prominent in the case of intracellular FCS measurements, since cytoplasm differs significantly in refractive index from a diluted aqueous solution of a reference fluorophore<sup>[33]</sup>. Additionally, there exist some discrepancies in published values of diffusion coefficient of some standard reference fluorescent dyes<sup>[36],[53]</sup>.

An additional positioning problem exists in the case of planar samples<sup>[17],[54]</sup>. Since the excitation beam is divergent above and below its waist, placing the planar sample above or below the focal plane results in larger effective detection area and, therefore,

higher values of  $\tau_D$  and  $N$ . Although uncertainties in the absolute determination of  $V_0$  do not represent a problem if only relative changes of diffusion coefficient or concentration are sought for, the positioning problem in the case of planar samples results in increased uncertainty in results of individual measurements, compromising their comparability. Therefore, several calibration-free FCS variants have been developed, which do not rely on external calibration, but contain an intrinsic measure of distance. The intrinsic calibration is typically achieved by scanning with the focus through the sample at well defined speed or with well defined steps (scanning FCS<sup>[55],[56]</sup>, Z-scan FCS<sup>[17]</sup>, ...) or by correlating intensity time-traces measured at points at well-defined distances from each other (multi-focus FCS<sup>[57],[58]</sup>, imaging FCS<sup>[59],[60]</sup>, raster image correlation spectroscopy<sup>[61]</sup>, ...).

## 7. Technique Overview

### Applications and Limitations of FCS

As has been already said in the Introduction, FCS can characterize time-scales of processes causing fluorescence intensity fluctuations as well as the concentration of independent fluorescence particles involved in those fluctuations. Movement of molecules in and out of the effective detection volume is in most cases the dominant source of fluorescence intensity fluctuations and provides information on mobility of the fluorescent particles (either diffusion coefficient or velocity of an oriented flow).

Diffusion coefficient measured by FCS can be interpreted in terms of the size of the diffusing fluorescent particles (and its changes) or in terms of viscosity and organization of the medium. The latter approach is typical for intracellular FCS measurements<sup>[43]</sup> and especially for FCS in biological membranes.

Following processes involving changes in diffusion coefficient of fluorescent particles are commonly addressed by FCS:

1. conformational changes of macromolecules; for example DNA compaction for gene therapy<sup>[9]</sup>;
2. binding of small fluorescently labelled ligands to large molecules or supramolecular structures (such as chromatin or biological membranes). Fractions of free and bound ligand can be resolved according to (13)<sup>[62],[63],[64]</sup>;
3. aggregation phenomena and determination of critical micelle concentrations<sup>[65],[66]</sup>;
4. lateral organization of biological membranes and their artificial models<sup>[28],[67],[68]</sup>.

The second parameter provided by FCS, the concentration of fluorescent particles, is useful complementary information, which is of particular importance for investigation of aggregation phenomena.

Since diffusion coefficient is approximately inversely proportional to cubic root of molecular mass (from Stokes-Einstein formula), relatively large changes in molecular mass are needed to be resolved by FCS. Oligomerization of fluorescent particles is, therefore, more reliably detected via changes in their concentration than via changes in their diffusion coefficient. The weak dependence of  $D$  on molecular mass also imposes a limitation on FCS binding studies. Association of a fluorescently labelled molecule with a binding partner of smaller or comparable molecular mass cannot be reliably resolved by FCS.

Following problems are commonly addressed by determining molecular concentrations by FCS:

1. oligomerization studies. By dividing the average photon count-rate by  $N$  determined by FCS the average brightness per particle is obtained. Comparing the obtained brightness per particle with the brightness of the monomeric fluorophore (measured ideally under identical conditions to avoid uncertainty resulting from environmental sensitivity of the fluorophore brightness) the average number of fluorophores per particle is obtained<sup>[69],[70],[71]</sup>;
2. determination of the absolute concentration of a molecules of interest within particular locations in the sample<sup>[72],[73]</sup>.

### Selected References

Theory of FCS	[8], [34], [35], [74], [76]
Artefacts and their prevention in FCS	[2], [10], [24], [30], [33], [37]
Reviews on biological or biochemical applications of FCS	[3], [18], [21], [27], [28], [36], [77], [81]
Comparison of FCS with other techniques	[82-86]

A commented bibliography on FCS can be found in the review of Thompson et al.<sup>[78]</sup>.

## 8. Conclusion

FCS analyses fluctuations of fluorescence intensity collected form a small effective detection volume (defined typically by the point spread function of a confocal microscope) and extracts information on the time-scale of processes underlying the fluctuations. Usual applications contain measurements of concentrations and diffusion coefficients of molecules or supramolecular structures moving through the detection volume or investigation of processes manifested by changes in diffusion coefficient. FCS implementation in a confocal microscope is straightforward and so is combination of FCS with confocal

imaging. It is well suited for measurements in living cells and has, therefore, promising biological applications. The basic principle behind FCS is very versatile and a range of related experimental techniques is based on it (fluorescence cross-correlation spectroscopy, image correlation spectroscopy, ...). Those FCS variants have overcome some limitations of the basic FCS approach and found a variety of biological applications.

## References and Further Reading

- [1] R. Rigler, U. Mets, J. Widengren, P. Kask, *Eur Biophys J Biophys Lett*, 1993, 22, 169-175.
- [2] J. Enderlein, I. Gregor, D. Patra, T. Dertinger, U.B. Kaupp, *Chemphyschem*, 2005, 6, 2324-2336.
- [3] J. Ries, P. Schwille, *BioEssays*, 2012, 34, 361-368.
- [4] P. Kask, P. Piksamr, U. Mets, *Eur Biophys J Biophys Lett*, 1985, 12, 163-166.
- [5] J. Sýkora, K. Kaiser, I. Gregor, W. Bonigk, G. Schmalzing, J. Enderlein, *Anal Chem*, 2007, 79, 4040-4049.
- [6] P. Kask, P. Piksamr, M. Pooga, U. Mets, E. Lippmaa, *Biophys J*, 1989, 55, 213-220.
- [7] J. Widengren, U. Mets, R. Rigler, *J Phys Chem*, 1995, 99, 13368-13379.
- [8] E. Elson, D. Magde, *Biopolymers*, 1974, 13, 1-27.
- [9] N. Adjimatera, T. Kral, M. Hof, I.S. Blagbrough, *Pharm Res*, 2006, 23, 1564-1573.
- [10] S.T. Hess, W.W. Webb, *Biophys J*, 2002, 83, 2300-2317.
- [11] S. Felekyan, R. Kuhnemuth, V. Kudryavtsev, C. Sandhagen, W. Becker, C.A.M. Seidel, *Rev Sci Instrum*, 2005, 76, 083104:083101-083104:083114.
- [12] P. Schwille, U. Haupts, S. Maiti, W.W. Webb, *Biophys J*, 1999, 77, 2251-2265.
- [13] P. Schwille, K.G. Heinze, *Chemphyschem*, 2001, 2, 269-272.
- [14] B. Kannan, J.Y. Har, P. Liu, I. Maruyama, J.L. Ding, T. Wohland, *Anal Chem*, 2006, 78, 3444-3451.
- [15] N. Bag, A. Ali, V.S. Chauhan, T. Wohland, A. Mishra, *Chem Commun (Camb)*, 2013, 49, 9155-9157.
- [16] T. Wohland, X.K. Shi, J. Sankaran, E.H.K. Stelzer, *Opt Express*, 2010, 18, 10627-10641.
- [17] A. Benda, M. Beneš, V. Mareček, A. Lhotský, W.T. Hermens, M. Hof, *Langmuir*, 2003, 19, 4120-4126.
- [18] S.T. Hess, S.H. Huang, A.A. Heikal, W.W. Webb, *Biochemistry*, 2002, 41, 697-705.
- [19] H. Blom, L. Kastrup, C. Eggeling, *Curr Pharm Biotechnol*, 2006, 7, 51-66.
- [20] J. Wenger, H. Rigneault, J. Dintinger, D. Marguet, P.F. Lenne, *J Biol Phys*, 2006, 32, SN1-SN4.
- [21] P. Schwille, *Cell Biochem Biophys*, 2001, 34, 383-408.
- [22] E. Haustein, P. Schwille, *Annu Rev Biophys Biomolec Struct*, 2007, 36, 151-169.
- [23] P. Liu, S. Ahmed, T. Wohland, *Trends Endocrinol Metab*, 2008, 19, 181-190.
- [24] L.M. Davis, G.Q. Shen, *Curr Pharm Biotechnol*, 2006, 7, 287-301.
- [25] A.J. Garcia-Saez, P. Schwille, *Methods*, 2008, 46, 116-122.
- [26] X. Pan, W. Foo, W. Lim, M.H.Y. Fok, P. Liu, H. Yu, I. Maruyama, T. Wohland, *Review of Scientific Instruments*, 2007, 78, 053711.
- [27] J. Ries, P. Schwille, *Phys Chem Chem Phys*, 2008, 10, 3487-3497.
- [28] S. Chiantia, J. Ries, P. Schwille, *Biochim Biophys Acta-Biomembr*, 2009, 1788, 225-233.
- [29] Z. Petrášek, P. Schwille, *Chemphyschem*, 2008, 9, 147-158.
- [30] I. Gregor, D. Patra, J. Enderlein, *Chemphyschem*, 2005, 6, 164-170.
- [31] P. Kask, R. Gunther, P. Axhausen, *Eur Biophys J Biophys Lett*, 1997, 25, 163-169.
- [32] J. Widengren, R. Rigler, *Bioimaging*, 1996, 4, 149-157.
- [33] J. Enderlein, I. Gregor, D. Patra, J. Fitter, *Curr Pharm Biotechnol*, 2004, 5, 155-161.
- [34] H. Qian, E.L. Elson, *Appl Optics*, 1991, 30, 1185-1195.
- [35] S.R. Aragon, R. Pecora, *J Chem Phys*, 1976, 64, 1791-1803.
- [36] I.V. Perevoshchikova, E.A. Kotova, Y.N. Antonenko, *Biochemistry-Moscow*, 2011, 76, 497-516.
- [37] S. Rüttinger, V. Buschmann, B. Kramer, R. Erdmann, R. Macdonald, F. Koberling, *J Microsc*, 2008, 232, 343-352.
- [38] P. Kapusta, M. Wahl, A. Benda, M. Hof, J. Enderlein, *J Fluoresc*, 2007, 17, 43-48.
- [39] L. Yu, J.L. Ding, B. Ho, T. Wohland, *Biochim Biophys Acta-Biomembr*, 2005, 1716, 29-39.
- [40] P. Kapusta, *Absolute Diffusion Coefficients: Compilation of Reference Data for FCS Calibration*, Rev. 1, PicoQuant GmbH., Berlin, (2010), <http://www.picoquant.com/scientific/technical-and-application-notes>, Accessed: 04/05, 2014.
- [41] N.L. Thompson, in *Topics in Fluorescence Spectroscopy*, ed. J.R. Lakowicz, Plenum Press, New York 1991, Vol. 1, pp. 337-378.
- [42] D.S. Banks, C. Fradin, *Biophys J*, 2005, 89, 2960-2971.
- [43] G. Guigas, C. Kalla, M. Weiss, *Biophys J*, 2007, 93, 316-323.
- [44] R. Macháň, M. Hof, *Int J Mol Sci*, 2010, 11, 427-457.
- [45] S.M. Guo, J. He, N. Monnier, G.Y. Sun, T. Wohland, M. Bathe, *Anal Chem*, 2012, 84, 3880-3888.
- [46] P. Sengupta, K. Garai, J. Balaji, N. Periasamy, S. Maiti, *Biophys J*, 2003, 84, 1977-1984.
- [47] N. Pal, S.D. Verma, M.K. Singh, S. Sen, *Anal Chem*, 2011, 83, 7736-7744.
- [48] P. Košovan, F. Uhlík, J. Kulová, M. Stěpánek, Z. Limpouchová, K. Procházka, A. Benda, J. Humpolíčková, M. Hof, *Collect Czech Chem*

- Commun, 2011, 76, 207-222.
- [49] K. Starchev, J.W. Zhang, J. Buffle, J Colloid Interface Sci, 1998, 203, 189-196.
- [50] B. Wu, Y. Chen, J.D. Muller, Biophys J, 2008, 94, 2800-2808.
- [51] J. Enderlein, I. Gregor, Review of Scientific Instruments, 2005, 76, 033102:033101–033102:033105.
- [52] P. Kapusta, R. Macháň, A. Benda, M. Hof, Int J Mol Sci, 2012, 13, 12890-12910.
- [53] R. Šachl, I. Mikhalyov, M. Hof, L.B.A. Johansson, Phys Chem Chem Phys, 2009, 11, 4335-4343.
- [54] S. Milon, R. Hovius, H. Vogel, T. Wohland, Chem Phys, 2003, 288, 171-186.
- [55] Q.Q. Ruan, M.A. Cheng, M. Levi, E. Gratton, W.W. Mantulin, Biophys J, 2004, 87, 1260-1267.
- [56] J. Ries, S. Chiantia, P. Schwille, Biophys J, 2009, 96, 1999-2008.
- [57] M. Burkhardt, P. Schwille, Opt Express, 2006, 14, 5013-5020.
- [58] T. Dertinger, V. Pacheco, I. von der Hocht, R. Hartmann, I. Gregor, J. Enderlein, Chemphyschem, 2007, 8, 433-443.
- [59] J. Sankaran, X.K. Shi, L.Y. Ho, E.H.K. Stelzer, T. Wohland, Opt Express, 2010, 18, 25468-25481.
- [60] J. Sankaran, N. Bag, R.S. Kraut, T. Wohland, Anal Chem, 2013, 85, 3948-3954.
- [61] M.A. Digman, C.M. Brown, P. Sengupta, P.W. Wiseman, A.R. Horwitz, E. Gratton, Biophys J, 2005, 89, 1317-1327.
- [62] M. Bierbaum, P.I. Bastiaens, Biophys J, 2013, 104, 1642-1651.
- [63] C. Caballero-George, T. Sorkalla, D. Jakobs, J. Bolanos, H. Raja, C. Shearer, E. Birmingham, H. Haberlein, ScientificWorldJournal, 2012, 2012, 524169.
- [64] R.H. Rose, S.J. Briddon, S.J. Hill, Br J Pharmacol, 2012, 165, 1789-1800.
- [65] L.L. Yu, M.Y. Tan, B. Ho, J.L. Ding, T. Wohland, Anal Chim Acta, 2006, 556, 216-225.
- [66] S. Nag, J. Chen, J. Irudayaraj, S. Maiti, Biophys J, 2010, 99, 1969-1975.
- [67] L. Wawrezinieck, H. Rigneault, D. Marguet, P.F. Lenne, Biophys J, 2005, 89, 4029-4042.
- [68] E. Sezgin, I. Levental, M. Grzybek, G. Schwarzmann, V. Mueller, A. Honigmann, V.N. Belov, C. Eggeling, U. Coskun, K. Simons, P. Schwille, Biochim Biophys Acta-Biomembr, 2012, 1818, 1777-1784.
- [69] T.A. Nguyen, P. Sarkar, J.V. Veetil, S.V. Koushik, S.S. Vogel, PLoS One, 2012, 7, e38209.
- [70] K. Herrick-Davis, E. Grinde, A. Cowan, J.E. Mazurkiewicz, Mol Pharmacol, 2013, 84, 630-642.
- [71] B. Ilien, N. Glasser, J.P. Clamme, P. Didier, E. Piemont, R. Chinnappan, S.B. Daval, J.L. Galzi, Y. Mely, J Biol Chem, 2009, 284, 19533-19543.
- [72] L. Erokhova, A. Horner, P. Kugler, P. Pohl, J Biol Chem, 2011, 286, 39926-39932.
- [73] S.R. Yu, M. Burkhardt, M. Nowak, J. Ries, Z. Petrasek, S. Scholpp, P. Schwille, M. Brand, Nature, 2009, 461, 533-536.
- [74] D.E. Koppel, Phys Rev A, 1974, 10, 1938-1945.
- [75] T. Wohland, R. Rigler, H. Vogel, Biophys J, 2001, 80, 2987-2999.
- [76] J. Enderlein, I. Gregor, D. Patra, J. Fitter, J Fluoresc, 2005, 15, 415-422.
- [77] Z. Földes-Papp, U. Demel, W. Domej, G.P. Tilz, Exp Biol Med, 2002, 227, 291-300.
- [78] N.L. Thompson, A.M. Lieto, N.W. Allen, Curr Opin Struct Biol, 2002, 12, 634-641.
- [79] A. Shahzad, G. Kohler, Appl Spectrosc Rev, 2011, 46, 166-173.
- [80] V. Vukojevic, A. Pramanik, T. Yakovleva, R. Rigler, L. Terenius, G. Bakalkin, Cell Mol Life Sci, 2005, 62, 535-550.
- [81] O. Krichevsky, G. Bonnet, Rep Prog Phys, 2002, 65, 251-297.
- [82] L.M. Davis, P.E. Williams, H.M. Cain, D.A. Ball, C.G. Parigger, E.D. Matayoshi, K.M. Swift, Biophys J, 2002, 82, 43A-43A.
- [83] Y. Chen, B.C. Lagerholm, B. Yang, K. Jacobson, Methods, 2006, 39, 147-153.
- [84] L. Guo, J.Y. Har, J. Sankaran, Y.M. Hong, B. Kannan, T. Wohland, Chemphyschem, 2008, 9, 721-728.
- [85] D.E. Koppel, D. Axelrod, J. Schlessinger, E.L. Elson, W.W. Webb, Biophys J, 1976, 16, 1315-1329.
- [86] D.M. Owen, D. Williamson, C. Rentero, K. Gaus, Traffic, 2009, 10, 962-971.

## Appendix

### FCS with SymPhoTime 64

Here we show how to perform basic FCS measurements and data analysis using the SymPhoTime 64 software (PicoQuant, Berlin, Germany). The software controls PicoQuant data acquisition cards, which record time-tagged time-resolved fluorescence data, and performs various types of analysis of those data, including calculation and fitting of FCS correlation functions. SymPhoTime 64 controls PicoQuant confocal microscopes (such as MicroTime 200); in the case of microscopes from other manufacturers upgraded with a PicoQuant data acquisition card, a dedicated microscope software is needed to control the settings of the microscope, acquire images and select a point for the FCS measurement. The subsequent recording of fluorescence intensity time-traces and their FCS analysis is performed by SymPhoTime 64. The software also controls PicoQuant pulsed laser drivers (Figure 1, 4), if it is included in the setup. Pulsed lasers are, however, needed only for time-resolved measurements are not necessary in an FCS setup.

#### Test Mode

After setting a point for measurement, acquisition of fluorescence intensity time traces by SymPhoTime 64 can begin. The main window of the program has 3 main panes: Test, Measurement and Analysis (Figure 1, 1). Data acquired in the Test mode are not saved; they are only displayed in real time on the screen to aid alignment of the instrument and optimizing settings for the measurement. Three modes are available for the real time display: TCSPC, Time Trace and FCS (Figure 1, 2). The TCSPC pane displays the photon arrival histogram; since TCSPC data are not required in standard FCS, we will not discuss this display mode further. Time Trace is the most basic mode displaying the real time value of detected fluorescence intensity (Figure 1). If signal from multiple detectors is fed to the data acquisition card, a time trace for each individual detector is shown. Besides the graphic display, numerical values of average and maximum count-rate for each detection channel are shown (Figure 1, 3).

The real time intensity time trace is useful for focusing to the structure of interest (e. g. if the fluorescently labelled molecules of interest are located in the plasma membrane of a cell, by changing the axial position of the focus two maxima of fluorescence intensity can be found corresponding to the lower and to the upper membrane). Besides that, the time trace can be used to optimize the pinhole position by measuring intensity originating from a fluorophore solution (it is advisable to use in this case a higher concentration of fluorophore than for FCS).

The FCS pane in the Test mode (Figure 2) shows correlation functions calculated in real time from the detected time traces (similarly to the output from a hardware correlator). Autocorrelations of signals from individual detectors and cross-correlation between them are shown. However, in the situation shown in Figure 2 only a single detector receives fluorescence signal; the other detector contributes only its thermal noise. Maximum and average count-rate and the amplitude of the displayed correlation function are shown next to the graphic display (Figure 2, 1). The particle number corresponding to the amplitude is also shown as well as the particle brightness obtained by dividing the average count-rate by the particle number. Brightness of a reference fluorophore is a good indicator of the quality of alignment of the setup. The optimal correction ring settings can be found by searching for the maximum brightness. To aid the alignment procedure, any of the values can be displayed in a larger window (by clicking on the displayed value) (Figure 2, 2).

#### Measurement Mode

After optimizing the data acquisition in the Test mode, we can switch to the Measurement pane (Figure 3 and 4), in which the recorded data are stored for subsequent analysis. Before starting the measurement, the file name for the dataset should be defined; additionally, any information on the instrument settings or on the sample details can be noted down to be saved together with the data (Figure 3, 1). The data acquisition is then started by the Start button and terminated by the Stop button (Figure 3, 2); alternatively the acquisition time can be defined and the acquisition then stops automatically after the defined time has elapsed (Figure 3, 3). The main window is divided into three panels; the upper one displays the correlation function calculated in real time, the lower left panel shows the TCSPC histogram and the bottom right panel the intensity time trace.

#### Analysis Mode

After the data acquisition has finished, we proceed to the analysis of the stored data. In the Workspace explorer on the left hand side of the main program window we select the file to be analysed (Figure 5). The real time calculated correlation functions (recognised by a filename of the following structure: Name\_OFCS.pqres) are stored alongside the raw data. We are, however, not going to use this correlation function. We will, instead, calculate the correlation function again from the stored raw data. This will allow us to correct for some common FCS artefacts as mentioned in the main text. After selecting the data file, we switch to the Analysis pane in which various modes of analysis are offered. We select the FCS

menu, which offers several FCS modalities, from which we choose the basic FCS analysis (Figure 5). The window for FCS correlation calculation is shown in Figure 6. The Intensity time trace is shown in the upper panel. By sliding the red start and stop markers (Figure 6, 1) an arbitrary part of the time trace can be selected for analysis. This is useful when a part of the time trace is affected by movement of large aggregates, by bleaching etc. The range of lag-times for which the correlation is calculated can be selected (Figure 6, 2). If Lagtime Min. is set to 0, the shortest lag-time will be determined by the software based on the temporal resolution of the data. If pulsed excitation is used, FLCS can be used to correct for background and detector afterpulsing (Figure 6, 3). Explanation of the method is beyond the scope of this appendix; we will use it here, therefore, only as a “black box” feature. If continuous wave excitation is used, distortion of the correlation function caused by afterpulsing can be prevented by splitting the fluorescence emission onto two detectors and cross-correlating signals from them (see Figure 4; the cross-correlation function does not contain the steep initial decay of correlation caused by detector afterpulses). After pressing the Calculate button (Figure 6, 4), correlation function is calculated and displayed in the main panel. The correlation function can be saved (Figure 6, 5) for further analysis.

Since the sample for which we have just obtained the autocorrelation function was the solution of a calibration dye, we will use it to calibrate the effective detection volume. We select the saved autocorrelation function in the Workspace explorer and in the FCS analysis menu (Figure 5) we choose FCS calibration. That brings us to a curve fitting window (Figure 7). The default fitting model offered is that with a single diffusion time and a single dark state, which is suitable for most calibration dyes. If we know that our calibration dye has no dark state, we can switch to a simpler model by pressing the Exclude Triplet button. If we are calibrating the effective detection volume using the known value of  $D$  of our calibration dye, we fill in the reference value of  $D$  (Figure 7, 1). We can start the fitting by performing Initial Fit (Figure 7, 2), which searches over broader ranges of parameter values and is, thus, more likely to converge even if the initial parameter values are far from the optimal ones. Subsequently we can perform the Fit till self-consistency is reached (parameter values do not change, only fluctuate around their minima, during further fitting iterations). If the quality of the fit is good and the parameter values are reasonable, we can save the obtained characteristics of the effective detection volume (its volume and structure parameter  $\kappa$ ) (Figure 7, 3). Those will be then used as default values in the FCS fitting window (Figure 8). Ideally we should perform multiple calibration

measurements to check the reproducibility of the parameters.

When we afterwards measure any other dataset and calculate the correlation function (Figure 6), we can choose to proceed to fitting of the correlation function (Figure 6, 6). By default, the simplest model for pure 3-dimensional diffusion (single  $D$ , no dark state) is offered in the fitting window (Figure 8, 1). If that model does not fit well the curve (as is the case in Figure 8), we can select a more complex model, for example the model with a dark (triplet) state (Figure 9, 1). A significantly better fit is obtained as can be seen from the residuals as well as from the  $\chi^2$  value (Figure 9, 2).

Another example of autocorrelation function fit is shown in Figure 10. It is obvious that the fit is not perfect (especially in the region around 10 ms). Nevertheless, knowing the non-ideal nature of the sample (liposomes prepared by sonication, which are intrinsically polydisperse and prone to aggregation; aggregates being most likely responsible for the deviations between the fit and the experimental curve around 10 ms lag-time), we may consider the fit to be an acceptable one giving a good estimate of the typical diffusion coefficient and concentration of the liposomes. A more complex model may yield a slightly better fit; however, the parameters thus obtained may be artificial and lacking direct physical interpretation.

The curve in Figure 11 cannot be satisfactorily fitted with the model with a single  $D$  and single dark state and definitely requires a more complex model for its description. The knowledge of the nature of the sample is helpful for selecting which model to use. Knowing that the sample contained a mixture of free dye and of fluorescently labelled liposomes, a model with two values of  $D$  (Figure 12, 1) and a single dark state is expected to describe the experimental data. That is indeed the case as shown in Figure 12. The individual values of  $D$  retrieved from the fit agree within the margin of error with the values obtained from measurements in samples containing only one of the components (free dye in Figure 7 and liposomes in Figure 10). This is, however, not always the case. Keeping at least one of the diffusion times fixed to a value obtained separately in a sample containing only one of the components significantly improves reliability of fitting with two diffusion times.

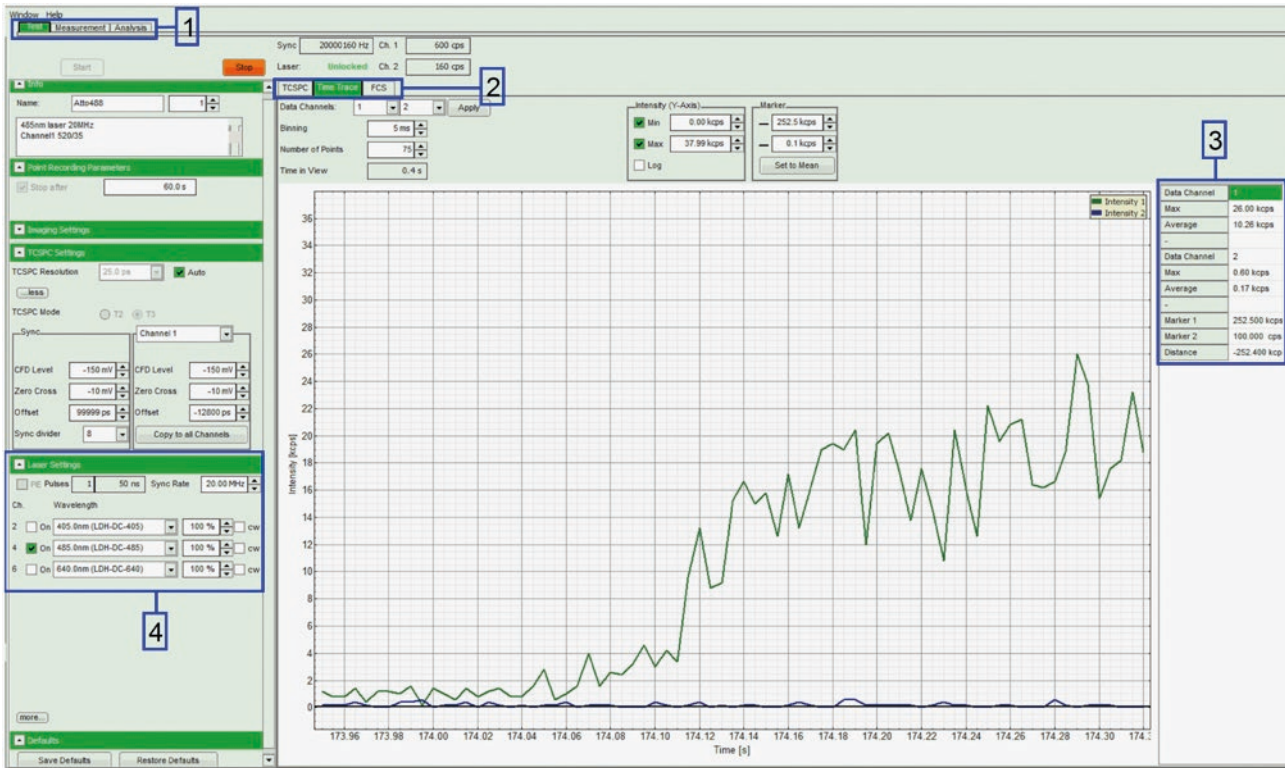


Figure 1

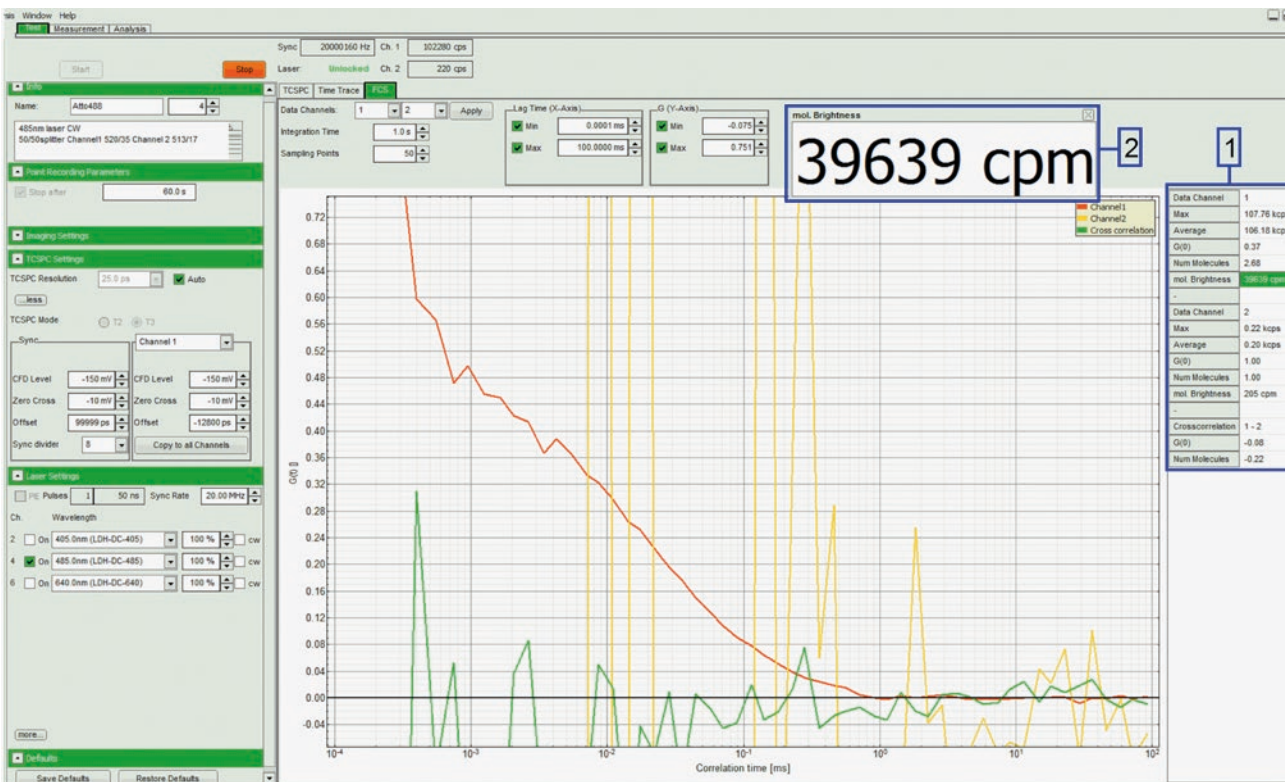


Figure 2

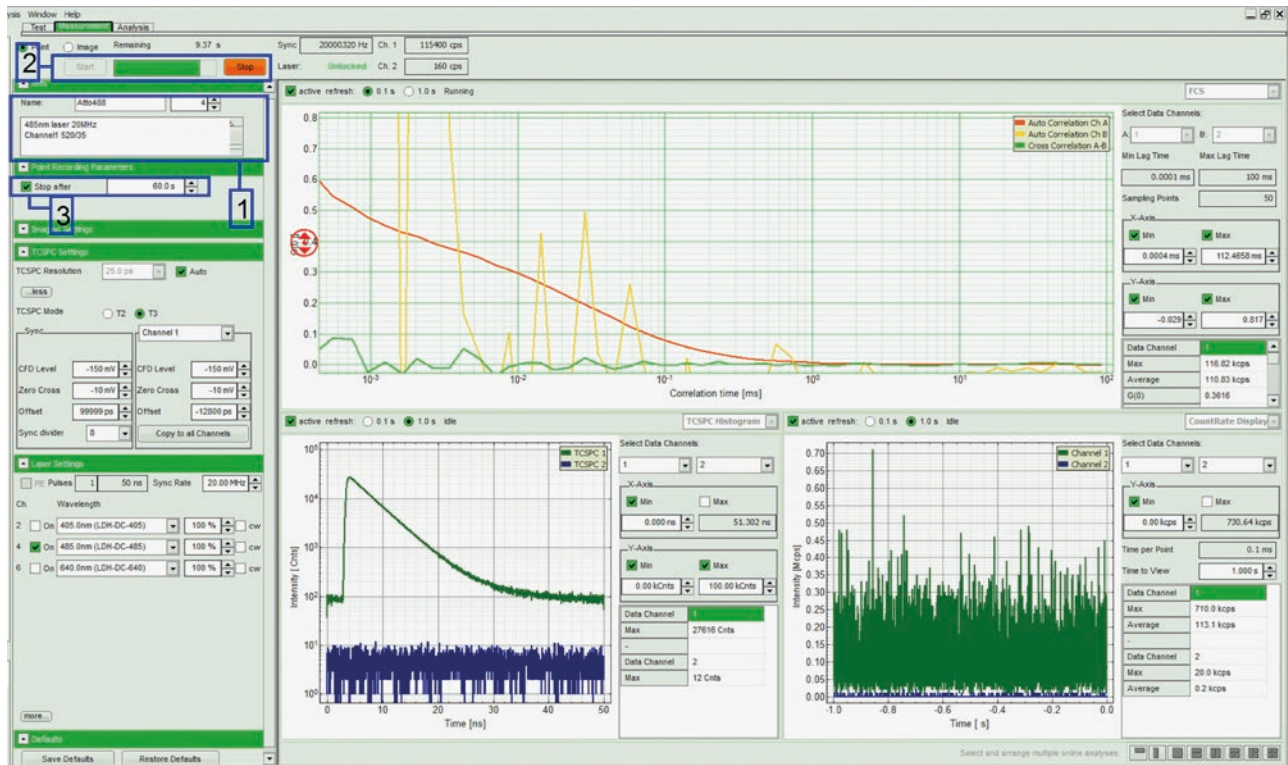


Figure 3

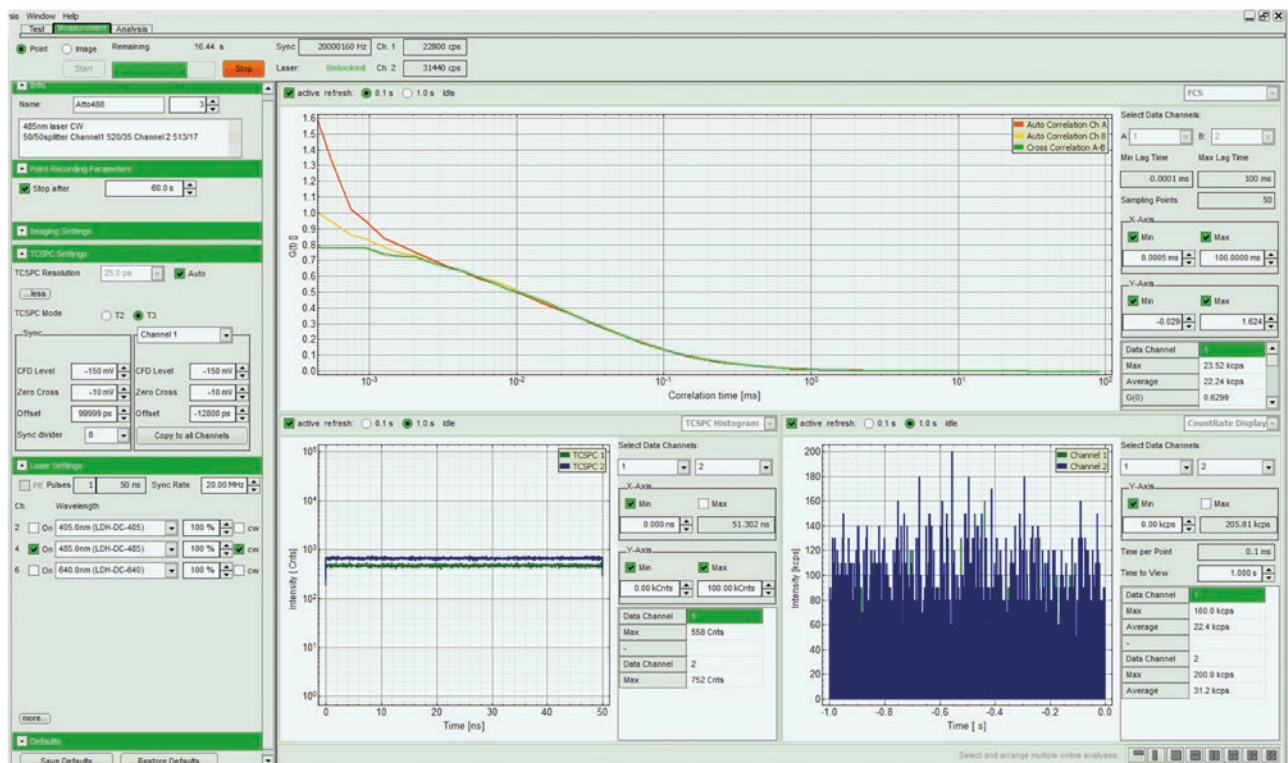
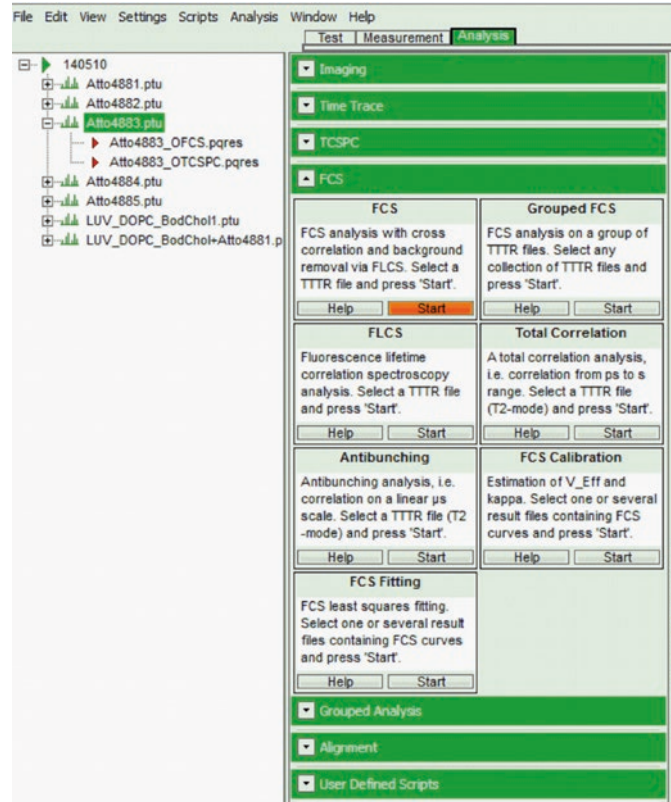
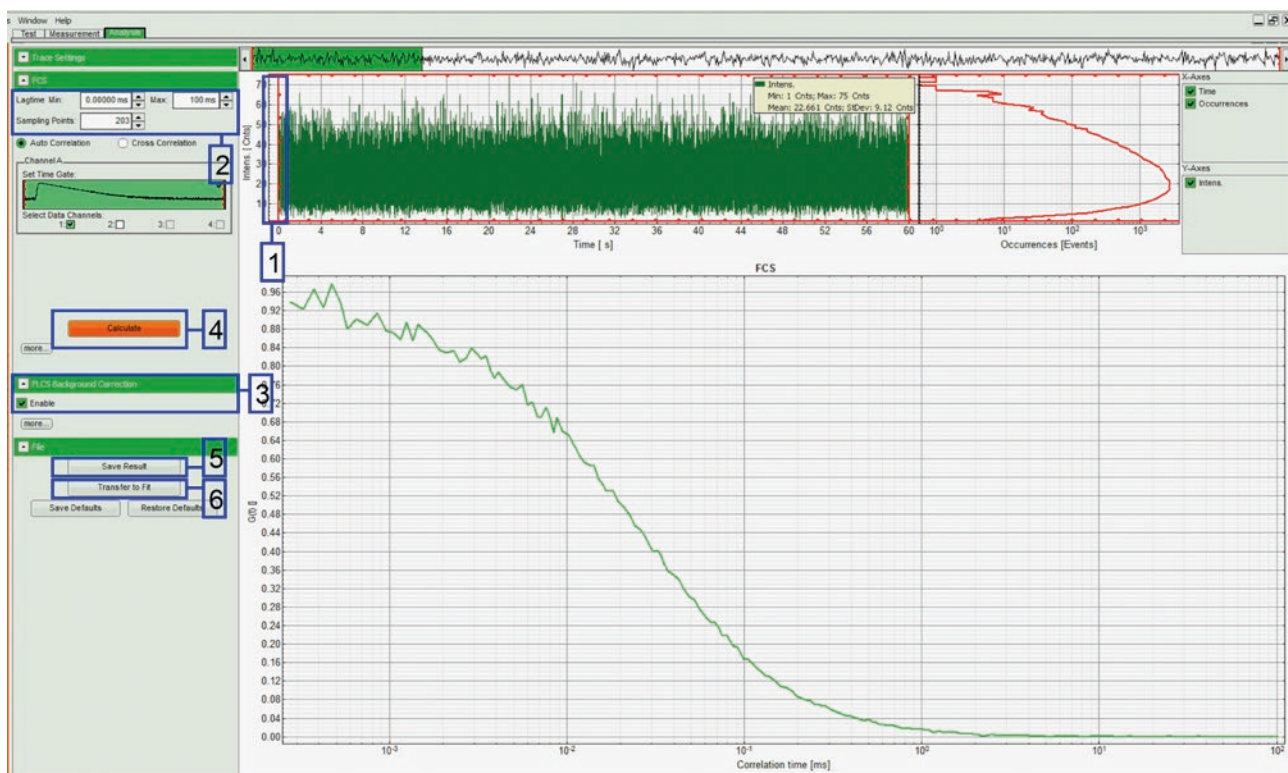
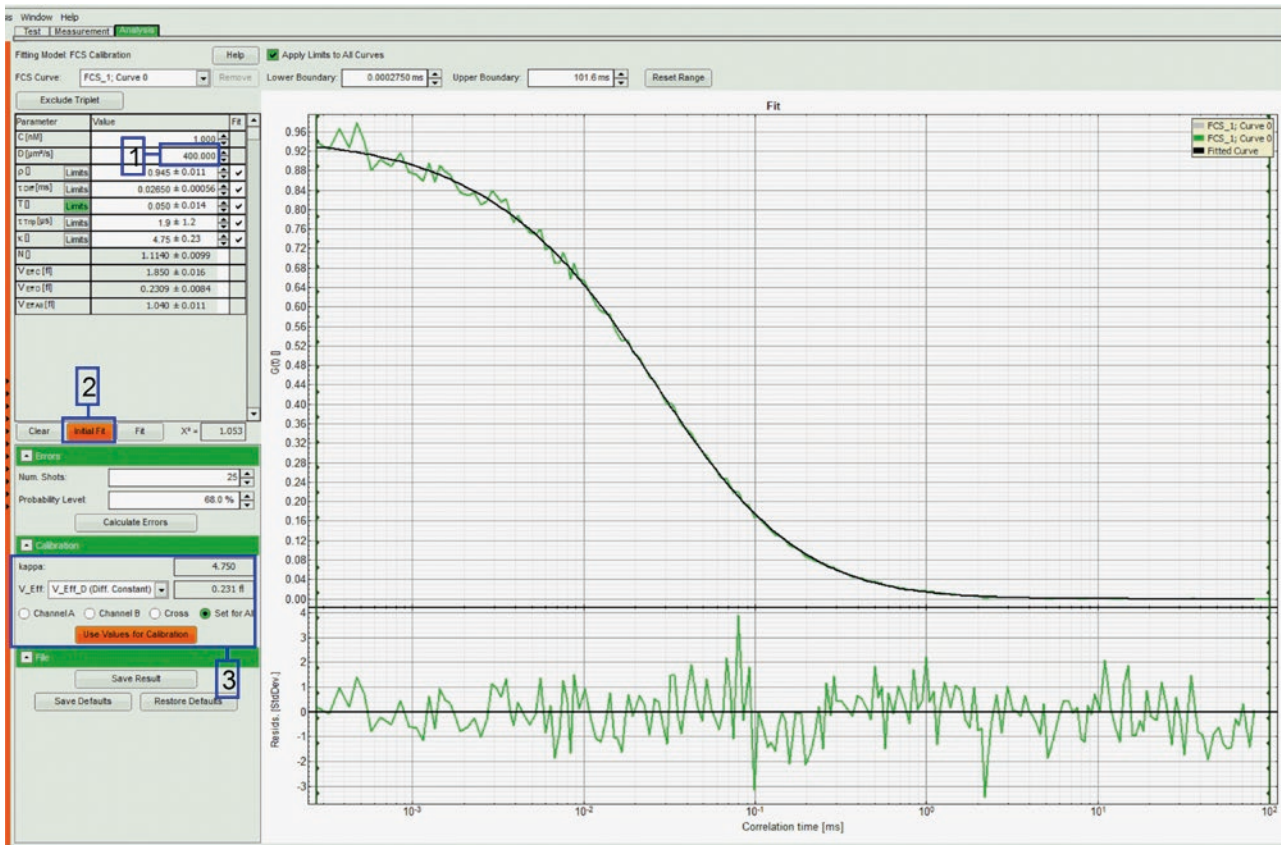
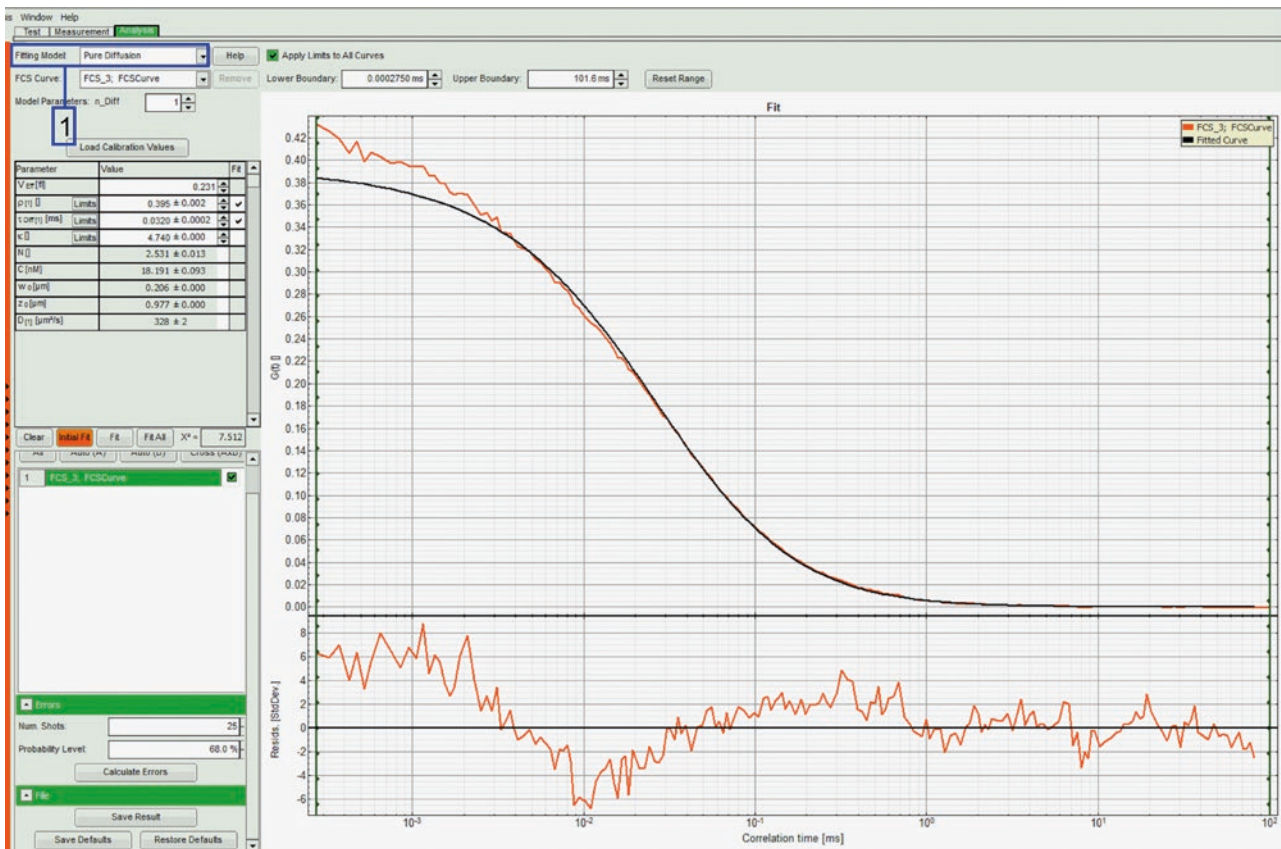


Figure 4

**Figure 5****Figure 6**

**Figure 7****Figure 8**

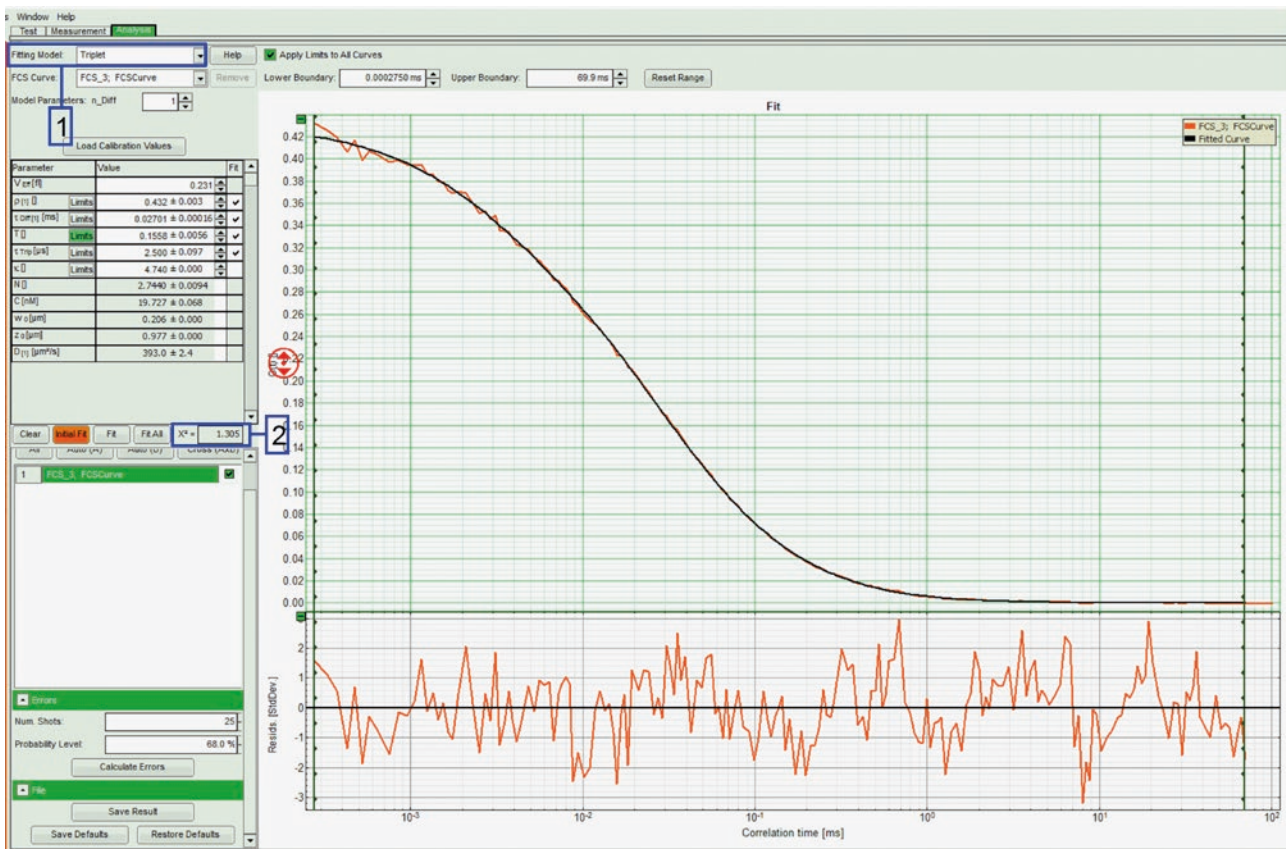


Figure 9

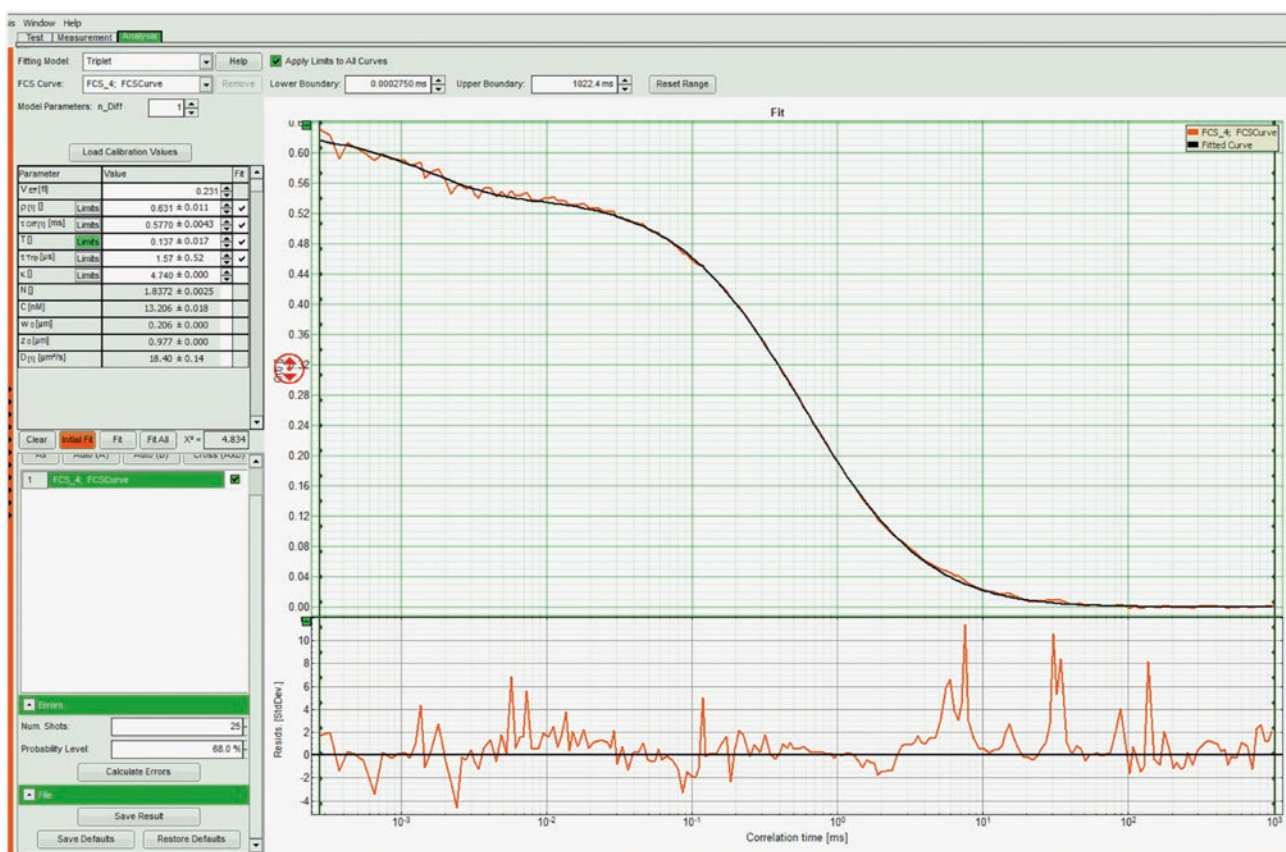


Figure 10

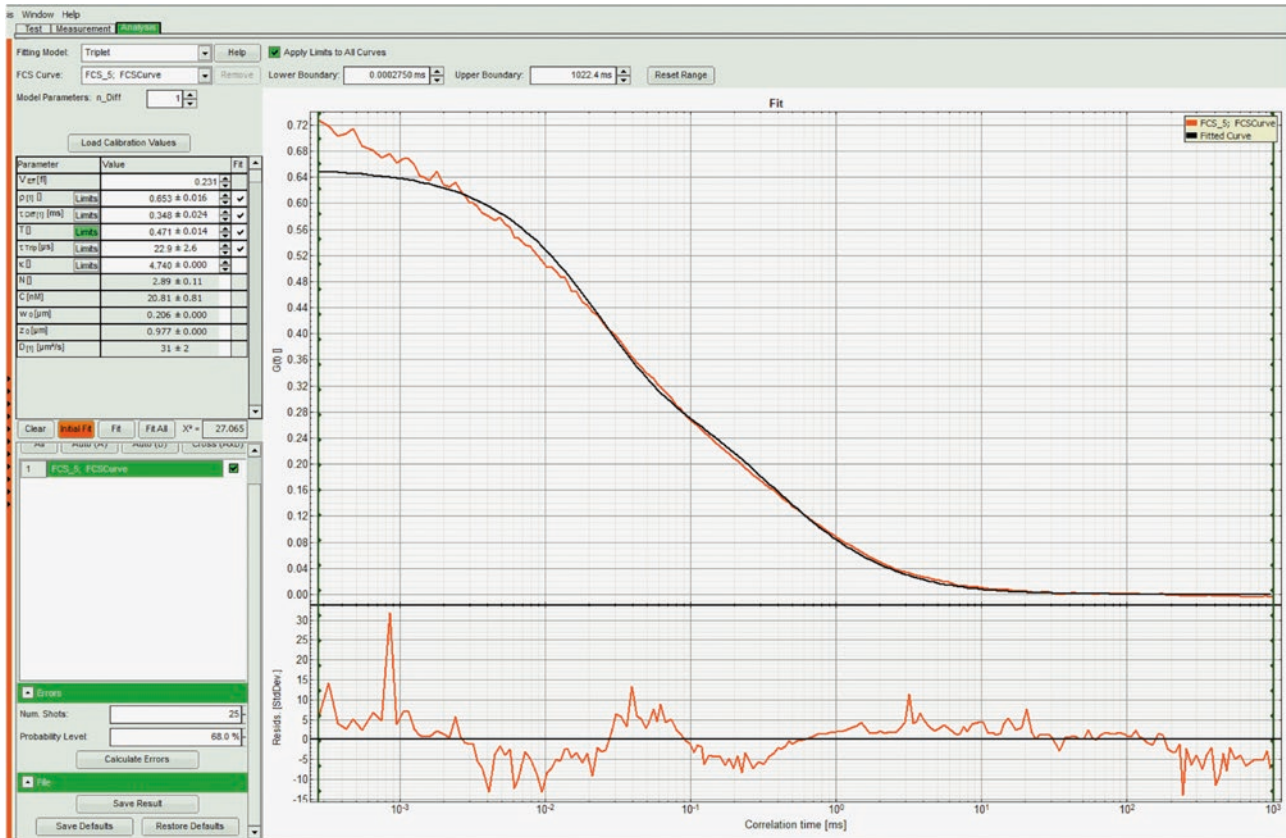


Figure 11

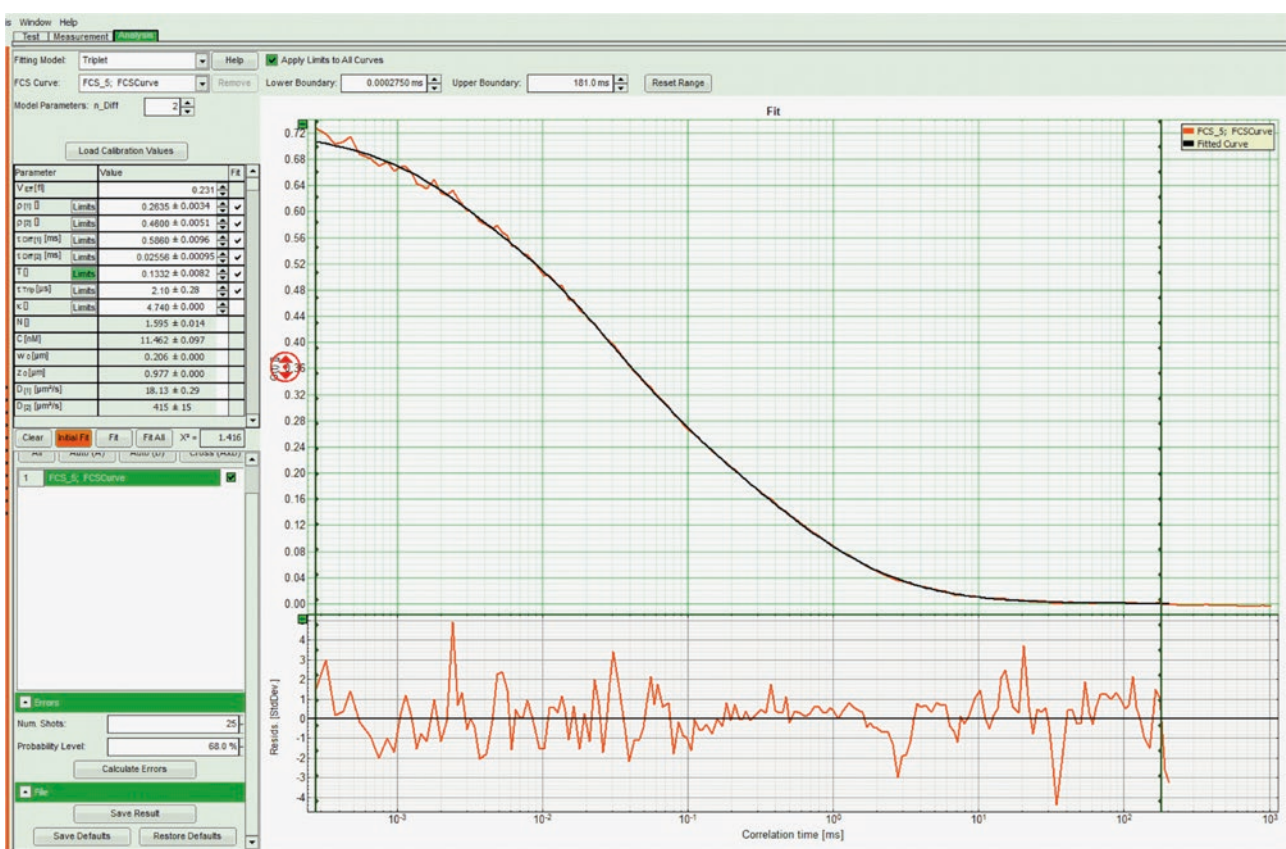


Figure 12

# Chapter

6

# Fluorescence Recovery After Photobleaching (FRAP)

Graham Wright<sup>1</sup> and Jean-Baptiste Sibarita<sup>2,3</sup>

<sup>1</sup> Institute of Medical Biology, A\*STAR, Singapore

<sup>2</sup> University of Bordeaux, Interdisciplinary Institute for Neuroscience,  
Bordeaux, France

<sup>3</sup> CNRS UMR 5297, Bordeaux, France

## Index

Abstract .....	3
1. Principle of FRAP .....	3
2. Qualitative Determination of Protein Dynamics .....	5
3. Models for Quantification of Diffusion and Chemical Exchange .....	6
Diffusion .....	6
Point Bleaching with Gaussian Profile (Axelrod Model) .....	6
Point Bleaching with Rectangular Profile (Soumpasis Model) .....	7
Line Bleaching .....	7
Chemical Interaction .....	7
4. Methods – FRAP Experiments .....	7
Instrumentation .....	7
Data Acquisition .....	8
Data Processing Prior to Quantification .....	10
5. Conclusion .....	10
Acknowledgements .....	10
Further Reading .....	11

## Abstract

Fluorescence recovery after photobleaching (FRAP) is a microscopy technique capable of quantifying the mobility of molecules within cells. By exploiting the phenomenon of photobleaching, fluorescent molecules within a region of interest can be selectively and irreversibly ‘turned off’. The analysis of the fluorescence recovery within the same region, due the redistribution of the molecules, provides information on their diffusion- and binding-dependent mobility. Both qualitative and quantitative analysis can then be applied to decipher the dynamic behavior of the molecules of interest.

## 1. Principle of FRAP

Fluorescence recovery after photobleaching (FRAP) is a popular fluorescence microscopy technique used to quantify the mobility of molecules within cells. The mobility is determined by the molecules’ properties of transport, diffusion and binding to immobile sites. Since the initial development by Axelrod et al.<sup>[1]</sup> and Peters et al.<sup>[2]</sup> in the 1970’s, the technique has been widely used in biological research to study cell

membrane diffusion, protein interactions and protein dynamics<sup>[3-12]</sup>.

Photobleaching is a natural phenomenon that manifests itself as decreasing intensity of fluorescence over time during fluorescence imaging. Exposing a fluorophore to a high level of light intensity in the presence of molecular oxygen causes permanent and irreversible chemical changes to that molecule, rendering it non-fluorescent<sup>[11],[13],[14]</sup>. Under a constant absorption of light, the fluorescence intensity will decrease over time following an exponential decay law:

$$I(t) = I_0 e^{-Kt}$$

where  $I_0$  represents the initial fluorescence intensity and  $K$  the bleaching rate constant of the fluorophore including the flux of illumination photons.

Generally, photobleaching is considered a problem for time-lapse and 3D imaging, leading to unwanted loss of the signal and resultant degradation of the signal-to-noise ratio during acquisition. In FRAP experiments, however, the photobleaching phenomenon is exploited to selectively ‘turn off’ a subset of the fluorescent molecules in the sample usually at a spot or in a specific area of interest using a short pulse of

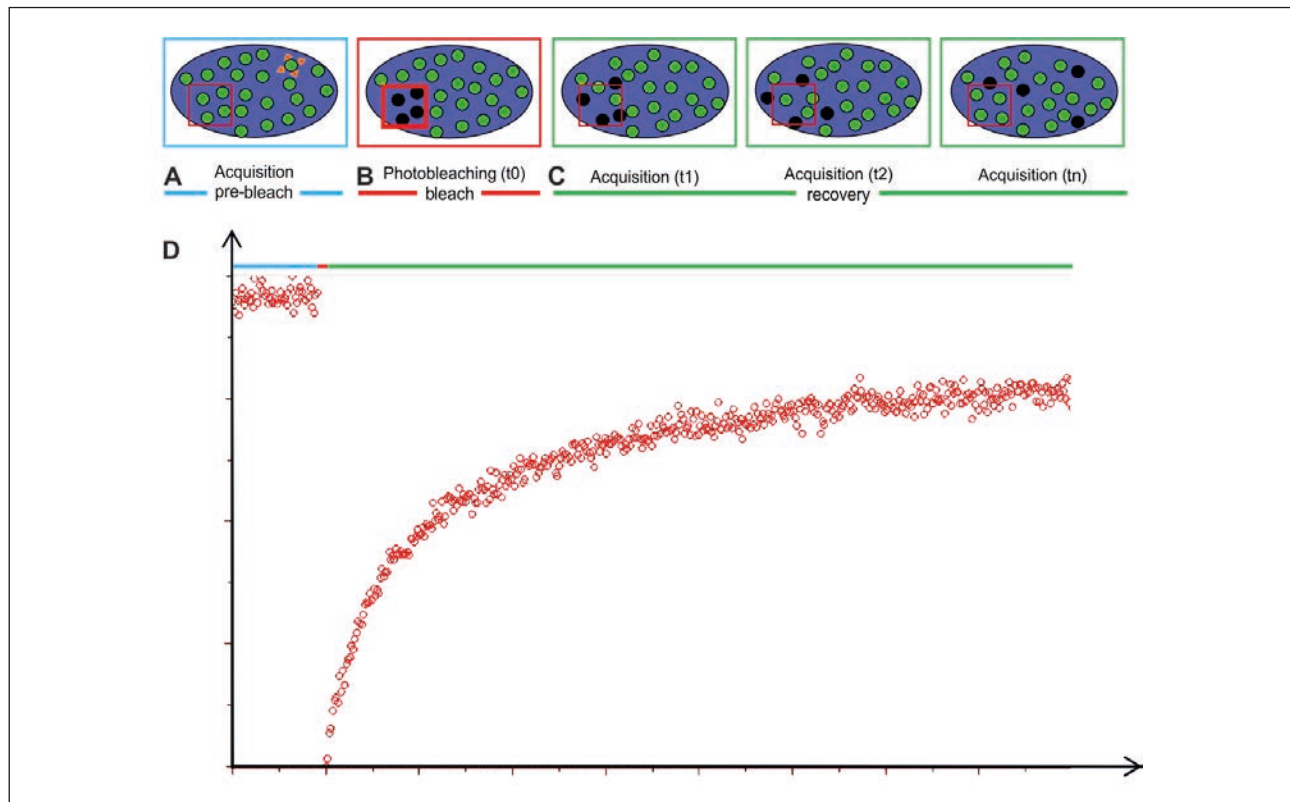


**Figure 1** Principle of FRAP experiments. **A** A cell or organelle is uniformly labeled with a fluorescent tag and a pre-bleach series of images collected. **B** A ROI is selectively photobleached using a short pulse of intense laser light. **C** A post-bleach recovery time series of images is collected and the intensity within the ROI monitored as the bleached dye diffuses out and new dye diffuses in. **D** Intensity changes within the ROI are measured, corrected, normalized and plotted on a graph for further quantification.

high intensity laser light that can be positioned to, or scanned over, the region of interest (ROI). Monitoring the recovery of intensity in the bleached ROI yields information on protein mobility (Figure 1).

The choice of fluorophore is an important consideration for all fluorescence imaging based experiments, and FRAP is no exception. Ideally it should be stable enough to undergo minimal photobleaching during the imaging phases - the pre- and post-bleach acquisitions – but bleach quickly and permanently during selective ROI photobleaching. Genetically encoded fluorescent proteins, like GFP, are generally used to label a molecule of interest with very high specificity<sup>[3],[14],[15]</sup>. They provide enormous power and scope to study biomolecules in living cells through transient expression or through producing stable transgenic cell lines. Importantly, it must be taken into consideration that these modifications may change the properties of the tagged molecule and it is noteworthy that high intensity illumination creates free radicals which are highly reactive and thus cytotoxic<sup>[16]</sup>. The induced photodamage may affect cell viability and result in artifactual results. It is therefore important to minimize the extent of bleaching, even during the bleaching step.

In practice, a FRAP experiment is a 3 step acquisition process, followed by data analysis, as follows (also refer to Figure 1)<sup>[11],[17],[18]</sup>:

- 1. Pre-Bleach:** A time-lapse acquisition containing the cell or sample of interest and ideally some empty background area. It is important to tune the acquisition settings to reduce the amount of photobleaching resulting from the imaging itself (Figure 1A)
- 2. Bleach:** A ROI is selectively photobleached using a short pulse of intense laser light, the intensity modulation is typically controlled through an acousto-optical tunable filter (AOTF). The ROI may be a single focused spot, or the laser beam may be scanned (in a raster or a whirlwind pattern) over the area through the action of galvanometric-mirrors. To avoid damaging the cell, just a fraction of the overall pool of fluorescent molecules should be turned off (Figure 1B)
- 3. Recovery:** A time-lapse acquisition with similar parameters as the pre-bleach phase, but longer

in duration, is performed. When appropriate, this can be done in up to 3 phases with a series of fast acquisitions to cover the fast dynamics of recovery, followed by phases of less frequent imaging as the recovery continues. Again, it is important to reduce the amount of photobleaching caused by the imaging itself to a minimum (Figure 1C).

- 4. Data analysis:** Following correction and normalization steps, the intensity fluctuations during the recovery phase within the ROI are analyzed quantitatively (Figure 1D). This allows the extraction of the recovery rate as a measure for molecular mobility as well as mobile and immobile fractions. Advanced fitting using biophysical models can be used under certain, precisely defined boundary conditions, to quantify the diffusion coefficient or chemical exchange rate.

FRAP can be used qualitatively to identify whether a particular molecule is turning over, thereby undergoing exchange with its environment, by basic analysis of the recovery curve. It allows the determination of:

1. the half-time of recovery ( $t_{1/2}$ ), and
2. the mobile ( $M$ ) and immobile ( $1-M$ ) fractions (Figure 4).

More advanced quantitative models allow the precise determination of the kinetics and molecular properties driving such dynamics. Fitting the experimental curve with advanced theoretical models allows the determination of additional parameters<sup>[19-27]</sup>:

1. the ratio between mobile ( $M$ ) and immobile ( $1-M$ ) fractions (Figure 4),
2. the effective diffusion coefficient ( $D$ ),
3. the binding time of proteins to sufficiently immobile macromolecular complexes ( $k_{on}$ ,  $k_{off}$ ), and
4. the interconnection of intracellular organelles.

A closely related technique to FRAP is Fluorescence Loss in Photobleaching (FLIP<sup>[11]</sup>; Figure 2). Again the experiment consists of a pre-bleach acquisition, but then a ROI in the cell is repeatedly bleached whilst a second ROI is analysed for the consequent loss of fluorescence. This technique gives information about

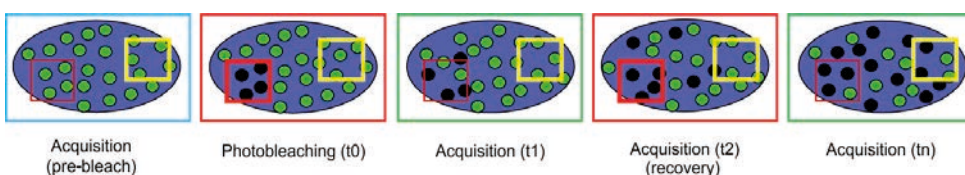


**Figure 2 Principle of FLIP experiments.** A cell or organelle is uniformly labeled with a fluorescent tag and a pre-bleach series collected. A ROI is selectively photobleached using a short pulse of intense laser light repeatedly whilst a second ROI is analysed for the loss of fluorescence.

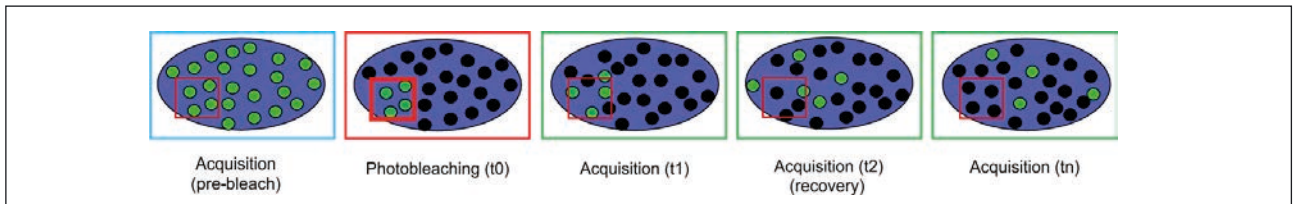


**Figure 3** Principle of iFRAP experiments. A cell or organelle is uniformly labeled with a fluorescent tag and a pre-bleach series collected. A ROI is selected and the area outside of it photobleached using a scanned pulse of intense laser light. The ROI is then analysed for the loss of fluorescence over a post-bleach acquisition. Due to the high likelihood of inducing photodamage on live cells, this technique has largely been replaced by photoactivation-type experiments.

molecules mobility and interconnection between cellular compartments. It will not be covered further within the scope of this chapter. This technique has to be used with caution to avoid photodamage due to repeated bleaching steps.

iFRAP (inverse-FRAP; Figure 3<sup>[28]</sup>) consists of bleaching everything but the ROI, essentially the reciprocal experiment of FRAP. The sample's fluorescence, save for a small area, is photobleached and the analysis concentrates on the loss of fluorescence from the ROI, rather than the recovery. This technique is typically more damaging to the sample due to the large areas that are exposed to high laser power. As a result it has been largely replaced by photoactivation (PA) experiments since the discovery of photoactivatable GFP and development similar proteins<sup>[13],[29-31]</sup>. With PA experiments the fluorescence can be selectively “turned on” in an ROI through a pulse of shorter wavelength light (typically 405 nm). These techniques will not be covered further within the scope of this chapter.

## 2. Qualitative Determination of Protein Dynamics

It is common, and quite straightforward, to characterize molecule dynamics from FRAP experiment by the half-time of recovery ( $t_{1/2}$ ) and the mobile ( $M$ ) and immobile ( $1-M$ ) fractions. Even if it has no direct relation with biophysical parameters, they provide a general semi-quantitative estimate on molecule dynamics and can be used to compare various biological conditions.  $t_{1/2}$  gives information on the average dynamics of moving molecules, whereas  $M$  quantifies the fraction of molecules which are moving and  $1-M$  describes the fraction of immobile molecules within the bleached area during the experiment. Immobile molecules strongly interact with a structural component of the cell or be ‘trapped’ within a multi-component protein complex, preventing them from moving away from the bleached ROI. From the recovery curves,  $t_{1/2}$  can easily be extracted (see Figure 4), provided the post-bleach recovery imaging segment was sufficiently long and appropriate intensity corrections have been performed. This value needs to be used with caution, since the

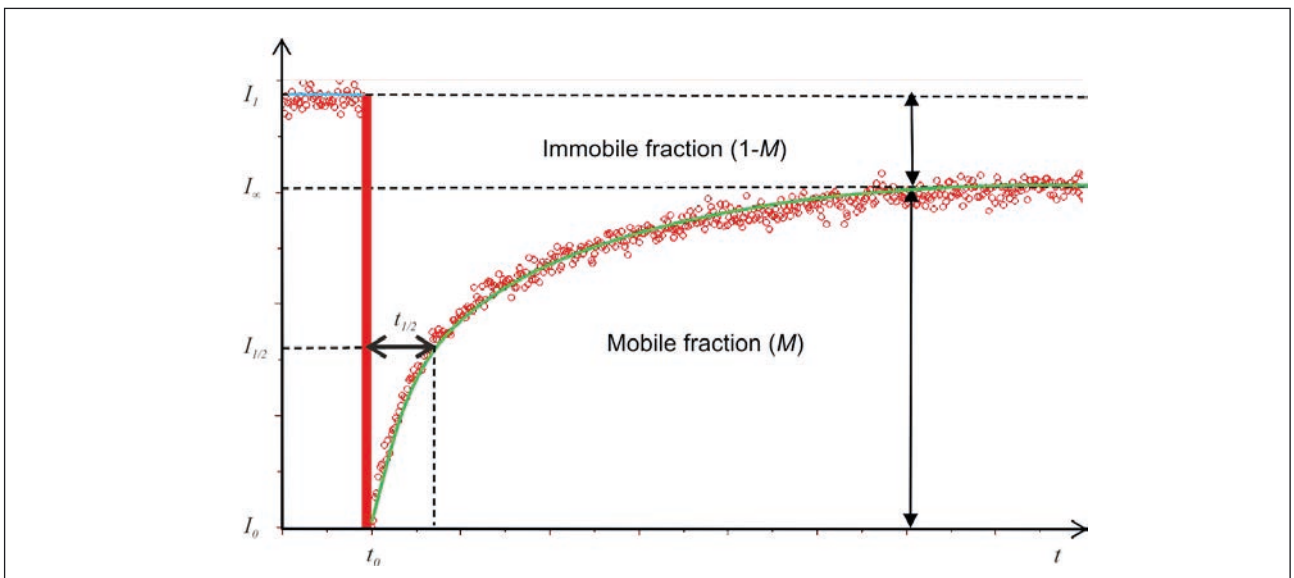


**Figure 4** Recovery curve of a FRAP experiment and determination of half-time of recovery ( $t_{1/2}$ ), mobile ( $M$ ) and immobile ( $1-M$ ) fractions.

cell geometry and bleached area properties (size, position with respect to the cell) can strongly influence  $t_{1/2}$  in addition to the molecules' behavior<sup>[11]</sup>.

The photobleaching depth  $B$  is given by the fraction between the remaining signal and the original signal in the bleached ROI. It is given by

$$B = \frac{I_1 - I_0}{I_1}$$

This fraction is important for quantitative analysis and has to be less than 80% in practice.

The mobile fraction is given by

$$M = \frac{I_\infty - I_0}{I_1 - I_0}$$

and gives information on proteins that are mobile or interact transiently with immobile binding sites during the observation time of the experiment. Again, caution needs to be taken since  $M$  may depend on acquisition parameters and bleaching dimensions.

### 3. Models for Quantification of Diffusion and Chemical Exchange

Molecular mobility is mainly due to diffusion, flow or chemical reaction (association/dissociation to an immobile molecular complex). The general equation of the fluorescence recovery is given by

$$\frac{\partial c(r,t)}{\partial t} = D \nabla^2 c(r,t) - V \frac{\partial c(r,t)}{\partial r} + (k_{off} - k_{on})c(r,t)$$

The first term describes the diffusion, the second the flow and the last term the association/dissociation processes. Unfortunately, this equation has no analytical solution, and it is easier to investigate each contribution individually. It therefore may be necessary to perform multiple experiments, bleaching for example areas with different sizes.

#### Diffusion

The diffusion coefficient of a molecule is given by the Stokes-Einstein relation:

$$D = \frac{kT}{6\pi\eta R}$$

Where  $k$  is the Boltzmann constant,  $T$  the temperature,  $\eta$  the viscosity and  $R$  the hydrodynamic radius of the molecule.

In most FRAP experiments,  $D$  is defined as

$$D = \frac{w^2}{4\tau_D}$$

where  $w$  is the waist of the bleached area,  $\tau_D$  a characteristic time constant extracted from mathematical model fitting, and  $n$  the number of spatial dimensions. In general  $\tau_D$ , has no direct relation with  $t_{1/2}$  defined in Figure 4.

#### Point Bleaching with Gaussian Profile (Axelrod Model)

It is possible to extract the diffusion coefficient by single-point bleaching with a Gaussian profile, using the Axelrod model<sup>[11]</sup> (Figure 5). Recovery curves are reconstructed by averaging the pixel intensity values within a circular region of interest of  $w$  in diameter,  $w$  being the waist of the laser at  $1/e^2$  (13.5%) of the peak intensity of the Gaussian. Using imaging information, the recovery sequence can be corrected by normalizing mean pixel intensities in another ROI located far from the bleaching area. This step makes it possible to take into account intensity fluctuations due to observational photobleaching or laser instabilities. Once corrected, the recovery curves are fitted with a 10<sup>th</sup> order limited development of the following equation.

$$F(t) = (1-M) \frac{1-e^{-Kt}}{K} + M \sum_{n=1}^{\infty} \left[ \frac{(-K)^n}{n!} \right] \left[ 1+n \left( 1+\frac{2t}{\tau} \right) \right]^{-1}$$

where  $M$  is the mobile fraction (accounting for the ability of the molecule to diffuse during the duration of the experiment),  $K$  is a bleaching constant parameter and  $\tau$  is the characteristic diffusion time. The diffusion coefficient  $D$  can be correctly estimated as follows:

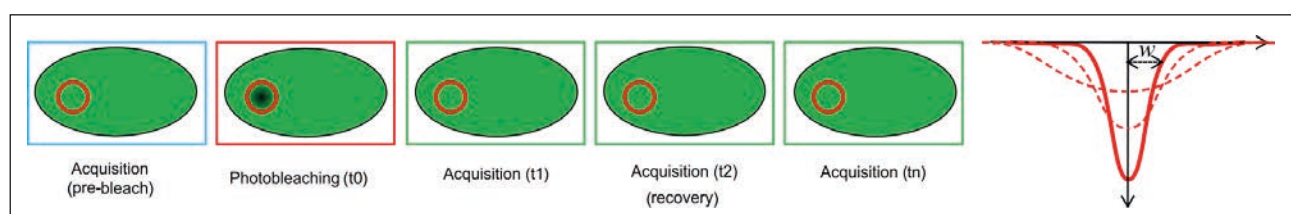


**Figure 5** Schematic and model of point bleaching with a Gaussian profile and recovery.

$$D = \frac{w^2}{4\tau}$$

$K$  can be obtained by fitting the following laser intensity distribution on the bleaching profile:

$$I(r, t=0) = I_0 e^{-KB(r)} \text{ with } B(r) = B(0) e^{-\frac{r^2}{2w^2}}$$

### Point Bleaching with Rectangular Profile (Sompasis Model)

Bleaching with a rectangular profile (Figure 6) allows avoiding the complexity to measure the bleaching constant  $K$  required to solve the Axelrod equation<sup>[1],[32]</sup>. In this case, the recovery curve can be fitted with the following equation:

$$I(t) = e^{\frac{-2\tau}{t}} \left( J_0 \frac{2\tau}{t} + J_1 \frac{2\tau}{t} \right)$$

Where  $J$  is the Bessel function and  $\tau = w^2 / 4D$ .

### Line Bleaching

The Sompasis model requires shaping of the beam with a square profile, which is not commonly available on standard FRAP equipments. A simpler solution consists of performing a line bleaching with a Gaussian beam profile<sup>[33],[34]</sup> (Figure 7). In this case, the recovery curve can be fitted by the following equation, a 1D approximation of the diffusion process:

$$I(t) = I_\infty \left( 1 - \sqrt{\frac{w^2}{w^2 + 4\pi Dt}} \right)$$

This model displays an accuracy of about 30%.

### Chemical Interaction

FRAP recovery curves of chemical reactions are the simplest case, since they can be solved by the following single exponential recovery function:

$$I(t) = A(1 - e^{-t/\tau}) \quad \text{with} \quad \tau = \frac{1}{k_{on} + k_{off}} \quad \text{and} \quad A = \frac{k_{off}}{k_{on} + K_{off}}$$

where  $k_{on}$  and  $k_{off}$  are the association and dissociation rates of the bleached molecules to their ligand. In practice, this case is very rare in living cells, and diffusion always plays a role<sup>[20]</sup>. Nevertheless, it is important to notice that in the case of pure binding, the recovery rate is independent of the bleaching radius, while it is a function of  $w$  in the case of Brownian diffusion.

## 4. Methods – FRAP Experiments

### Instrumentation

The hardware required for FRAP experiments comprises a fluorescence microscope equipped with light sources (arc lamps, LEDs or lasers) and filter sets for imaging as well as a light source for bleaching (typically lasers) with some method of selectively bleaching a region of interest (ROI). Of course, a sample labeled with a fluorescent molecule attached to the protein of interest is required and is one of the challenges the biologist is facing. The fluorophore used should be selected both for its spectral properties in order to match the laser lines and filters available, as well as for having favourable photophysical properties, i.e., negligible bleaching probability at low illumination intensities and high bleaching probability at high intensities. As most biological experiments involve living cells, there is a prerequisite for the

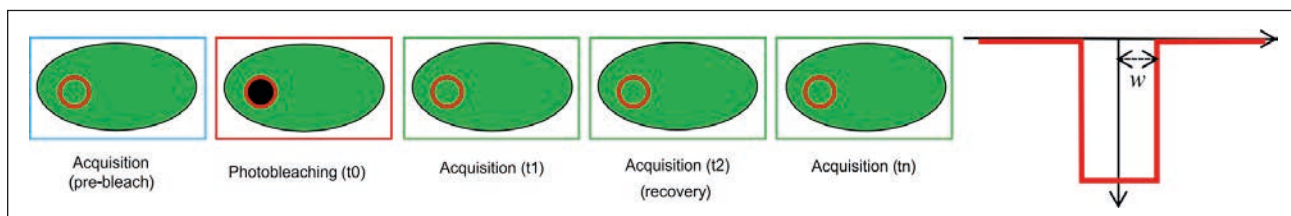


Figure 6. Schematic and model of point bleaching with a rectangular profile and recovery.

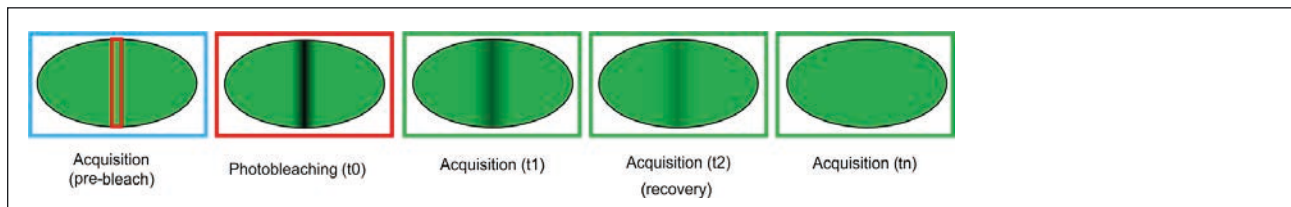
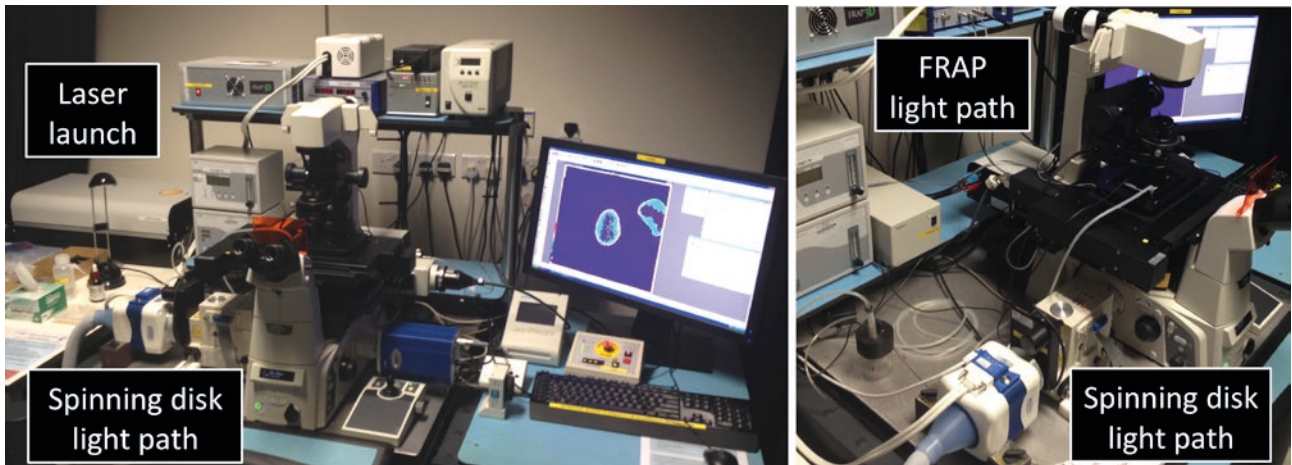
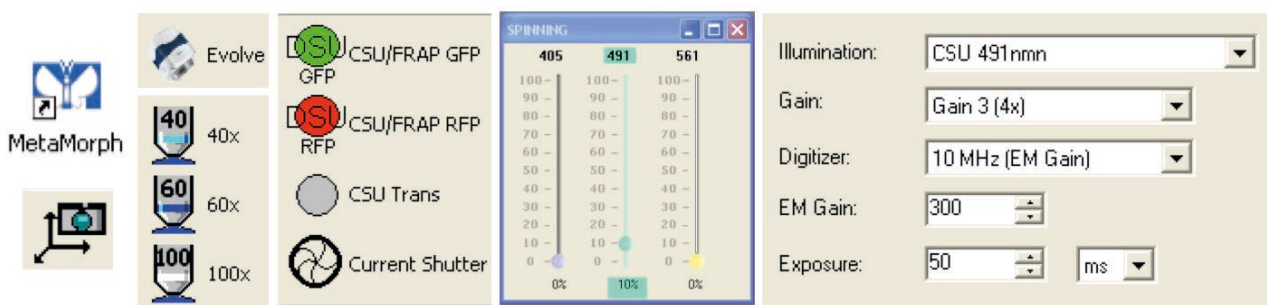


Figure 7. Schematic of line bleaching and recovery.



**Figure 8** Photographs of an implementation of the Roper iLas2 FRAP-3D system at the Institute of Medical Biology, A\*STAR, Singapore. The microscope stand is an inverted Nikon Eclipse Ti equipped with a Yokogawa CSU-22 spinning disk confocal head and a liquid-cooled Photometrics Evolve EM-CCD camera. It is operated through the MetaMorph and iLas2 acquisition software. The lasers (405/491/561 nm) inside the laser launch are used for both imaging and FRAP, with an AOTF to rapidly control the intensity of laser reaching the sample, and a galvo mirror to rapidly switch between the spinning disk (mounted on the left of the microscope) and FRAP light paths (mounted at the rear of the microscope).



**Figure 9** Establishing and refining the imaging conditions in the MetaMorph software through selection of the correct camera mode, objective lens, filter combination, laser power, camera gain and exposure conditions appropriate for the sample. Photobleaching and photodamage, as a consequence of tuning these imaging conditions, should be reduced to a minimum – lower laser power and shorter exposures, whilst maintaining sufficient dynamic range in the images for quantification and imaging frequency for sampling of the recovery.

microscope to be equipped with an incubator and a supply of humidity and CO<sub>2</sub>, as dictated by the cell type.

The most common way to achieve selective photobleaching is to use galvanometer-driven mirrors to steer the laser beam, which is momentarily switched to a higher intensity, to a diffraction limited spot or to a scanned region (in raster or whirlwind pattern) over a pre-selected ROI. For this reason, many FRAP experiments have been carried out on confocal laser scanning microscopes (CLSMs) as they are equipped with high-power lasers and galvo mirrors<sup>[35-37]</sup>. FRAP scanning heads are now also commercially available for widefield fluorescence systems (e.g. DeltaVision Elite from GE), spinning disk confocal or TIRF systems (e.g. iLas2 FRAP-3D from Roper (Figure 8), UltraView VoX from PerkinElmer and Revolution XD from Andor). In these setups the microscope's excitation illumination light-path and the FRAP illumin-

nation light-path are independent from one another, offering very fast switching between, or even simultaneous, photobleaching and imaging. Typically, such systems will have some calibration routine to correlate a given pixel's position with the corresponding galvo position. Some of the CLSM manufacturers have also developed systems with dual scanners to enable this (e.g. the SIM scanner on the Olympus FV1000 and FV1200 confocal systems).

The short-lived increase in the laser intensity for photobleaching is achieved either by using an acousto-optical tunable filter (AOTF), by modulating the laser output power directly, or by using a fast switching mirror to steer the beam into an independent light-path with reduced attenuation.

### Data Acquisition

Acquisition and photo-perturbation parameters need to be carefully adjusted in order to minimise errors

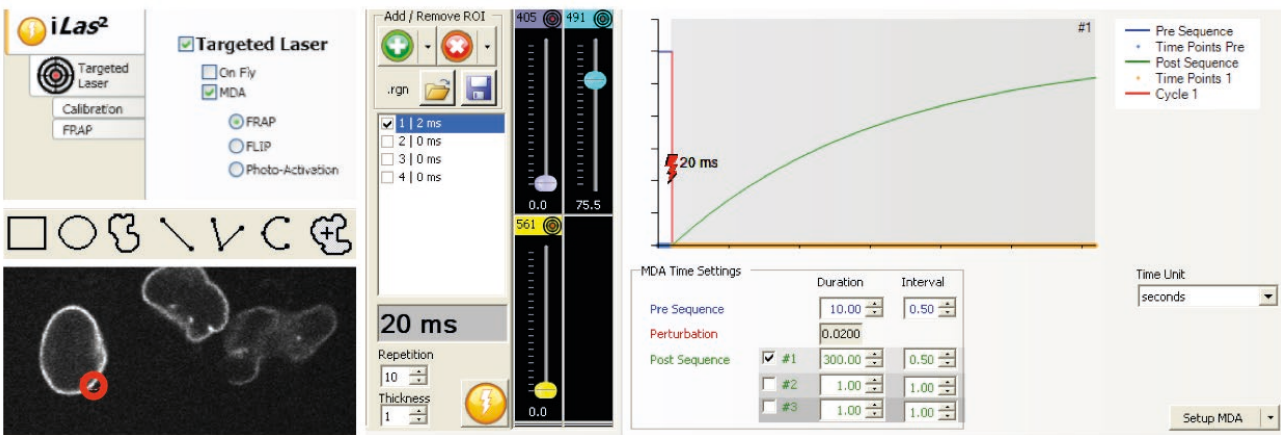


**Figure 10** Establishing and refining the FRAP conditions in the iLas<sup>2</sup> module through selection of the appropriate mode of operation (On-Fly or MDA), ROI shape, size and location, duration/repetitions of bleach and laser intensity to be used, as well as the temporal frequency and number of images in the pre- and post-bleach acquisition steps. They have to be adjusted according to the protein dynamics and cell and fluorophore stability. This data, once established, is then sent back to the Multi Dimensional Acquisition tool in MetaMorph.

in quantification and interpretation<sup>[27]</sup>. This is a rule of thumb for qualitative and quantitative FRAP experiments. Prior to carrying out a FRAP experiment, one should perform empirical tests to establish time-lapse image acquisition settings that minimise photo-bleaching and match protein dynamics. This usually requires a compromise between sufficient dynamic range for quantification and sufficient imaging speed to properly sample the recovery dynamics. Acquisition frequency and photo-perturbation duration need to be adjusted according to the recovery speed as well. This will involve selection of the appropriate objective lens, fluorescence filter set, laser power, camera settings, exposure duration (or corresponding confocal acquisition settings) and imaging frequency according to the sample preparation and protein dynamics (Figure 9). Subsequent empirical tests should be carried out to tune the FRAP settings like the ROI shape, size and location, bleaching duration and laser intensity (Figure 10). It is important that the duration of the photobleaching step should be short enough to prevent any molecules from entering or leaving the ROI during the bleach. In addition, acquisition of the post-bleach sequence must be fast enough to capture the fluorescence recovery. Finally, the delay between the end of the bleaching and the beginning of the recovery must be as short as possible. In a general manner, one can use the rule of ten:

- bleaching duration must be at least 10 times faster than the half time of recovery ( $t_{1/2}$ ).
- delay between the end of the bleaching step and the beginning of the recovery sequence must be shorter than a 10<sup>th</sup> of  $t_{1/2}$ .
- acquisition frequency of the recovery sequence must be at least 10 times faster than  $t_{1/2}$  (at least

until  $t = t_{1/2}$ , then the acquisition frequency can be reduced to avoid observational photobleaching).

- recovery sequence duration must be about 10 times longer than  $t_{1/2}$ .

When the size of the bleaching ROI affects the half time recovery, which is the case for example for diffusional or flow-induced mobility, it can be adjusted for the rule of ten to hold (e.g., bleaching a larger area in a fast mode will increase the  $t_{1/2}$ , allowing slower acquisition frequency).

In the following example, we show the data acquisition parameters that require consideration for the iLas<sup>2</sup> FRAP-3D system (Roper, France), integrated onto the MetaMorph acquisition platform (Molecular Devices; Figure 9). Whilst the considerations are similar on other hardware/software platforms, the terminology and implementation may differ.

Once the appropriate imaging and FRAP conditions are established, single or multiple ROIs are selected in a preview image and the iLas<sup>2</sup> software sends the data as a journal (macro) to the MetaMorph Multi Dimensional Acquisition (MDA) tool. This handles the complex time-lapse acquisition routine established in the iLas<sup>2</sup> window. When the time resolution of the experiment is critical the FRAP-On-Fly method can be used instead of the MDA. In this case a stream acquisition is setup in which the hardware is pushed to its limits to maximize frame-rate. During the acquisition, the user can then manually select the position of the FRAP ROI with the mouse whilst the stream acquisition continues. The frame rate is then limited by the exposure time and read-out speeds of the camera/computer system.

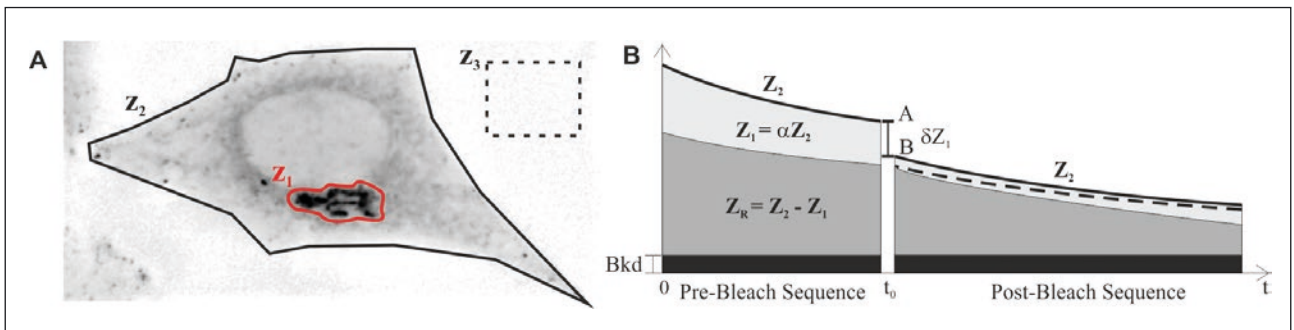


**Figure 11** Image correction prior quantification. All the information for a given cell is used to measure the cell fluorescence eliminated by bleaching and to compensate for observational photobleaching over time throughout the experiment. **A** Three distinct ROI are defined:  $z_1$  is the region targeted by the laser bleaching pulses;  $z_2$  includes the whole cell and is assumed to contain a fixed number of fluorophores, regardless of whether those fluorophores are bleached or fluorescent;  $z_3$  is defined for the estimation of background level, mostly due to the CCD dark signal. **B** The average level over  $z_3$  is subtracted from all the images. Signal levels  $Z_1$  and  $Z_2$ , in regions  $z_1$  and  $z_2$ , are analysed after background subtraction. They are processed to account for observational bleaching and for the limitation of recovery in  $z_1$  by the total loss over  $z_2$ .

### Data Processing Prior to Quantification

It is of major importance to process the acquired data before quantification in order to correct for observational photobleaching and avoid artifacts in the quantification<sup>[27]</sup>. Image sequences can be corrected for observational photobleaching using the fact that a closed volume ( $Z_2$  in Figure 11A) contains a finite number of fluorescent molecules<sup>[5]</sup>. Changes in the average intensity inside this volume over time results from both bleaching pulses and observational photobleaching, following a first-order decay with time constant  $\tau$ . Observational photobleaching can be assessed with  $Z_2$  before ( $t < t_0$ ) and after the pulse ( $t > t_0$ ), and corrected by multiplying  $Z_2$  by  $e^{(t-t_0)/\tau}$ . In this normalization process, the step points A and B are fixed points, and the normalized  $Z_2$  curve (second plot) has two constants:  $Z_2(t < t_0) = A$  and  $Z_2(t > t_0) = B$ .

Let  $\alpha$  be the ratio  $Z_1/Z_2$ , with  $Z_1$  the average intensity over the volume  $z_1$  (see Figure 11A). Before the bleaching pulse, at  $t < t_0$ ,  $\alpha$  remains constant at steady state.  $Z_1$  (light grey) and the difference signal  $Z_R = Z_2 - Z_1$  over the complementary region (dark grey) therefore both decay like  $Z_2$ . Consequently,  $Z_1$  and  $Z_R$  are constant before the pulse on the normalized graph. Immediately after the photobleaching of  $z_1$ , at  $t = t_0$ ,  $Z_1/Z_2$  no longer equals  $\alpha$ , but instead falls to  $\alpha - \delta Z_1/Z_2$ . If full recovery to the initial steady state occurs during the experiment, this proportion then returns to  $\alpha$ , and  $Z_1$  recovers at the expense of  $Z_R$ . With the exception of very limited bleached areas and/or bleaching depths, full recovery in  $z_1$  is attenuated by a loss factor  $B/A$ . Recovery curves are thus compared to their asymptotic limit  $Z_1(B/A)$ , so that the mobile fraction can still be measured correctly. To enable comparisons between multiple experiments a normalisation step is typically carried out.

Once the data are processed and normalized,

recovery curves can be analyzed following the procedure introduced earlier.

### 5. Conclusion

FRAP is carried out on microscopes equipped with components that allow the user to selectively expose regions of interest (ROI) to intense pulses of laser light. This is usually possible on research grade microscopes such as confocal instruments. In doing so the fluorescent molecules (usually proteins of interest tagged with fluorophores like GFP) within that region are photobleached into an 'off' state. By subsequently analysing that ROI the dynamics of the recovery of that fluorescence can be used to give a greater understanding of the molecule being studied like: (1) the half-time of recovery, (2) the ratio between mobile and immobile fractions, (3) the effective diffusion coefficient, (4) the binding time of proteins to immobile macromolecular complexes, and (5) the interconnection of intracellular organelles and the existence of protein complexes.

### Acknowledgements

Thanks to Emma Feng Yu (microLAMBDA Pte Ltd, Singapore) for help and advice with the iLas2 and MetaMorph software. Also, we thank Malte Wachsmuth for the critical reading and advice on the preparation of this manuscript.

## Further Reading

- [1] Axelrod, D., et al., Mobility measurement by analysis of fluorescence photobleaching recovery kinetics. *Biophys J*, 1976. 16(9): p. 1055-69.
- [2] Peters, R., et al., A microfluorimetric study of translational diffusion in erythrocyte membranes. *Biochim Biophys Acta*, 1974. 367(3): p. 282-94.
- [3] White, J. and E. Stelzer, Photobleaching GFP reveals protein dynamics inside live cells. *Trends Cell Biol*, 1999. 9(2): p. 61-5.
- [4] Snapp, E.L., N. Altan, and J. Lippincott-Schwartz, Measuring protein mobility by photo-bleaching GFP chimeras in living cells. *Curr Protoc Cell Biol*, 2003. Chapter 21: p. Unit 21 1.
- [5] Phair, R.D. and T. Misteli, High mobility of proteins in the mammalian cell nucleus. *Nature*, 2000. 404(6778): p. 604-9.
- [6] Lippincott-Schwartz, J., T.H. Roberts, and K. Hirschberg, Secretory protein trafficking and organelle dynamics in living cells. *Annu Rev Cell Dev Biol*, 2000. 16: p. 557-89.
- [7] Houtsmuller, A.B., et al., Action of DNA repair endonuclease ERCC1/XPF in living cells. *Science*, 1999. 284(5416): p. 958-61.
- [8] Houtsmuller, A.B. and W. Vermeulen, Macromolecular dynamics in living cell nuclei revealed by fluorescence redistribution after photobleaching. *Histochem Cell Biol*, 2001. 115(1): p. 13-21.
- [9] Klonis, N., et al., Fluorescence photobleaching analysis for the study of cellular dynamics. *Eur Biophys J*, 2002. 31(1): p. 36-51.
- [10] Hoogstraten, D., et al., Rapid switching of TFIIH between RNA polymerase I and II transcription and DNA repair in vivo. *Mol Cell*, 2002. 10(5): p. 1163-74.
- [11] Bancaud, A., et al., Fluorescence perturbation techniques to study mobility and molecular dynamics of proteins in live cells: FRAP, photoactivation, photoconversion, and FLIP. *Cold Spring Harb Protoc*, 2010. 2010(12): p. pdb top90.
- [12] Reits, E.A. and J.J. Neefjes, From fixed to FRAP: measuring protein mobility and activity in living cells. *Nat Cell Biol*, 2001. 3(6): p. E145-7.
- [13] Lippincott-Schwartz, J., N. Altan-Bonnet, and G.H. Patterson, Photobleaching and photoactivation: following protein dynamics in living cells. *Nat Cell Biol*, 2003. Suppl: p. S7-14.
- [14] Lippincott-Schwartz, J. and G.H. Patterson, Development and use of fluorescent protein markers in living cells. *Science*, 2003. 300(5616): p. 87-91.
- [15] Weber, W., et al., Shedding light on the dark and weakly fluorescent states of green fluorescent proteins. *Proc Natl Acad Sci U S A*, 1999. 96(11): p. 6177-82.
- [16] Magidson, V. and A. Khodjakov, Circumventing photodamage in live-cell microscopy. *Methods Cell Biol*, 2013. 114: p. 545-60.
- [17] Swift, S.R. and L. Trinkle-Mulcahy, Basic principles of FRAP, FLIM and FRET. *Proc Roy Microsc Soc*, 2004. 39: p. 3-10.
- [18] Terjung, S. and R. Pepperkok, FRAP-teaching module, in European Advanced Light Microscopy Network (EAMNET). 2005.
- [19] Sprague, B.L. and J.G. McNally, FRAP analysis of binding: proper and fitting. *Trends Cell Biol*, 2005. 15(2): p. 84-91.
- [20] Sprague, B.L., et al., Analysis of binding reactions by fluorescence recovery after photobleaching. *Biophys J*, 2004. 86(6): p. 3473-95.
- [21] Bulinski, J.C., et al., Rapid dynamics of the microtubule binding of ensconsin in vivo. *J Cell Sci*, 2001. 114(Pt 21): p. 3885-97.
- [22] Lambert, N.A., Uncoupling diffusion and binding in FRAP experiments. *Nat Methods*, 2009. 6(3): p. 183; author reply 183-4.
- [23] Sullivan, K.D., A.K. Majewska, and E.B. Brown, Single- and two-photon fluorescence recovery after photobleaching, in *Imaging: A Laboratory Manual*. 2011, Cold Spring Harbor Press: Cold Spring Harbor.
- [24] Gordon, G.W., et al., Analysis of simulated and experimental fluorescence recovery after photobleaching. Data for two diffusing components. *Biophysical Journal*, 1995. 68(3): p. 766-778.
- [25] Phair, R.D. and T. Misteli, Kinetic modelling approaches to in vivo imaging. *Nat Rev Mol Cell Biol*, 2001. 2(12): p. 898-907.
- [26] Lippincott-Schwartz, J., E. Snapp, and A. Kenworthy, Studying protein dynamics in living cells. *Nat Rev Mol Cell Biol*, 2001. 2(6): p. 444-56.
- [27] Weiss, M., Challenges and artifacts in quantitative photobleaching experiments. *Traffic*, 2004. 5(9): p. 662-71.
- [28] Rabut, G. and J. Ellenberg, Photobleaching techniques to study mobility and molecular dynamics of proteins in live cells: FRAP, iFRAP and FLIP, in *Live-cell Imaging: A Laboratory Manual*, R.D. Goldman and D.L. Spector, Editors. 2005, Cold Spring Harbor Press: Cold Spring Harbor. p. 101-127.
- [29] Lippincott-Schwartz, J. and G.H. Patterson, Fluorescent proteins for photoactivation experiments. *Methods Cell Biol*, 2008. 85: p. 45-61.
- [30] Patterson, G.H., Photoactivation and imaging of photoactivatable fluorescent proteins. *Curr Protoc Cell Biol*, 2008. Chapter 21: p. Unit 21 6.
- [31] Patterson, G.H. and J. Lippincott-Schwartz, A photoactivatable GFP for selective photolabeling of proteins and cells. *Science*, 2002. 297(5588): p.

1873-7.

- [32] Soumpasis, D.M., Theoretical analysis of fluorescence photobleaching recovery experiments. *Biophys J*, 1983. 41(1): p. 95-7.
- [33] Ellenberg, J., et al., Nuclear membrane dynamics and reassembly in living cells: targeting of an inner nuclear membrane protein in interphase and mitosis. *J Cell Biol*, 1997. 138(6): p. 1193-206.
- [34] Braeckmans, K., et al., Line FRAP with the confocal laser scanning microscope for diffusion measurements in small regions of 3-D samples. *Biophys J*, 2007. 92(6): p. 2172-83.
- [35] McNally, J.G. and C.L. Smith, Photobleaching by confocal microscopy, in *Confocal and two photon microscopy*, A. Diaspro, Editor. 2001, Wiley-Liss: New York. p. 525-538.
- [36] Hauser, G.I., S. Seiffert, and W. Oppermann, Systematic evaluation of FRAP experiments performed in a confocal laser scanning microscope--part II: Multiple diffusion processes. *J Microsc*, 2008. 230(Pt 3): p. 353-62.
- [37] Seiffert, S. and W. Oppermann, Systematic evaluation of FRAP experiments performed in a confocal laser scanning microscope. *J Microsc*, 2005. 220(Pt 1): p. 20-30.

PicoQuant GmbH  
Rudower Chaussee 29  
12489 Berlin  
Germany

Material can be downloaded from [www.picoquant.com](http://www.picoquant.com)

© 2016 PicoQuant GmbH

All rights reserved. No parts of it may be reproduced, translated or transferred to third parties without written permission of PicoQuant GmbH.

[www.picoquant.com](http://www.picoquant.com)